DEVELOPMENT OF LOAD INTERACTION DESIGN RULES

FOR PRESSURISED COMPONENTS SUBJECTED TO

COMBINED LOADING

Thesis submitted in accordance with the

requirements of the University of Liverpool for

the Degree of Doctor of Philosophy by

AMRAN BIN AYOB

April 1994

ABSTRACT

In practice, many pressure vessel and piping components are subjected to load combinations which can be quite complex. The standard design codes make a simplifying assumption that peak stresses for different loads occur at the same location, resulting in a conservative rule.

A plain pipe, pipe bend, tee branch and torispherical head with nozzle were modelled using the PATRAN code and stress analysis studies were conducted using the finite element codes ASAS and ABAQUS. The components were subjected to individual loads of internal pressure, axial thrust, bending moment and torque. A computer program was developed to examine the behaviour of the structures subjected to combined loads and to plot first yield load interaction diagrams for any combination of loads. A limited geometrical nonlinear analysis with combined loading was also carried out for two pipe bends and the branch junction to assess the effect of excessive deformation and nonlinear load coupling on load interactions.

In general, the results showed that the load interaction relations predicted by the linear elastic finite element method (FEM) and linear superposition of stresses are less conservative than those proposed by the design rules. For the pipe bends, when the geometrical nonlinearity and nonlinear load coupling are taken into consideration, the present prediction becomes more unconservative than both the linear FEM and standard design rules. Proposals are being made for a change in the current British Standard design code.

i

ACKNOWLEDGEMENTS

TABLE OF CONTENTS

NOMENCLATURE

The nature of the study makes it impractical to standardise the symbols for all the components. The symbols which are unique to a component are defined under its own listing.

R	radius of pipe
D	diameter of pipe
T	thickness of pipe
σ	normal stress
τ	shear stress
P	internal pressure
T_o	torque
M	bending moment
F	axial force
$\underline{Y}$, σ_Y	uniaxial yield stress
$\underline{P}$	$= P/P_Y$, non-dimensionalised first yield pressure
$\underline{T}_o$	$= T_o/T_{oY}$, non-dimensionalised first yield torque
$\underline{M}$	$= M/M_Y$, non-dimensionalised first yield bending moment
$\underline{F}$	$= F/F_Y$, non-dimensionalised first yield axial force
I	second moment of area
Z	section modulus
E	elastic modulus
ν	Poisson's ratio
C	ASME III secondary stress index

Suffices

h, a, r	hoop, axial and radial directions of pipe
max	maximum
x, y, z	Cartesian coordinates
Y	at first yield
1, 2, 3	principal values
i, o, m	inner, outer and mean
vM, TR	von Mises, Tresca
n	nominal

Note
1. Diameters and radii without suffices are assumed to be mean values.
2. Other notations are defined in the text as they appear.
3. When quoting from a Code, the notation/definition of that particular Code will apply.

Pipe bend

r	mean radius of pipe
R	bend radius of elbow
b	$=R/r$, bend radius ratio
λ	$=TR/r^2$, pipe factor
ϕ	axial direction, $\phi=0°$ at elbow mid-section
θ	hoop direction, $\theta=0°$ at extrados

Tee branch

D, R, T	diameter, radius and thickness of run pipe
d, r, t	diameter, radius and thickness of branch pipe
ϕ	hoop direction of branch pipe
θ	hoop direction of run pipe
w_h	height of weld, measured from intersection
w_l	horizontal width of weld, measured from intersection
M_{xr}	moment about the x-axis, acting on the run pipe i.e. run pipe torsional moment (other moments can similarly be identified and defined by the suffices)

suffices
b, r	branch, run
c, f	crotch, flank

definition of terms
crotch line	the intersection line between the branch and run pipes inside surfaces
crotch corner	the point where the crotch line intersects the longitudinal plane
diameter ratio	d_m/D_m
thickness ratio	t/T

Torispherical head with nozzle

D	diameter of cylindrical shell
R	radius of cylindrical vessel
d	diameter of nozzle
T	thickness of vessel
t	thickness of nozzle
r_k	knuckle radius
L	crown radius
H	head height (to mid-wall)

CHAPTER 1.   INTRODUCTION

In recent times, the severe operating conditions of power and process plants have become more demanding on the design of the piping systems and pressure vessels. The function of these components is to contain and transport fluids, sometimes under high pressure and temperature. The most important design aspect is to ensure satisfactory service of the component under a combination of loads.

The design procedures are recommended by standard design codes such as the American ASME and British BS design codes. Although they have been used for many years, until recently a limited amount of stress analysis information existed by which the safety margin of the codes could be judged. Many attempts have been made to eliminate design weaknesses in the codes, with limited success over a narrow range of the geometric parameters. However the design procedures are constantly being revised as a result of many studies. The most rapid change in piping design criteria started in the 1950s which was brought about by the concern for nuclear accident safety and by the need to update the codes based on new understanding of piping behaviour. In cases where the data are still limited or the results are unsatisfactory, the finite element approach has been used to confirm or establish a more thorough understanding.

The various codes contain simplified design formulae for placing bounds on maximum stresses in the piping systems. A simple equation is given in terms of stress indices or stress intensification factors which reflect the capacity of various piping components to carry load without a specific stress or deformation being exceeded. In the ASME code, the limit on the calculated stress is based on its location, distribution and origin. In the Codes, the rules for combining the maximum calculated stress for combined loads are set - in Section NB-3652

1

of ASME III and in Section 4.11 of BS 806. The equations aim to ensure that every point in the structure conforms to the limiting stress. However, the equations which are based on the simple pipe theory are too simplified for use with the more complex tee branch. The development of numerical techniques has made it possible to determine stresses in detail. It is not reasonable any more to retain the same values of stress factor, allowable stress or even the method of combining stresses, as had been used. The aim would be either to shift from the use of standard design rules toward detailed analysis or to improve on the existing set of rules.

The stress state at any point in a structure may be defined by the three principal stresses by which the designer must compare and interpret against failure modes such as excessive deformation, fracture, creep deformation, incremental collapse or fatigue. The designer must also consider a suitable failure theory in order to define how the various stresses react and contribute to the strength of the structure. In relation to the ASME code provision on failure mode, the present first yield study is similar to limiting the primary and secondary stresses.

The elastic analysis does not describe the full situation. Even in cases where yielding has occurred, the vessel could be successful in containing a higher load. On the other hand, there are cases where vessels show excessive distortion at a load lower than expected. In this study, the structures are assumed not to fail by other modes before initial yielding takes place. The linear elastic finite element method (FEM) has been applied to a range of piping components such as the plain pipe, pipe bend, tee branch and torispherical head with nozzle, and the results evaluated against relevant theories and design rules. The study provides a description of the procedure to determine the stress field in a structure and to verify its proximity to yielding when subjected to a series of combined loads.

The principle of superposition of stresses from individual loading has been applied to produce interaction curves. The method is questionable where large cross-sectional ovalization from bending affects pressure stresses. This nonlinear coupling has been studied in detail in pipe bends where the (Haigh) effect is most significant. The calculation of the yield loci are laborious, hence a computer program and curves are presented for all the components.

The plain pipe is the simplest component with only one independent geometric parameter, i.e. D/T, while the more complicated tee branch and the torispherical head have more than two independent parameters. For this study, four models of the plain pipe and sixteen models of the pipe bend were sufficient to evaluate the effects of geometric parameters on stress behaviour and load interaction. A single model of the tee branch and torispherical head was studied. Depending on the component, the models were subjected to separate loadings of internal pressure, torsion, bending moment and axial force. The individual stresses were then combined to determine the first yield behaviour of the model when subjected to the loads.

In the plain pipe, four models were selected with D/T=5, 10, 15 and 24.5. After performing convergence tests on the thinnest model, a finite element mesh was chosen and implemented for all the plain pipe models. The moment loads were induced by nodal forces applied at the end the pipes. Together with internal pressure and axial force, the stresses from these individual loads were compared with the exact pipe solutions to verify the finite element model. The present study introduces a superposition method which uses the individual stress result to determine the yield behaviour when any two loads interact. In the plain pipe, the method of dealing with combined loads is well understood. The stresses are readily available from the theory of solid mechanics. The method was also compared to the BS code to evaluate its yield criterion and assumptions. The discussions in Chapter 4 assesses the results from the FEM in the light of the current design rules.

3

In the pipe bend, the models were grouped into four values of bend radius ratios, i.e. b=2, 3, 5 and 7. For each value of b, there were four models with different pipe thicknesses, i.e. D/T=10, 20, 80 and 150. The finite element mesh and the methods of loading of the pipe bends were based on the plain pipe. The elbow models were subjected to individual loads of internal pressure, torque and in-plane bending moment. The individual stresses in the elbows were compared to an energy method and the BS and ASME codes. The superposition method was again utilised to determine the first yield load interaction of the models. A computer program was written to interpolate stresses for any given intermediate values of b and D/T. The superposition method which was incorporated into the program could determine the load interaction behaviour for any given elbow. A geometrically nonlinear FE analysis was carried out to investigate the extent of cross-sectional ovalization in two elbow models due to individual loads. The nonlinear analysis was then extended to include simultaneous application of in-plane bending moment and internal pressure to evaluate the nonlinear coupling between the two loads. An experimental test was also carried out to determine the stress behaviour of an elbow subjected to internal pressure and an opening in-plane moment.

The tee branch and torispherical head with nozzle are more complex than the plain pipe and pipe bend in terms of finite element modelling and the geometric effects on the stress behaviour. However, a single particular geometry of both components were modelled and analyzed. Convergence tests were carried out to find a suitable mesh and element type. In the tee branch, two weld profiles were modelled to see the effect of the weld size on stresses at the intersection. In a preliminary study to determine stress convergence, a tee branch model with two layers of elements through the wall thickness was analyzed for pressure load. The hoop stress distribution on the inner surface of the intersection, from the 1-element and 2-element thick models were compared.

The torispherical head with nozzle was based on an experimental model which was tested at Liverpool. The load interactions of the tee branch and torispherical head were generated by the superposition method and compared to results compiled at Liverpool and to design codes.

CHAPTER 2.   STRESS ANALYSIS OF PIPING COMPONENTS

2.1. GENERAL REVIEW

2.1.1. Plain pipe

The purpose of pipe design is to ensure that it is able to withstand deadweight, pressure, thermal load and bending stress caused by external loads. The present analysis is concerned with initial yield of straight pipes when subjected to combined loads which are often simplified to internal pressure, bending moment, torque and axial force on the pipe. For the various load categories, yielding occurs at specific locations but when these loads act simultaneously, the yield behaviour becomes more complicated because the location of initial yield shifts as the load combination varies.

Stokey et al [1] and Larson et al [2] theoretically investigated yielding of thick- and thin-walled pipes subjected to internal pressure, axial force, bending and torsion; the analyses were done using the Tresca yield criteria. Franzen and Stokey's [3] work was concerned with the experimental elastic-plastic behaviour of pipes.

Comparisons are made herein with thick-walled pipe theory using the von Mises strength criterion. Some of the results will be compared to the experimental results of Reilly [4] and BS 806 [5] code. Exact solutions are available for stresses in cylindrical straight pipes by which numerical methods and standard design rules can be assessed.

It is desirable that during the loading process, the pipe should retain its circular cross-section and in the case of bending, the pipe should bend with a uniform radius of curvature. For pipes with (D/T < 40), it is known that departure from ideal bending is not of great

importance. Pipes with relatively thinner walls are more prone to the above problems and may develop local buckles. Pipes with D/T lower than 100 are commonly used in power and process plants and in offshore structures.

2.1.2. Pipe bend

Elbows are used in piping systems for layout requirements and to give additional flexibility which is achieved at the expense of higher stress levels than would be expected from simple bending theory. In the operating condition, various loads such as dead weight, anchor loads and thermal loads are transmitted to the curved region. It is important to be able to determine how the elbows behave under these loads. The geometrical aspect of the pipes, together with the loading conditions which are used in this study, are typical of those used in the chemical industry and power plants.

The study will look at some parameters which affect the pipe performance such as the effect of variation of dimensions, the influence of attached pipes and the effect of various load combinations on yielding in elbows. This work considers in-plane bending, torsional moment and internal pressure. A torsional moment at one end of the elbow is converted to an out-of-plane bending moment on the other elbow end. Hence for this load it is also necessary to study the stress behaviour along the meridional direction of the elbow. The case of torsional moment load shall sometimes be referred to as out-of-plane moment load.

Many studies on elbows have been reported. Early work on pipe bends was carried out by von Karman [6] who developed a theoretical formulation for in-plane moment on elbows using the Rayleigh-Ritz method. Later works have resulted in formulae for out-of-plane bending by Vigness [7] and combined in-plane bending with internal pressure by Barthelemy [8]. Within the geometrical limits of the elbow ($\lambda \geq 0.5$), the solutions of Karman and Vigness

still give sufficiently accurate design. The effects of internal pressure were studied by Kafka and Dunn [9] and the effects of attached pipes were investigated out by Rodabaugh, Iskander and Moore [10], Natarajan and Blomfield [11], Thomson and Spence [12], Thomas [13] and by Ohtsubo and Watanabe [14].

The energy methods developed by Von Karman [6] and Vigness [7] were extended by Rodabaugh and George [15] in an attempt to analyze the coupling effect of internal pressure on stresses when subjected to in-plane or out-of-plane moment. Using strain energy methods, they developed theoretical formulations to establish hoop and axial stresses which will be used in the present study. Prior to the above study, the effect of pressure was thought to be negligible because thick-walled pipes were being used commonly.

Findlay and Spence [16] presented a theoretical solution for in-plane bending of pipe bends with flanged ends, based on energy methods. The solution of the problem with membrane theory was given by Flugge [17] and later by Ory and Wilczek [18]. In recent years, Lang [19] provided a complete description of stress fields in bend pipes based on the method of toroidal elasticity. Lang commented that a defect in the ASME code for pipe bends is the absence of compatibility equations to determine topologically correct deformation fields. The toroidal elasticity method [19] was said to give an accurate model of ovalization which is useful in determining the discontinuity stress fields between an elbow and the tangent pipe.

For in-plane closing bending moment, the outer fibres on the extrados are displaced towards the neutral plane and the tube flattens so that the cross-section becomes oval in shape. It is well-known that the progressive ovalization of thin-walled elbows is more prominent than in thick-walled elbows. The deformation is less at the elbow ends where it is usually restricted by flanges or attached pipes. Unlike in-plane moment, torsional moment causes deformation

which is not symmetrical about the elbow mid-section; maximum ovalization occurs nearer to the end with pure out-of-plane moment. Many simple theories are based on the assumption that 'end effects' can be neglected. These theories assume that all cross-sectional planes of the elbow respond to applied loads in the same way, regardless of any end attachment. Dhalla [21], Kano et el [22] and Thomas [13] addressed the end effects of elbows and noted that the presence of constraints at the bend ends increases stiffness and reduces stresses in the elbows, similar to Spence and Thomson's [23] finding on flange-ended elbows.

Hoffmann and Roche [24] and Solal [25] noted that the behaviour of thin-walled elbows is different when they are subjected to a closing or opening in-plane bending moment. In an experimental investigation, Wassermann [26] noticed that internal pressure increased the bending hoop stress by as much as 11%. A closing moment gave a higher increase than an opening moment.

Fujimoto and Soh [27] carried out finite element and experimental stress analyses on elbows with $D_m/T \geq 100$ and $0.01 \leq \lambda \leq 0.2$, in an attempt to determine the stress indices of thin-walled elbows. These parameters are beyond the application limits of the ASME [28] code and the behaviour of such geometries are scantily reported. The problem of finite element analysis is the suitability of element formulation and meshing.

There were many attempts to address the stress indices of the ASME [28] code. The flexibility of elbows has been studied extensively and has resulted in equations which form the basis of the present ASME [28] piping system design. A number of assumptions and approximations were used to simplify these formulae such as linear elastic material, linear shell theory, initially geometrically perfect pipe and no end effects. Natarajan [29] proposed empirical formula of stress indices due to moment loadings and so did Ohtsubo and Watanabe

[14] and Thomson [30]. All the authors gave values of 'C' indices which were lower than ASME [28], very slightly for the in-plane and quite substantially for the out-of-plane moment.

The aim of this study is to provide, by the use of the finite element method, an understanding of the elastic behaviour of elbows and to assess some standard design rules and analysis methods. The first part of the analysis is aimed at confirming the elastic behaviour of a wide range of elbows by comparing the results with those from theoretical analyses and design codes. The next part deals with the first yield behaviour of elbows when two types of load act simultaneously. The load interaction diagrams allow the engineer to assess the amount of conservatism of standard design rules. The structural behaviour of a sample carbon steel elbow was also investigated experimentally. The elbow was loaded with internal pressure or/and in-plane opening moment to study the effects of single and combined loads.

2.1.3. Tee branch

In power plants and petrochemical industries, a pressure vessel with a nozzle or a pipe intersecting another pipe is a common configuration. In pressure vessels, the nozzle diameters are comparatively small but piping tee connections of equal diameters occur commonly in many industrial applications. Standard design rules and theoretical formulations for junctions with large diameter ratios are either not available or do not predict actual stresses satisfactorily.

In normal operation, a tee branch junction is mainly subjected to the pressure of the fluid which it transmits. The pressure loading generates one of the highest stresses. Other significant stresses may occur due to the pipe deadweight, thermal effects, anchor and hanger loads and seismic loads. In a tee branch junction, the external loads acting on the limbs transmit moments and forces to the intersection region. Very little is known about the

response of pipe connections to a complete set of all the moments and internal pressure. However, a fair amount of information exists on certain sets of loadings such as a combinations of moment loads on the branch pipe.

This study is intended to provide the designer with a method of predicting the maximum von Mises effective stress at the intersection of a particular branch junction when subjected to a combination of internal pressure and external moment loads. The butt welding forms a weld fillet at the outer intersection between the branch and run pipes. The branch junction was assumed to be fully fixed at one end of the run pipe. External loads of in-plane, out-of-plane and torsional moment were applied at the free ends of the pipe limbs. Fig. 1 shows the 'cantilever' method of supporting the structure and the moment loads.

The present study is to present a finite element model to study the stresses near the intersection of the branch junction for a d/D ratio of 0.8 and a D/T ratio of 20. The model utilised a single layer of 3-D isoparametric elements throughout the structure. The loads were assumed to produce small deformations of the structure shell, hence the solution of geometrically linear analysis was assumed. The terms 'tee', 'tee branch', 'branch junction', 'tee junction' and 'tee connection' shall be used synonymously. The terms 'vessel' and 'nozzle' are also used in a similar context to 'run pipe' and 'branch pipe' respectively.

From the start, the stress analysis of tee branches was recognised to be complicated because of its non-axisymmetric nature and the number of variables involved. Any solution would require both theoretical and experimental efforts. Designers have used the American Pressure Vessel and Piping codes since the 1940s. Up to the 1970s, a large amount of information has been gathered which indicated that the design codes were conservative. Up to the mid 1970s most of the work on pipe intersections was experimental. From then on analytical treatment

has been given more serious attention.

Before the 1980s, not much effort has been expended to look into branch junctions with d/D > 0.5. The available results for such diameter ratios were limited to specific geometries of D/T and t/T. Hence even to this moment, there is a gap between theoretical and experimental results for various D/T and t/T ratios for branches with d/D > 0.5.
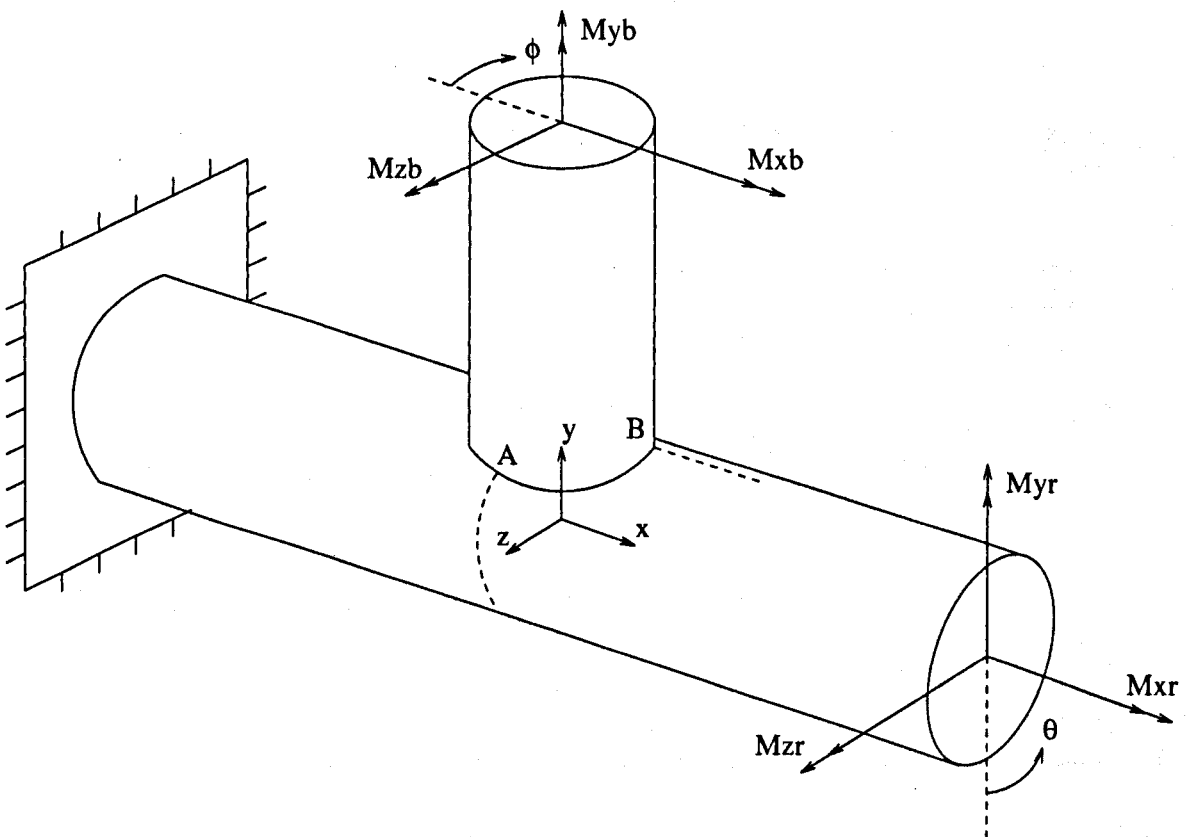

FIG. 1.   CANTILEVER MODEL OF TEE BRANCH JUNCTION, SHOWING MOMENT LOAD VECTORS ACTING ON LIMBS.

Theoretical formulations, such as that developed by Bijlaard and Steele, have found their way into Welding Research Council [31][32] formulations and US design codes. The application of earlier formulations was limited by the assumptions made in their derivation. In the 1960s, the development of the finite element method increased the capability of solving complicated engineering problems. Nowadays this approach has been facilitated by advances made in computational methods to solve complex problems efficiently and economically. The finite element method is now considered to be the most useful method of analysis. The experimental method of analysis has been employed using electrical strain gauges or the photoelastic method. Very accurate results have been obtained on carefully prepared test specimens. The following literature review represents a brief summary of studies which have contributed to the development of the present state of understanding. More detailed surveys on the work of other investigators can be found in Refs. [33] and [34].

The experimental determination of elastic stresses in shell intersections has been the subject of numerous studies. In 1969, Gwaltney et al [35] combined finite element analysis and experimental tests to determine stresses on the inner and outer surfaces of machined tee branches (with $D/T = 50$ and 100 and d/D of up to 1.0) undergoing six moment categories and internal pressure. In 1972, Corum et al [36] carried out theoretical and experimental analyses on thin piping tees of up to $d_o/D_o = 1.0$, for forces, moments and pressure loads.

Corum et al [36] reported the pioneering analytical solution of Reidelbach in 1961. In 1965 under the sponsorship of ASME's Pressure Vessel Research Committee, Wichman et al [31] produced a document providing guidance for the evaluation of localized stresses in pressurised shells due to external loads. The analytical work was based on theoretical results derived by Bijlaard [37] using the 'flexible loading surface' approach, thus limiting the usefulness of the results to $d_m/D_m \leq 0.25$. In Bijlaard's model, the branch pipe thickness does not influence

stresses in the run pipe because he assumed that the branch pipe moments acted directly on the run pipe shell through a pad loading. In 1967 Bijlaard et al [38] formulated a solution to include the case where the vessel and nozzle were of equal diameter.

In 1969, using Donnell's equations for both pipes, Eringen et al [39] improved on Reidelbach's solution and provided numerical results for tee branches when subjected to internal pressure, but the diameter ratio was limited to less than 1/3. In 1972 Lekkerkerker [40] treated the problem of thin-walled and small diameter branch pipe intersections using Flugge's equations.

In 1980, McBride and Jacobs [41] proposed a simplified method for calculating membrane and bending stresses in branches with large diameter ratios. The method provided an estimate of average primary membrane and primary bending stresses, on which the proposed allowables in ASME are based.

In 1985, an experimental study at Liverpool by Moffat [34] on branches of equal diameter ratio and with D/T ratios ranging from 11.4 to 41.4, resulted in parametric equations for maximum stresses. Combining test results from other studies, Moffat presented a set of plots showing the effect of R_m/T ratio on Tresca effective stresses, for external moment loads.

Load interaction in tee branches was the subject of another experimental investigation by Moffat and Mistry [42] in 1988. In 1991, in an attempt to investigate the influence of d/D, D/T and t/T ratios on the stress levels due to seven load categories, Moffat et al [43] presented effective stress factor (ESF) values for a wide range of branch junctions using the finite element method together with the experimental test results in Ref. [34]. Moore and Rodabaugh [44] realised the complexity of the problems of interacting loads. They mentioned

the theories of Schroeder and Ellyin and Turkkan [45] which required computer programs for evaluation.

The ASME and BS codes on tee branches are the result of many studies. Boyle [46] quoted the works of Money, Leckie and Penny, Decock and Markl that had contributed to the present BS formulations. The pressure loading stress indices in ASME were developed by Rodabaugh and Moore [47] from the correlation of experimental and finite element analysis data.

A theoretical and experimental investigation into pressure and branch pipe bending moment interactions was carried out by Schroeder et al [48] in which theoretical curves for limit interaction were presented and compared with test data. In Schroeder's test, the branch intersection was at a distance of 2.5 D_m away from the ends and the tests were done with the run pipe limbs fully fixed.

Most theoretical methods described in the literature were based on the shallow shell theory which was applied to junctions without fillets at the intersection. In the shallow shell theory, the problem was simplified by having the branch pipe diameter comparatively small to that of the run pipe. The curve of the intersection is then nearly a circle in the developed shell surface as long as the diameter ratios are less than 1/4. Many analytical equations were based on this shallow shell assumption, among others, the solutions which were presented by Leckie and Penny [49], Donnell [50] and Flugge [17]. The solutions by Donnell and Flugge formed the basis of many later works which extended the limitations to include wider ranges of thickness and diameter ratio. An example is Bijlaard et al's [38] work which presented results for thick tee branches with equal diameters using Flugge's equations for both shells. The shallow shell theory gives doubtful results in connections with large diameter ratios because the assumptions of axisymmetric nozzle and circular vessel cutout no longer holds. Analytical

14

solutions for diameter ratios with less than 1/3 have been obtained satisfactorily but ratios greater than 0.5 are still being studied.

Ref. [31] was updated in 1984 by Mershon et al [32] who provided further improvements in the methods for determining local stresses in branch junctions of up to $d_m/D_m \leq 0.5$. Mershon indicated that Bijlaard's solutions could be inaccurate for axial thrust and out-of-plane nozzle load when d/D ratios are large. Mershon's design proposals were based on Steele and Steele's [51] theory using Flugge-Conrad and Sanders-Simmonds' shell theory solutions. Later Steele [52] extended the analysis to include large diameter ratios and flexible nozzles.

In 1991, Mokhtarian and Endicott [53] presented formulations for maximum bending and membrane stresses in the vessel and nozzle, due to pressure, from a parametric study performed with a computer program developed by Steele and Steele [51]. Within the limits of the program, the results were reported to be accurate up to d/D = 0.5.

More recently, the problem of externally applied loads on tee branches has been investigated using finite element procedures to verify and supplement experimental and theoretical results. Without proper criteria to assess the quality of finite element solutions, errors in element selection and setting up the model, can lead to undetected errors. Most earlier analyses using shell or flat plate elements gave reasonably good agreement with experimental data in areas away from the pipe junction, but the comparison was poor at the junction. In 1969, Prince and Rashid [54] demonstrated the use of triangular plate elements in tee branches subjected to internal pressure.

During the 1970s, a number of studies called for improved element formulations and for finer meshing at the pipe junction. In 1972, Corum et al [36] used flat plate shell elements to

model thin intersecting cylinders subjected to all load categories. They found that the finite element predictions agreed well for cases involving loadings on the nozzle, except for nozzle torsional moment. Subsequent analyses employing 3-D elements gave better results in the vicinity of the junction. The use of such higher order 3-D elements was not common due to lack of the element in some packages. In 1973, Bakhrebah [55] modelled the structure by using 3-D elements in the critical intersection region and 2-D curved shell elements in regions away from the intersection. In 1978, a study by Gantayat and Powell [56] on the characteristics of different elements showed that the use of unmodified 8-node elements on thick- and thin-walled tubular tee gave poor performance.

The use of the finite element method to study tee branches of equal diameter was carried out by in 1985 by Lock et al [57]. They studied in-plane moment loadings and internal pressure using 20-node brick elements. The program was extended to include out-of-plane and twisting moments by Kirkwood et al [58]. Rodabaugh and Moore [59] compared several FEM results with those from experimental test and cautioned about the accuracy of both methods. They noted that the stress gradients on nozzle corners were quite steep and needed accurate placement of suitable gauges, and the finite element mesh would have to be extremely fine to provide accurate results. In 1991, Zhixiang et al [60] carried out experimental and finite element analyses on equal diameter tee branches and presented the relation between D/T and the stress concentration.

2.1.4. Torispherical head with nozzle

The most common method of sealing the ends of cylindrical pressure vessels is by means of using torispherical or ellipsoidal heads. When pressure vessels need to be connected to a piping system, the attachment of nozzles to the crown sometimes becomes inevitable. There have been numerous detailed analyses of torispherical shells with radial nozzles, undergoing

various loadings. In this configuration the nozzle has been singled out as a potential source of weakness in the sense that high stresses occur at the crown-nozzle intersection.

Many studies have been initiated by the failure of thin-walled pressure vessel heads under hydrostatic pressure. The design of pressure vessels requires a careful study of many important factors. In principle, the most difficult is the design of the knuckle region. Torispherical heads with various knuckle radii (for each head height) have been investigated by other researchers to establish the geometrical proportions of the torispherical heads which had the lowest maximum stresses, i.e. an 'optimum' torispherical head. For torispherical heads of constant head height to cylinder radius ratio, Batchelor and Taylor [61] found a peak in limit pressure when plotted against knuckle radius, indicating 'optimum' values of the geometrical parameter H/R in the range of 0.33 to 0.5. For a given head height to cylinder radius ratio, H/R, there is an infinite number of torispherical heads having different dome and knuckle radii. Torispherical head design may achieve the optimum head height but cannot produce biaxial tension in the knuckle; the knuckle must carry circumferential compression.

If the knuckle wall is thick enough compared to the knuckle radius, buckling is avoided. However, for thin heads, buckling in the knuckle region is now recognised as a classical failure mode. A thin-walled sharply curved knuckle region is much weaker than the spherical portion of the dome or the cylindrical vessel. On the other hand, if the knuckle is less sharply curved and the wall is relatively thick compared to the knuckle radius, the knuckle region is strong and acts as a stiffening ring between the cylindrical vessel and the spherical cap.

The design of nozzles in pressure vessels subjected to internal pressure is sometimes provided for in the Codes by the 'area replacement' method. The radial nozzles which are welded to the vessels are designed by considering pressure loading but not the external loadings imposed

by the piping system onto the nozzle. The external loads on the nozzles are not generally included because the configuration of the attached piping system is not established yet. However, stresses due to the external loads on the nozzle can be more critical than those due to internal pressure. The piping system which is connected to the nozzle is often redesigned several times at later stages to reduce the reactions at the nozzle, so that the resulting stresses at the nozzle are within acceptable limits. It is therefore useful to know the behaviour of the vessel under the nozzle loads, if they can be predetermined. This procedure can then be incorporated into the nozzle design. The design of nozzles in shells also depends on the nature of the loading. If a constant pressure were applied, the limit factor would be the logical basis of design. For cyclic pressure, shakedown or fatigue is the relevant design criterion.

The present structure consists of a torispherical shell of revolution attached to a radial nozzle at the crown and to a cylindrical vessel at the torus end. The nozzle is flush with the inside surface of the vessel. Apart from internal pressure, the external loadings considered were axial force, F, bending moment, M, and torsional moment, T_o, acting at the free end of the nozzle. In practice, it is common for the above loads to act simultaneously.

The stress behaviour in the vicinity of the vessel-nozzle intersection can be treated as a problem of a radial nozzle in a spherical segment. The stress is assumed not to be influenced by the knuckle geometry. Comparison of results with other authors is somewhat difficult because there are more than one basis of comparison. There are at least three interacting geometric parameters which influence the stress field at the junctures, and the maximum stress could occur at any of these junctures, namely, sphere-nozzle or cylinder-knuckle or knuckle-sphere. However, for the present study the maximum ESFs used to determine the first yield load interaction are taken from stresses at the juncture between the vessel and the nozzle.

Cylinders with torispherical ends have been the subject of numerous investigations over the last 70 years and satisfactory experimental and numerical correlations have been achieved. However the subject of nozzles in pressure vessels received considerable attention only in the late 1950s. The first theoretical work on sphere-cylinder intersections was done by Galletly [62] who utilized the theory of two intersecting thin shells. In 1959, Galletly [63] cautioned that torispherical shells designed according to the ASME code could lead to failure during testing, and the use of shell theory would result in poor results when applied to the toroidal region of the shell. This was because of the approximation of membrane forces and deformations in the differential equations. Most studies were concerned with determining limit pressures, such as studies by Onat and Prager [64] in 1954, Drucker and Shield [65] in 1959, Rose and Thompson [66] in 1961, Lind [67] in 1964, Leckie and Penny [49] in 1963, Gill [68] in 1964 and Rodabaugh and Cloud [69] in 1968. Elastic and shakedown analyses of spherical vessel with radial nozzle structures were presented by Penny and Leckie [49] and Leckie [70]. A good summary of past work on pressure vessels is briefly given by Bushnell [71].

Various investigators have used shell computer programs to determine the collapse behaviour of pressure vessels but theories which are based on thin shells neglect the influence of local geometry of the intersection. The early programs used small deflection shell theory but have been superseded by programs which uses large deflection theories, such as the BOSOR5 [74].

2.2. STRESS ANALYSIS OF PLAIN PIPES

2.2.1. Theoretical load interaction

The analysis was carried out using the thick-walled theory where the calculation for properties of cross-sectional area was not simplified and Lame's equations were used to calculate pressure hoop and axial stresses. In thick pipes, the pressure and shear stresses (from torsion) are not uniform across the wall thickness. In Stokey et al's [1] thick pipe analysis, these stresses were assumed to be uniform, although Stokey emphasized that the assumptions were not exact. The theory of solid mechanics was used to calculate the principal stresses σ_1, σ_2 and σ_3 which were then substituted into the von Mises strength criterion. Depending on the dominance of a load, the maximum von Mises effective stress may occur on either the inner or outer surface. The interaction relationships were evaluated for all possible load pairs.

2.2.1.1. Torque:Internal pressure

When pressure is dominant, first yield occurs on the inner surface of the pipe. Since there is no contribution to the hoop stress from torque, the total hoop stress is comprised of the pressure stress. From Lame's equations, the pressure hoop stress on the inner surface is:-

$$\sigma_h = P(R_o^2 + R_i^2)/(R_o^2 - R_i^2)$$

and the total axial stress is:-

$$\sigma_a = PR_i^2/(R_o^2 - R_i^2)$$

The total radial stress on the inner surface is:-

$$\sigma_r = -P$$

The associated shear stress is contributed by the torque load, i.e.

$$\tau = 2T_oR_i/\pi(R_o^4 - R_i^4)$$

The principal stresses, σ_1 and σ_2, are calculated from basic solid mechanics, i.e.

$$\sigma_{1,2} = \tfrac{1}{2}(\sigma_h + \sigma_a) \pm \tfrac{1}{2}\sqrt{((\sigma_h - \sigma_a)^2 + 4\tau^2)}$$

20

While $\sigma_3 = \sigma_r = -P$

Yielding is assumed to occur when the maximum von Mises effective stress reaches the yield stress, i.e.

$$\sigma_1^2 + \sigma_2^2 + \sigma_3^2 - \sigma_1\sigma_2 - \sigma_2\sigma_3 - \sigma_3\sigma_1 = Y^2 \tag{1}$$

After calculating the principal stresses, substituting into Eqn. (1), gives:-

$$\frac{3P^2R_o^4}{(R_o^2-R_i^2)^2} + \frac{12T_o^2R_i^2}{\pi^2(R_o^4-R_i^4)^2} = Y^2 \tag{2}$$

From basic solid mechanics, the thick pipe theory gives first yield pressure and torque loads:-

$$P_Y = \frac{R_o^2-R_i^2}{\sqrt{3}\,R_o^2}Y \tag{3}$$

$$T_{oY} = \frac{\pi(R_o^4-R_i^4)}{\sqrt{12}\,R_o}Y \tag{4}$$

Eqn. (2) can be made non-dimensionalised by combining with Eqns. (3) and (4), giving:-

$$(R_i/R_o)^2\,\overline{T}_o^2 + \overline{P}^2 = 1 \tag{5}$$

When torque is dominant, first yield occurs on the outer surface, with σ_1 positive, $\sigma_2 = \sigma_r = 0$ and σ_3 negative. Substituting the principal stresses into Eqn. (1) gives:-

$$\frac{3P^2R_i^4}{(R_o^2-R_i^2)^2} + \frac{12T_o^2R_o^2}{\pi^2(R_o^4-R_i^4)^2} = Y^2 \tag{6}$$

Combining Eqns. (3), (4) and (6) gives:-

$$\overline{T}_o^2 + (R_i/R_o)^4\,\overline{P}^2 = 1 \tag{7}$$

2.2.1.2. Moment:Internal pressure

When pressure is dominant, yielding starts on the inner surface. The principal stresses σ_1 ($=\sigma_h$) and σ_3 ($=\sigma_r$) remain unchanged from above while the total axial stress is:-

$$\sigma_2 = \sigma_a = 4MR_i/\pi(R_o^4 - R_i^4) + PR_i^2/(R_o^2 - R_i^2)$$

The first yield moment load in a thick cylinder is given by:-

$$M_Y = \pi(R_o^4 - R_i^4)Y/4R_o \tag{8}$$

Substituting the principal stresses into Eqn. (1) and then non-dimensionalised by combining with Eqns. (3) and (8), the load interaction is:-

$$(R_i/R_o)^2\overline{M}^2 + \overline{P}^2 = 1 \tag{9}$$

When moment is dominant, yield occurs on the outer surface, and the principal stresses are:-

$$\sigma_1 = \sigma_a = 4MR_o/\pi(R_o^4 - R_i^4) + PR_i^2/(R_o^2 - R_i^2)$$

$$\sigma_2 = \sigma_h = 2PR_i^2/(R_o^2 - R_i^2)$$

and $\quad \sigma_3 = \sigma_r = 0$

Substitution of principal stresses into Eqn. (1) and combining with Eqns. (3) and (8), the load interaction is:-

$$\overline{M}^2 + (R_i/R_o)^4\,\overline{P}^2 = 1 \tag{10}$$

2.2.1.3. Axial force:Internal pressure

When pressure is dominant, yield occurs on the inner surface. The principal stresses are:-

$$\sigma_1 = \sigma_h = P(R_o^2 + R_i^2)/(R_o^2 - R_i^2)$$

$$\sigma_2 = \sigma_a = F/\pi(R_o^2 - R_i^2) + PR_i^2/(R_o^2 - R_i^2)$$

and $\quad \sigma_3 = \sigma_r = -P$

The first yield axial force is:-

$$F_Y = \pi(R_o^2 - R_i^2)Y \tag{11}$$

Using similar procedure as before, the interaction is circular, i.e.

$$\overline{F}^2 + \overline{P}^2 = 1 \tag{12}$$

When the axial force is dominant, the magnitudes of σ_1 and σ_2 are reversed and a similar circular relation is obtained.

2.2.1.4. Moment:Torque

Irrespective of dominance of moment or torque, the formulation for principal stresses remain the same, and first yield occurs on the outer surface. The total axial and shear stresses are:-

$$\sigma_a = 4MR_o/\pi(R_o^4 - R_i^4)$$

and $\quad \tau = 2T_oR_o/\pi(R_o^4 - R_i^4)$

The total hoop stress is zero.

It is obvious that the principal stresses σ_1 is positive, σ_3 is negative and :-

and $\quad \sigma_2 = \sigma_r = 0$

Substituting the principal stresses into Eqn. (1) and combining with Eqns. (4) and (8), a circular relation is obtained, i.e.

$$\bar{M}^2 + \bar{T_o}^2 = 1 \tag{13}$$

2.2.1.5. Torque:Axial force

At all load combinations, yielding occurs on the outer surface and the formulations for σ_1 and σ_3 remain unchanged, while $\sigma_2=0$. Substituting the principal stresses into Eqn. (1) gives:-

$$\frac{F^2}{\pi^2(R_o^2-R_i^2)^2} + \frac{12T_o^2R_o^2}{\pi^2(R_o^4-R_i^4)^2} = Y^2 \tag{14}$$

to give a circular relation:-

$$\bar{F}^2 + \bar{T_o}^2 = 1 \tag{15}$$

2.2.1.6. Moment:Axial force

At all load combinations, yielding occurs on the outer surface from a uniaxial stress system.

The principal stress, $\quad \sigma_1 = \sigma_a = 4MR_o/\pi(R_o^4 - R_i^4) + F/\pi(R_o^2 - R_i^2)$

and $\quad \sigma_2 = \sigma_3 = 0$

The von Mises yield criterion is reduced to $\sigma_1 = Y$, or:-

$$\bar{M} + \bar{F} = 1 \quad \text{i.e. a linear relation.} \tag{16}$$

2.2.2. The BS code

BS 806 [5] allows the calculation of combined stresses in a straight pipe when pressure, bending moment and torque act. The symbols are defined in BS 806, with the exception of T_o which is substituted for T.

2.2.2.1. <u>Torque:Internal pressure</u>

The total hoop, axial and shear stresses from pressure and torque loads are, respectively:-

$$f_T = pd/2t + 0.5p$$

$$f_L = pd^2/4t(d + t)$$

and $f_s = T_o(d + 2t)/4I$

Irrespective of whether pressure or torque is dominant, the hoop stress is always larger than the axial stress, i.e.

$$f_T > f_L$$

hence the combined effective stress, f_c, as defined in BS 806 (based on Tresca) is then:-

$$f_c = \sqrt{\left[\left[\left(\frac{pd}{2t}+0.5p\right)^2 + 4\left(\frac{T_o(d+2t)}{4I}\right)^2\right]\right]} \tag{17}$$

Assuming that the design is based on the limitation of the effective stress by the yield stress,

$$f_c = Y \tag{18}$$

The first yield pressure is determined by setting $\overline{T_o}=0$ in Eqn. (17), giving:-

$$pd/2t + 0.5p = Y$$

or $P_Y = 2tY/(d + t)$ (19)

and the first yield torque is determined by setting P=0 in Eqn. (17), giving:-

$$T_{oY} = 2IY/(d + 2t) \tag{20}$$

Eqns.(17) and (18) can be made non-dimensionalised by combining with Eqns. (19) and (20) to give a circular relation, $\overline{T_o}^2 + \overline{P}^2 = 1$ (21)

2.2.2.2. Moment:Internal pressure

When moment is dominant, the axial stress is larger than the hoop stress, i.e. $f_L > f_T$. The total axial stress consists of pressure and moment stresses, i.e.

$$f_L = pd^2/4t(d + t) + (d + 2t)M/2I$$

and the torsional stress, f_s, is zero.

The effective combined stress, f_c, becomes:-

$$f_c = \sqrt{\left[\frac{pd^2}{4t(d+t)} + \frac{d+2t}{2I}M\right]^2 + 0} \qquad (22)$$

The first yield moment load is determined by equating $f_c = Y$ and setting $P=0$, i.e.

$$M_Y = 2IY/(d + 2t) \qquad (23)$$

Limiting the effective stress, f_c, from Eqn. (22) to Y and combining with Eqns. (19) and (23), the interaction is a linear plot which does not pass through $\bar{P}=1$, i.e.

$$d^2/2(d+t)^2 \, \bar{P} + \bar{M} = 1 \qquad (24)$$

When pressure is dominant, the hoop stress is larger than the axial stress. The total hoop stress is then:-

$$f_L = pd/2t + 0.5p$$

and $\quad f_s = 0$

The combined effective stress, f_c, becomes:-

$$f_c = \sqrt{\left[\frac{pd}{2t} + 0.5p\right]^2} \qquad (25)$$

Limiting the effective stress, f_c, to the yield stress Y and combining with Eqn. (19), results in a linear interaction which is independent of $\bar{M}$, i.e.

$$\bar{P} = 1 \qquad (26)$$

25

2.2.2.3. Moment:Torque

Irrespective of the magnitude of torque, the axial stress is always larger than the hoop stress.

The total axial and shear stresses are given by:-

$$f_L = (d + 2t)M/2I + 0$$

and $\quad f_s = T_o(d + 2t)/4I$

The combined effective stress, f_c, is then:-

$$f_C = \sqrt{\left[\frac{d+2t}{2I}M\right]^2 + 4\left[\frac{T_o(d+2t)}{4I}\right]^2} \tag{27}$$

Equating f_c to the yield stress Y and combining with Eqns. (20) and (23), results in a circular relation for all values of $\overline{M}$ and $\overline{T}_o$, i.e.

$$\overline{M}^2 + \overline{T}_o^2 = 1 \tag{28}$$

2.3. STRESS ANALYSIS OF PIPE BENDS

2.3.1. Experimental investigation

Experimental tests on elbows are usually concerned with establishing the limit load. The present test gave an opportunity to assess the stress levels from the yield curves generated from the finite element method. This involved measuring the strains at a few points at the elbow mid-section and obtaining the angular rotation between the ends of the elbow. The elbow was first loaded, step-wise, by a single load of in-plane moment or internal pressure and then by a series of combined loads. The rotation between the elbow ends provided an approximate means of determining the elastic limit of the elbow. The test provided a limited amount of information about the location and extent of elasticity which would confirm the adequacy of the FE method of prediction of yielding. The experimental test is briefly described.

2.3.1.1. Test elbow dimensions

The elbow was manufactured according to the requirements of ASTM WPB Schedule 40 of long radius welding elbow specifications. The pipe thickness, which was determined using the ultrasonic method, revealed non-uniform thickness in the hoop direction of the elbow mid-section. Thickness measurements taken at hoop intervals of 45° showed wall thickening at the intrados and thinning at the extrados, as shown in Table 1. At the crowns ($\theta = \pm 90°$), the shell was of different thicknesses, i.e. 6.19 mm and 5.60 mm. The wall thickness at the intrados could not be measured accurately due to large shell curvature and unsuitably large measuring probe. The final thickness of the pipe was taken to be the mean value of all the measurements in Table 1.

Table 1. <u>Wall thickness variation at elbow mid-section.</u>

$\theta(°)$	0	45	90	135	180	225	270	315
Thickness (mm)	5.74	5.65	5.60	6.23	-	6.35	6.19	5.92

The nominal dimensions of the elbow were:-

Outer radius of pipe, R_o	= 44.73 mm
Wall thickness of pipe, T	= 5.95 mm
Deduced inner radius of pipe, R_i	= 38.78 mm
Bend radius of elbow, R	= 115.0 mm
Pipe factor, λ	= 0.39
Bend radius ratio, b	= 2.75

2.3.1.2. <u>Tensile test</u>

A tensile test specimen was cut out from the crown region of an elbow identical to the test elbow. The curved (from the pipe curvature) grip ends were flattened and the gauge section was ground. The specimen was heat treated at 650°C for 1 hour and then left to cool in the furnace. The faces were then lightly ground to the final dimensions. The tensile specimen had a gauge section 10.90 mm wide, 4.04 mm thick and 45.0 mm in length and was strain gauged with longitudinal and transverse gauges mounted on opposite sides of the gauge section.

The test specimen was located in an Instron universal testing machine and the gauges were connected to a strain indicator. Testing was commenced by setting the machine platen speed at 2 mm/min. The plot of load and average strain (from two opposite surfaces) are shown in Fig. 2. The elastic modulus of the elbow material was calculated from this set of data. Fig. 3 shows the complete stress-strain behaviour of the tensile test, from which the yield stress and other properties of the material were derived.
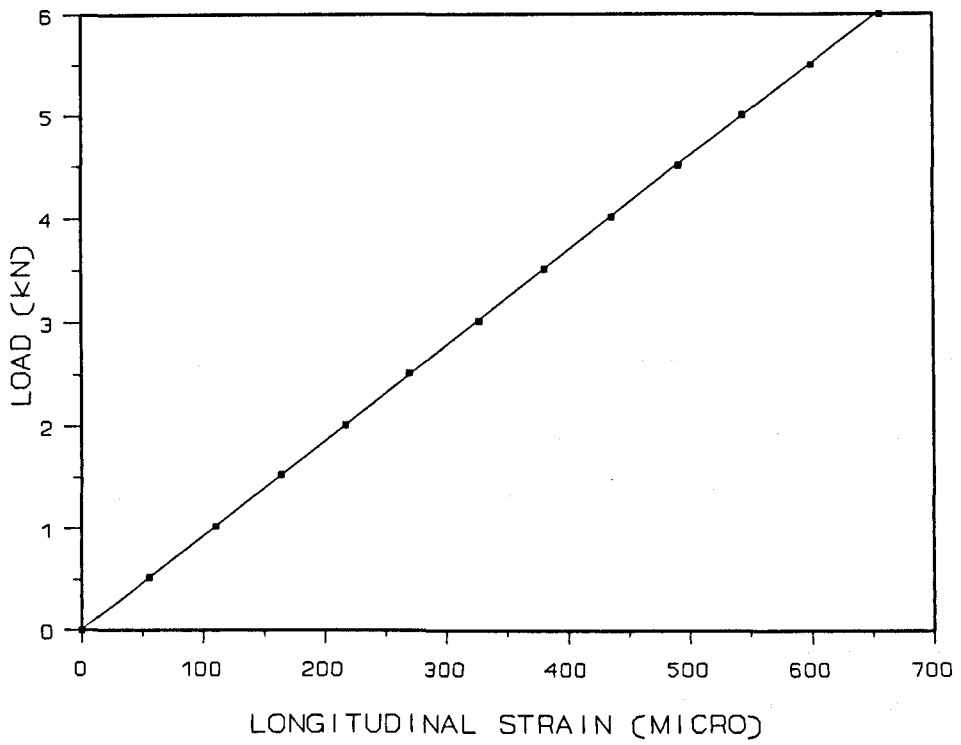
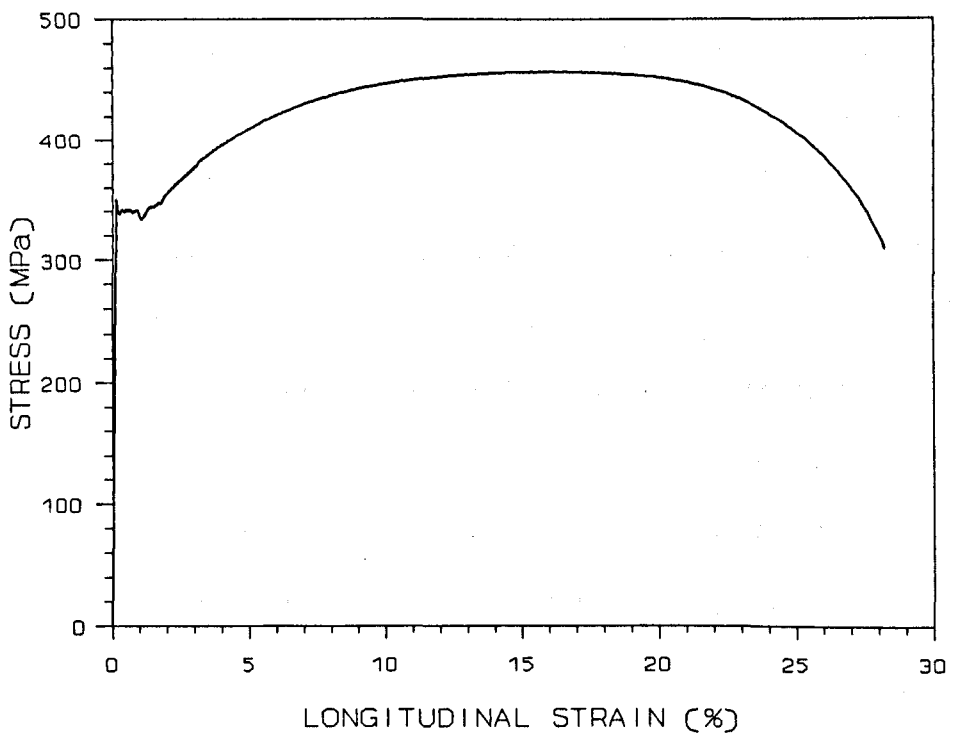FIG. 2. ELASTIC LOAD-STRAIN BEHAVIOUR FROM TENSILE TEST.

FIG. 3. COMPLETE STRESS-STRAIN CURVE FROM TENSILE TEST.

The following material properties were calculated from the tensile test:-

Yield stress, σ_Y	= 337.6 MPa
Elastic modulus, E	= 207.7 GPa
Tensile strength, σ_{UTS}	= 457.5 MPa
Poisson's ratio	= 0.275
Elongation at break point	= 28.2%

2.3.1.3. The experimental setup

Due to testing similarities, it was decided to utilise an existing rig. The in-plane bending moment was applied from a four-point loading acting on the tangents pipes. Pipe collars were used to transmit the loads (from actions and reactions of the rams and tensile links) to the test specimen. Rectangular strain rosettes were bonded on the outer surface of the elbow crowns and intrados. The 6 mm gauges in the rosettes were aligned along the hoop and longitudinal directions of the elbow. Elbow end rotations were measured indirectly by using a system of dial indicators mounted onto measuring arms. The measuring arms were situated 152 mm away from the end of the elbow to eliminate the recording of local deformations. The schematic diagram of the setup is shown in Fig. 4.

2.3.1.4. The loading system

The four point loading system consisted of a pair of hydraulic rams and a pair of tensile links which were strain gauged to act as load cells. This loading system provided pure in-plane opening bending moment on the curved pipe section. In the present experimental and FEM work, a closing moment is taken to be positive and an opening moment to be negative. Knowing that the distance between the ram and the tensile link was 0.5m, the moment applied to the elbow could be calculated from the load cell reading.
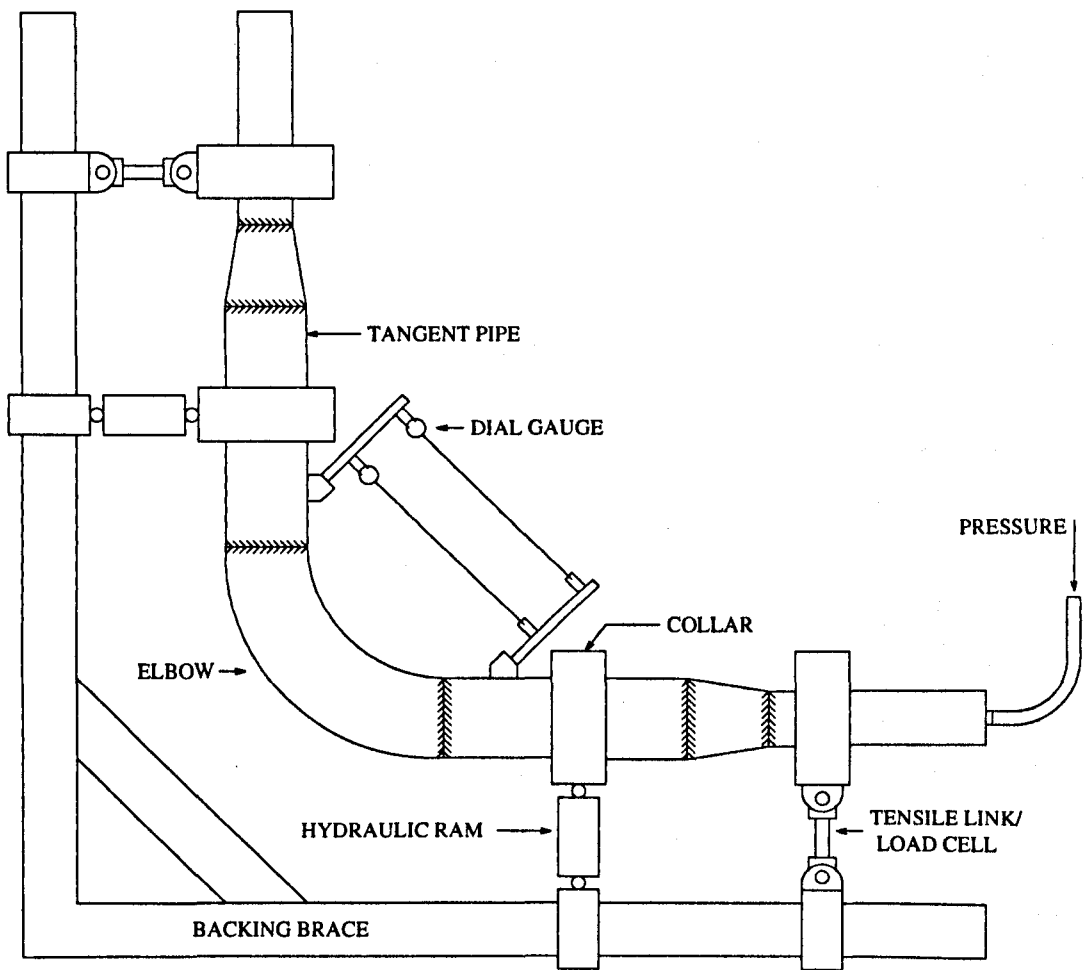
FIG. 4. SCHEMATIC DIAGRAM OF EXPERIMENTAL SETUP. (NOT TO SCALE).

31

The internal pressure was applied via a hand pump through an opening at the end of one of the tangent pipes. A pressure transducer connected to the pump gave indication of the pressure level. The critical components of the experimental rig such as the backing brace, tensile links, pins as well as the elbow tangent pipe were checked to ensure that at maximum load, the stresses in the components were acceptable.

2.3.1.5. The testing procedure

A series of 5 tests were conducted, with the last test carried out beyond the elastic limit of the elbow. Each test was conducted by applying the loads step-wise. At each load increment, the dial indicator readings were noted and the strains were recorded with an automatic strain gauge scanning and indicating system.

From the dimensions and material properties of the elbow, a geometric nonlinear FE analysis was run in which the yield loads P_Y and M_Y were determined, i.e.

$$P_Y = 30.4 \text{ MPa} \qquad \text{and} \qquad M_Y = -3.18 \text{ kN-m (i.e. opening moment)}$$

The elbow was loaded with an opening moment (Test No. 1) until the moment reached about 70% of M_Y. After unloading, the elbow was pressurised (Test No. 2) until the pressure reached about 70% of P_Y. To account for any extraneous out-of-plane bending of the elbow, the mean strain from the two crown locations was taken. Assuming that the material was linear elastic up to the final load, the stresses could be calculated from the normal constitutive relations.

When subjected to a combined load, it was assumed that the elbow would not yield below the most conservative linear relation. To study the elastic stress behaviour of the combined loads, the elbow was loaded to about 70% of this linear yield locus. In Test No. 3, the elbow was

pressurised to 15 MPa followed by an additional moment of -0.75 kN-m. In Test No. 4, the elbow was loaded with a pressure and moment load combination of about $\overline{P}:\overline{M}=2:1$ until the maximum deduced effective stress achieved about 50% of the yield stress which corresponded to a final load of P=10 MPa and M=-0.5 kN-m.

In Test No. 5, the elbow was subjected to an incremental combined load of about $\overline{P}:\overline{M}=1:2$ until the maximum limitation of the loading ram travel. During the test, when the elbow started to yield, the elbow rotated by a large amount, causing the rams and tensile links not to be perpendicular to the tangent pipes. The perpendicular offset was measured before the specimen was unloaded. The next loading was compensated by the amount of offset. This ensured a satisfactory moment calculation when the elbow was subjected to the final load combination.

2.3.2. Energy method

Ref (34.)

Rodabaugh and George [15] employed the thin shell theory, wherein the pipe thickness is small compared to the bend radius and the ratio R/r is large compared to unity. The basis of Rodabaugh and George [15] series-type equations are similar to von Karman's [6] formulation. Rodabaugh's method is to express the integral term of the strain energy formulation in Fourier series by the use of trigonometric equivalents. For greater accuracy, higher order terms need to be included. The rate of convergence of the series expression for the various stresses is not uniform and depends on pressure and the factor $\lambda = TR/r^2 \sqrt{(1-\nu^2)}$. If the first order approximation on in-plane and out-of-plane moments is used, Rodabaugh's equations are reduced to von Karman and Vigness's [7] equations. The formulations are briefly described here.

The basic von Karman's and Vigness's equations for in-plane and out-of-plane moments express the elastic energy stored in a unit centreline of the curved pipe due to tangential and radial displacements. For in-plane moment, the energy, in Ref. [15] nomenclature, is:-

$$U_1 = \frac{rtE}{2R^2} \left[\int_0^{2\pi} \left(\frac{r\Delta\alpha}{\alpha}\sin\phi + w_t\cos\phi + w_r\sin\phi \right)^2 d\phi + \frac{t^2R^2}{12r^4(1-\nu^2)} \int_0^{2\pi} \left(\frac{d^3w_t}{d\phi^3} + \frac{dw_t}{d\phi} \right)^2 d\phi \right]$$

(29)

The tangential displacement is assumed to be of the form:-

$$w_t = \sum_{n=1}^{\infty} a_n \sin(2n\phi)$$

(30)

Assuming inextensibility in the hoop direction, the radial displacement is given by:-

$$w_r = -dw_t/d\phi$$

(31)

The assumption of inextensibility can be removed by using the 'Gross correction' [73]. The trigonometric series expression for w_t can be substituted into the energy equation and the integral performed, to give:-

$$U_1 = \frac{\pi rtE}{2R^2} [r^2(\frac{\Delta\alpha}{\alpha})^2 + 3r\frac{\Delta\alpha}{\alpha}a_1 + \frac{9}{4}a_1^2 + \frac{1}{4}\sum_{n=1}^{\infty} a_n^2(1-2n)^2$$

$$-2a_n a_{n+1}(2n-1)(2n+3) + a_{n+1}^2(2n+3)^2 + \frac{\lambda^2}{12}\sum_{n=1}^{\infty} a_n^2(8n^3-2n)^2]$$

(32)

Rodabaugh's analysis was to study the effect of internal pressure on the flexibility and stress factors of curved pipes. When internal pressure is considered, an additional work is done by the pressure acting against the change in volume. The energy per unit centre length is:-

$$U_2 = P\Delta A$$

(33)

The coefficients a_n are determined by differentiating U ($=U_1-U_2$) with respect to each a_n, and by the principle of least work, each resulting equation is set to zero. This gives a set of n linear equations with (n+1) unknown a's. By assuming $a_{n+1}=0$, all the constants, a's, may

34

be calculated.

The axial and hoop strains on which Eqn. (29) is based are:-

$$e_a = \frac{1}{R}(\frac{\Delta\alpha}{\alpha}r\sin\phi + w_t\cos\phi + w_r\sin\phi) \qquad (34)$$

and

$$e_h = \pm\frac{t}{2(1-\nu^2)r^2}(\frac{d^3w_t}{d\phi^3} + \frac{dw_t}{d\phi}) \qquad (35)$$

The strains may be converted to stresses by the following equations:-

$$\sigma_a = \frac{E}{1-\nu^2}(e_a + \nu e_h) \qquad (36)$$

$$\sigma_h = \frac{E}{1-\nu^2}(e_h + \nu e_a) \qquad (37)$$

The computer program for calculating the hoop and axial effective stresses on the inner and outer surfaces is presented in the Appendix A. A tenth order approximation of solution is used for satisfactory convergence. The strain energy formulation for out-of-plane moment may be obtained in the same manner [15].

2.3.3. Hoop and axial stresses from ASME

Most simplified elbow analyses and the ASME [28] code predict a more flexible response than the shell analysis because the end stiffening effects are neglected, resulting in overprediction of stresses. ASME realises this and work to rectify this shortcoming is underway.

Table NB-3685.1-1 and NB-3685.1-2 of ASME III [28] give the equations for the stress

indices for the inner and outer hoop and axial stresses around the circumference of the elbow

mid-section. When internal pressure acts, the hoop stress is given, in ASME nomenclature,

by:-

$$\sigma_\theta = \left[\frac{D_o - 0.8\, t_m}{2\, t_m}\right] \left[\frac{0.5\ (2R + r\ \sin\phi)}{R + r\ \sin\phi}\right] P \tag{38}$$

and axial stress,

$$\sigma_\phi = D_i P / 4 t_m \tag{39}$$

Due to in-plane and out-of-plane moments, the hoop and axial stresses, σ_θ and σ_ϕ, are given

by:-

on the outer surface, $\qquad \sigma_\theta = (\nu \sigma_{tm} + \sigma_{nb}) M / Z$
on the inner surface, $\qquad \sigma_\theta = (\nu \sigma_{tm} - \sigma_{nb}) M / Z$
on the outer surface, $\qquad \sigma_\phi = (\sigma_{tm} + \nu \sigma_{nb}) M / Z$
on the inner surface, $\qquad \sigma_\phi = (\sigma_{tm} - \nu \sigma_{nb}) M / Z$

For in-plane moment,
$\qquad \sigma_{tm} = \sin\phi + [(1.5 X_2 - 18.75)\sin 3\phi + 11.25\sin 5\phi] / X_4$
and $\qquad \sigma_{nb} = \lambda(9 X_2 \cos 2\phi + 225\cos 4\phi) / X_4$

For out-of-plane moment,
$\qquad \sigma_{tm} = \cos\phi + [(1.5 X_2 - 18.75)\cos 3\phi + 11.25\cos 5\phi] / X_4$
and $\qquad \sigma_{nb} = -\lambda(9 X_2 \sin 2\phi + 225\sin 4\phi) / X_4$

where $\quad X_1 = 5 + 6\lambda^2 + 24\psi$
$\qquad X_2 = 17 + 600\lambda^2 + 480\psi$
$\qquad X_3 = X_1 X_2 - 6.25$
$\qquad X_4 = (1 - \nu^2)(X_3 - 4.5 X_2)$
$\qquad \lambda = TR / (r^2 \sqrt{(1 - \nu^2)})$
$\qquad \psi = PR^2 / ErT$

The equations are valid for elbows with $\lambda \geq 0.2$ only. This book title.

ref: 38

36

2.4. STRESS ANALYSIS OF TEE BRANCH

2.4.1. Stress concentration and classification

Like other fittings such as reducers and elbows, branch junctions introduce stress intensification. The stress concentration factor (SCF) is defined as a multiplier to be applied to the nominal stresses in an equivalent plain pipe to account for geometric discontinuity effects of the connection. The stress concentration at the intersection is mainly due to the main shell being weakened by the intersection opening and varies with the shape and size of the opening. However, the intensified stresses are highly localised leaving the surrounding material lowly stressed.

Due to internal pressure, the high stresses at the pipe intersection are a result of self-equilibrating discontinuity shear forces and moments which maintain compatibility at the junction. Together with membrane forces, the discontinuity forces give rise to high local stresses. The discontinuity effect which is caused by the change of direction between the run and branch pipes varies around the opening and is maximum along the longitudinal plane where the local stresses are maximum.

Although the most critical stresses are usually caused by pressure, considerable stresses at pipe junctions may also occur from external nozzle loads. Stresses around the intersection produced by external loads must be classified into primary, secondary and peak stresses. These stresses have different degrees of significance and must be assigned different stress limits.

The following definitions and behaviours of the stress categories are given by Smith and Van Laan:-

" *Primary stress is developed by imposed mechanical loadings (forces). Primary stress is not self-limiting. Therefore, if the yield strength is exceeded through the entire cross section of the structural material used in piping design, then failure can be prevented only by removal of the loading or strain hardening in the material.*

Primary stresses can further be categorized as general primary membrane stress, local primary membrane stress, and primary bending stress. These three categories are of interest because the pipe will not fail until the entire cross section has reached the yield strength. Local primary stresses may exceed yielding; however, under this stress state they will behave as secondary stresses and redistribute themselves as the local pipe wall distortion occurs. The failing moment would be that required to put the entire cross section of the pipe in plastic behavior, not just the extreme fiber. Therefore, the permissible primary bending moment (and likewise the calculated stress) may be increased over the yielding moment by the shape factor.

Secondary stress is developed in a structure owing to constraint of that structure against displacements, whether thermal expansion or imposed anchor and restraint movements. Under secondary loading the piping system must conform to imposed strains, rather than imposed forces, so that the loading can be satisfied by system distortions. Distortion of the piping system as well as local yielding tends to relieve the developed stresses due to imposed displacements, so these stresses are said to be self-limiting.

Given that secondary stresses are classified as those stresses caused by constraints of displacements which cause distortion, peak stresses are those which cause virtually no distortion and therefore high stress levels. Examples would be thermal gradients through a pipe wall or stress concentration at a discontinuity such as a pipe fitting or a weld. Peak stress is the highest stress in a local region and is responsible for causing fatigue failure. "

- Smith P.R. and Van Laan T.J. - Piping and Pipe Support Systems. Design and Engineering.

In general, pressure vessel and piping components exhibit both primary and secondary behaviour and it is not immediately obvious how the stresses should be categorised. A value of stress means little until it is associated with its location, distribution in the structure and the type of load producing it. The Codes have their own stress classification procedures on which the stress allowables are based.

The effective stress factor (ESF) at the junction was obtained by normalizing the Mises stress with the nominal stress, regardless of location of the maximum stress. Some uncertainty was encountered when Moffat et al [43] tried to determine the effect of t/T on ESF. For the branch pipe loads, the nominal stress σ_n would also have varied with t/T if σ_n was based on the actual branch pipe thickness. Following the argument of Moffat, it was decided that an effective thickness be used so that σ_n for the branch pipe would remain constant. The effective thickness t^* is defined as, $t^* = (d/D)T$. The nominal stresses of the branch pipe were based on the effective thickness, hence:-

for torsional run pipe moment,	$\sigma_n = T_o D_o / 2I_r$
for torsional branch pipe,	$\sigma_n = T_o d_o / 2I_b^*$
for run pipe bending moment,	$\sigma_n = M D_o / 2I_r$
for branch pipe bending moment,	$\sigma_n = M d_o / 2I_b^*$
for internal pressure	$\sigma_n = P D_m / 2T$

where I^* is based on the effective thickness.

2.4.2. Load interaction

A general moment load acting on a pipe limb can be resolved into three moments acting along 3 mutually perpendicular axes of the limb, to give a total of 9 sets of moment, i.e. three in each of the three connecting limbs. Using the 'cantilever model', as in Fig. 1, with one of the run pipe limbs rigidly fixed, the 9 moments can be reduced to 6 independent moments acting at the free ends of the two limbs. If the pipe limbs are sufficiently long, the shear effects of force loads can be neglected. Including internal pressure, a total of 7 load categories can thus act on the tee branch, each giving a complex stress behaviour. In practice, these loads occur together in a combination of 2 or more load cases and the stress levels arising from the multiple load interaction must be considered.

2.5. STRESS ANALYSIS OF TORISPHERICAL HEAD WITH NOZZLE

2.5.1. Experimental investigation at Liverpool

In order to verify any theoretical formulation or numerical results, experimental tests on similar structures are needed. The experimental test was part of a test programme carried out by Drabble [74] at Liverpool to determine the shakedown behaviour of a torispherical head with nozzle, under the action of internal pressure, axial force and bending moment applied to the nozzle. The whole vessel was made of mild steel and had a uniform thickness. The weld formed a fillet, 0.5 inch high and 0.25 inch wide, at the juncture between the nozzle and the main vessel. From Drabble's report, there was no mention of initial geometric imperfections.

The model was instrumented with 39 pairs (hoop and meridional) of 0.0625-inch foil rectangular strain gauges bonded to the outer and inner surfaces of the shell. These gauges were located between $S=-0.1$ and $S=0.5$ along an meridional plane. The non-dimensional meridional distance S is taken to be the ratio of the actual distance (measured along the shell surface) from the crotch corner to the inner radius of the spherical crown. On the outer surface, the distance was measured from the weld-crown juncture. The distance was taken to be positive in the main vessel and negative distance in the nozzle.

The model was subjected to combinations of internal pressure, compressive axial force and bending moment. A detailed experimental procedure of the test is given in Ref. [74].
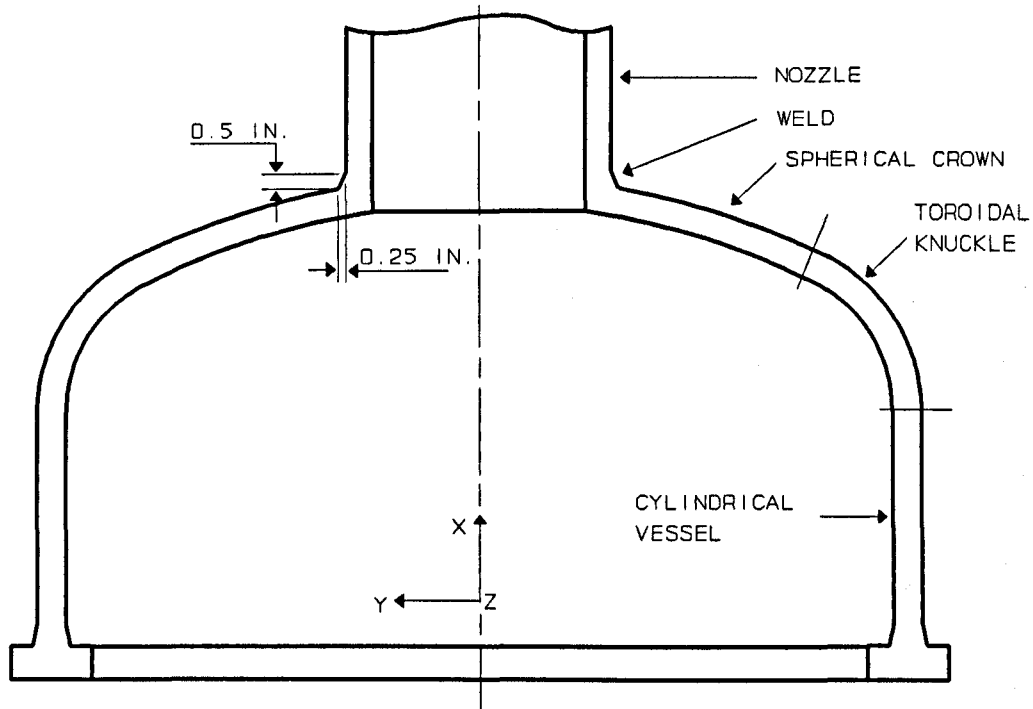
FIG. 5. TORISPHERICAL HEAD WITH NOZZLE. (DRAWN TO SCALE).

The torispherical head with nozzle is shown in Fig. 5. The dimensions of the vessel were as follows:-

Mean diameter of cylindrical shell, D_m	= 16.0 in. (406.4 mm)
Mean knuckle radius, r_{km}	= 2.95 in. (74.93 mm)
Mean crown radius, L_m	= 16.0 in. (406.4 mm)
Mean diameter of nozzle, d_m	= 4.5 in. (114.3 mm)
Thickness of vessel, T	= 0.5 in. (12.7 mm)
Thickness of nozzle, t	= 0.5 in. (12.7 mm)
Head height (to mid-wall), H	= 3.967 in. (100.8 mm)
Length of cylindrical vessel	= 4.0 in. (101.6 mm)

which give parametric ratios:-

d_m/D_m	= 0.281
D_m/T	= 32.0
d_m/t	= 9.0
2L/T	= 64.0
H/D_m	= 0.248
$\lambda = D_m/2H$	= 2.017
$\rho = (r_m/L_m)\sqrt{(L_m/T)}$	= 0.795

40

CHAPTER 3.   THE FINITE ELEMENT METHOD

The finite element modelling in all the piping components utilised the computer aided engineering software package PATRAN [75]. Unlike the tee branch, the geometric modelling of the plain pipe, elbow and torispherical head was straightforward. The main difficulty for the tee branch lies in generating the non-axisymmetric weld profile and assigning a single layer of elements to the intersection region. For reference, the modelling of the tee branch is described in detail.

The various ways of constraining and inducing bending loads on the tee branch are also detailed. For all the components, the models were constructed with PATRAN [75] HEX20 20-node isoparametric hexahedral elements. The element has nodes at the corners and mid-sides, and each node has three degrees of translational freedom. The element has the advantage of correctly representing the curved boundaries with a fewer number of elements and is known to converge rapidly with a lesser number of elements. In a convergence test, the plain pipe and tee branch were also modelled with two layers of the 20-node element through the wall thickness.

The resulting finite element model was run through the PATRAN features of automated nodal equivalencing, node removal, node compaction and resequencing and element compaction. The elements were checked for free edge and crack to ensure structural integrity. All the load categories for a component used the mesh which was generated for that component, so that all the models would give identical node numbers at corresponding locations. The PATRAN [75] neutral output files were translated to make them readable by the ASAS [76] finite element analysis program.

Linear elastic and geometrically nonlinear finite element analyses were carried out on two elbow models, EL01 and EL07, to study the effect of geometric nonlinearity and nonlinear coupling between internal pressure and in-plane bending moment. The objective was to determine the extent to which the linear superposition method of load interaction could be used to predict first yield in thin elbows. Another pressure coupling investigation was carried out on the tee branch, with the out-of-plane branch pipe moment as the other interacting load. The effect on other components was not carried out because the cross-sectional ovalization is reported to be considerably lower than in the elbow.

3.1. PLAIN PIPES

3.1.1. Geometrical parameters and FE model

The geometric parameters of the four pipe models PIP1, PIP2, PIP3 and PIP4 are shown in Table 1. Each model is 1 metre long and has the following material properties:-

$$E = 200 \text{ GN/m}^2 \text{ and } \nu = 0.3$$

Table 1. <u>Geometric parameters of plain pipe models</u>

Model	PIP1	PIP2	PIP3	PIP4
R_o	0.136	0.136	0.136	0.136
R_i	0.125	0.119	0.111	0.091
T	0.0107	0.0170	0.0247	0.0453
D_m/T	24.5	15.00	10.00	5.00

(All linear dimensions are in metres)

A preliminary convergence test was carried out on two models to establish a suitable mesh. Models PIP1 and PIP4, with $D_m/T=24.5$ and 5 respectively, which represent 'thin' and 'thick' pipes, were subjected to internal pressure. The pipes were first modelled with 8-node

isoparametric hexahedral elements with a single layer of elements through the thickness, 24 elements in the hoop direction and 28 in the axial direction. The pipes were then modelled with two elements through the thickness and finally the 20-node element was used. The mesh was then refined to provide 40 elements in the axial direction and 36 elements in the hoop direction. It was found that the 20-node element models gave satisfactory agreement with the Lame's solutions, but did not significantly give better results with the finer mesh. Hence the coarser 1x24x28 (radial x hoop x axial) mesh with a single layer of 20-node elements was adopted for all the pipe models. A total of 672 elements and 4824 nodes was generated, and each uniform element measured 35.6mm x 35.7mm.

The torsional moment on the end of the pipe was induced by means of 48 equal tangential nodal forces acting at the outer edge of the pipe end, at intervals of $\theta = 7.5°$. The uniform tangential nodal forces were obtained from:-

$$\text{Force} \quad = \quad T_o/(R_o \times 48) \tag{40}$$

The bending moments on the pipe were induced by 48 graded axial forces applied at intervals of $\theta = 7.5°$ on the nodes at the outer edge of the pipe end. The loading technique produced consistent nominal stresses within a distance of one pipe diameter from the loaded end. The graded nodal forces were calculated from:-

$$\text{Force} = M(\frac{2}{D_m}) \frac{\sin \frac{\pi(\theta - 90°)}{180°}}{\sum\limits_{\theta - 90°}^{270°} \sin^2 \frac{\pi(\theta - 90°)}{180°}} \tag{41}$$

For the axial force, a total of 48 uniform nodal axial forces acted in the axial direction:-

$$\text{Force} = F/48 \tag{42}$$

43

The methods of inducing the loads in a plain pipe by means of nodal forces are shown in Figs. 6. The methods are similarly utilised in the pipe bends, tee branches and the torispherical head at the pipe ends where the loads are needed. For internal pressure, an additional axial stress acted on the end of the closed pipe. To prevent rigid body motion of the structure, suppression of all displacements were applied at the other end of the pipe. Similar load modelling was used for other piping components.
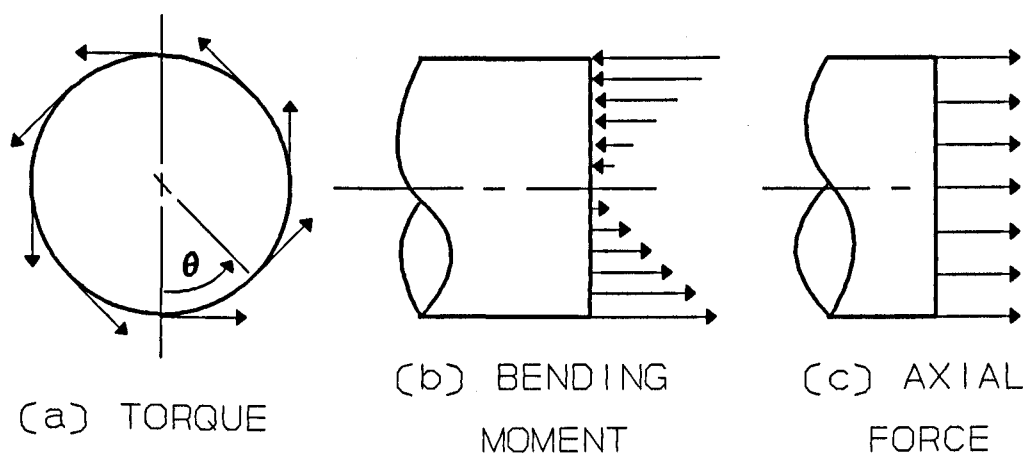
FIG. 6. LOAD MODELLING IN PIPES

3.2. PIPE BENDS

3.2.1. Geometrical parameters

The geometrical features of all sixteen models, representing a wide range of b and λ, are given in Table 2. The models have a bend angle of 90° and mean pipe radius of r=0.1 m. The elbows are grouped into four bend radius ratios b (=R/r) of 2, 3, 5 and 7. For each bend ratio, four elbow models of varying D_m/T ratios were selected, i.e. D_m/T=150, 80, 20 and 10. Model EL01 with λ=0.0267 and D_m/T=150 may be considered a 'thin-walled' and 'small-radius' elbow, while model EL16 with λ=1.4 and D_m/T=10, may be considered a 'thick-walled' and 'large-radius' elbow. The categorisation of elbows into thin- and thick-walled and into small and large radii varies with the authors; ASME categorises elbows with b≥3 to be large-radius elbows.

Table 2.   Geometric parameters of elbow models

Model	b	λ	D_m/T	Model	b	λ	D_m/T
EL01	2	0.0267	150	EL09	5	0.0667	150
EL02	2	0.05	80	EL10	5	0.125	80
EL03	2	0.2	20	EL11	5	0.5	20
EL04	2	0.4	10	EL12	5	1.0	10
EL05	3	0.04	150	EL13	7	0.0933	150
EL06	3	0.075	80	EL14	7	0.175	80
EL07	3	0.3	20	EL15	7	0.7	20
EL08	3	0.6	10	EL16	7	1.4	10

3.2.2. The FE model

The elbows, shown in Table 2, were modelled and subjected to identical loads of torque, in-plane moment and internal pressure. Figs. 7(a) and (b) show the basic geometry, boundary conditions and moment vectors, while Fig. 8 shows the finite element mesh at the curved section of model EL07.

45

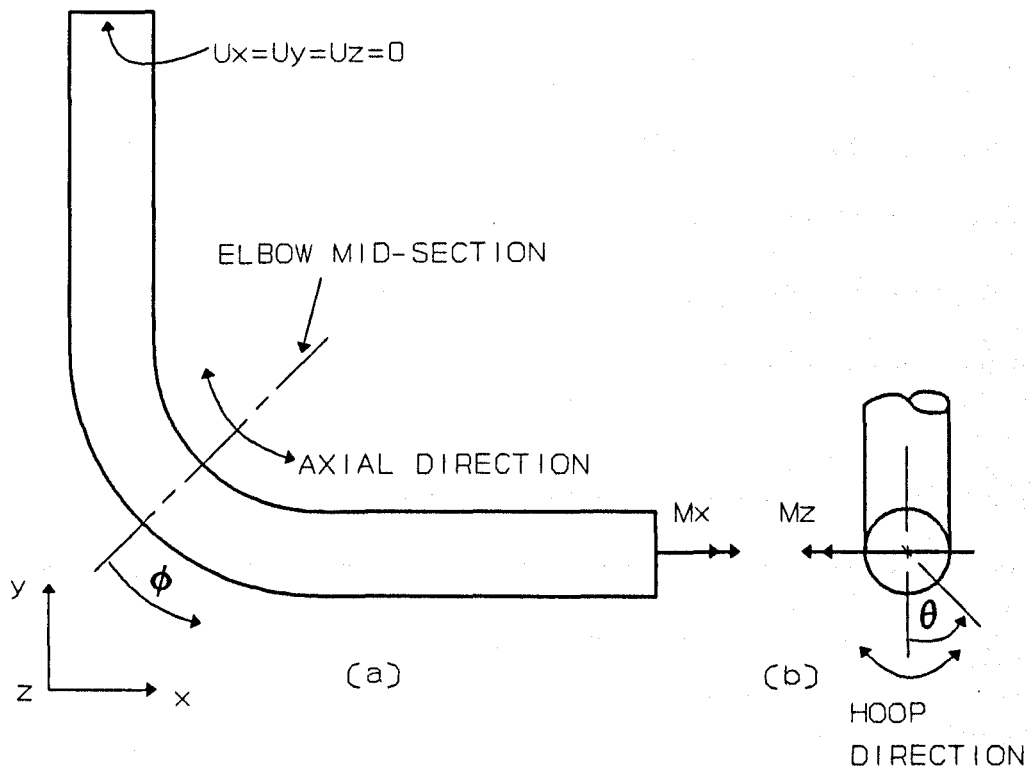FIG. 7.   GEOMETRY, BOUNDARY CONDITIONS AND MOMENT VECTORS IN
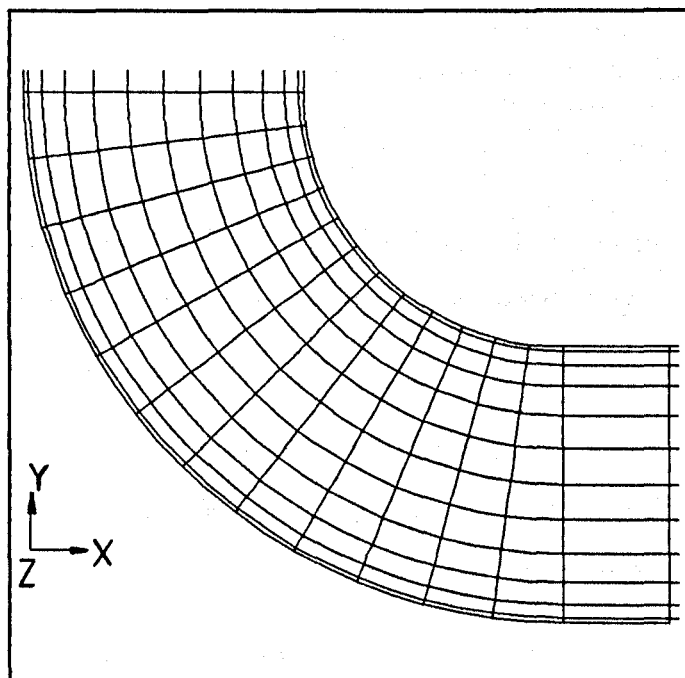   ELBOW. (Note: U = displacement).

FIG. 8.   FINITE ELEMENT MESH OF CURVED SECTION OF ELBOW EL07.

46

The choice of mesh, geometric and load modellings was partly based on the previous work performed on plain pipes. Initial pressure stress comparison with the toroidal theory of solid mechanics proved that the mesh was satisfactory. The length of the attached tangent pipes was four times the mean pipe diameter, and was considered to be adequate to prevent propagation into the curved section of the effects of boundary condition and applied loads at the free ends. It has been shown by Dhalla [21] that the effects due to end restraint and cross-section ovalization do not propagate for a distance of more than three times the diameter along the attached pipe. The curved section had 24 and 12 uniform elements in the hoop and axial divisions respectively. The tangent pipes had 10 and 24 axial and hoop divisions respectively. Altogether a total of 768 20-node hexahedral elements and 5496 nodes were generated.

The elbows were loaded separately by internal pressure as well as a closing in-plane moment and torque applied at the free end of a tangent pipe. The load modelling was similar to that used in plain pipes. An opening moment is assumed to give identical stress result as a closing moment, but with reversed signs. Hence results from the positive model of the moment M_z was used for the negative opening moment.

The full structure was analyzed because there was no common plane of symmetry of geometry and applied loads. Furthermore, the ASAS [76] brick element which does not restrain rotational displacements at the nodes would give dubious data along any plane of symmetry. The free end of the vertical tangent pipe, in Fig. 7(a), was constrained from linear displacement in three mutually perpendicular directions.

3.2.3. Geometrical nonlinear FE analysis

In the linear analysis, the stresses at each load step were not affected by the progressive geometric deformation as the elbow was loaded up to the final pressure or moment. In the

numerical solution of geometrical nonlinearity, the deformed configuration at every iterative increment is used for equilibrium conditions.

A geometrically nonlinear stress analysis was carried out on two elbow models, EL01 and EL07. Model EL01 represents a thin elbow with a small bend radius and elbow model EL07 represents a moderate elbow which is commonly used in industries. The analysis of the two models with separate loads of torque, in-plane moment and internal pressure was intended to assess the extent of geometrical nonlinearity. This was followed by an analysis with combined loadings to show the nonlinear coupling between pressure and moment loads.

3.3. TEE BRANCH

3.3.1. Geometrical parameters

A tee branch piping is shown in Fig. 1. The four main parameters of a tee branch are the branch and run pipe mean diameters and thicknesses. In a welded branch junction, the weld details, i.e. the height and width, provide additional parameters. Hereafter, the term 'weld' will be used to denote a triangular weld fillet without transition radii. This geometry gives a sharp change in contour between the weld and the pipes.

The geometric ratios are useful when comparing with other studies. In this study, one specific tee branch with ratios $D_m/T = 20$, $d_m/D_m = 0.8$ and $t/T = 1.0$ was modelled, with weld details identical to the one used by Moffat et al [43]. Figs. 9(a) and (b) show the weld details used in the present FEM and Moffat et al's [43] models. The following tee branch with the weld details shall be referred to as the FEM first model:-

mean diameter of run pipe, D_m = 200 mm
mean diameter of branch pipe, d_m = 160 mm
thickness of run pipe, T   = 10 mm

thickness of branch pipe, t .... = 10 mm
weld height at crotch corner, w_{hc} .... = 15.5 mm
weld height at flank, w_{hf} .... = 15.5 mm
weld width at crotch corner, w_{lc} .... = 8.75 mm
weld width at flank, w_{lf} .... = 8.75 mm

The material was assumed to be carbon steel with properties E = 200 GPa and ν = 0.3.

To study the stress level due to the intersection alone, other sources of stress concentration must be removed from the vicinity of the intersection. If the limb lengths are not sufficiently long, the end effects from the loadings applied at the free pipe ends may interfere with the stress concentration due to the intersection. Mokhtarian and Endicott [53] and ASME [28] suggested pipe lengths of not less than $2.5\sqrt{\text{(radius x thickness)}}$. Mershon et al [32] noted limb lengths of at least $2\sqrt{\text{(radius x thickness)}}$ for attenuation of other stress concentrations. The pipe lengths used in this study were taken to be four times the mean diameters, i.e.

length of branch pipe .... = 640 mm from the run pipe centreline
length of run pipe limbs .... = 800 mm each side of the branch pipe centreline
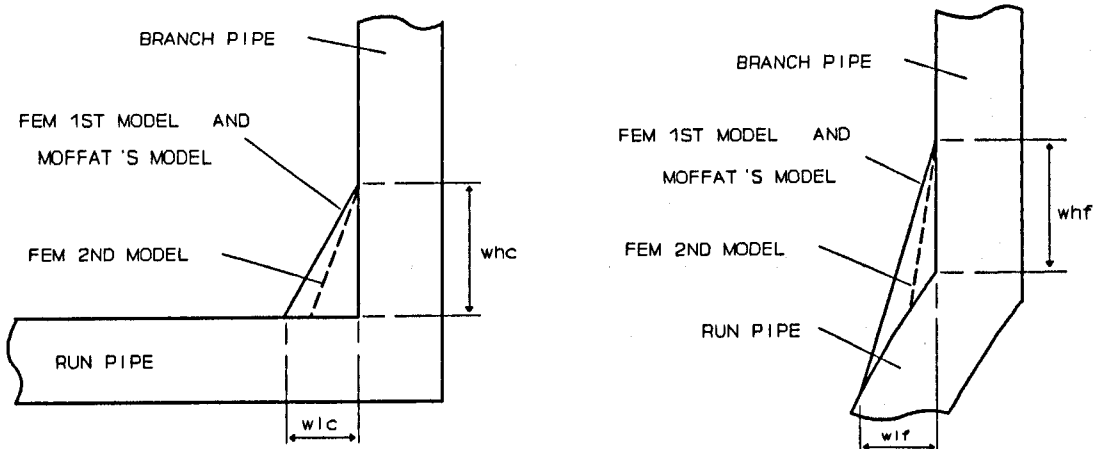
(a) LONGITUDINAL PLANE   (b) TRANSVERSE PLANE

FIG. 9. WELD DETAILS OF TEE BRANCH. COMPARISON BETWEEN FEM FIRST (AND MOFFAT'S) MODEL AND FEM SECOND MODEL. (DRAWN TO SCALE).

3.3.2. The FE model

The basic concept of the finite element method is the idealization of the structure as an assemblage of subdivisions. Fig. 10 shows the various areas for subdivision of the structure. Two areas were identified for different meshing; the critical area around the intersection and the remote regions. The critical area is shown as region PBCDELKMN. The edge EL is of a distance of about $0.36D_m$ from the intersection at S, and the edge PB is $0.44d_m$ from point S.

The outer surfaces of regions RSEHJ and PBSR were generated first. Edges EH and PB were located at distances of $\pi D_m/4$ along the run pipe from the centreline of the branch pipe and $1.75R_m$ along the branch pipe from the run pipe centreline, respectively. The above dimensions also ensured that the elements in region RSELK were not much distorted. The line of intersection, RS, between the two outer surfaces formed a reference line from which the weld dimensions were measured. The weld horizontal width at the longitudinal plane was set to $SD = w_{lc}$ and at the flank and the horizontal projection of RM was set to w_{lf}. These two weld bases, D and M, were connected by a quarter ellipse, MD, scribed along the outer surface of the run pipe. The weld height at both the longitudinal and transverse planes, i.e. SC and RN, was set to a value of w_h, which is the greater of w_{hc} and w_{hf}. The weld toe line, NC, was formed by translating the intersection line, RS, by a distance w_h along the branch pipe. The weld surface was then blended together with the run and branch pipe outer surfaces to form an outer patch. The inner surfaces of regions RSEHJ and PBSR were generated by using the inner pipes dimensions. These inner surfaces intersect at the crotch line. The inner and outer surfaces of the remote regions QABP and EFGH were formed in a more straightforward procedure.
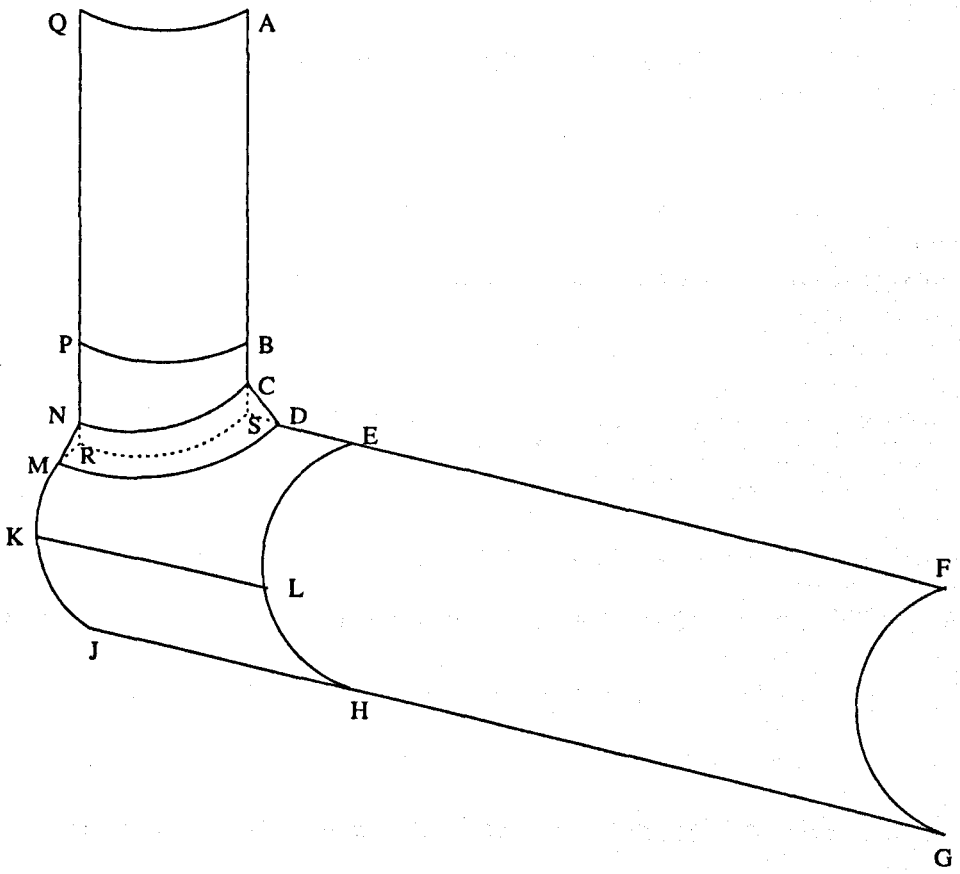
FIG. 10.   A QUARTER TEE BRANCH SHOWING REGIONS FOR SUBDIVISION.

A solid quarter model was created by joining the outer to the inner patches. The final full model was formed by mirroring the quarter model about the longitudinal and transverse planes. A full three-dimensional tee branch model was considered because there were no common planes of symmetry for all the seven load cases.

The discretization of the tee branch into finite elements of suitable size and shape is no less important than the selection of the element itself. In the finite element method, the difficulty in obtaining accurate results is due to the high stress gradient in the intersection region. This may be overcome by using a fine mesh in the critical region where a coarse mesh may cause violation of local equilibrium and gives unsatisfactory results. It is known that the stress gradients in remote regions are low, thus justifying the use of coarser meshes.

In the FEM, shell and beam elements have been specially written for thin geometries and are widely used in the analysis of shell structures. In tee connections, apart from nominal stress and stress concentration from the nozzle intersection, the local stress due to the weld profile must be considered. If shell elements are used, the intersection lies inside the wall thickness and the predicted stress at this location is a rough estimate of the stress at the weld toe. If the tee connection is thin walled the weld has significant stiffness which is ignored by a shell model. To compensate for this many methods have been devised such as the multi point constraint approach to create a rigid block representing the weld or using a stiffer shell element at this particular location. To model the weld reinforcement in cylinder-cylinder intersections, it is desirable to use solid elements because they give a more accurate representation of the structure geometry.

A study was undertaken at Liverpool, by Mwenifumbo [77] and Moffat et al [43], on the performance of the solid elements in tee branches and the effect of mesh refinement. Working

with the 8-node and 20-node brick elements on tee branches, several finite element idealizations were carried out [43][77] for convergence tests. Mwenifumbo [77] showed that the 8-node model needed six times more elements in the critical region than the 20-node model for satisfactory convergence. A finer element mesh does not provide improvement if the finite element formulation is not properly developed. This was realised by Corum et al [36] who was using an analysis which was developed at the University of California, Berkeley by Clough.

It is well known that when thin members are subjected to bending, the strain variation throughout the thickness is linear. The first order elements represent this variation poorly. With second order elements, one layer of elements through the shell thickness is adequate especially if the elements are rectangular in shape. Previous studies at Liverpool [43][77], as well as by Natarajan et al [78], on tee branches showed that the use of one element through the thickness of the branch was acceptable provided the mesh was well refined. For accurate radial stresses, Bryson et al [79] commented on the use of at least two layers when the 8-node element was used. Chen and Schnobrich [80] analyzed the use of 3-D multi-layered elements at the critical area of the intersection. To avoid the abrupt change of stiffness from the fine to the coarse mesh, they gradually reduced the number of layers of elements in transition regions.

The number of elements in a region is governed by the criterion that the elements should be as cubical in shape as possible, and should be consistent with the degree of mesh refinement. The most awkward part of the model was the weld and intersection region where the strains and stresses must be predicted accurately. To ensure that no tetrahedron and wedge elements were utilised, proper modelling and division of the intersection region was thoroughly done. It was also ensured that any discontinuity such as the weld toe curve coincided with element

edges.

The quarter model of the tee branch was divided into six mesh areas. The most critical regions were the weld and two areas along the pipe limbs adjacent to the weld. The weld NCDM had 4 elements along the weld width CD and 12 elements in the circumferential direction NC. The area PBCN had a one-way transitional mesh from 8 elements along PB to 12 elements along NC, while the edge BC had 6 elements. The third critical region, MDELK, had edges EL and LK with 6 elements each, and were considered to be the opposing sides to edge MD, which also had 12 elements. This method ensured that the element mesh became finer nearer the intersection. The other opposing edges DE and MK had 6 elements each. Region KLHJ contained a uniform rectangular mesh of 6x6 elements. Regions QABP and EFGH were the least critical and contained non-uniform rectangular meshes of 8x6 and 6x6 elements respectively. The non-uniform node spacings were in the longitudinal directions of the pipe limbs, with the mesh becoming finer nearer the intersection.

The finite element representation at the intersection of the tee is shown in Fig. 11. Figs. 12 and 13 show the meshes on the longitudinal and transverse planes of the tee branch. A total of 1328 elements were generated, 704 of which were in the critical intersection region. The total number of nodes was 9493. The structure had one element through the thickness. Further mesh refinement was not desirable since the thickness direction would have contributed to unacceptable aspect ratios.

Mesh refinement and maintaining proper element aspect ratio are important in order to get good results. In Natarajan et al's [78] study using 20-node brick elements, the hoop stress distribution along the run pipe gave poor agreement with experimental results. Increasing the number of elements near the intersection resulted in a much lower predicted stress peak. In

the next model they reduced the elements aspect ratio (near the intersection) from 1:3 to 1:2 but still got poor results. They carried on refining the mesh while keeping the aspect ratio of 1:2 and obtained good agreement.
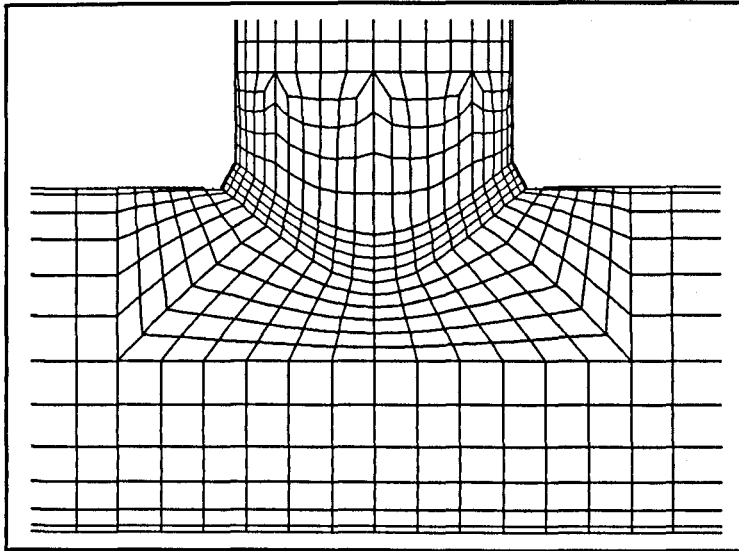

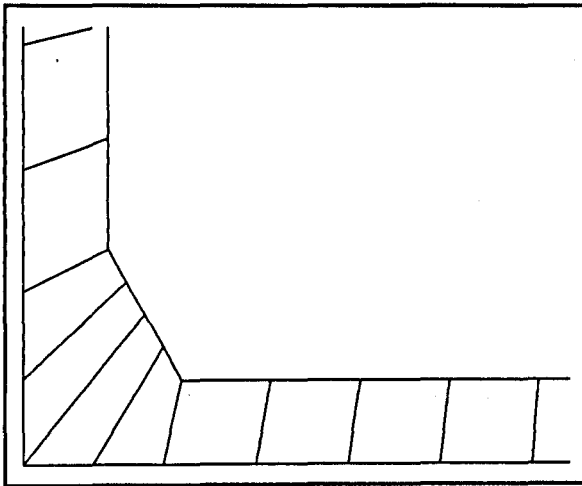FIG. 11. FINITE ELEMENT MESH AT INTERSECTION REGION OF TEE BRANCH
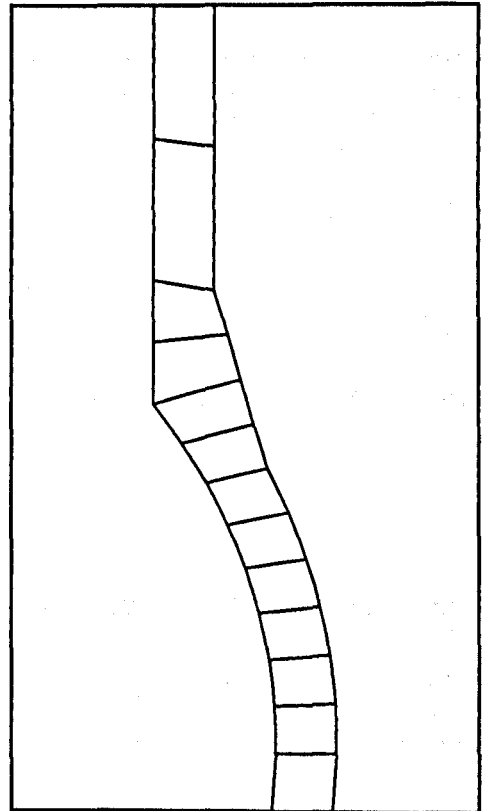

FIG. 12.   FE MESH ON LONGITUDINAL PLANE.

FIG. 13. FE MESH ON TRANSVERSE PLANE.

3.3.3. Boundary conditions

The response of the pipe connection to moment loads depends on how the loads are reacted

at the end where the structure is fixed. The ASME code calls for every limb to be checked

separately for the respective resultant limb moment but is unclear about boundary conditions.

The 'cantilever' method of constraint was applied but not before other methods were

considered. To prevent rigid body motion of the structure, suppression of all displacements

were applied at one end of the run pipe. Similarly, there are many ways in which moment

loads can be applied to the branch junction. Moffat [34] provided a detailed discussion on the

subject and the effect on resulting stresses. The two most commonly used methods to

constrain the branch are discussed below.

Case (a) <u>Cantilever model. One end of run pipe fixed</u>

The present study was based on the cantilever model. In this model, the tee branch is fully

constrained at one end of the run pipe while the free ends are applied with moment loads.

Experimental studies on tee branches with the cantilever model were carried out by Gwaltney

et al [35], Moffat [34] and Zhixiang et al [60].

Case (b) <u>Two ends of pipe fixed</u>

The resulting stresses from this case are sensitive to the short run pipe lengths, but otherwise

the resulting stresses due to branch pipe moments are not different from the above case (a).

The branch moments are reacted out through both run pipe limbs. The in-plane run pipe

moment is obtained by a branch thrust. Rodabaugh [81] speculated that for branch moments,

the difference in resulting stress factors between case (a) and case (b) would be small if r/R

is less than 3/4, but if r/R=1 the stress factor for case (b) is less than case (a). Among

others, Mershon et al [32] and Fujimoto and Soh [27] based their analyses on this loading

case.

Another method of constraining the structure is where the ends of the run pipe are simply supported. If the run pipes in case (b) are sufficiently long, the stress distributions in these cases would be similar, a point which was proven by Moffat [34]. In another method, if moment is applied at a pipe end, the other two pipe ends are fixed. Experimental studies in which two pipe ends are fixed were carried out by Hardenbergh and Zamrik [82], Riley [83], Ellyin [84] and Decock [85].

3.3.4. Load modelling

The loads on the tee branch may consist of internal pressure, bending or torsional moments acting at the ends of the run or branch pipes. The in-plane and torsional moment loads were applied to ends of the pipes in a way similar to the plain pipes. For pressure, axial stresses were also applied to the ends of the pipes to model the close-ended condition. Fig. 1 shows the method of constraining the structure and the moment vectors being applied on the pipes. The hoop angular directions of the run and branch pipes θ and ϕ are defined in the figure.

The branch pipe had 32 elements around the circumference, hence a total of 64 nodal forces acted at intervals of $\phi = 5.625°$ to induce branch moment loads. For out-of-plane moment on the run pipe, the nodal forces are given by:-

$$\text{Force} = M_{yr}\left(\frac{2}{D_m}\right)\frac{\sin\frac{\pi\theta}{180°}}{\sum\limits_{\theta=0°}^{180°}\sin^2\frac{\pi\theta}{180°}} \tag{43}$$

The nodal forces to induce out-of-plane moment load on the branch pipe are similar to the above equation, except that the moment was replaced by M_{xb}, D_m was replaced by d_m and the angular direction in the run pipe θ was replaced by ϕ in the branch pipe.

3.4. TORISPHERICAL HEAD WITH NOZZLE

3.4.1. The FE model

To get a correct correlation with Drabble's [74] experimental results, it is necessary to model the loading, geometry and boundary conditions of the experimental test exactly. The experimental nozzle-shell geometry shown in Fig. 5 was adopted for the finite element analysis. One of the difficulties facing investigators is the lack of accurate knowledge of boundary conditions in experiment tests. The use of a flange for clamping at the cylindrical vessel was represented by a fully fixed boundary condition. The structure was loaded with internal pressure and external compressive axial force, bending moment and torsional moment at the nozzle end in a similar way as the plain pipe.

At geometric discontinuities, the loadings could create high stress gradients in the radial, hoop and meridional directions. The FE mesh size in these directions was considered in a preliminary convergence test on the model subjected to internal pressure. The peak von Mises effective stress on the inner surface of the knuckle was compared. The number of elements in the hoop direction that will adequately model the structure is critical to the analysis. In the full hoop direction, 24- and 48-element models were carried out. The convergence of stresses due to meshing in the meridional direction was also considered. The number of elements in the meridional direction was increased from 2+2+1 (i.e. number of elements in knuckle+crown+weld) to 5+4+1 and finally to 8+8+2, which will be referred to as coarse, medium and fine meshes respectively. Increasing the number of elements from 24 to 48 in the hoop direction improved the result marginally but in the meridional direction, the coarse and medium meshes gave a lower peak stress by about 20% than the experimental value. The final fine mesh was about 4% higher than measured; i.e. a good agreement with the test result. A model with two layers of elements in the wall was run but it did not give

significant improvement over the one-layer model; so the one-layer model was used subsequently. In the hoop direction, the 48-element model was selected mainly because it gave an aspect ratio close to unity at the critical intersection region. The results of the mesh investigations led to the selection of the final FE idealization in the meridional direction; 8+8+2 elements in the knuckle, crown and weld regions, 6 elements in the main cylinder and 7 in the nozzle. A longitudinal section of the discretized geometry is shown in Fig. 14. The full model utilized 1488 20-node brick elements with a total of 10656 nodes. The vessel material was mild steel which is characterized by elastic modulus of 30×10^6 psi and Poisson's ratio of 0.3.
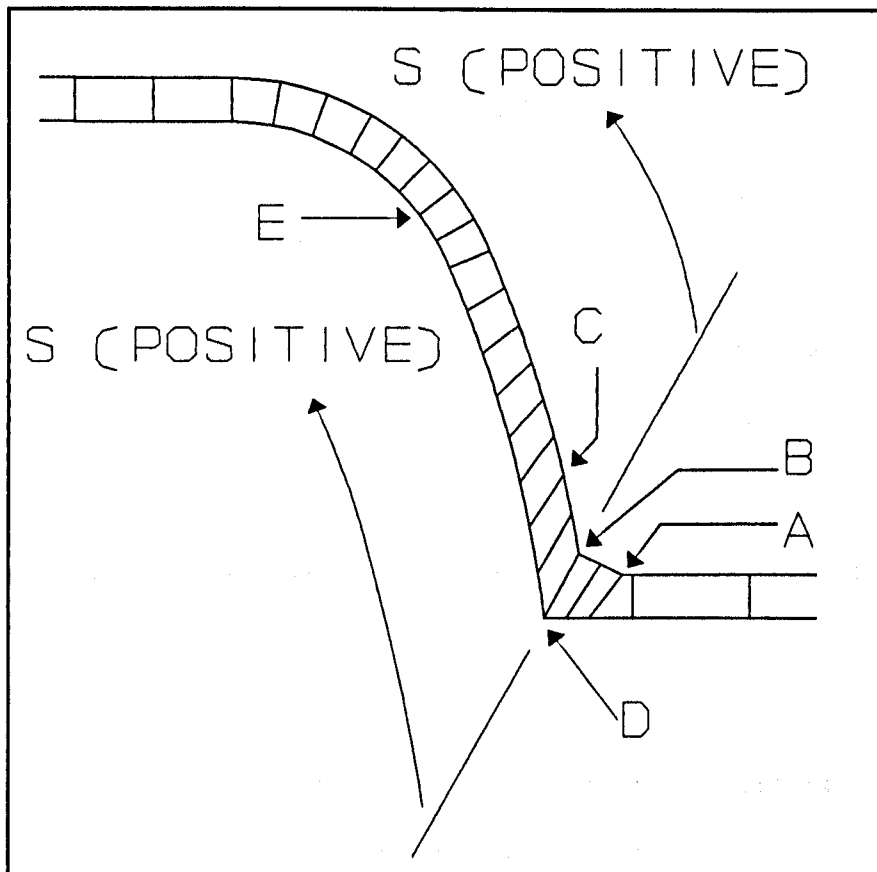
FIG. 14.   FINITE   ELEMENT   MESH   ON   MERIDIONAL   PLANE   OF
TORISPHERICAL HEAD WITH NOZZLE.

3.5. STRESS AND LOAD INTERACTION CALCULATIONS FROM FEM DATA

The numerical stress analysis was performed using the linear elastic finite element program ASAS [76]. For each loading category, the finite element results gave normal and shear nodal stresses with reference to the global x-, y- and z-axes. To eliminate undesired end effects from the boundary conditions and external loads, only the stress data around the region of interest was stored in a database. For the tee branch and torispherical head, the region around the intersection was the area of interest. For the pipe bends, only the curved pipe section was considered and in the plain pipes, it was the central area which was about one diameter away from the ends.

The stresses were then normalised using the respective nominal stresses. For pressure, the nominal stresses are:-

$$\sigma_n = PR_m/T \quad \text{for plain pipe, elbow and tee branch} \tag{44}$$

$$\sigma_n = PL_m/2T \quad \text{for torispherical head} \tag{45}$$

and for torque and in-plane moment, the nominal stresses are, respectively:-

$$\sigma_n = M \times \text{outer radius} /I \tag{46}$$

and $$\sigma_n = T_o \times \text{outer radius} /I \tag{47}$$

where 'outer radius' and I refer to the parameters of the pipe or nozzle on which the load acts.

For each piping component, a computer program was written to manipulate the FEM stress data output, for load interaction and other calculations. It was based on the program TSTRESS written by Mistry [42]. The program FINALE.FOR which was used to analyze pipe bends is listed in Appendix B. The slight modifications to the programs for each component are due to different numbers of load categories and different locations of stress

distributions. The following procedure describes the program FINALE.FOR written for the pipe bends.

From the FE analysis of an elbow, three subsets of stress data were obtained, one for each load category of torque, pressure and moment. Assuming a linear load-stress relation and the absence of nonlinear load coupling, the six stress components, σ_x, σ_y, σ_z, τ_{xy}, τ_{yz} and τ_{zx}, at every node could be proportioned and summed algebraically for any combined load and loading category. These stresses were used to determine the von Mises effective stresses at all the nodes in the structure. The principal stresses σ_1, σ_2 and σ_3 at each node were obtained from the three equations of stress invariants, namely,

$$\sigma_1 + \sigma_2 + \sigma_3 = \sigma_x + \sigma_y + \sigma_z \tag{48a}$$

$$\sigma_1\sigma_2 + \sigma_2\sigma_3 + \sigma_1\sigma_3 = \sigma_x\sigma_y + \sigma_y\sigma_z + \sigma_z\sigma_x - \tau_{xy}^2 - \tau_{yz}^2 - \tau_{zx}^2 \tag{48b}$$

and $\quad \sigma_1\sigma_2\sigma_3 = \sigma_x\sigma_y\sigma_z + 2\tau_{xy}\tau_{yz}\tau_{zx} - \sigma_x\tau_{yz}^2 - \sigma_y\tau_{zx}^2 - \sigma_z\tau_{xy}^2 \tag{48c}$

from which the von Mises effective stress at each node, σ_{vM}, could be obtained:-

$$2\sigma_{vM}^2 = (\sigma_1 - \sigma_2)^2 + (\sigma_2 - \sigma_3)^2 + (\sigma_1 - \sigma_3)^2 \tag{49}$$

The computer program FINALE.FOR provides the following capabilities:-

1. Effective stress distribution on inner and outer surfaces, at elbow mid-section for any combined load. Determination of location and magnitude of the maximum effective stress.
2. Two-load interaction diagrams.
3. Three-load interaction diagrams.
4. Distribution of von Mises ESF, from individual loads.

The program is able to interpolate stresses for any given elbow geometry which is within the range of the present models under study. For a given elbow geometry, the program FINALE.FOR carries out a two dimensional cubic spline interpolation for the two interpolating parameters (D_m/T and bend ratio, b), from sixteen sets of data which were obtained from the FE analysis of sixteen elbow models. If adequate data were obtained from the FE analysis on tee branches (27 sets at least), a similar three dimensional interpolation

could be done for any given tee branch. The three independent interpolating parameters would then be the ratios D/T, d/D and t/T.

The main feature of the computer program is the ability to analyze load interaction behaviours of pipe bends. A load interaction diagram is drawn by combining the loads in various proportions to form a first yield locus. From the FEM stress data, the maximum von Mises effective stress for any load combination can be located and calculated by the program. By limiting the maximum effective stress to the yield stress of the material, the limiting combining loads can be found.

For any two interacting loads, a vector is formed from the maximum resultant effective stress. A yield point on the vector is located by calculating the factor required for the resultant stress to equal the yield stress. Other yield points are obtained by rotating the vector in an incremental step of 1 degree (by combining the interacting loads in various proportions) to form a locus of first yield. Negative moments imply that the nodal loads needed to induce the moments are applied in the opposing directions. The stress data for the negative moments were not regenerated but instead were taken from the results of positive moments, with the signs of the stresses reversed.

CHAPTER 4.   RESULTS AND DISCUSSION

4.1. PLAIN PIPES

4.1.1. FEM stress results

The accuracy of the load interaction depends entirely on results produced by the FEM. The stresses in the pipes from separate loads were calculated from Lame's theory. The comparison of the FEM results with the thick pipe solution for the models with extreme D/T ratios is summarised in Table 3. The difference between the two methods is negligible.

Table 3.   Stresses from FEM and theory.

Model	Load	Max. stress	Stresses (MPa) Theory	FEM
PIP1	Torque = 1 MN-m	shear	909.36	909.41
	Moment = 1 MN-m	axial	1818.73	1815.10
	Pressure = 1 MN/m^2	axial	5.628	5.645
		hoop	11.256	11.273
	Axial force = 1 MN	axial	114.25	114.25
PIP4	Torque = 1 MN-m	shear	316.15	316.16
	Moment = 1 MN-m	axial	632.29	630.30
	Pressure = 1 MN/m^2	axial	0.811	0.859
		hoop	1.621	1.658
	Axial force = 1 MN	axial	31.027	31.026

4.1.2. Load interactions

Figs. 15-20 show the interaction curves for load pairs $\bar{T_o}{:}\bar{P}$, $\bar{M}{:}\bar{P}$, $\bar{F}{:}\bar{P}$, $\bar{M}{:}\bar{T_o}$, $\bar{T_o}{:}\bar{F}$ and $\bar{M}{:}\bar{F}$ for varying D/T ratio. Figs. 21-24 show the comparisons between the FEM, theoretical, BS and Reilly's [4] experimental results, for pipe models PIP1 (D/T=5) and PIP4 (D/T=24.5). Table 4 shows the BS and the two yield formulations. The BS formulations are derived from the equations of hoop, axial, shear and equivalent combined stress.

The finite element method of predicting first yield gives accurate results. The BS uses the Tresca yield criterion and hence the results differ significantly for some load pairs. From the effective stress formulations, the von Mises and Tresca stresses tend to be equal if the intermediate principal stress approaches zero. This condition is not met if pressure is one of the interacting loads, hence the difference in yield prediction of the load pairs $\bar{T_o}{:}\bar{P}$, $\bar{M}{:}\bar{P}$ and $\bar{F}{:}\bar{P}$.

When a combined load causes a uniaxial stress system over the whole load range, the interaction is linear, otherwise the interaction is at least (conservatively) circular. When the location of first yield shifts between the inner and outer surfaces of the pipe at different load combinations, the interaction is made up of two separate relations which are dependent of the D/T ratio. Out of six load pairs, only the $\bar{T_o}{:}\bar{P}$ and $\bar{M}{:}\bar{P}$ pairs are influenced by D/T as shown in Figs. 15 and 16. The interaction diagrams are symmetrical in all quadrants, indicating that the maximum effective stress behaviour of the pipe does not depend on the signs of the loads.

Table 4.   Load interaction relations with von Mises and Tresca yield criteria using thick pipe theory - a comparison with the BS.

| | Thick cylinder theory | | BS 806 |
	von Mises	Tresca	
$\dfrac{\overline{T}_o}{P}$	$\overline{T}_o^2 + (R_i/R_o)^4\overline{P}^2 = 1$[a] $(R_i/R_o)^2\overline{T}_o^2 + \overline{P}^2 = 1$[b]	$\overline{T}_o^2 + 0.25(R_i/R_o)^2\overline{P}^2 = 1$[a] $0.25(R_i/R_o)^2\overline{T}_o^2 - 0.5\overline{P}^2 + 1.5\overline{P} = 1$[b]	$\overline{T}_o^2 + \overline{P}^2 = 1$
$\dfrac{\overline{M}}{P}$	$\overline{M}^2 + (R_i/R_o)^4\overline{P}^2 = 1$[c] $(R_i/R_o)^2\overline{M}^2 + \overline{P}^2 = 1$[b]	$\overline{M} + 0.5(R_i/R_o)^2\overline{P} = 1$[c] $\overline{P} = 1$[b]	$\overline{M} + \overline{P}d^2/2(d+t)^2 = 1$[c] $\overline{P} = 1$[b]
$\dfrac{\overline{F}}{P}$	$\overline{F}^2 + \overline{P}^2 = 1$	$\overline{F} + 0.5\overline{P} = 1$[d] $\overline{P} = 1$[b]	-
$\dfrac{\overline{T}_o}{M}$	$\overline{T}_o^2 + \overline{M}^2 = 1$	$\overline{T}_o^2 + \overline{M}^2 = 1$	$\overline{T}_o^2 + \overline{M}^2 = 1$
$\dfrac{\overline{T}_o}{F}$	$\overline{T}_o^2 + \overline{F}^2 = 1$	$\overline{T}_o^2 + \overline{F}^2 = 1$	-
$\dfrac{\overline{M}}{F}$	$\overline{M} + \overline{F} = 1$	$\overline{M} + \overline{F} = 1$	-

[a]   when torque load dominates
[b]   when pressure load dominates
[c]   when moment load dominates
[d]   when axial force dominates
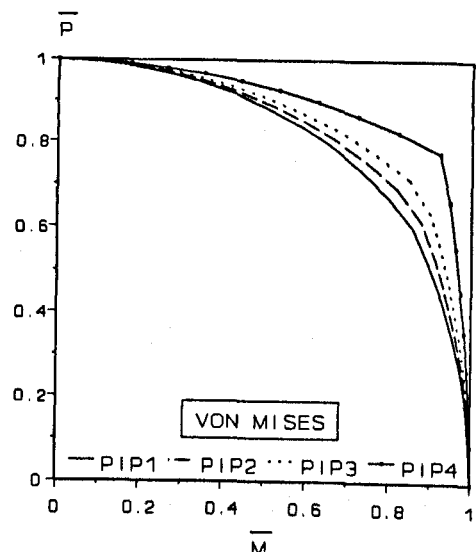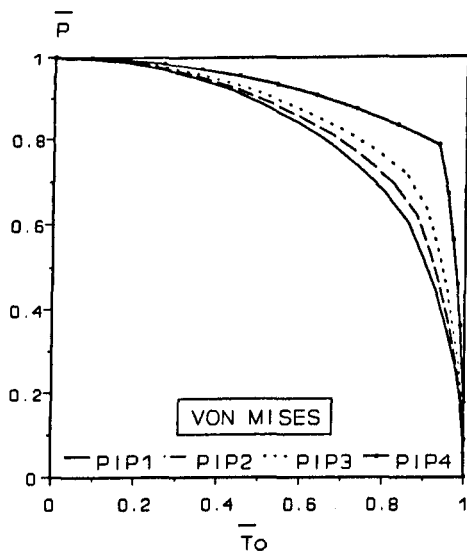
FIG. 15. TORQUE:PRESSURE INTERACTION

FIG. 16. MOMENT:PRESSURE INTERACTION

FIGS. 15-16.   EFFECT OF D/T ON FIRST YIELD LOAD INTERACTIONS OF PLAIN PIPES. (Note D/T for PIP1=24.5, PIP2=15, PIP3=10, PIP4=5).
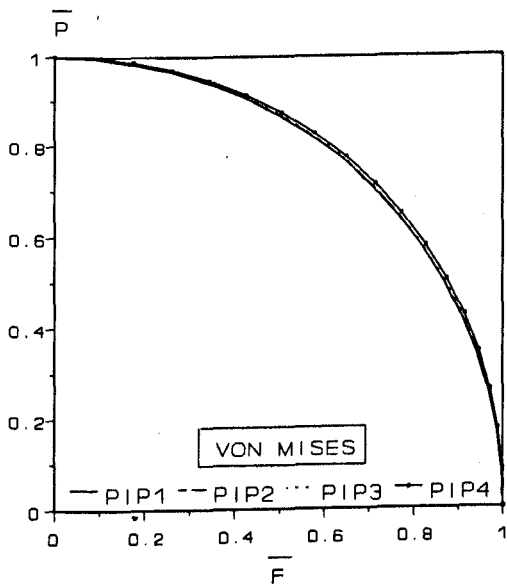
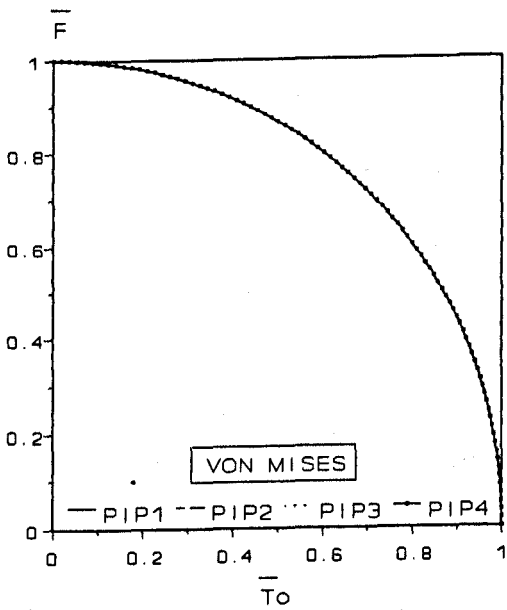FIG. 17. AXIAL FORCE:PRESSURE
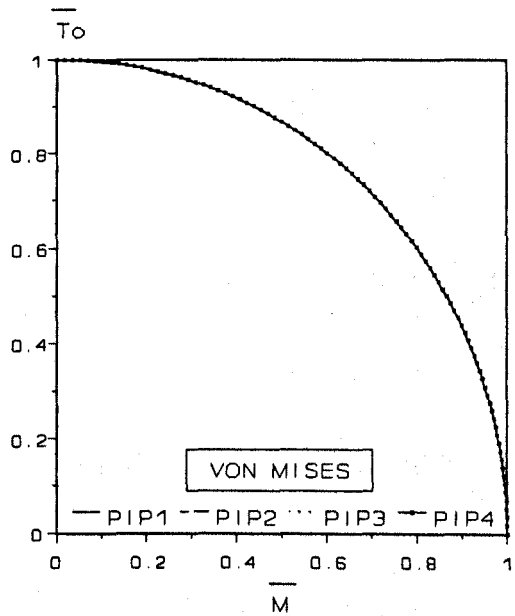
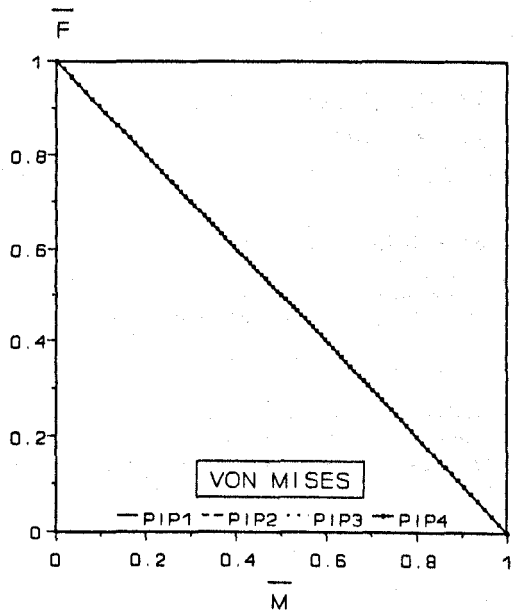FIG. 18. MOMENT:TORQUE

FIG. 19. TORQUE:AXIAL FORCE

FIG. 20. MOMENT:AXIAL FORCE

FIGS. 17-20.   EFFECTS OF D/T ON FIRST YIELD LOAD INTERACTIONS OF PLAIN
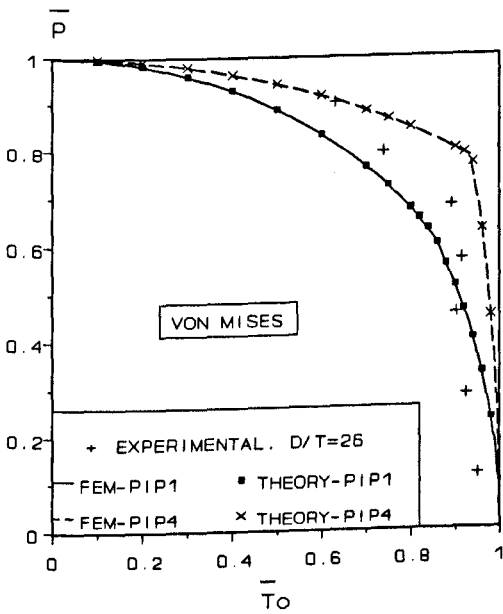PIPES. (Note D/T for PIP1=24.5, PIP2=15, PIP3=10 and PIP4=5).
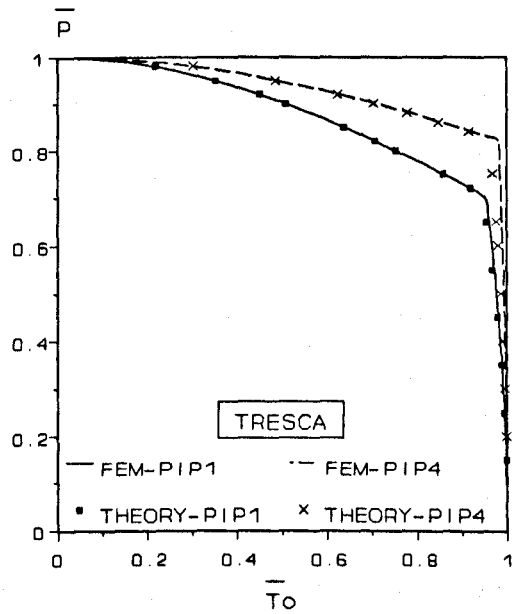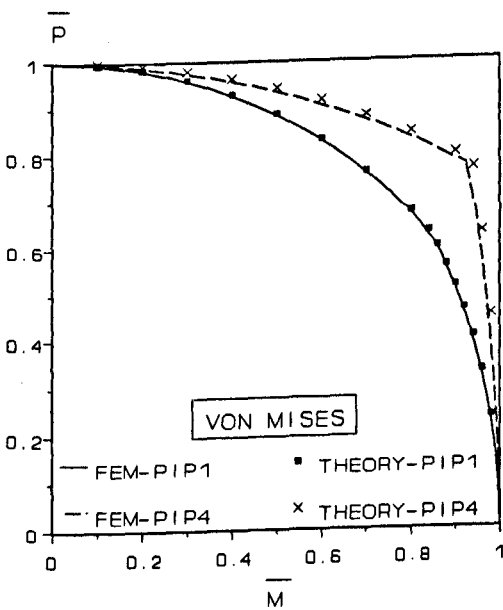
66

FIG. 21. TORQUE:PRESSURE

VON MISES

+ EXPERIMENTAL. D/T=26

— FEM-PIP1   ▪ THEORY-PIP1

-- FEM-PIP4   × THEORY-PIP4

$\overline{P}$ ... $\overline{T_o}$

FIG. 22. TORQUE:PRESSURE

TRESCA

— FEM-PIP1   ·— FEM-PIP4

▪ THEORY-PIP1   × THEORY-PIP4

$\overline{P}$ ... $\overline{T_o}$

FIG. 23. MOMENT:PRESSURE

VON MISES

— FEM-PIP1   ▪ THEORY-PIP1

·— FEM-PIP4   × THEORY-PIP4

$\overline{P}$ ... $\overline{M}$

FIG. 24. MOMENT:PRESSURE

TRESCA

▪ BS-PIP1   × BS-PIP4

— FEM-PIP1   ·— FEM-PIP4

$\overline{P}$ ... $\overline{M}$
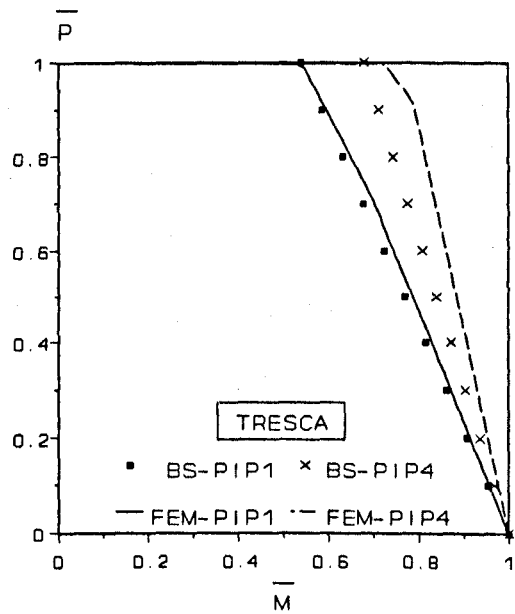
FIGS. 21-24. COMPARISON BETWEEN THEORETICAL AND FEM $\overline{T}_o:\overline{P}$ AND $\overline{M}:\overline{P}$ LOAD INTERACTIONS - VON MISES AND TRESCA CRITERIA. REILLY'S [4] EXPERIMENTAL TEST RESULT ALSO SHOWN. (Note D/T for PIP1=24.5, PIP2=15, PIP3=10 and PIP4=5).

4.1.2.1. Torque:Internal pressure

When a pipe is subjected to torque and internal pressure, the first yield is dependent on the D/T ratio of the pipe. From Fig. 15, as the pipe becomes thicker (lower D/T ratio), yielding occurs at higher loads. The yield loci predicted by the finite element method (Fig. 21) agree excellently with the thick pipe theory, for both PIP1 (D/T=24.5) and PIP4 (D/T=5). The location of yield shifts from the outer surface, when torque is dominant, to the inner surface when pressure is dominant and is marked by a sudden change of slope. Theoretically, the discontinuity may be explained by Eqns. (5) and (7) - it is more pronounced in thicker pipes (Fig. 15). The BS gives a circular interaction which agrees well with thinner pipes but the discrepancy with FEM increases as the pipes become thicker. Fig. 21 also shows the comparison with Reilly's [4] experimental tests on a pipe with D/T=26. When torque dominates, the test [4] indicated that yielding was reached earlier than predicted; this may be due to local buckling of the pipe. In fact, the trend of Reilly's results is closer to the Tresca criterion. The Tresca results in Fig. 22 are presented to show the difference between the FEM and the BS circular relation. The large discrepancy arises from the BS use of the mean diameter hoop stress, the neglect of radial stresses and the Code's assumption that the minimum stress is always zero. This means that the BS results will only approach the theoretical (and FEM) prediction when the pressure load dominates.

4.1.2.2. Moment:Internal pressure

The moment:pressure interaction from the FEM is identical to that of torque:pressure. Eqns. (9) and (10) give two sets of curves, each of which is applicable for a range of combined load. Fig. 16 shows a set of curves which are dependent on the D/T ratios. The results agree excellently with the maximum von Mises effective stresses which use thick pipe stresses. The BS interaction is different because the Tresca yield criterion being used does not consider the intermediate principal stress. When compared with the FEM Tresca criterion (Fig. 24), the

68

agreement is good, unlike the above $\overline{T}_o:\overline{P}$ interaction. In the $\overline{M}:\overline{P}$ interaction, stresses σ_1 and σ_2 are always positive so that the stress $\sigma_3(=0)$ is taken into account in both the BS and finite element methods. The implied thin pipe theory from the BS gives slight conservatism which, as expected, vanishes as the pipe becomes thinner. The derived Eqn. (24) from BS shows the effect of D/T and the derived Eqn. (26) shows that yielding is unaffected by moment when pressure dominates.

4.1.2.3. Axial force:Internal pressure

The FEM and theoretical interaction for the von Mises criterion shows a circular relation (Fig. 17). The Tresca criterion results in a bi-linear interaction which is not influenced by D/T ratio, i.e. when the force load is dominant, the linear relation is:-

$$\overline{F} + 0.5\overline{P} = 1 \qquad (50)$$

and when pressure is dominant, the relation is:-

$$\overline{P} = 1 \qquad (51)$$

At all values of combined loads, yielding occurs on the inner surface because the axial tensile force does not give preference to any particular yield location.

4.1.2.4. Moment:Torque

The FEM shows a circular interaction which is consistent with the theoretical von Mises. The BS (Eqn. (28)) and Tresca criterion shows a similar circular interaction. Yielding at all loads occurs on the outer surface of the pipe.

4.1.2.5. Torque:Axial force

The FEM results show circular interaction which is confirmed by thick and thin pipe analyses for both von Mises and Tresca criteria. Yielding occurs on the outer surface.

69

4.1.2.6. Moment:Axial force

The FEM shows a linear interaction. The thick and thin pipe analyses for both von Mises and Tresca criteria give a similar linear interaction. Yielding occurs on the outer surface.

4.2. PIPE BENDS

For initial stress verification, two models were considered in detail. The models EL05 and EL07 (see Table 2, page 45) have a bend ratio b=3 but with extreme D/T ratios of 150 and 20 respectively. The results of other elbows in the series are taken into consideration in the general discussion. Comparison with the energy method and standard design codes will reveal the adequacy of the FEM in predicting stresses in thick- and thin-walled elbows.

4.2.1. von Mises effective stresses

The von Mises ESFs are characterized by three factors, i.e. thickness, bend radius and mean diameter, which can be grouped into two parameters, b (=R/r) and D/T. The von Mises effective stress factor (ESF) distributions around the circumference at the elbow mid-section of elbows EL05 and EL07 are shown in Figs. 25-27. Due to torque (Fig. 25), maximum stresses occur on the outer surface with ESF peaks on either side of the crown, at $\theta=75°$ and 120°. The peaks are more pronounced in thinner (D/T ≥ 80) elbows. At the intrados and extrados, the ESFs do not vary much with elbow thickness but elsewhere the stresses increase with thinner elbows, with stresses on the outer surface greater than on the inner surface.

In Fig. 26, an in-plane moment gives the same response as in torque except that maximum stresses occur at $\theta=90°$. However, in thicker elbows, there is a tendency for stresses on the outer surface at the intrados to approach the high stresses at the crown. Increasing the thickness and bend radius result in levelling of the peaks and reduction of stresses. For

70

internal pressure (Fig. 27), the stresses on both surfaces increase gradually from the extrados to the intrados, with stresses on the inner surface higher than on the outer surface but the stress gradient across the wall becomes smaller as the elbow gets thinner.

The pipe factor λ is defined as:-

$$\lambda = (T/r)(R/r) \qquad or \qquad \lambda = (T/r)b$$

If b is constant, the pipe factor λ is then inversely proportional to the D/T ratio. On many occasions, in trying to show the effect of the bend ratio and pipe factor on stresses, many analysts present the stress variation with λ and b, as in Figs. 28-30. For torque and moment loads, the stresses increase with decreasing λ, but there is no definite trend of stress variation with b because λ is not an independent parameter which affects stress. If λ is kept constant, varying b results in a change of D/T too. This may explain the conflicting reports on the effect of λ on stress although the effect from D/T ratio and b (=R/r) is very clear. Fujimoto and Soh [27], Natarajan and Blomfield [11] and Thomson and Spence [86] reported a slight increase of stress with increasing bend radius when the pipe factor is kept constant. On the other hand, the stress indices from BS [5] as well as Turner and Ford [87] show the opposite trend of stress increase. When the ESF results are presented as functions of D/T and b (Figs. 31-33), a definite trend is observed, i.e. the ESFs increase with decreasing bend ratio b. For torque and moment loads, when the pipe becomes thicker (low D/T), the ESFs becomes less affected (in absolute terms only) by the pipe bend, as shown in Figs. 31 and 32. It is also observed that in very thin pipes (D/T > 150), the maximum ESFs tend to be less affected by the D/T ratio. For pressure loading, the D/T ratio does not influence maximum ESFs but when the pipe becomes thicker (D/T > 40), the ESFs increase appreciably with decreasing D/T (Fig. 33). A tabular comparison of maximum ESFs due to the three load cases is shown in Table 5.
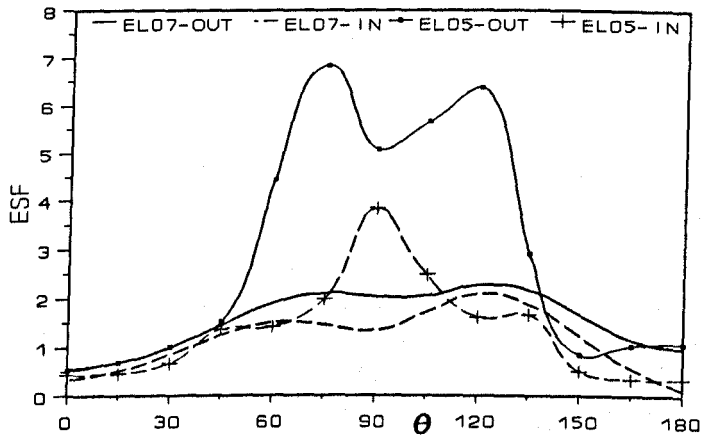
FIG. 25.   MISES STRESS ON INNER AND OUTER SURFACES. MODELS EL05
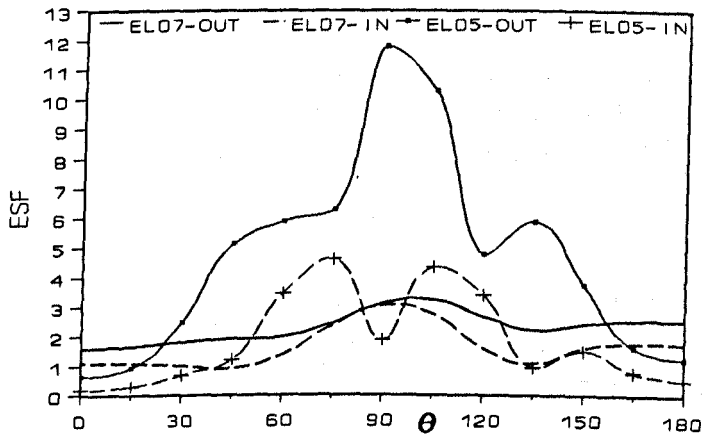AND EL07 SUBJECTED TO TORQUE LOADING.

FIG. 26.   MISES STRESS ON INNER AND OUTER SURFACES. MODELS EL05
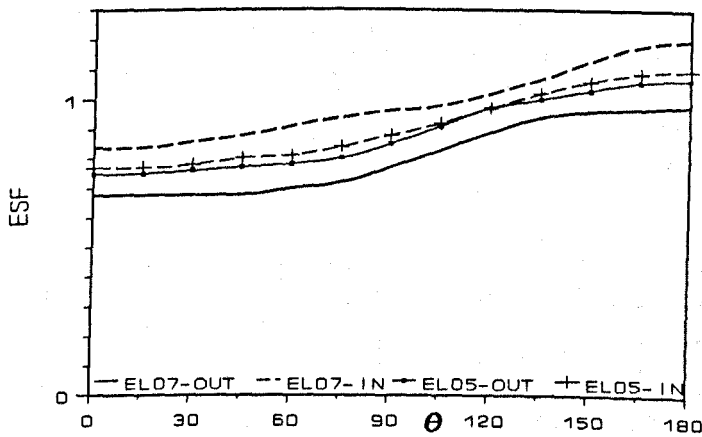AND EL07 SUBJECTED TO MOMENT LOADING.

FIG. 27.   MISES STRESS ON INNER AND OUTER SURFACES. MODELS EL05
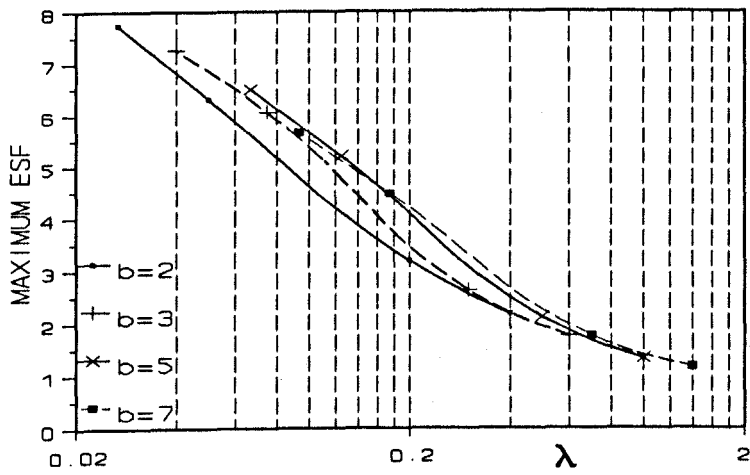AND EL07 SUBJECTED TO PRESSURE LOADING.

72

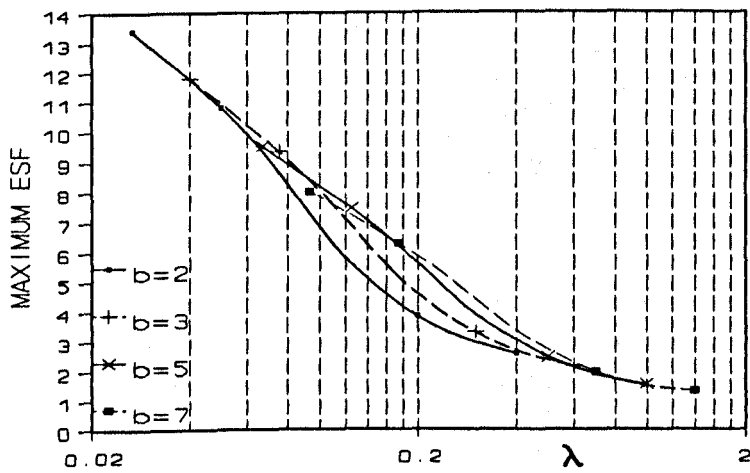FIG. 28.   EFFECTS OF b AND λ ON MAXIMUM ESF. TORQUE LOADING.

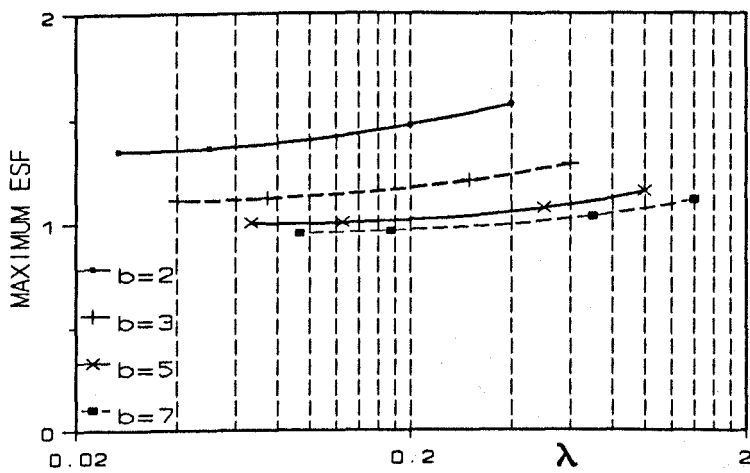

FIG. 29.   EFFECTS OF b AND λ ON MAXIMUM ESF. MOMENT LOADING.

FIG. 30.   EFFECTS OF b AND λ ON MAXIMUM ESF. PRESSURE LOADING.

73
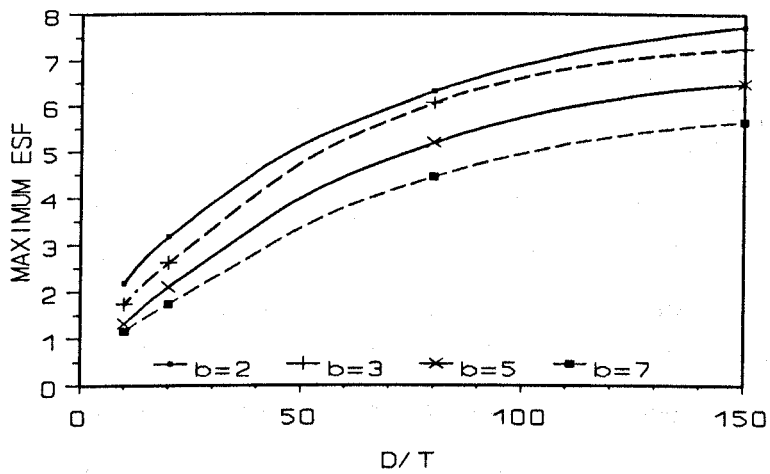
FIG. 31.   EFFECTS OF b AND D/T ON MAXIMUM ESF. TORQUE LOADING.
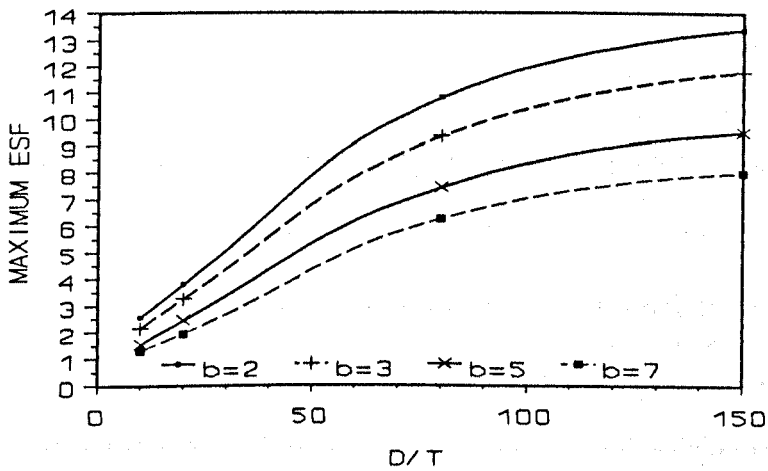
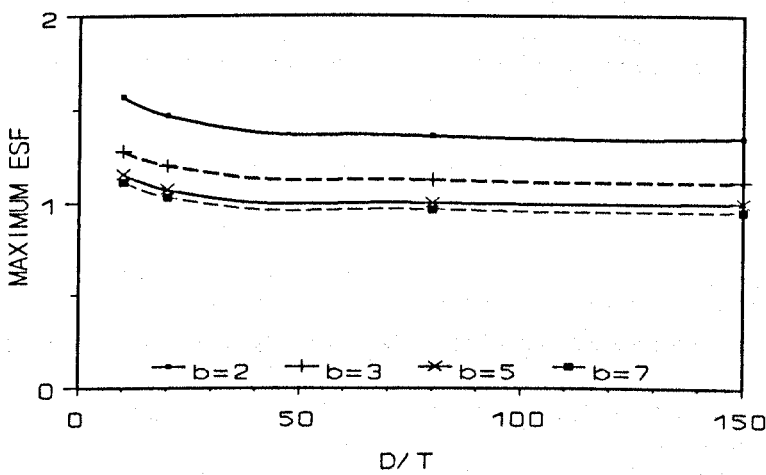FIG. 32.   EFFECTS OF b AND D/T ON MAXIMUM ESF. MOMENT LOADING.

FIG. 33.   EFFECTS OF b AND D/T ON MAXIMUM ESF. PRESSURE LOADING.

Table 5.   Maximum von Mises ESFs of elbows EL01 to EL16.

Model	Max.	Mises	ESF	Model	Max.	Mises	ESF
	Torque	Moment	Pressure		Torque	Moment	Pressure
EL01	7.74	13.39	1.35	EL09	6.48	9.5	1.0
EL02	6.33	10.8	1.36	EL10	5.19	7.44	1.0
EL03	3.17	3.8	1.47	EL11	2.10	2.44	1.07
EL04	2.17	2.56	1.57	EL12	1.32	1.53	1.15
EL05	7.25	11.79	1.11	EL13	5.65	7.99	0.95
EL06	6.05	9.33	1.12	EL14	4.45	6.24	0.96
EL07	2.61	3.25	1.20	EL15	1.74	1.93	1.03
EL08	1.74	2.14	1.28	EL16	1.16	1.30	1.11

If the von Mises yield criterion is used, yield occurs in the elbow when the maximum Mises effective stress at any location approaches the yield stress of the material. This is on assumption that elastic buckling does not precede first yield. In Lang's [88] theoretical analysis of elbows subjected to in-plane moment, he attempted to define thick and thin elbows from the locations of first yield. In thick elbows, Ref. [88], yielding is initiated by the maximum hoop stress on the inner surface at $\theta = 90^\circ$ and in thin elbows, initial yielding starts either on the inner surface at the extrados or on the outer surface at the intrados because of maximum axial stress at this location. By equating the stresses at these locations, Lang defined thick and thin elbows by the transition point given by the equation,

$$2\epsilon - \frac{v\eta^2}{24\epsilon^3} \frac{[144v^2 - 399v + 165]}{64v} - \frac{\eta^2}{32\epsilon}(6 + 5v^2 - 6v) + 15v\eta = 0 \tag{52}$$

where $\epsilon = T/2r$, $\eta = r/R$ and v is Poisson's ratio.

A thick elbow mode of yielding occurs when the left hand side of the above equation is greater than zero, otherwise a thin elbow mode of yielding occurs. However, Lang's finding does not agree with the present study. From the present study, the axial stresses at the intrados or extrados approach zero values.

4.2.2. Hoop and axial stresses

The hoop and axial stress distribution at the elbow mid-section of models EL05 and EL07 are shown in Figs. 34-45. Although the stresses are plotted for the range of $\theta = 0°$ to 180°, it may be taken that the stress distribution is symmetrical about the intrados-extrados plane for moment and pressure loadings, and antisymmetrical for torque loading. The FEM results are compared to the theoretical analysis of Rodabaugh and George [15] and the ASME [28] design code.

For torque loading, the hoop and axial stresses for models EL05 and EL07 are shown in Figs. 34, 35, 40 and 41. In general, stresses are higher in thinner pipes and the hoop stresses are slightly higher than axial stresses but all the stresses are negligible at the intrados and extrados. The largest stress is the hoop stress on the outer surface which peaks at hoop locations of $\theta \approx 60°$ and $\theta \approx 125°$ but in thicker pipes, the hoop stress on the inner surface at $\theta \approx 125_o$ may approach the maximum stress. The maximum axial stress occurs on the outer surface at $\theta \approx 105°$. Longer bend radius does not change the distribution trend but lowers the overall stress magnitude.

Due to in-plane closing moment, the maximum stress is the hoop stress at the outer surface of the crown. As the elbow becomes thicker, the hoop stresses at the outer surface of the intrados as well as at the inner surface of the crown may approach the maximum stress. The maximum axial stress occurs on the outer surface at $\theta \approx 75°$ but in thicker elbows, the outer axial stress at about $\theta \approx 135°$ may approach the maximum value. The stresses at the intrados and extrados of thin elbows approach zero but reach peak values in thick elbows. When the bend radius becomes larger, the main difference occurs at the intrados and extrados of the elbows. In elbows with large b, the outer fibres are not easily displaced towards the centre of the pipe (compared to small radius elbows), thus the fibres at the extrados and intrados

experience higher additional tensile and compressive axial stresses respectively. The hoop stresses at these locations are not lowered because of the Poisson's effect of axial stresses. Elsewhere, the effect of increasing b results in lowering of stresses.

Due to pressure loading, the hoop and axial stresses are not affected significantly by pipe thickness and bend ratio. The hoop stresses increase very slightly from the extrados to the intrados, with stresses on the inner surface higher than on the outer surface. The axial stresses on the inner and outer surfaces are equal and remain unchanged in the hoop direction.

The FEM hoop and axial stresses are compared to theoretical results which are computed from the energy method of Rodabaugh and George [15] and Subsection NB-3685 of ASME Section III [28] design code. The energy method [15] has been described in Section 2.3. For moment loading (Figs. 36, 37, 42 and 43), the FEM results for the thicker model EL07 are in good agreement with theory but for the thinner model EL05, the energy theory [15] can overpredict stresses by more than 100%. For torque loading, the theoretical stresses are higher than the FEM especially for the thinner model. For pressure, the stresses predicted by ASME [28] are satisfactory. Thin elbows are likely to suffer from geometric nonlinear behaviour when subjected to moment and torsional loads, resulting in higher stresses than predicted by the present linear analysis. Elbow EL05 has geometric parameters $\lambda = 0.04$ and $D/T = 150$, which accounts for the large stress discrepancies with theory [15]. The agreement with model EL07 is satisfactory for moment and pressure loads but fair with torsional moment.
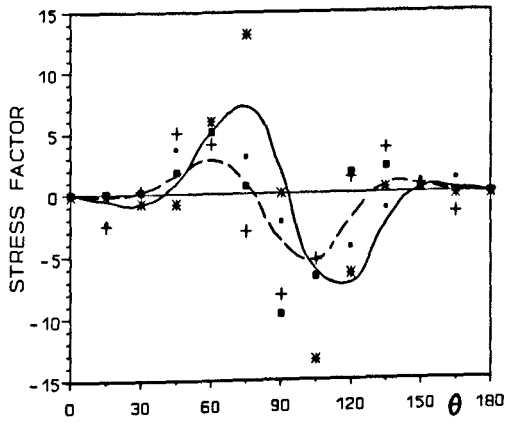
FIG. 34. HOOP AND AXIAL STRESSES ON OUTER SURFACE.
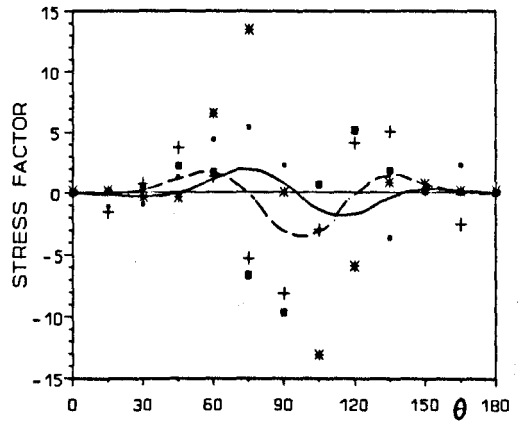MODEL EL05 SUBJECTED TO TORQUE.

FIG. 35. HOOP AND AXIAL STRESSES ON INNER SURFACE.
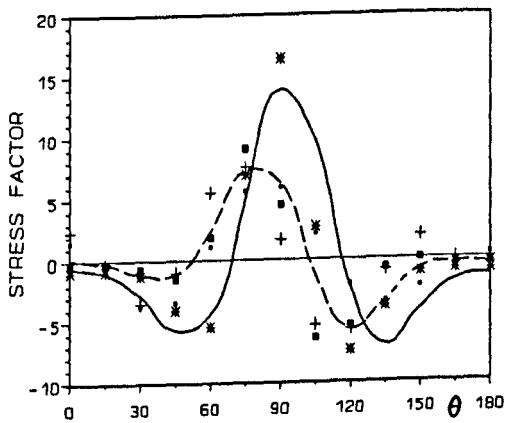MODEL EL05 SUBJECTED TO TORQUE.

FIG. 36. HOOP AND AXIAL STRESSES ON OUTER SURFACE.
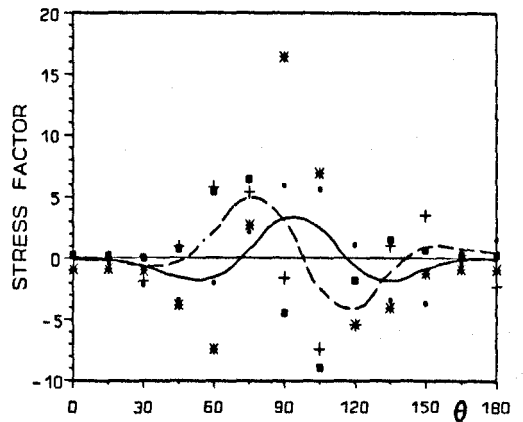MODEL EL05 SUBJECTED TO MOMENT.

FIG. 37. HOOP AND AXIAL STRESSES ON INNER SURFACE.
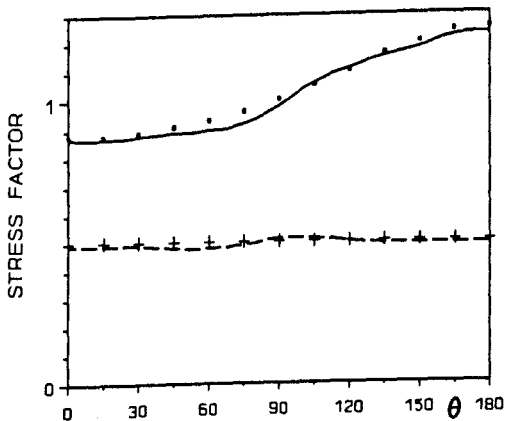MODEL EL05 SUBJECTED TO MOMENT.

FIG. 38. HOOP AND AXIAL STRESSES ON OUTER SURFACE.
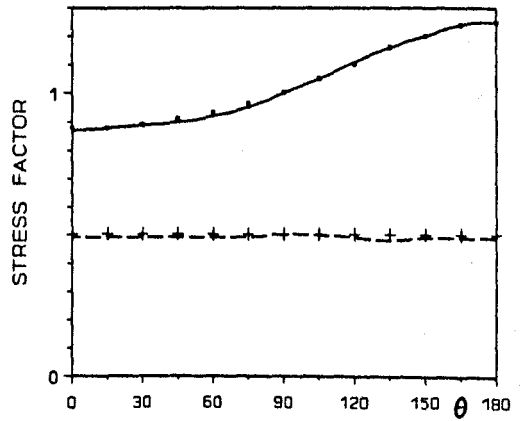MODEL EL05 SUBJECTED TO PRESSURE.

FIG. 39. HOOP AND AXIAL STRESSES ON INNER SURFACE.
MODEL EL05 SUBJECTED TO PRESSURE.

Key to markers   — FEM hoop   - - - FEM axial   ■ ASME [28] hoop
    + ASME [28] axial   * Rodabaugh [15] hoop   ■ Rodabaugh [15] axial
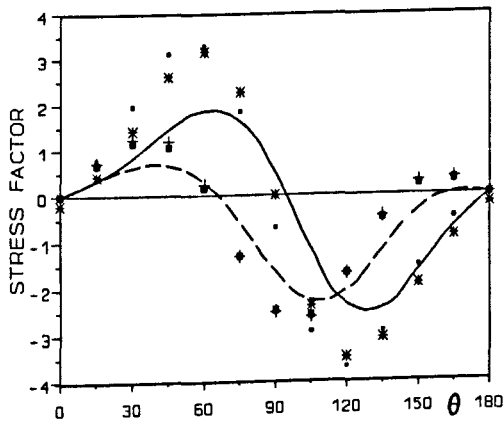
78

FIG. 40. HOOP AND AXIAL STRESSES ON OUTER SURFACE.
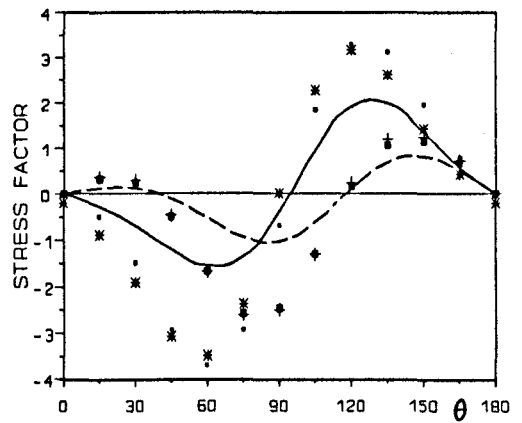MODEL EL07 SUBJECTED TO TORQUE.

FIG. 41. HOOP AND AXIAL STRESSES ON INNER SURFACE.
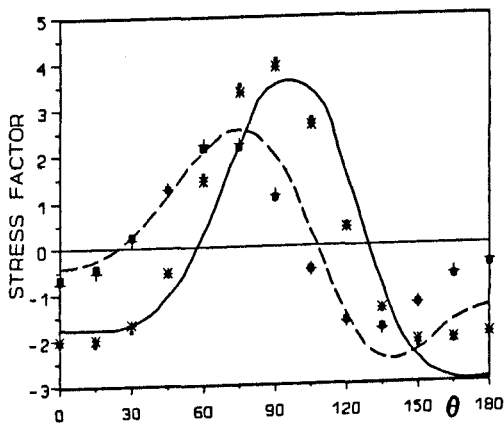MODEL EL07 SUBJECTED TO TORQUE.

FIG. 42. HOOP AND AXIAL STRESSES ON OUTER SURFACE.
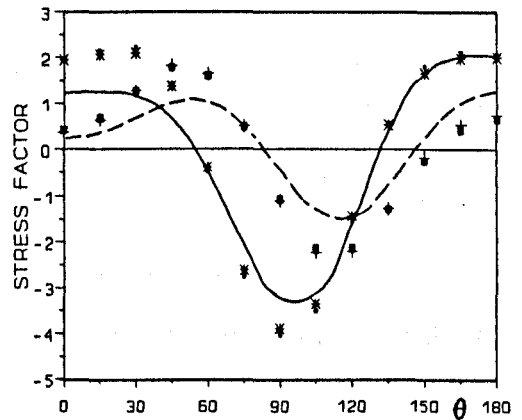MODEL EL07 SUBJECTED TO MOMENT.

FIG. 43. HOOP AND AXIAL STRESSES ON INNER SURFACE.
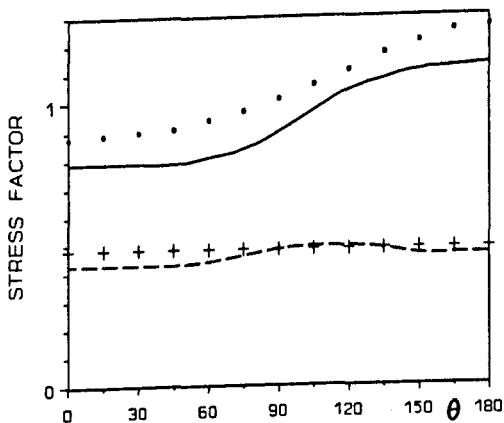MODEL EL07 SUBJECTED TO MOMENT.

FIG. 44. HOOP AND AXIAL STRESSES ON OUTER SURFACE.
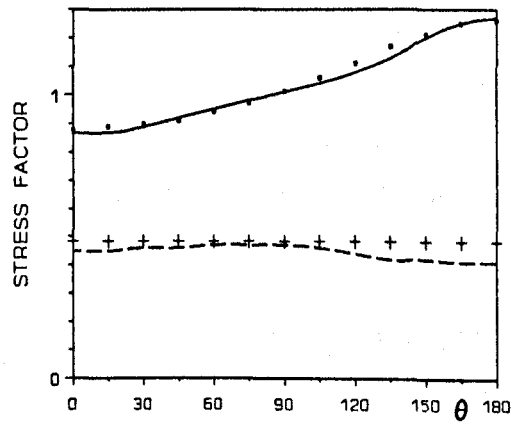MODEL EL07 SUBJECTED TO PRESSURE.

FIG. 45. HOOP AND AXIAL STRESSES ON INNER SURFACE.
MODEL EL07 SUBJECTED TO PRESSURE.

Key to markers   — FEM hoop   - - - FEM axial   ■ ASME [28] hoop

+ ASME [28] axial   * Rodabaugh [15] hoop   ■ Rodabaugh [15] axial

79

Due to torque or moment loading on thick elbows, the hoop stress distributions on the inner and outer surfaces have approximately the same magnitude but opposite signs, whereas in thin elbows the hoop stresses are equal in sign. The stress difference between the outer and inner surfaces can be used to interpret bending and membrane stresses induced by external loads. Hence, thicker elbows are subject to more bending and the thinner elbows to more membrane stresses in the hoop direction.

Some authors place great importance on the exact location of maximum axial or hoop stresses and how the stress peaks move along the hoop direction as the geometric parameters vary. It is detected here that the stress peaks shift closer to the crown as the elbow becomes thinner. With respect to this, the FEM shows good agreement with the findings of Fujimoto and Soh [27] and Sobel and Newman [89]. Chan and Boyle [90] compared their simple analysis with Thomson's [30] theoretical and experimental results and remarked on a 7° shift of the maximum axial and hoop stresses. In the FEM, the exact locations of the stresses may vary with the meshing and mesh refinement. Findlay and Spence [16] performed theoretical and experimental tests on elbows with in-plane moment loading. Their experiments were limited to long radius elbows with λ between 0.1 and 1.0. Their finding of the positions of the maximum hoop stress is consistent with the present study. In another analysis, Thomson and Spence [86] found that due to in-plane bending, the maximum hoop stress occurs at $\theta = 95°$ which was said to increase with radius ratios. The FEM shows that depending on λ, this location is either at $\theta = 90°$ or at $\theta = 180°$ but other authors specifically give the location at $\theta = 90°$. The ASME [28] code implies that the position to be $\theta = 90°$ and experimental works of Imamasa and Uragami [91] gave $\theta = 85°$.

Figs. 46 and 47 shows the variation of outer hoop stresses (at the crown and elbow mid-section) with b and λ. In fact the variations of hoop and axial stresses with λ and b from the three load cases are similar to the ESF variation. The graphs are presented in a similar way as other analysts to show the reversal of maximum stresses in long and short radii elbows for different ranges of λ. For torque and moment loadings, when λ is small, maximum hoop stresses occur in short radius elbows whereas if λ is high, they occur in long radius elbows. Table 6 shows the range of λ when the maximum hoop stress changes over between short and long radii elbows. For torque and moment, the hoop stress is taken at the outer surface of the crown and for pressure, the inner surface of the intrados. A similar observation was also reported by Fujimoto and Soh [27]. Their finite element analysis of elbows with b=2 and 3 resulted in a changeover point of λ=0.03. The same analysis was carried out to see the effect of D/T and b on hoop stresses. Similar to the case of maximum ESF, the hoop stress increases with decreasing b or increasing D/T.

Table 6.   Effect of b and λ on σ_h.

Load	Range of λ	Maximum hoop stress in:-
Torque	$\lambda < 0.12$ $\lambda > 1.4$	short radius elbow long radius elbow
Moment	$\lambda < 0.04$ $\lambda > 0.18$	short radius elbow long radius elbow
Pressure	all values of λ	short radius elbow
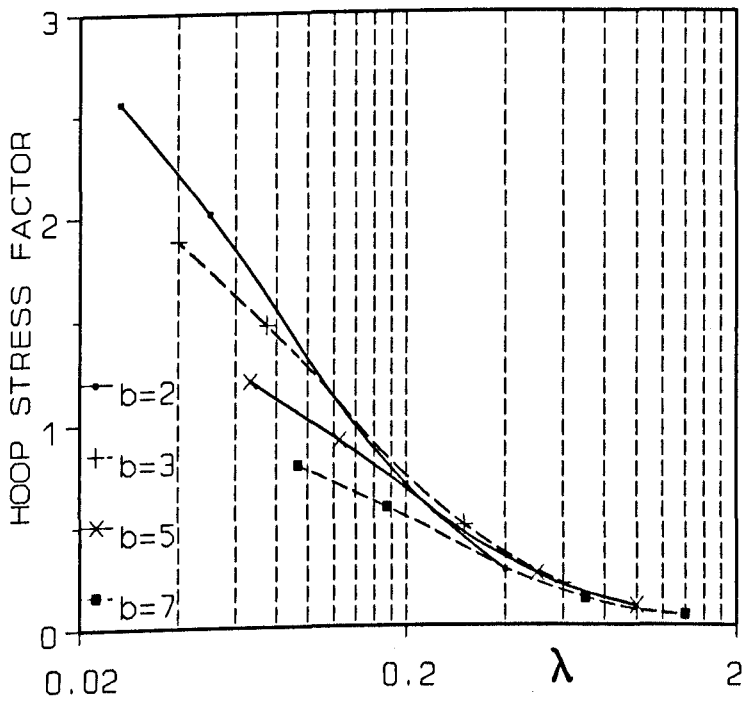
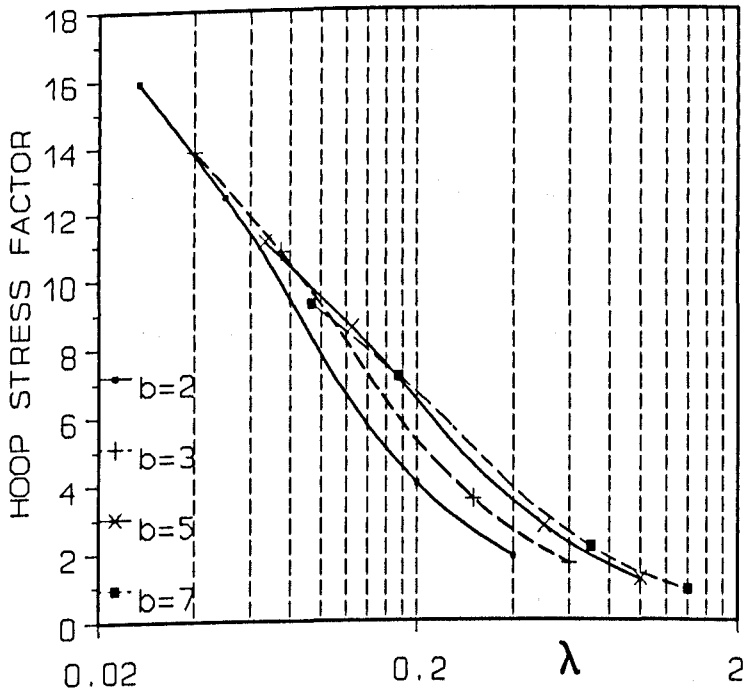FIG. 46.   EFFECTS OF b AND λ ON HOOP STRESS. TORQUE LOADING.

FIG. 47.   EFFECTS OF b AND λ ON HOOP STRESS. MOMENT LOADING.

82

4.2.3. von Mises ESFs along axial direction of bend

The end conditions of the curved section affect elbows with small pipe factors. The tangent pipes resist ovalization of the cross-section so that the stresses near the ends of the elbow are lower than at the mid-section where deformation is largest. When torque acts on the elbow, maximum stresses occur between the mid-section and the end which has pure out-of-plane moment. For pressure loading there is no ovalization and the stresses do not increase along the axial direction of the curved section.

Figs. 48 and 49 show the von Mises ESF distributions, on the outer surface, along the axial (meridional) direction of the bend. For torque and moment loads, the stresses are taken along the crown and for pressure, along the intrados. Due to torque loading, the ESF peaks at a section nearer to the elbow end which experiences pure out-of-plane bending moment. For both elbow models, these stress peaks, which occur at $\phi \approx -20°$, are about three times those at the torque end. The ESF peaks shift slightly towards the elbow mid-section as the elbow becomes thinner and as b decreases. In-plane moment load produces symmetrical distributions about the elbow mid-section with ESF peaks at $\phi = 0°$. These peaks are about 1½ times those at the end of the bends, irrespective of pipe thickness. For pressure loading, the ESFs do not vary along the axial direction of the bend, although in thicker pipes there is a tendency for the overall ESF in the bend to be slightly higher than in the tangent pipes.

The ASME [28] rules do not consider the effects of tangent pipes, resulting in overprediction of stresses, i.e. more conservative stresses, but if geometrical non-linearities are considered in the FEM, these results should agree well. The bend radius too affects the interaction between the end effects and the ovalization at the curved section. The ESFs (at the outer surface of the crown) in elbows EL13 and EL16 are reduced by about 50% from the mid-

section to the elbow ends, while in models EL01 and EL04, the reduction is about 35%. The pipe thickness does not significantly affect the stress reduction from the curved section to the tangent pipe junctions.
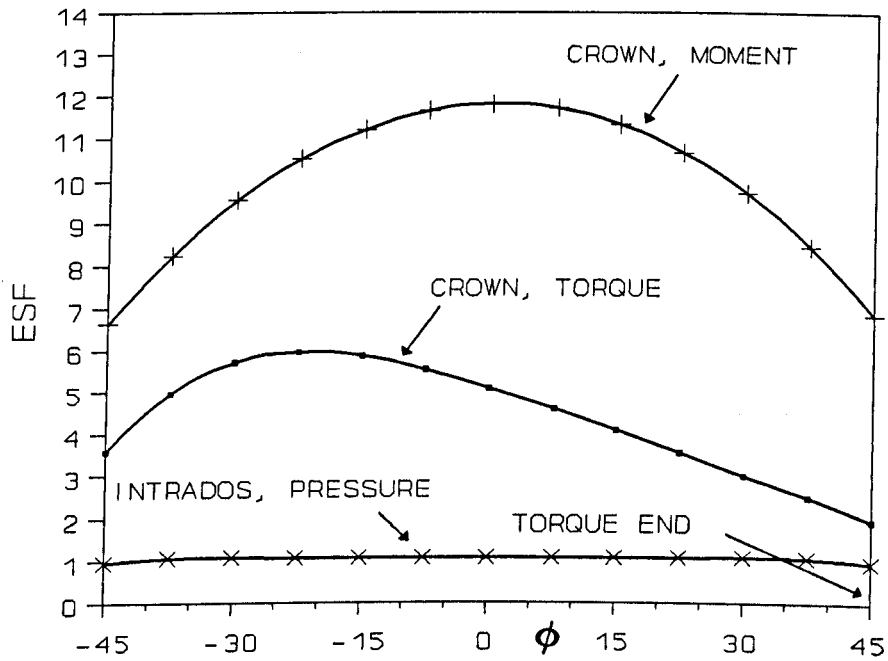

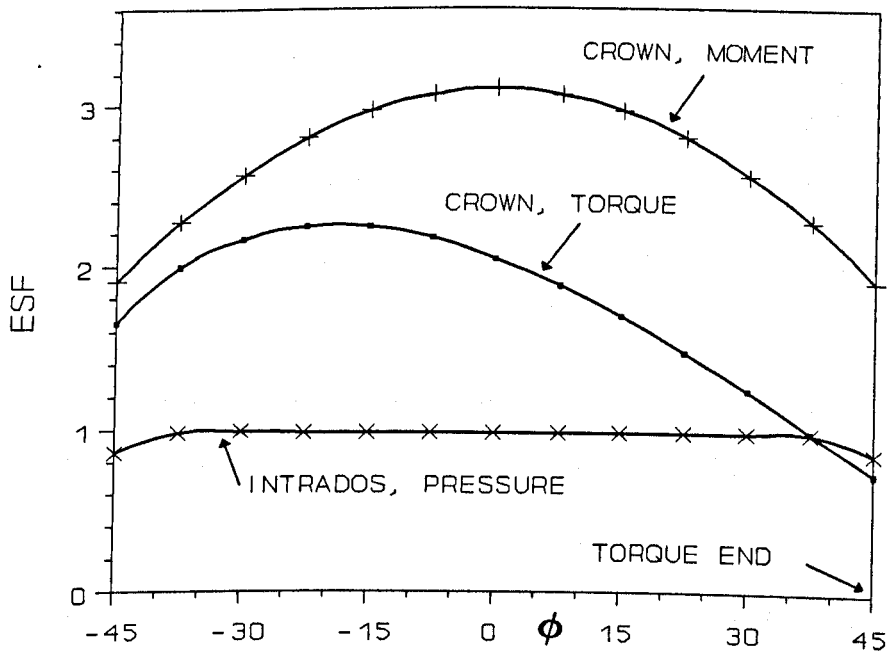FIG. 48. MISES STRESS DISTRIBUTION IN AXIAL DIRECTION OF ELBOW EL05.

FIG. 49. MISES STRESS DISTRIBUTION IN AXIAL DIRECTION OF ELBOW EL07.

84

4.2.4. Stress indices from Codes

The stress indices C_1 and C_2 in ASME [28] are essentially maximum elastic stress factors due to pressure and moment loads respectively. They are expressed in terms of the elbow geometric parameters. The symbols used are defined in ASME [28]. From Subsection NB-3683.7 of ASME III [28] code, the stress indices C_1 and C_2, for pressure and moment loading respectively, are:-

$$C_1 = (2R-r_m)/2(R-r_m) \tag{53}$$

$$C_2 = 1.95/\lambda^{2/3} \tag{54}$$

The BS 806 [5] code presents the axial and hoop stress factors for in-plane and out-of-plane moments in graphical forms. For the BS code, the hoop stress factors are selected as they are the larger values for the range of elbows under study. Table 7 compares the maximum ESF from the FEM with the stress indices from the ASME and BS codes.

From Table 7, the ASME and BS results are quite similar in the way they differ from the FEM results at various values of D/T and b. The table shows the overall conservatism of the Codes especially for torque loading. The discrepancies between the FEM results and the Codes become larger as the elbows get thinner and the bend radii get smaller. For in-plane moment, for elbows with $D/T \geq 80$ and $b \leq 3$, the Codes stress factors are always higher than the FEM values by 17.5-72%. From Fujimoto and Soh's [27] examination, the ASME code formulae overestimate stress by about 40% for lower values of the pipe factor. For torque loading, for $D/T \geq 80$, the Codes stress factors are higher by at least 40%, for all bend radius ratios. The Codes emphasise the increase of stress index as λ decreases because of progressive flattening of the cross-section. The ASME stress index for pressure C_1 does not differ much with the FEM results; the stress varies with D/T but not with b.

4.2.5. FEM first yield load interaction

Figs. 50-52 show the first yield interaction diagrams for load pairs $\bar{M}:\bar{T}_o$, $\bar{T}_o:\bar{P}$ and $\bar{M}:\bar{P}$ drawn from linear superposition of individual effects. For each load pair, the elbows are grouped into their respective bend ratio b, hence the curves in each graph show the effect of D/T ratio on first yield. From Fig. 50, the pipe thickness does not seem to affect first yield in a particular trend nor does it result in an appreciable increase or decrease of the maximum ESF. The bend radius slightly affects the maximum ESF, with larger values of b result in a lower ESFs. The interaction is best represented by a circular relation:-

$$\bar{M}^2 + \bar{T}_o^2 = 1 \tag{55}$$

Table 7.   Maximum stress factors from FEM and the Codes.

Model	Method	Max.	stress	factor[1]
		Torque	Moment[a]	Pressure
EL01	FEM	7.74	13.39	1.35
	ASME	21.85	21.85	1.5
	BS	19.5	23.0	
EL02	FEM	6.33	10.8	1.36
	ASME	14.37	14.37	1.5
	BS	14.0	15.0	
EL03	FEM	3.17	3.8	1.47
	ASME	5.7	5.7	1.5
	BS	6.2	6.2	
EL04	FEM	2.17	2.56	1.57
	ASME	3.59	3.59	1.5
	BS	4.3	4.0	
EL05	FEM	7.25	11.79	1.11
	ASME	16.67	16.67	1.25
	BS	14.5	17.0	
EL06	FEM	6.05	9.33	1.12
	ASME	10.96	10.96	1.25
	BS	10.0	11.5	
EL07	FEM	2.61	3.25	1.20
	ASME	4.35	4.35	1.25
	BS	4.4	4.5	
EL08	FEM	1.74	2.14	1.28
	ASME	2.74	2.74	1.25
	BS	2.9	2.9	

Table 7(contd.). Maximum stress factors from FEM and the Codes.

Model	Method	Max.	stress	factor[1]
		Torque	Moment[a]	Pressure
EL09	FEM	6.48	9.5	1.0
	ASME	11.86	11.86	1.25
	BS	10.7	11.5	
EL10	FEM	5.19	7.44	1.0
	ASME	7.8	7.8	1.25
	BS	6.6	7.8	
EL11	FEM	2.10	2.44	1.07
	ASME	3.1	3.1	1.25
	BS	2.9	3.0	
EL12	FEM	1.32	1.53	1.15
	ASME	1.95	1.95	1.25
	BS	1.9	1.8	
EL13	FEM	5.65	7.99	0.95
	ASME	9.48	9.48	1.08
	BS	8.4	9.6	
EL14	FEM	4.45	6.24	0.96
	ASME	6.23	6.23	1.08
	BS	5.4	6.0	
EL15	FEM	1.74	1.93	1.03
	ASME	2.47	2.47	1.08
	BS	2.1	2.2	
EL16	FEM	1.16	1.30	1.11
	ASME	1.56	1.56	1.08
	BS	1.3	1.2	

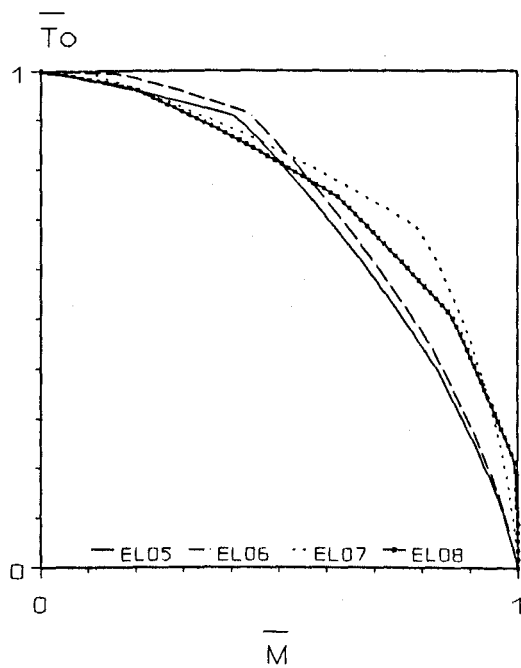[1] for FEM, maximum Mises effective stress factor
for BS, maximum hoop or axial stress factor
for ASME, maximum hoop stress factor

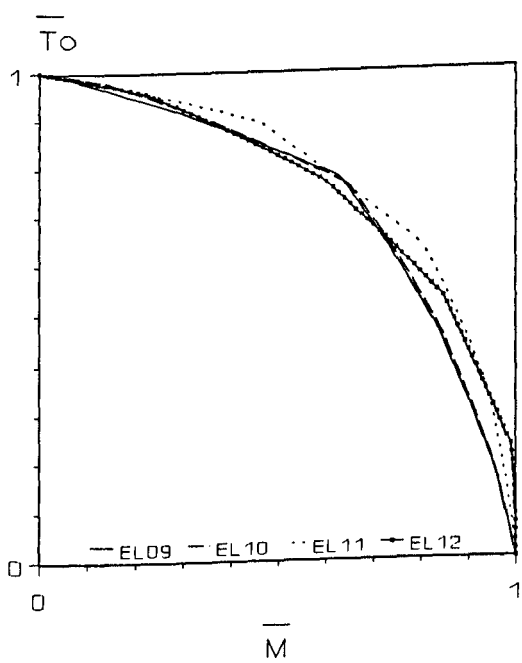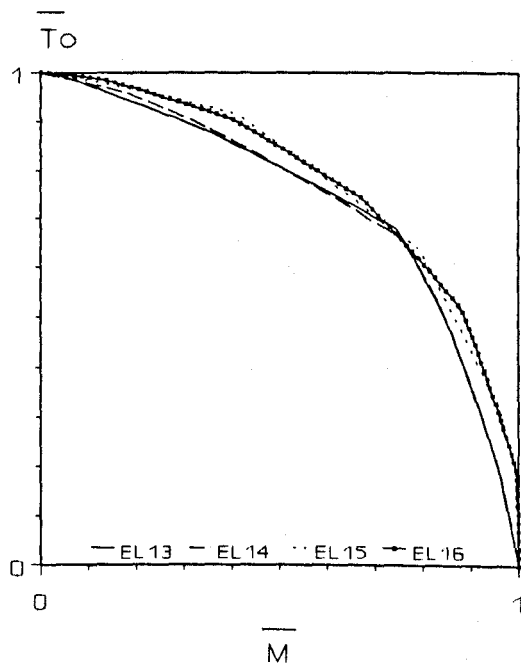[a] a closing moment is taken to be positive, and an opening moment to be negative
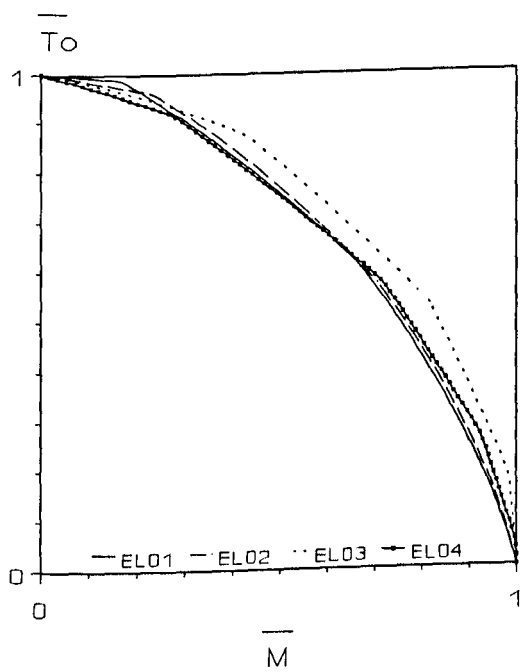
(a) b=2

(b) b=3
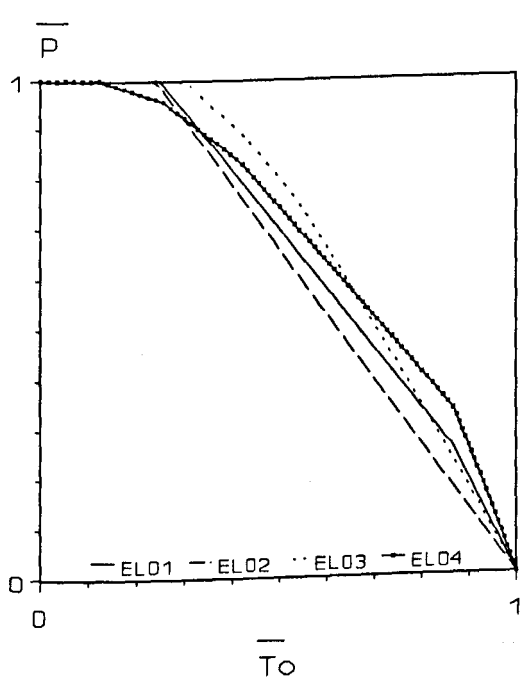
(c) b=5

(d) b=7

FIG. 50.   EFFECTS OF D/T AND b ON MOMENT:TORQUE INTERACTIONS.

88
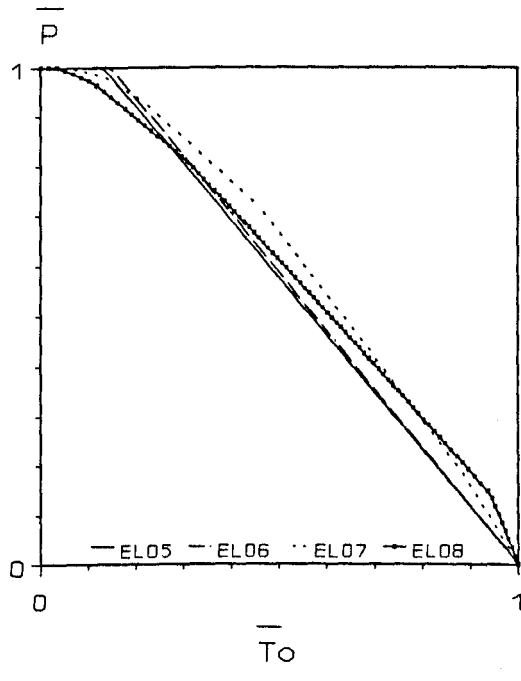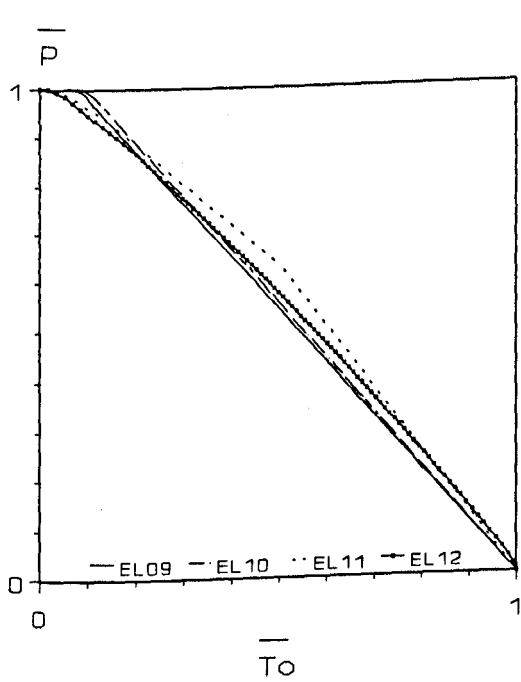
FIG. 51.   EFFECTS OF D/T AND b ON TORQUE:PRESSURE INTERACTIONS.

89
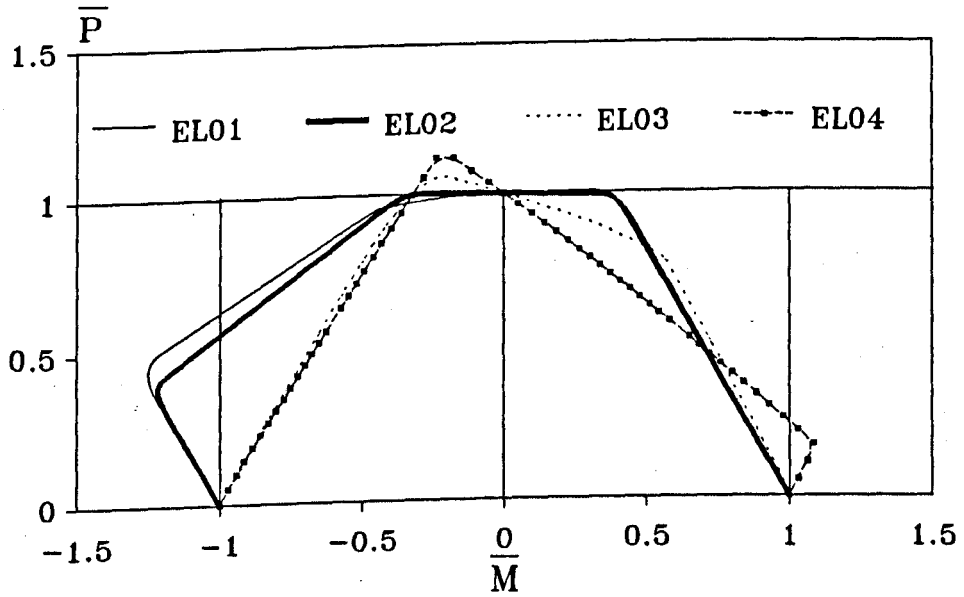
(a) b=2

(b) b=3
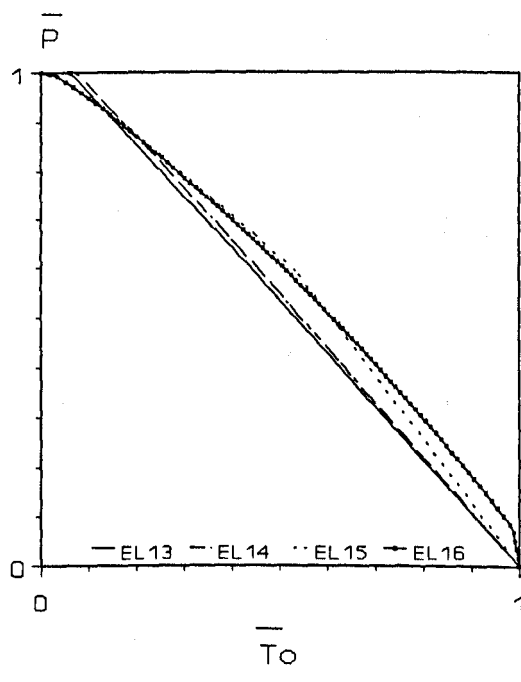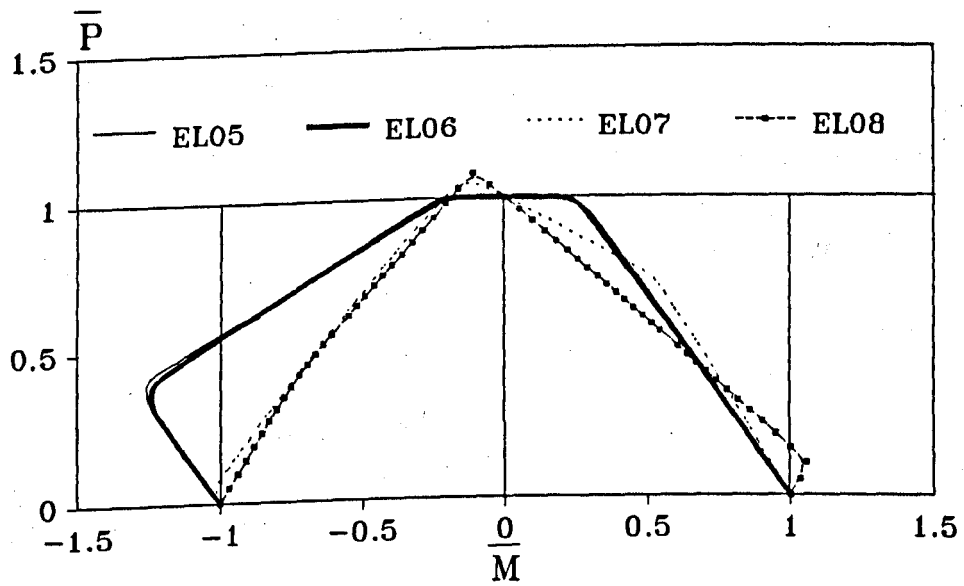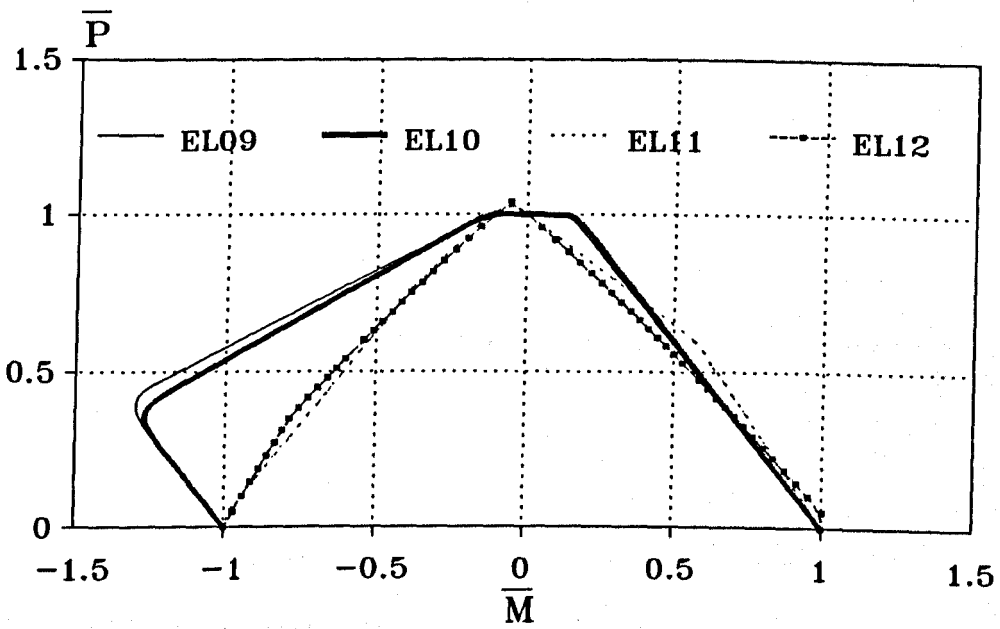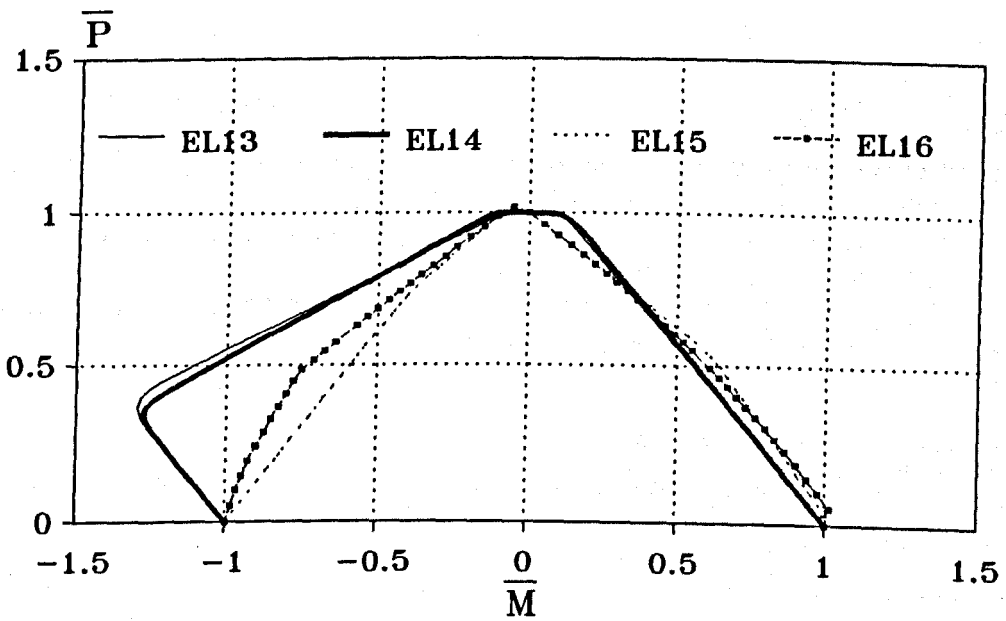
FIG. 52.   EFFECTS OF D/T AND b ON MOMENT:PRESSURE INTERACTIONS

90

(c) b=5

(d) b=7

FIG. 52(CONTD.).   EFFECTS OF D/T AND b ON MOMENT:PRESSURE
                    INTERACTIONS.

Similarly, the $\bar{T}_0:\bar{P}$ load pair in Figs. 51 is not much affected by D/T and b except when b=2. In the case of b=2, the stresses are lower when internal pressure dominates, giving a slightly larger yield locus. The interaction is best represented by a linear relation:-

$$\bar{T}_0 + \bar{P} = 1 \qquad\qquad (56)$$

The interaction between pressure and in-plane bending moment is different from the two previous interactions because it can result in a maximum stress lower than that given by the individual load. From Figs. 52, the bend radius does not influence maximum stresses as much as the D/T ratio. Different D/T ratios result in different load capacities being increased beyond their first yield individual value. In thin elbows, such as EL01, EL02, EL05, EL06, EL09, EL10, EL13 and EL14 (where D/T $\geq$ 80), the first yield opening moment capacity is increased by at least 22% when $\bar{P} \approx 0.4$. In thick elbows (D/T $\leq$ 10), the closing moment capacity is increased by as much as 9% when $\bar{P} \approx 0.15$. In addition, thick elbows (D/T $\leq$ 20) show a 15% increase in first yield pressure capacity when an opening moment of $\bar{M} \approx 0.2$ is present. Taking into consideration the behaviour of the range of elbows being studied, the best interaction is a linear relation:-

$$\bar{M} + \bar{P} = 1 \qquad\qquad (57)$$

In reality, the load interaction behaviour is more complex than the linear superposition from the individual loadcases because of the effect of flexibility of one loadcase upon the other. Spence and Boyle [92], Rodabaugh and George [15] and Wassermann [26] analyzed the effect of in-plane moment on stress behaviour due to stiffening from internal pressure.

4.2.6. Nonlinear coupling of in-plane moment and pressure

A detailed analysis of load interaction which involves moment and internal pressure is complex. It is well known that especially in thin elbows, an in-plane or torsional moment causes severe ovalization of the pipe cross-section. The stresses in an elbow subjected to internal pressure departs from simple pipe theory if the cross-section is not circular. This results in a nonlinear coupling between pressure and moment loads, and in a reduction of flexibility and stresses. Rodabaugh and George [15] studied the influence of internal pressure on the in-plane and out-of-plane moment stresses, and formulated reduced stresses when pressure is present. The reduction of stresses is also noted by Spence and Boyle [92]. However experimental investigation by Wassermann [26] on thick and long radius elbows (b > 6 and D/T ≈ 10) showed a reverse effect i.e. an increase of hoop stress when pressure is present. Wassermann also showed that with pressure the closing moment causes a larger increase of hoop stress than an opening moment. The following results from the nonlinear analysis should be read as a supplement to the linear analysis results.

Torque

Both elbow models EL01 and EL07 show a very slight effect of geometric nonlinearity. In model EL01, the maximum von Mises effective stress increases with torque but the increase is reduced progressively (see Fig. 53), whereas in model EL07 the effect is reversed (see Fig. 54). The trend of whether the stress increases progressively or not depends on the location on the elbows. This is due to the effect of cross-section ovalization on shell bending at different locations.

In-plane moment

From Figs. 55 and 56, the elbows behave differently when subjected to an opening or closing in-plane bending moment. A closing moment on the elbows causes the maximum effective

stresses at the crown to increase progressively with the load, compared to the linear analysis, but an opening moment causes a progressive reduction in the stress increase. Although small, the effect of geometric nonlinearity in model EL01 is about twice that of EL07. Tables 8 and 9 give an example of the reduction or increase of the maximum von Mises effective stress from various loadings, when compared to the linear analysis.

Pressure

In both elbow models, the maximum effective stresses increase linearly with pressure. There are no signs of geometric nonlinearity, as shown by the coincident lines in Figs. 57 and 58.

Pressure:Moment interaction

Tables 8 and 9 show the differences between the stresses obtained from linear and nonlinear analyses. The particular magnitude of pressure was chosen to cause a maximum stress of about 100 MPa in the elbows, while the choice of magnitude of the positive moment would cause an arbitrary maximum stress (of 617.26 MPa) in both elbows. The stresses were evaluated at the nodes where the combined stresses are maximum.

FIG. 53.
MAXIMUM MISES STRESS (AT NODE 2754) FROM
LINEAR AND NONLINEAR ANALYSES. ELBOW EL01
SUBJECTED TO TORQUE.

FIG. 54.
MAXIMUM MISES STRESS (AT NODE 3233) FROM
LINEAR AND NONLINEAR ANALYSES. ELBOW EL07
SUBJECTED TO TORQUE.

FIG. 55.
MAXIMUM MISES STRESS (AT NODE 2744) FROM
LINEAR AND NONLINEAR ANALYSES. ELBOW EL01
SUBJECTED TO IN-PLANE MOMENT.
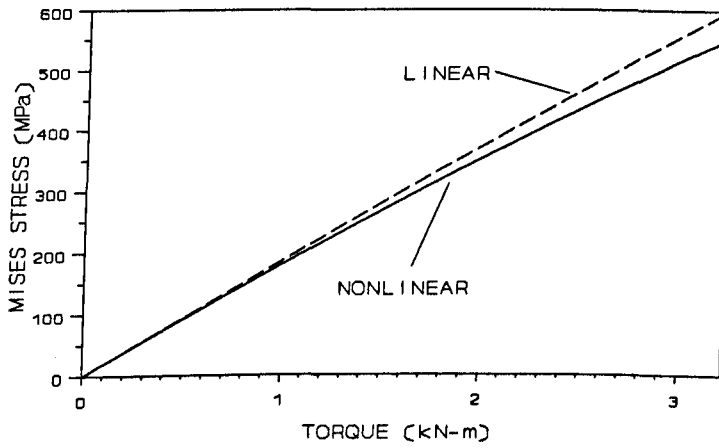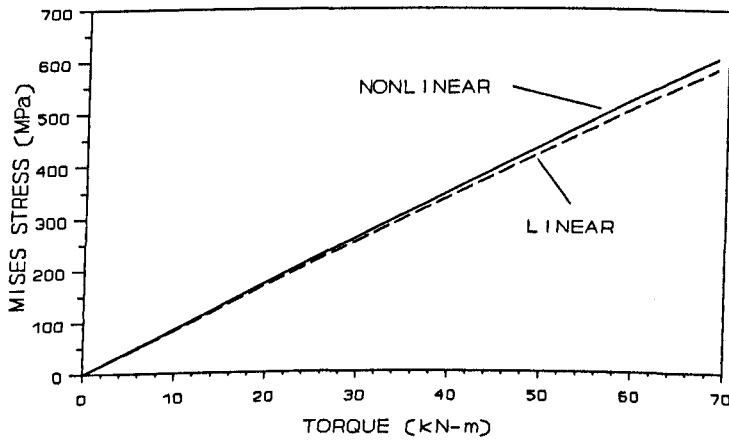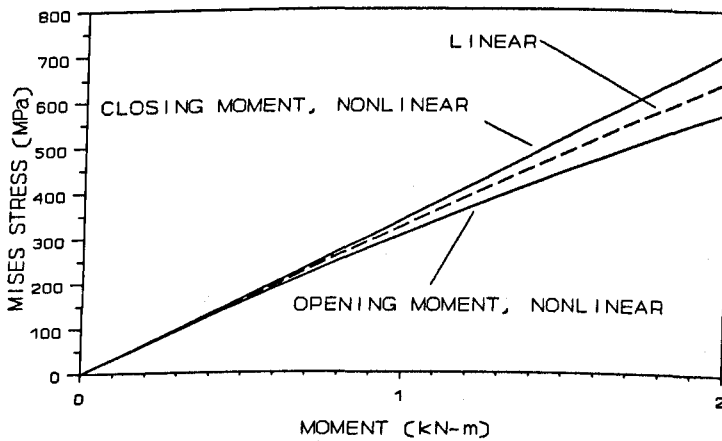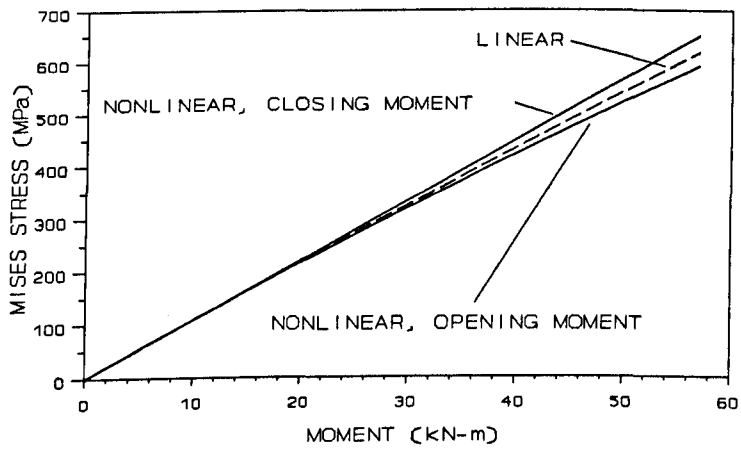
95

FIG. 56.   MAXIMUM MISES STRESS (AT NODE 2739) FROM
LINEAR AND NONLINEAR ANALYSES. ELBOW EL07
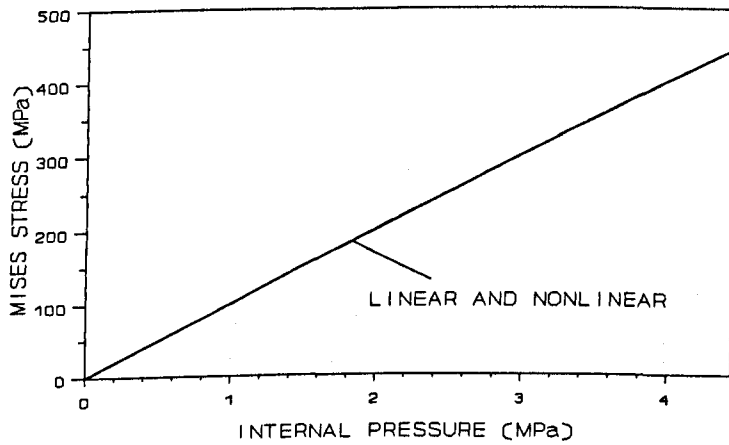SUBJECTED TO IN-PLANE MOMENT.

FIG. 57.   MAXIMUM MISES STRESS (AT NODE 2692) FROM
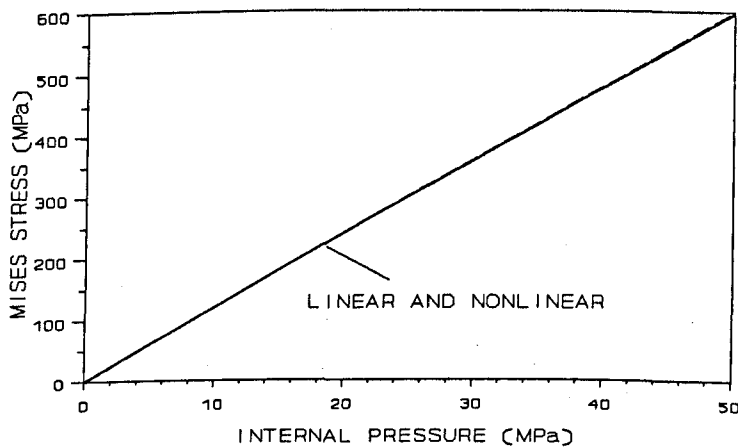LINEAR AND NONLINEAR ANALYSES. ELBOW EL01
SUBJECTED TO INTERNAL PRESSURE.

FIG. 58.   MAXIMUM MISES STRESS (AT NODE 2692) FROM
LINEAR AND NONLINEAR ANALYSES. ELBOW EL07
SUBJECTED TO INTERNAL PRESSURE.

96

Table 8. Elbow model EL01. Effective stresses from linear and nonlinear FEM analyses.

| Loadings | Max. σ_{vM} from linear and nonlinear analyses | | | | |
| | Linear[a] | Geometric nonlinear[b] | | Geometric pressure | nonlinear and interaction[c] |
	Max. σ_{vM}	Max. σ_{vM}	% difference from linear analysis	Max. σ_{vM}	% difference from linear analysis
P[d]	62.7	62.7	0	-	-
M[e]	617.3	673.6	9.1	-	-
-M[f]	617.3	535.4	-13.3	-	-
P+M[g]	679.9	736.2	8.3	454.1	-33.2
P+(-M)[h]	554.6	490.7	-11.5	272.4	-50.9

All the stresses in Table 1 occur at node 2744, at the crown.

Table 9. Elbow model EL07. Effective stresses from linear and nonlinear FEM analyses.

| Loadings | Max. σ_{vM} from linear and nonlinear analyses | | | | |
| | Linear[a] | Geometric nonlinear[b] | | Geometric pressure | nonlinear and interaction[c] |
	Max. σ_{vM}	Max. σ_{vM}	% difference from linear analysis	Max. σ_{vM}	% difference from linear analysis
P[d]	70.0[k] 80.5[j]	70.0[k] 80.5[j]	0 0	-	-
M[e]	617.3[k]	651.7[k]	5.6	-	-
-M[f]	579.2[j]	553.8[j]	-4.4	-	-
P+M[g]	687.3[k]	721.7[k]	5.0	664.2[k]	-3.4
P+(-M)[h]	659.6[j]	634.3[j]	-3.9	598.0[j]	-9.3

[a]   geometrically linear FEM for single loads and use of linear superposition (from single loads data) for combined loads

[b]   geometrically nonlinear FEM for single loads and use of linear superposition (from single loads data) for combined loads

[c]   geometrically nonlinear FEM for combined loads (i.e. includes pressure interaction)

[d]   internal pressure to cause maximum $\sigma_{vM} \approx 100$ MPa in elbow

[e]   closing in-plane moment=1.9 kN-m in EL01, =57 kN-m in EL07

[f]   opening in-plane moment=1.9 kN-m in EL01, =57 kN-m in EL07

[g]   pressure + closing in-plane moment, i.e. a combination of [d] and [e]

[h]   pressure + opening in-plane moment, i.e. a combination of [d] and [e]

[j]   at node 2745

[k]   at node 2739

In general, due to internal pressure, the maximum effective stress occurs at the inner surface of the intrados, while an in-plane moment causes a maximum stress at the outer surface of the crown. When the two loadings occur together, the maximum stress in the elbow can happen at other locations, depending on the magnitude of the loads and the geometric parameters of the elbow. As an example, Figs. 59 and 60 show the maximum stress occurring at different nodes when the moment is increased, while the internal pressure is being kept constant. The node locations of the elbows are listed in the Appendix C. In model EL01 (see Fig. 59), when pressure acts alone, the maximum stress is just on the inner surface of the intrados, and when the moment is increased, the location shifts to the outer surface at a hoop location of $\theta = 135°$, at node 2719. Finally, when the moment load predominates, the location of the maximum stress moves, as expected, to the outer surface of the crown.

In the elbow model EL07, Fig. 60 shows that when pressure acts alone, the maximum stress is at the inner surface of the intrados, but after that as the moment increases, the maximum stress occurs at the inner surface of the crown. There is no indication of the stress peaking at the outer surface of the crown, even at large moment loads.

Many researches have been devoted to the study of combined pressure and in-plane moment loads on elbows. The influence of pressure on combined loadings can be seen in Tables 8 and 9 where the combined stresses are derived from three methods. In the linear analysis, the combined stresses are obtained from linear elastic finite element analyses on individual loading. The second method combines the stresses which are obtained from geometrically nonlinear finite element analyses on individual loading. The third method is the result of geometric nonlinear analyses on combined loadings, thus automatically including any nonlinear load interaction.
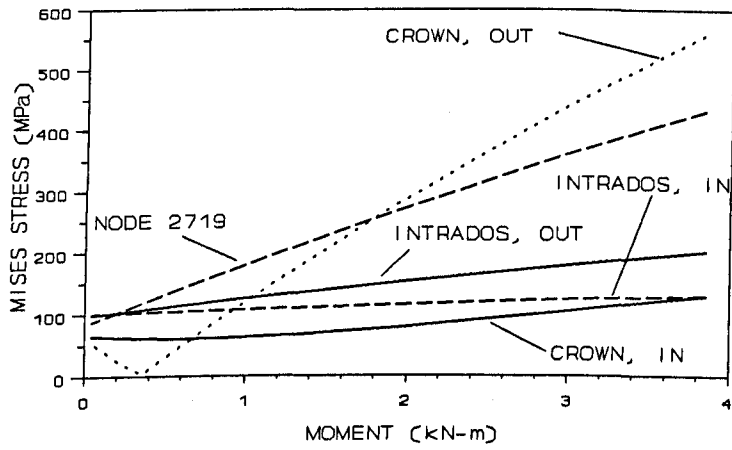
FIG. 59.
MAXIMUM MISES STRESS OCCURRING AT
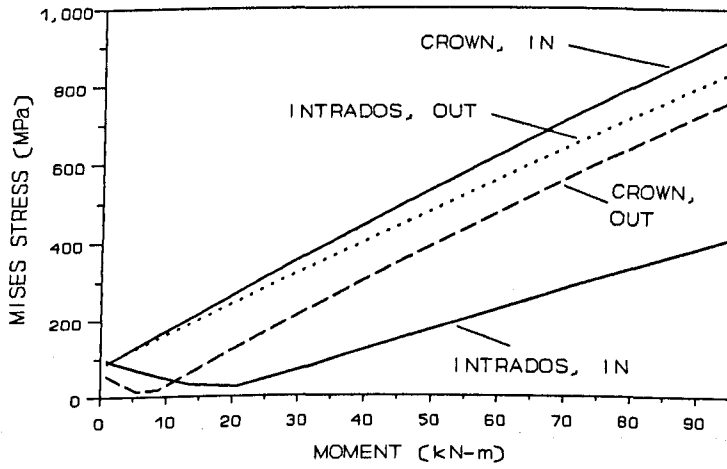DIFFERENT NODES. ELBOW EL01 SUBJECTED
TO P=0.997 MPa AND OPENING MOMENT.

FIG. 60.
MAXIMUM MISES STRESS OCCURRING AT A NODE. ELBOW
EL07 SUBJECTED TO P=8.4 MPa AND OPENING MOMENT.
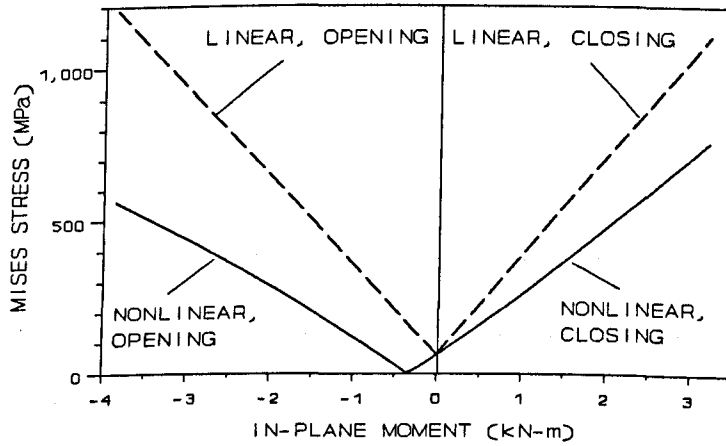
FIG. 61.
MISES STRESS AT NODE 2744 FROM LINEAR AND
NONLINEAR ANALYSES. ELBOW EL01 SUBJECTED
TO PRESSURE P=0.997 MPa AND MOMENT.

99

The third method evidently shows the stiffening effect of internal pressure on in-plane moment, especially on the thinner model EL01. With the specified combination of pressure and opening moment, the stress is reduced by 50.9%, and with a closing moment the reduction is 33.2%. The thicker model EL07 shows smaller corresponding reductions of 9.3% and 3.4%.

The effect of geometric nonlinearity with stiffening of the cross-section shows interesting results. A closing moment increases the maximum effective stress, and an opening moment reduces the stress. Although small, the stress increase and decrease in elbow EL01 are larger than in elbow EL07. When the results from both geometric and interaction nonlinear analyses are examined closely, the trend of the stress increase and decrease becomes apparent. In the geometric nonlinear analysis, the increase is due to the tensile stresses from the closing moment being added to the tensile pressure stresses at the outer surface of the crown. An opening moment produces compressive stresses at the same location, hence providing a reducing effect to the pressure stresses. When the load interaction is taken into account, the stiffening effect from internal pressure reduces ovalization and has a cancelling effect on the stress produced by geometric deformation. The effects of load interaction nonlinearity are quite large in the thinner model.

Fig. 61 helps to explain the large difference between the effects produced by opening and closing moments especially in elbow EL01. Internal pressure loading loads the elbow to a particular stress level. When a small magnitude of in-plane moment is then introduced, the maximum stress increases or decreases, depending on whether a closing or an opening moment is applied. An opening (negative) moment introduces a cancelling effect so that the effective stress at node 2744 (outer surface of the crown) is reduced to zero, whereas a closing (positive) moment increases the stress beyond the initial stress caused by internal

pressure. In addition, the different stress behaviour between an opening and a closing moment determines whether the stresses increase progressively with the moment. Hence, for an opening moment, the difference between linear and nonlinear analyses is larger for the same magnitude of moment which eventually accounts for the opening moment stress to be less than for a closing moment.

Fig. 62 shows the first yield locus, from the linear analysis, when the two loadings occur together in different combinations of magnitude. The yield points at selected load combinations are also plotted to emphasize the effect of nonlinear interaction on yielding at yield stresses of 200, 300 and 400 MPa. Since the nonlinear analysis results in lower maximum stresses, the yield envelopes are larger. Elbows with higher yield stresses have larger yield envelopes because the stresses become progressively reduced as the moment is increased. The key to the markers used in Fig. 62 as well as Figs. 64, 69 and 70 are defined in Appendix C.

The $\overline{M}$:$\overline{P}$ interaction of model EL07, shown in Fig. 63, does not exhibit much nonlinear interaction. Unlike model EL01, the maximum effective stress in the thicker model occurs at different locations for the closing and opening moments. For the same magnitude of closing and opening moments, the maximum stresses are quite close and the nonlinear analysis gives slightly lower maximum stress values than in linear analysis. Comparing the curves of Fig. 63 to those in Figs. 56 and 58, it can be seen that the reduction in maximum stress is due to a small contribution of geometric nonlinearity and nonlinear interaction. Fig. 64 shows the linear analysis yield envelope to be only slightly more conservative (i.e. overestimation of maximum effective stress) than the nonlinear envelope.
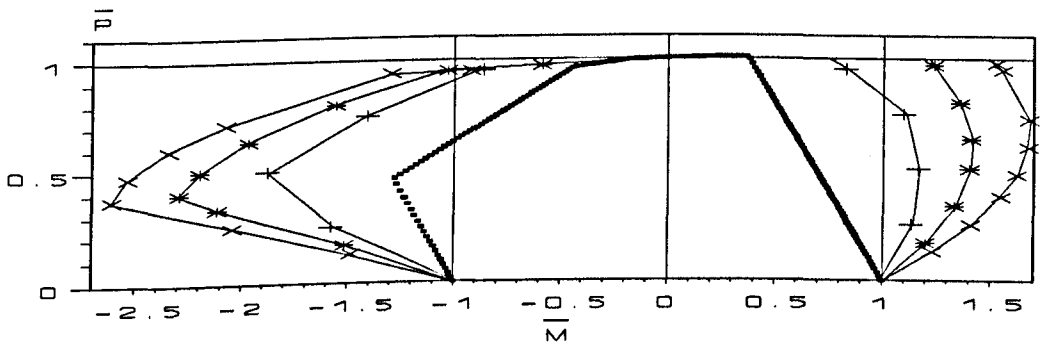
FIG. 62. LINEAR AND NONLINEAR $\overline{M}$:$\overline{P}$ INTERACTION. ELBOW MODEL EL01.
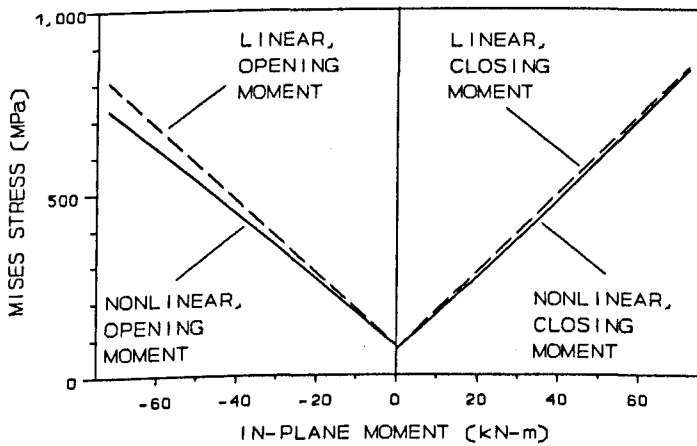
FIG. 63. MAXIMUM MISES STRESS FROM LINEAR AND NONLINEAR ANALYSES. ELBOW EL07 SUBJECTED TO PRESSURE P=8.4 MPa AND MOMENT. (AT NODE 2739 FOR CLOSING, AT 2745 FOR OPENING MOMENTS)
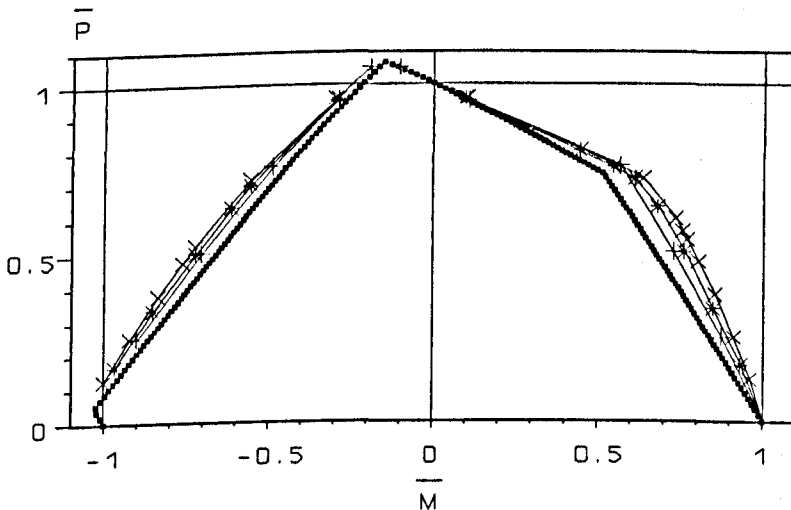
FIG. 64. LINEAR AND NONLINEAR $\overline{M}$:$\overline{P}$ INTERACTION. ELBOW MODEL EL07.

Key to markers in Figs. 62 and 64.
■ linear analysis
* nonlinear analysis, σ_Y=300 MPa

+ nonlinear analysis, σ_Y=200 MPa
x nonlinear analysis, σ_Y=400 MPa
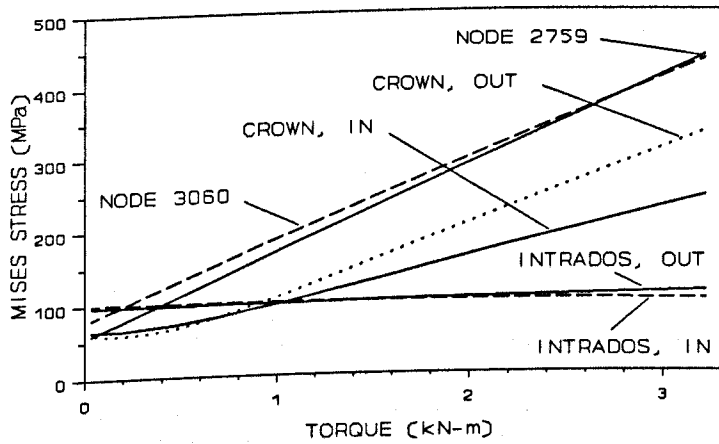
FIG. 65.

MAXIMUM MISES STRESS OCCURRING AT
DIFFERENT NODES. ELBOW EL01 SUBJECTED
TO P=0.997 MPa AND TORQUE.
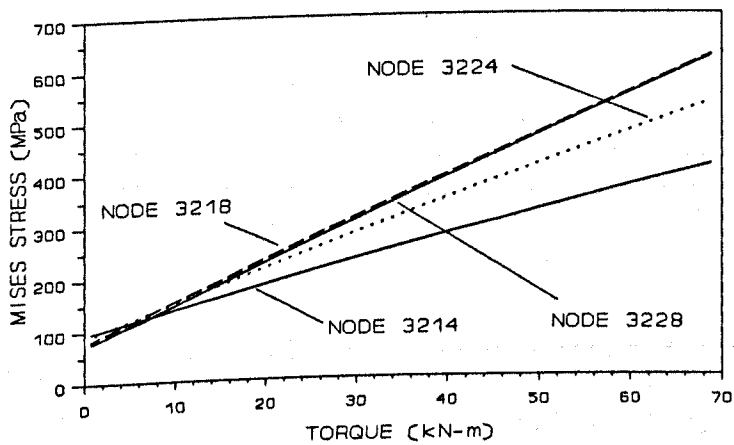
FIG. 66.

MAXIMUM MISES STRESS OCCURRING AT DIFFERENT
NODES FOR DIFFERENT TORQUE. ELBOW EL07
SUBJECTED TO P=8.341 MPa AND TORQUE.
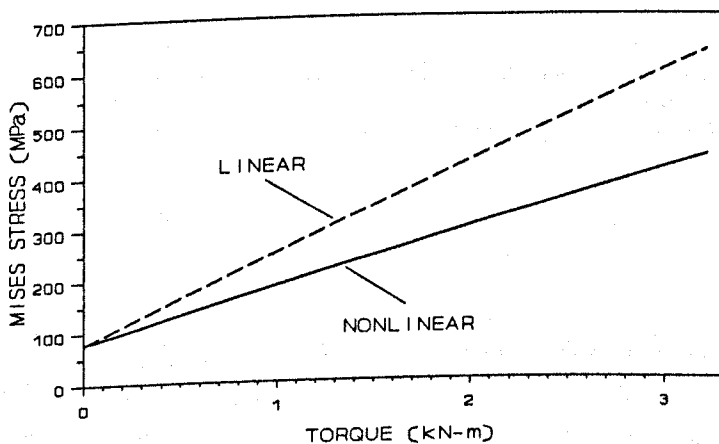
FIG. 67.

MISES STRESS AT NODE 3060 FROM LINEAR AND
NONLINEAR ANALYSES. ELBOW EL01 SUBJECTED
TO PRESSURE P=0.997 MPa AND TORQUE.

103
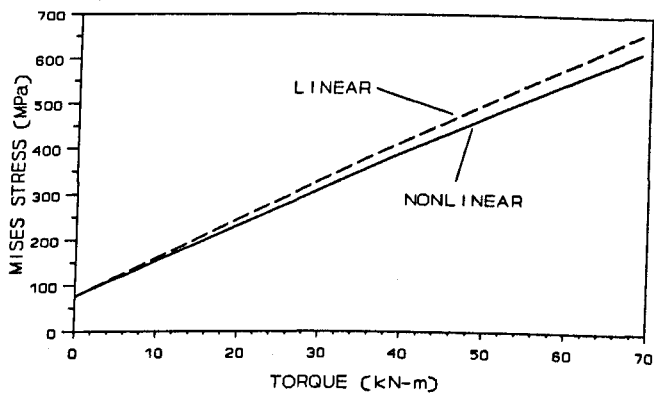
FIG. 68.

MAXIMUM MISES STRESS (AT NODE 3218) FROM LINEAR AND NONLINEAR ANALYSES. ELBOW EL07 SUBJECTED TO PRESSURE P=8.4 MPa AND TORQUE.
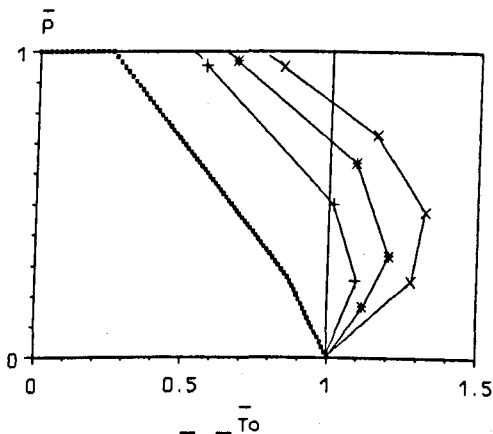
FIG. 69. LINEAR AND NONLINEAR $\overline{T}_o$:$\overline{P}$ INTERACTION. ELBOW MODEL EL01.
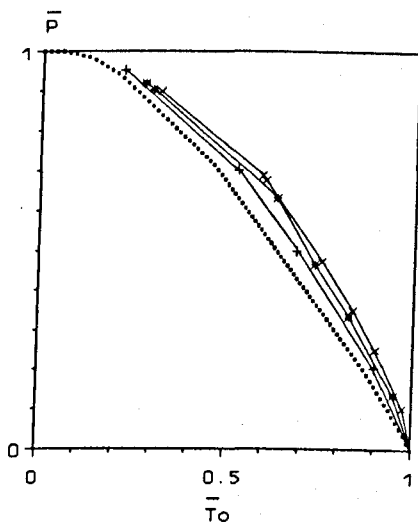
FIG. 70. LINEAR AND NONLINEAR $\overline{T}_o$:$\overline{P}$ INTERACTION. ELBOW MODEL EL07.

Key to markers in Figs. 69 and 70.
■ linear analysis   + nonlinear analysis, σ_Y=200 MPa
* nonlinear analysis, σ_Y=300 MPa   x nonlinear analysis, σ_Y=400 MPa

104

Table 10 shows the approximate maximum increase in the (opening) first yield moment-carrying capacity of the elbows due to both geometric and nonlinear load interaction. The first yield closing-moments also show increases but not as high as the opening moments. The yield locus trends indicate that for the thicker elbow, there is a slight increase in the opening moment-carrying capacity at very low internal pressures. There are also increases in internal pressure capacity at low values of opening moment, which are not shown by the thinner elbow nor for closing moments.

Table 10. Increase in moment carrying capacity of elbows.

| Limit	Magnitude of pressure and increase in first yield	maximum % moment (absolute) capacity
stress	Model EL01	Model EL07
200 MPa	At $P=0.5P_Y$, opening moment increase by $\approx 88\%$	At $P=0.05P_Y$, opening moment increase by $<5\%$
300 MPa	At $P=0.4P_Y$, opening moment increase by $\approx 130\%$	At $P=0.05P_Y$, opening moment increase by $<5\%$
400 MPa	At $P=0.37P_Y$, opening moment increase by $\approx 160\%$	At $P=0.05P_Y$, opening moment increase by $<5\%$

P_Y denotes the pressure to cause first yield in the respective elbows.

Pressure:Torque interaction

In model EL01, with constant internal pressure, the maximum effective stress changes location with torque, as shown in Fig. 65. As the torsional moment is increased from zero, the location shifts from the inner surface of the intrados to the outer surface at ($\theta=240°$ and $\phi=-15°$) and finally to the outer surface at ($\theta=75°$ and $\phi=0°$) as the torque predominates. In model EL07, the maximum stress starts at the inner surface of the intrados and finally moves to the outer surface at ($\theta=240°$ and $\phi=-22.5°$) at large values of torque, as shown in Fig. 66. From the analysis on other elbow models, these maximum locations depend on elbow

geometric parameters.

The phenomena of geometric and nonlinear load interaction is similarly encountered in the $\bar{T}_o:\bar{P}$ interaction. When subjected to torque, the thinner model EL01 again shows larger geometric and interaction nonlinearity and than the thicker elbow.

Comparing the graphs in Fig. 53 to Fig. 67 and Fig. 54 to Fig. 68, it can be seen that the reduction in maximum stress is due to a combination of both phenomena. Fig. 69 shows the nonlinear yield envelope of the thinner model to be very conservative compared to a slight conservatism in the thicker model, shown in Fig. 70. In model EL01, since the effect of geometric and interaction nonlinearity becomes increasingly large at higher limit (yield) stress, the torque-carrying capacity of the elbow increases with the stress limit. At all stress limits, the torque is increased beyond T_{oY} at $\bar{P} \leq 0.5\ P_Y$, as can be seen from Fig. 69.

4.2.7. Load interactions from Codes

4.2.7.1 BS 806

In the BS 806 [5], the hoop, axial and shear stresses are based on the thin cylinder theory. To make the procedure more conservative, the effects of pressure and moment are not coupled. The stress factors, F_{Ti} and F_{Li} were derived by Turner and Ford [87], while the factors F_{To} and F_{Lo} by Smith [93]. The symbols refers to those used in the BS.

i. Torque:Pressure

The total hoop stress, f_T, is the sum of separate effects from internal pressure and torque loadings and is given by:-

$$f_T = pd/2t + 0.5p + 0$$

and similarly, the total axial stress is:-

$$f_L = pd^2/4t(d + t) + 0$$

Since there is no contribution of shear stress from pressure, the total shear stress is:-

$$f_s = M_T(d + 2t)/4I$$

Since $f_T > f_L$, the effective stress is:-

$$f_c = \sqrt{(f_T^2 + 4f_s^2)} = Y$$

or $$(pd/2t + 0.5p)^2 + 4[M_T(d + 2t)/4I]^2 = Y^2$$

to give a circular interaction between pressure and torque, i.e. $\bar{T}_o^2 + \bar{P}^2 = 1$ (58)

ii. Moment:Pressure

Similarly, when internal pressure and in-plane moment act on the elbow,

$$\text{Total } f_T = pd/2t + 0.5p + rM_iF_{Ti}/I$$

$$\text{Total } f_L = pd^2/4t(d + t) + rM_iF_{Li}/I$$

For a given value of pipe factor λ, $F_{Ti} > F_{Li}$, so that $f_T > f_L$.

Since M_T is not acting, the shear stress $f_s = 0$.

Substituting for the value of f_T into the equation for f_c:-

$$(pd/2t + 0.5p + rM_iF_{Ti}/I)^2 + 0 = Y^2$$

The above equation gives a linear relation, i.e. $\bar{M} + \bar{P} = 1$ (59)

iii. Moment:Torque

And similarly,

$$\text{Total } f_T = 0 + rM_iF_{Ti}/I$$

$$\text{Total } f_L = 0 + rM_iF_{Li}/I$$

As before, $f_T > f_L$, hence giving $F = f_T$.

From the torque loading, $f_s = M_T(d + 2t)/4I$

The effective stress, $f_c = \sqrt{(F^2 + 4f_s^2)} = Y$

or $$(rM_iF_{Ti}/I)^2 + 4[M_T(d + 2t)/4I]^2 = Y^2$$

The above equation gives a circular relation, i.e. $\overline{M}^2 + \overline{T}_o^2 = 1$ (60)

4.2.7.2. ASME III

Equation (10) of Subsection NB-3653.1 ASME III [28] code is meant to control primary plus secondary loads so as to place an upper bound on deformations. Neglecting thermal effects, Equation (10) of ASME [28] is:-

$$C_1 P_o D_o/2t + C_2 D_o M_i/2I \leq 3S_m$$

where the resultant moment $M_i = \sqrt{(M_x^2 + M_y^2 + M_z^2)}$.

It can be shown that the $\overline{M}:\overline{T}_o$ interaction is circular and the $\overline{T}_o:\overline{P}$ and $\overline{M}:\overline{P}$ interaction are linear.

In the Codes, the maximum stresses due to the individual loads are summed up, regardless of the location on the pipe. In the ASME code, the interactions are similar to the FEM but in the BS code, only the circular $\overline{T}_o:\overline{P}$ interaction is different from the FEM.

4.2.8. Experimental test

4.2.8.1. Strain behaviour

Figs. 71 and 72 show the strain behaviour for the single loading of increasing pressure and moment, while Figs. 73 and 74 show the plots for the combined loadings.

From the figures, it can be seen that within the elastic limit of the material, in all loading conditions, the maximum measured strain occurs in the hoop direction at the intrados. It must be remembered that due to the limited number of gauge locations, the strain behaviour on the inner surface and other locations could not be determined. The strains at the locations which were not gauged could be higher than the test results.
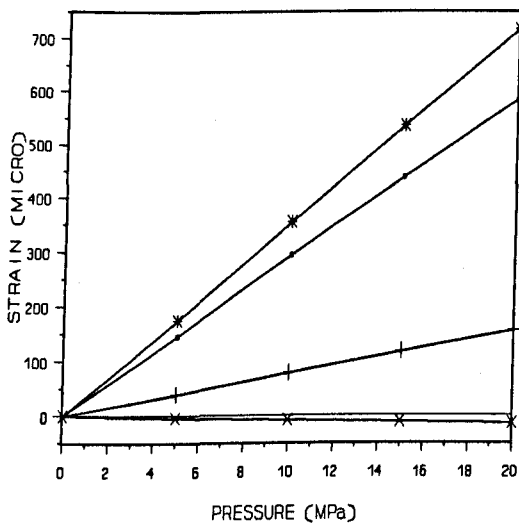
INTERNAL PRESSURE ONLY.

FIG. 71
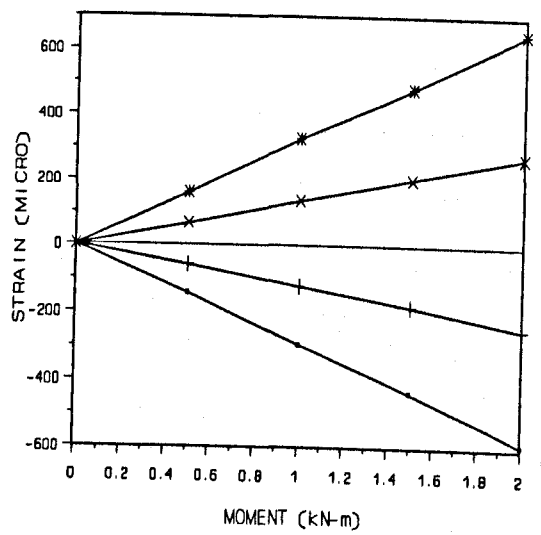
IN-PLANE OPENING MOMENT ONLY.

FIG. 72
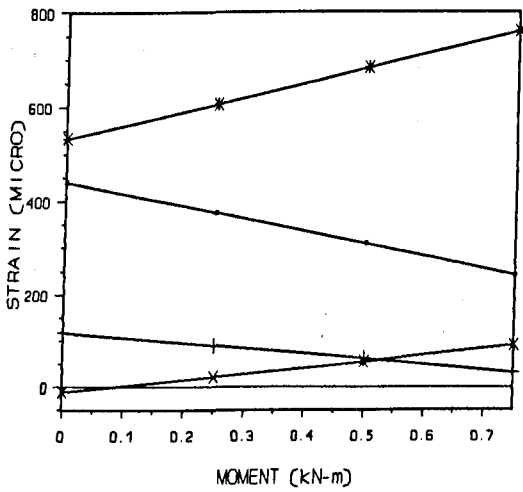
IN-PLANE OPENING MOMENT WITH
CONSTANT INTERNAL PRESSURE=15 MPa.

FIG. 73
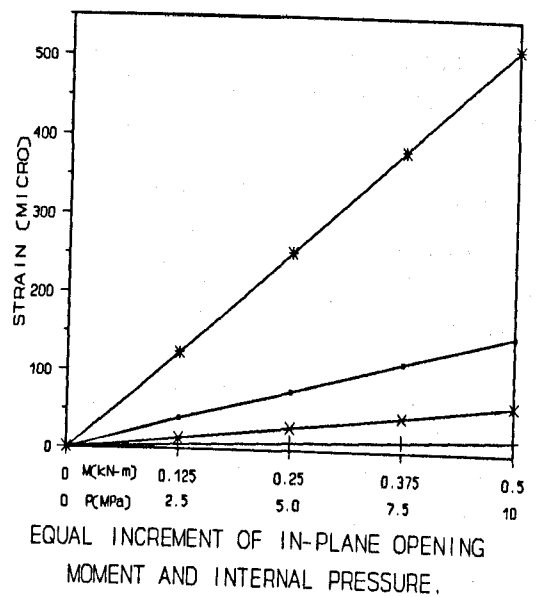
EQUAL INCREMENT OF IN-PLANE OPENING
MOMENT AND INTERNAL PRESSURE.

FIG. 74

FIGS. 71-74.   LOAD-STRAIN CURVES OF TEST ELBOW FROM VARIOUS LOADS.

Key to markers
■ hoop strain at crown   + axial strain at crown
* hoop strain at intrados   x axial strain at intrados

109

Fig. 75 shows the strains and rotation between the elbow ends for the incremental combined load for Test No.5. The curves show initial elastic response and the gradual transition to predominantly plastic behaviour. From the finite element linear load interaction analysis, it was calculated that the elbow would have experienced first yield at a load combination of pressure=13.23 MPa and moment=-2.646 kN-m; a combination which is shown in Fig. 75. At this load combination, neither the strains nor the rotation of the elbow indicate any sign of nonlinearity. In fact the strains and rotation start to become nonlinear at a much higher load combination of pressure=20 MPa and moment=-4 kN-m. This is not unusual; an experiment carried out by Kirkwood and Moffat [94] to determine the plastic loads in branch pipe connections also showed first yield moment and pressure well before any sign of deviation from nonlinear response. In another similar experimental investigation by Greenstreet [95], an elbow (λ=0.25, b=2.84 and ψ=0.0045) indicated a first yield load of 2193 lb and a load of 2450 lb at onset of nonlinearity, and another elbow (λ=0.167, b=1.89 and ψ=0.0019) gave corresponding loads of 1065 lb and 2500 lb, again proving the point made earlier. ψ is a pressure parameter which is equal to $PR^2/R_m T$.

In Test No. 5, as shown in Fig. 75, at high loads, the strains at two locations levelled off and then dropped, which could be due to stress redistribution.

4.2.8.2. Effective stress

In Test Nos. 1-4, the elbow was assumed to be in the elastic regime. In Test No.5, the elbow was elastic up to a load combination of Pressure=13.23 MPa and Moment=-2.646 kN-m. Table 11 compares the von Mises effective stress obtained from experiment to the theoretical energy method [15] and geometrically linear FEM. Rodabaugh and George's [15] method accounts for the stiffening effect of pressure on the pipe cross-sectional ovalization brought about by in-plane bending moment. Rodabaugh's theory and formulation is thoroughly dealt

with in a previous work. From Table 11, the effective stresses are larger at the intrados but the maximum effective stresses do not necessarily occur at the gauged locations.

The FEM results cannot strictly be compared to the experimental results because of the effects of incremental deformation from single loads, and stiffening of cross section ovalization due to pressure in the case of combined loadings. When internal pressure and moment occur together, the stresses at the intrados are lower than the FEM results. The Rodabaugh and George's [15] method gives lower effective stresses in both the single and combined loadings. This result cannot be used to confirm finding from earlier nonlinear FE analysis concerning the slight stiffening effect in thick elbows because the difference may be due to the experimental elbow which may not be modelled exactly in the FE analysis. With respect to this, Greenstreet [95] reported that the pretest ovality of elbows can be as high as 2%.

However, the stiffening effect of internal pressure can be seen by combining the experimental data of the single loads and comparing them with the combined loadings, as shown in Table 12. In Test No. 5, an elastic point is taken for comparison. In this study, the discussion is limited to quoting the stresses from only two gauged locations. The larger of the effective stresses occurs at the intrados. When the elbow is subjected to combined loadings, the larger effective stresses are reduced by an amount which is influenced by the ratio $\bar{P}:\bar{M}$ of the combining loadings but at other locations the stresses may increase.

Table 11.   Comparison of von Mises effective stress.

Test No.	Combined loads M (kN-m) P (MPa)	Location	Stresses (MPa) Experiment σ_h and σ_a	σ_{vM}	Rodabaugh [15] σ_{vM}	FEM σ_{vM}
1	M=0 P=20	crown	σ_h=141.0 σ_a=71.3	122.1	123.4	101.6* 103.1+
		intrados	σ_h=160.3 σ_a=41.2	144.2	160.6	135.6* 136.0+
2	M=-2.0 P=0	crown	σ_h=-147.0 σ_a=-91.2	128.5	152.9	147.0* 146.6+
		intrados	σ_h=163.6 σ_a=102.0	143.1	117.0	151.2* 161.7+
3	M=-0.75 P=15	crown	σ_h=55.9 σ_a=21.9	48.8	40.7	22.3* 26.0+
		intrados	σ_h=176.4 σ_a=67.2	154.2	161.6	156.8* 158.8+
4	M=-0.5 P=10	crown	σ_h=35.0 σ_a=13.4	30.6	26.3	14.9* 16.1+
		intrados	σ_h=119.2 σ_a=45.7	104.2	108.3	104.5* 106.3+
5	M=-2.0 P=10	crown	σ_h=-62.7 σ_a=-47.3	56.6	84.7	96.7* 89.2+
		intrados	σ_h=208.3 σ_a=105.6	180.4	192.3	216.9* 222.5+

*   geometrically linear FEM for single loads and use of linear superposition (from single loads data) for combined loads

+   geometrically nonlinear FEM for single loads and pressure load interaction included for combined loads

h   hoop stress

a   axial/longitudinal stress

Table 12.   Stiffening effect of pressure on effective stress in combined loadings.

Test No.	Combined loads M (kN-m) P (MPa)	Location	From single loads σ_{vM}	Combined loads	% reduction
3	M=-0.75	crown	51.9	58.5	-12.7
	P=15	intrados	193.8	184.7	4.7
4	M=-0.5	crown	34.6	36.6	-5.8
	P=10	intrados	129.2	124.8	3.4
5	M=-2.0	crown	80.9	67.8	16.2
	P=10	intrados	257.8	216.1	16.2

4.2.8.3. Load interaction

The experimental load interaction for first yield could not be determined from tests on a single elbow. An experimental load interaction diagram could only be obtained from tests beyond the elastic limit on several identical elbows which are extensively strain gauged. Fig. 76 shows the deduced interaction diagram for the experimental elbow using the FEM data of a range of elbow models. The proximity to first yield for the tests shown in Table 11 are also plotted (numbered 1-5) on the interaction diagram. In addition, a point, which is numbered 6, is also plotted. This point corresponds to a combined loading of pressure=20 MPa and moment=-4 kN-m, which from Fig. 75 is the start of rotation nonlinearity. This shows that even when a response (in this case, rotation) indicates the beginning of nonlinearity, the elbow has already yielded.

A 2-load curve for the first yield locus can be simplified by either a square, circular or linear interaction. From Fig. 76, the $\overline{P}:\overline{M}$ interaction in both quadrants can simply and conservatively be represented by a linear relation, i.e.

$$|\overline{P}| + |\overline{M}| = 1 \tag{61}$$
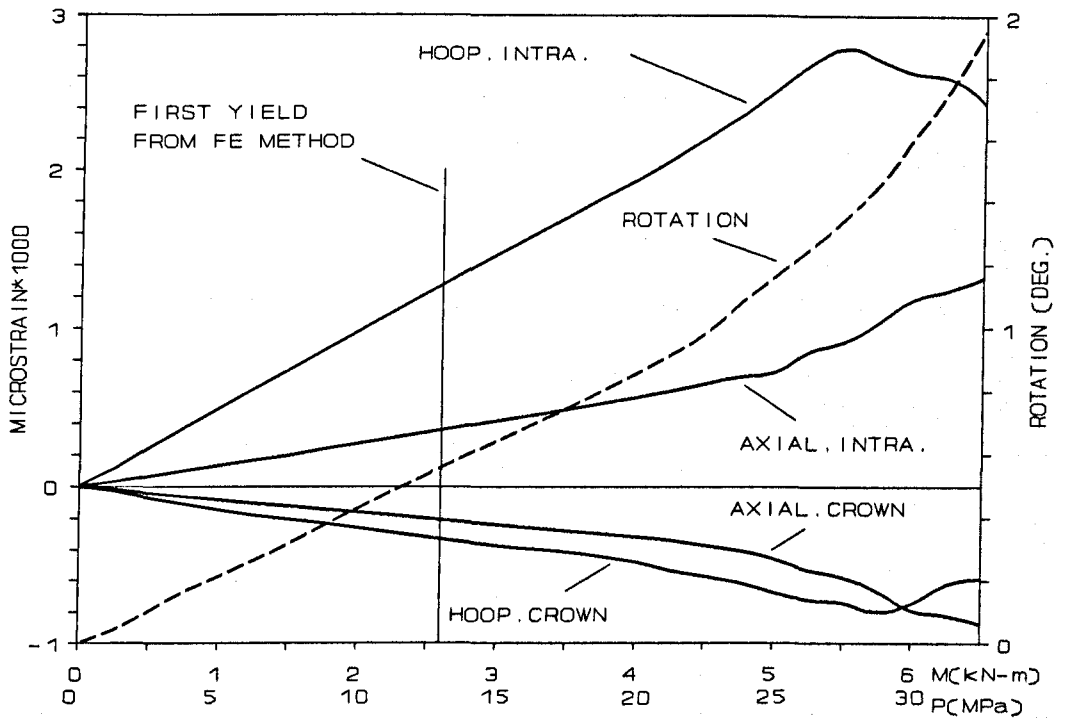
FIG. 75.   EQUAL INCREMENT OF IN-PLANE OPENING MOMENT AND
INTERNAL PRESSURE. (LOADING PATH 0→5→6 IN FIG. 76).
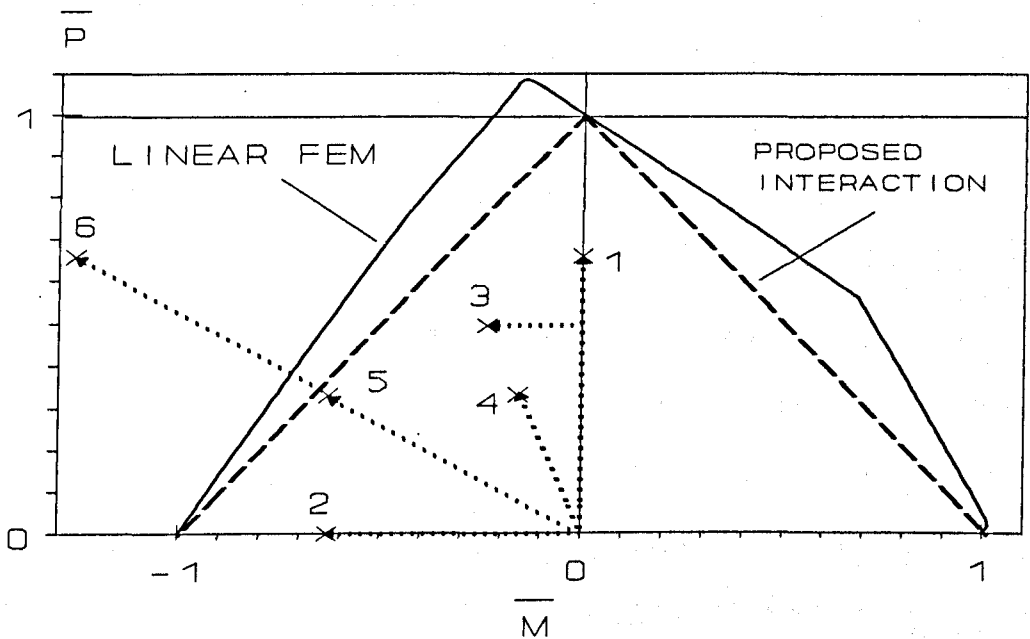
FIG. 76.   FIRST YIELD $\overline{M}$:$\overline{P}$ INTERACTION DIAGRAM OF EXPERIMENTAL
ELBOW FROM FEM. EXPERIMENTAL TESTS ARE NUMBERED 1-6.

4.2.8.4. Stress concentration factor from Codes

The stress concentration factor (SCF) is defined as the ratio of the maximum stress in an elbow to the nominal stress of an equivalent straight pipe subjected to the same loading. The BS 806 Code is considered for comparison. Due to in-plane moment, from the elbow dimensions (pipe factor $\lambda=0.393$ and bend ratio $b=2.75$), the BS 806 Code gives separate SCF values in the transverse and longitudinal directions. The correlation between the measured and BS values of SCF is satisfactory. Table 13 shows a comparison between the experimental results and the BS Code. The experimental value of SCF=3.8 is the larger between two locations, so the maximum SCF in the elbow could be higher.

Table 13.   SCF from experimental and BS Code.

	Transverse SCF	Longitudinal SCF	Maximum SCF
BS 806	3.7	2.4	3.7 (Transverse SCF)
Experimental	at crown, 3.4 at intrados, 3.8	at crown, 2.1 at intrados, 2.4	3.8[+] (intrados-out- transverse)

+   The larger of the stresses between intrados-out and crown-out

4.2.9 Location of yield

Unlike the procedures of the Codes where the maximum hoop stresses from individual loads are added, the stresses from the present method are determined for nearly every load combination followed by the location of the maximum stress. Hence, the resultant maximum stresses may not be at the locations which are predicted by the individual loads. Table 14 shows the yielding locations in EL07 (thick elbow) and EL05 (thin elbow) for different load combinations. The load combinations can be represented in quadrants which are similar to those in the interaction diagrams. The change of yield location is especially pronounced when there is a sudden change of yield locus slope.

Due to torque, the yield location along the axial direction of the curved portion of the elbow is $\phi \approx -20°$ whereas an in-plane moment causes yield at the elbow mid-section. When these loads acts simultaneously, yielding is likely to occur between $\phi = -20°$ and $\phi = 0°$ and between $\theta = 75°$ and $\theta = 120°$.

Generally, internal pressure causes yielding on the inner surface but as the elbow gets thinner, the difference between the ESF on the inner and outer surfaces is minimal. Furthermore, the ESF distribution along the axial direction and across the thickness is not much affected by D/T. Moment and torque cause yielding on the outer surface. Therefore when any two loads interact in a thin elbow, yielding is most likely to occur on the outer surface at a location dictated by torque or moment loading. Thick elbows do not have pronounced stress peaks and hence the yield locations are not as definite as thin elbows.

Table 14.   Location of first yield due to two interacting loads, in thick and thin elbows, Quadrant 1 - Both loads positive. Quadrant 2 - First load negative and second load positive.

In-plane moment (M) + Pressure (P)

Quadrant	Thick/Thin	Load	ϕ (deg.)	θ (deg.)	Surface in/out
1	Thick Thin	M alone	0 0	90 90	out out
	Thick Thin	M dominates	0 0	90 90	out out
	Thick Thin	P dominates	0 0	180 90	in out
	Thick Thin	P alone	0 0	180 180	in in
2	Thick Thin	P dominates	0 0	105 135	in out
	Thick Thin	M dominates	0 0	90 135	in out
	Thick Thin	M alone	0 0	90 90	out out

Torque (T_o) + Pressure (P)

1					
	Thick Thin	T alone	-22.5 -15	120 75	out out
	Thick Thin	T dominates	-22.5 -22.5	135 120	out out
	Thick Thin	P dominates	-22.5 -22.5	135 120	in out
	Thick Thin	P alone	0 0	180 180	in in

Moment (M) + Torque (T_o)

1					
	Thick Thin	M alone	0 0	90 90	out out
	Thick Thin	M dominates	-22.5 -15	135 90	out out
	Thick Thin	T dominates	-22.5 -22.5	135 90	out out
	Thick Thin	T alone	-22.5 -15	120 75	out out

4.3. TEE BRANCH

4.3.1. Maximum stresses - comparison with Codes and other methods

The present stress factors in the Codes are the results of recommendations from many studies. If the design stress factors are too high the economic penalty is in providing expansion loops and additional supports and if too low then the stress limit is not sufficient to prevent 'failure'.

The ASME III [28] code uses stress intensity as a measure of stress concentration. Depending on the mode of failure, the stress intensity is based on the primary, secondary or peak stress. If the primary-plus-secondary stresses are to be limited, the 'C' stress index is used, in which case the stress intensity is twice the maximum shear stress. The ASME code is applicable for branch junctions with $d_m/D_m \le 0.5$ and $D_m/T \le 100$ and the stress index is intended to be

conservative to account for the effects of transverse shear forces on the pipe. The BS 806 [5] stress factors are presented as a set of curves for in-plane and out-of-plane branch moments, for varying pipe factor λ where, for welded branch junctions, $\lambda = (T/R_m)(1 + t/R_m)$.

If the maximum stress occurs at the weld junction, the magnitude of the maximum stress is likely to be sensitive to the weld details as well. A second, nominally identical tee branch was modelled with a smaller weld seam ($w_h = 15.0$ mm, $w_{lc} = 6.0$ mm, $w_{lf} = 3.2$ mm) based on the BS and Babcock [96] design. Hereafter the model with the smaller weld seam shall be referred to as the second FEM model. The weld details of the two FEM models are shown in Figs. 9(a) and (b). In the ASME code, the formulations have been modified to describe the weld as best as possible. The unreinforced nozzle design in ASME III Fig. NB-3643.3(a)-1(d) has the closest geometry to the present FEM model. A minimum weld, with fillet radius r_2 = T/2, is assumed.

The ASME stress factors for M_{zb} and M_{xb} (see Fig. 1) include the three geometric parameters, given in the form of:-

$$\text{stress factor} = Q(R/T)^a(r/R)^b(t/T)^c \qquad (62)$$

If a single geometric parameter, (R/T), is used, such as:-

$$\text{stress factor} = Q(R/T)^n \qquad (63)$$

as in Ref. [34], the values of 'Q' and 'n' are usually given for a set of d/D and t/T values.

From finite element analysis on a wide range of welded tee branches (t/T=1, t/T=d/D, 0.2<(d/D)<0.8 and 10<(D/T)<60) and experimental data from equal diameter tee junctions, Moffat et al [43] produced fitted ESF curves for various D/T and d/D ratios. Their results in Table 15 are calculated from the following associated polynomial which was used to plot the curves:-

118

$$ESF = a_0 + a_1x + a_2x^2 + a_3x^3 + a_4x^4 \qquad (64)$$

where $x = d/D$ and the coefficients 'a' are dependent on the geometric parameters. From Moffat et al's [43] ESF curves, there is not much difference in the general trend between the curves of $t=T$ and $t/d = T/D$. The main difference is when d/D approaches zero; the ESFs are different between $t=T$ and $t/d=T/D$, except for pressure and M_{yr} loads. For the case of $t=T$, the lowest limit of diameter ratio is $d/D = T/D$. For the case of $t/d = T/D$, the lowest limit of d/D is when the nozzle aperture and nozzle thickness tend to zero values, and Moffat's ESFs at $d/D = 0$ were extrapolated from values estimated by using solid mechanics principles.

The comparison between the FEM and other methods are shown in Table 15, even though the present tee branch falls outside the range of applicability of some of the equations.

Table 15.   Stress factors from FEM, the Codes and other methods.

Loads	FEM[a]	FEM[b]	FEM[c]	Decock[c]	ASME[d]	Fujimoto	Moffat[43][e]	BS[c]
	ESF$_{vM}$	ESF$_{vM}$		SCF	C	C$_{2b}$	ESF	
M_{xr}	3.95	4.11	4.19	-	-	-	4.00	1.0
M_{zr}	3.58	3.85	3.84	-	1.93	-	3.81	6.2[f]
M_{yr}	1.46	1.55	1.55	-	1.93	-	1.41	7.7[g]
M_{yb}	2.65	2.77	2.83	-	-	-	2.77	1.0
M_{zb}	2.66	3.32	2.69	-	11.72	4.48	2.92	6.2[f]
M_{xb}	4.51	5.77	5.40	-	11.72	14.66	5.01	7.7[g]
P	4.08	4.13	4.06	4.17	2.47	-	4.36	3.91[h]

[a]   FEM 1st model
[b]   FEM 2nd model; smaller weld seam than first model
[c]   based on maximum principal stress
[d]   based on twice maximum shear stress
[e]   based on Tresca criterion
[f]   BS value of B_i
[g]   BS value of B_o
[h]   BS value of stress multiplier, m

4.3.1.1. Internal pressure

In most practical applications, internal pressure is the basic loading for a tee branch. Therefore the study of stress concentration and the influence of geometric parameters on stresses in the shell for this loading is of great importance. It has been reported that the locations of maximum ESF due to moment loads may vary with r/R and D/T ratios but due to internal pressure the location in most pipe connections is at the crotch corner.

From various studies, the general effects of the geometric parameters can be generally summarized. In thin shells, the maximum effective stresses peak prominently at about $d_m/D_m \approx 0.4$. The maximum stresses peak at higher values of d_m/D_m as the shells become thicker and in shells where $D_m/T < 30$, the stresses are maximum when $d_m/D_m = 1$. If the thickness ratio t/T is small, the maximum effective stress occurs in the branch pipe, otherwise it occurs in the run pipe.

Mershon [97] presented a compilation of SCF data around openings in shell intersections subjected to internal pressure. For equal pressure strength of the run and branch pipes and for constant D_m/T ratio, Mershon noted that in most cases, the stresses increase in magnitude up to a diameter ratio of 0.8, after which the stresses either level off or are reduced. Studies by other analysts show that the effect of d/D is not very significant, especially when D/T is small. The following subsections briefly summarise various formulations of stress factor, with their validity of application. Some of the symbols used in the various methods have been modified to suit the present notation system. The results from various formulations are compared to the corresponding stress factors from the first FEM model. The ASME and Moffat's use the Tresca effective stress factor and the rest use maximum stress factor.

Based on a compilation of available experimental data, Decock [98] formulated an empirical

120

equation for maximum stress in tee branch junctions due to pressure loading. The relationship is:-

$$SCF = \frac{2 + 2\frac{d}{D}\sqrt{(\frac{d}{D} \cdot \frac{t}{T})} + 1.25\frac{d}{D}\sqrt{\frac{D}{T}}}{1 + \frac{t}{T}\sqrt{(\frac{d}{D} \cdot \frac{t}{T})}} \qquad (65)$$

Later, Decock [99] compared his equation with experimental results from 8 different welded tee branches. The maximum deviation was about 19% but the deviations did not correlate with the geometric parameters, except that higher deviations came from smaller t/T ratios. Rodabaugh [100] reported an experimental pressure test on a pipe connection (with D/T = 230, d/D = 0.529, t/T = 0.981 and fillet radius $\approx$ 1/8 inch) where the maximum stress occurred on the weld at $\phi = 68°$. The maximum SCF was reported to be about twice that at the crotch. The above Decock's equation correctly predicted the magnitude of the maximum SCF but the formulation was derived for stresses at the crotch corner.

The rules in BS 806 are based on Money's [101] empirical relation of SCF based on maximum stress and give a two-step value of SCF which is independent on d/D. The BS equations are:-

$$SCF = 2.5(r/t)^{0.4084}(T/R)^{0.2415} \quad \text{for } 0 < (d/D) \le 0.7 \qquad (66)$$

or $\qquad SCF = 2.5(r/t)^{0.4829}(T/R)^{0.2415} \quad \text{for } 0.7 \le (d/D) < 1.0 \qquad (67)$

The stress index in ASME III NB-3683.8 was incorporated from the SCF formulation developed by Rodabaugh and Moore [47]. The ASME code formulation is:-

$$C_1 = 1.4(D/T)^{0.182}(d/D)^{0.367}(T/t)^{0.382}(t/r_2)^{0.148} \ge 1.2 \qquad (68)$$

with $0.5 < (r_2/t) < 12.5$

From Table 15, the Decock and the BS formulae agree well with the FEM results, while

Moffat's value was higher by nearly 10%. In the finite element analysis, Moffat et al [43] modelled a branch junction with weld seam identical to the present model. Moffat used a lesser number of elements than the present model and remarked of a further stress increase if the number of elements was increased.

Using the 'area replacement method' and the maximum normal stress failure theory, Lind [102] derived two SCF formulations, the larger of which gives the maximum stress factor:-

$$SCF = \frac{\left[1 + 1.77\lambda + (d/D)^{1.5}(t/T)^{0.5}\right]Z}{1 + (d/D)^{0.5}(t/T)^{1.5}} \qquad (69)$$

$$SCF = \frac{\left[1.67\left[(d/D)(D/T)/(t/T)\right]^{0.5} + 0.565(d/D)\right]Z}{0.67\left[(d/D)(D/T)/(t/T)\right]^{0.5} + 0.565(t/T)} \qquad (70)$$

where $Z = 1 + [(t/T)/(d/D)]^{0.5}/(D/T)$ and $\lambda = (T/R)(1+t/R)$

Lind's analysis assumes that the influence of corners and fillets are small. The larger of the two gives a maximum SCF of 4.10, which agrees well with the FEM result.

From 184 experimental data, Xie and Lu [103] proposed an empirical equation for predicting maximum stress factor, in the form of a polynomial obtained by the least square method. Their equation for the stress concentration factor, K, is:-

$$K = 2.87 + [1.38 - 0.72(t/T)^{0.5}](D/T)^{0.43}(d/D)^{0.9} - (t/T)^{0.5} \qquad (71)$$

and gives a value of 4.83 for the present model. For the curve fitting, Xie used data in the ranges of:- $1.4 < (D/T)240$, $0.004 < (d/D) < 1.0$ and $0.048 < (t/T) < 2.8$

4.3.1.2. Out-of-plane branch moment, M_{xb}

For out-of-plane branch moment loading, Wordsworth and Smedley [104] showed that the maximum stress is strongly influenced by d/D and reaches a peak value at $d/D \approx 0.75$.

Although the study was on tubular joints, Wordsworth offered an explanation on the variation of the maximum stress with d/D. For d/D $\approx$ 1, the bending stress in the branch pipe is said to be smoothly transferred to the run pipe in the transverse plane, thus minimizing the run pipe shell bending. For d/D approaching zero, the branch pipe is too small to impose large bending in the run pipe. When d/D $\approx$ 0.75 Wordsworth explained that the bending stress in the branch pipe is transferred to the run pipe through severe geometric discontinuity, thus creating large shell bending and maximum stress. In the longitudinal plane the change in geometry between the run and branch pipes does not vary with d/D so that when the load M_{zb} acts, there is no significant stress peak. Decock's [99] results for both in-plane and out-of-plane branch moments also show the trend of the stress peaking between d/D =0.5 and 1.0. On the contrary, Moffat et al [43] suggested that the stress keeps increasing up to d/D =1.

Fujimoto and Soh [27] observed a different trend, for in-plane and out-of-plane branch moments; the values of C_{2b} increase with increasing D/T but are not much affected by d/D. Fujimoto's equation for the branch moment stress factor is:-

$$C_{2b} = 1.8(D/T)^{0.7} \tag{72}$$

based on maximum principal stress, limited to 0.5 < (d/D) < 0.95, 50 < (D/T) < 300 and t = T

The ASME C_b and C_r stress indices are fictitious stress concentration factors because they are multipliers to the resultant branch and run pipe moments. Strictly, these indices cannot be compared to the individual effective stress factors from the present study. The ASME Section III NB-3863.8(c) stress index for M_{xb} is:-

$$C_{2b} = 3.0(R/T)^{2/3}(r/R)^{1/2}(t/T)(r/r_o) \geq 1.5 \tag{73}$$

based on twice maximum shear stress, limited to (r/R) $\leq$ 0.5, (D_o/T) $\leq$ 100 and 0.09 < (t/T) < 4.3

123

The BS 806 formulation for the out-of-plane SCF, B_o, is:-

$$B_o = 1.8/\lambda^{2/3} \qquad (74)$$

based on maximum hoop or axial stress. $\lambda = (T/R)(1+t/R)$

It must be noted that the definition of λ as used in the above BS formulation is different to that used by authors such as Money, Lind and Decock. Moffat's result is higher than the present result by about 11% and the BS result agrees well with the present FEM value. The ASME code and Fujimoto overpredict by more than twice the FEM value.

4.3.1.3. In-plane branch moment, M_{zb}

The location of maximum stress from Decock's [99] experimental results for in-plane branch pipe moment, M_{zb}, varied from the weld toe in the longitudinal plane to ϕ of between 45° and 60°, without showing any particular trend with respect to the geometric parameters of the tee branches. The respective stress factors are:-

ASME: $\qquad C_{2b} = 3.0(R/T)^{2/3}(r/R)^{1/2}(t/T)(r/r_o) \geq 1.5 \qquad (75)$

Fujimoto: $\qquad C_{2b} = 0.7(D/T)^{0.62} \qquad (76)$

BS 806: $\qquad B_i = 1.35/\lambda^{2/3} + 0.5 \qquad (77)$

where λ is defined in Eqn. (74) and B_i is the in-plane SCF.

Moffat's result gives higher maximum stresses than the present model but the BS and Fujimoto's value are very conservative.

4.3.1.4. Out-of-plane run moment, M_{yr}

In a branch junction where the branch pipe is small and an out-of-plane moment acts on the run pipe, the run pipe stress is the dominating factor in the design. Intuitively for $(r/R) < 0.5$ the maximum stress would not be greater than M_{yr}/Z_r. The Codes' stress factors are:-

ASME: $\qquad C_{2r} = 1.15(r/t)^{0.25} \geq 1.5 \qquad (78)$

and the BS 806 formulation for out-of-plane SCF, B_o, is:-

$$B_o = 1.8/\lambda^{2/3} \qquad (79)$$

Moffat's value gives a good correlation with the present FEM prediction but the BS stress factor is too high.

.4.3.1.5. <u>In-plane run moment, M_{zr}</u>

The Codes' stress factor formulations are:-

ASME: $\qquad C_{2r} = 1.15(r/t)^{0.25} \geq 1.5 \qquad (80)$

BS 806: $\qquad B_i = 1.35/\lambda^{2/3} + 0.5 \qquad (81)$

$\qquad$ where B_i is the in-plane SCF.

Moffat's result is slightly higher but the BS value is about 24% higher.

In summary, due to M_{xb}, the present tee branch (d/D =0.8, D/T =20 and t=T) gives a maximum effective stress factor which is markedly higher than any other loading. Surprisingly, the in-plane branch loading M_{zb} gives a smaller ESF than internal pressure loading. In fact the stress factor for M_{zb} is at the same level as the less critical M_{yb} loading. The least critical M_{yr} shows concentration of stress just above the nominal stress. Steele and Steele [51] reported the general discrepancies given by different approaches when vessels are subjected to nozzle loads. They found that the pad load method of analysis, the finite element method and their own method gave good agreement with experimental results for regions away from the intersection but underestimated the peak stresses at the intersection. Bijlaard's pad load method was said to seriously underestimate the peak stress and Steele's solution slightly underestimated the measured peak stress.

The BS and ASME codes assume there is no stress intensification from twisting branch and

run pipe moments but the results from other sources show the stresses for these loads, depending on geometrical parameter, can be quite substantial. Rodabaugh and Moore's [47] finite element results indicated that for $d/D \leq 0.5$ and $D/T \leq 100$, the maximum stress factor for branch pipe twisting moment does not exceed 1.5, but has been shown to be as high as 2.5 in a FE analysis by Corum et al [36]. Referring to this discrepancy, a report by Rodabaugh [81] indicates a need for a change.

The ASME stress index C_{2b} is based on the out-of-plane branch moment. Moffat et al [43] extrapolated the ASME's values of C_{2b} beyond the limit of application and compared the indices to their own ESF data. Beyond $d/D = 0.5$, Moffat found the ASME values to diverge significantly. This probably explains the reason why ASME's stress indices are much higher than the present FEM ESF values, for branch moment loads. On the other hand, the ASME stress indices are low for internal pressure and M_{zr}. To supplement the ASME stress index, Khan and Shah [105] proposed separate peak stress factors for the branch and run pipes, for tee connections subjected to out-of-plane branch moment. The equations which are applicable for the diameter range $d/D > 0.5$ are:-

$$C_{2b} = 1.8917(d/D)^{-0.2758}(R/T)^{0.6503}(t/T)^{0.1441} \qquad \text{for the branch pipe} \qquad (82)$$

and $\quad C_{2b} = 1.3701(d/D)^{-0.2816}(R/T)^{0.7399}(t/T)^{1.3521} \qquad \text{for the run pipe} \qquad (83)$

Eqns. (82) and (83) give peak stress factors of 8.99 and 8.02 in the branch and run pipe respectively. These high values (compared to 5.4 from present FEM study) can be attributed to the equations being derived for tee connections without a weld seam between the pipes, but the stress indices are at least less conservative than the extrapolated ASME values of 11.72. As for torsional moments, the ASME design guidance are not available.

The BS 806 does not distinguish between bending moments applied at to the branch and

through the run pipes. From the values of the stress factors B_o and B_i, it seems that these stress factors are intended for branch pipe loads. From non-intensified shear stresses in the BS equation for the Tresca effective stresses, it is deduced that the BS stress factors for torsional moments is a very unconservative value of unity.

4.3.2. Effects of weld

The weld at the pipes intersection produces a significant local stress concentration. Effectively the weld fillet lowers peak stresses and smooths the stress distribution. The effect of the weld on the stress distribution is seldom reported. Ellyin and Turkkan [45] found that without the weld, branches in the range of $0.5 < d/D < 0.6$ suffer from higher stresses. In an experimental test on the effects of run pipe moments, Zhixiang et al [60] noted that when the butt-welded tees were subjected to branch moment loads, the ESFs were reduced by about 15-20%. The effect of the weld was lessened in thick tee branches. Mershon [97] remarked that minor details of the weld fillet at the intersection can have a major influence on the resulting stress level. This is due to the fact that even a small weld reinforcement can constitute a sizeable increase in the effective nozzle wall thickness at the critical location and is said to be more pronounced at small diameter ratios. The study by Bryson et al [106] also concluded that weld reinforcement at the intersection reduces maximum stresses.

In a load interaction study, Schroeder et al [48] determined the branch limit moments for tee junctions with and without fillet. They noticed that fillets have a greater strengthening effect for in-plane than for out-of-plane bending moments, but Zhixiang found that the stresses were reduced more for out-of-plane moment. The present study supports Zhixiang's finding.

Zhixiang et al [60] carried out tests on geometrically similar tees and observed that a specific welding seam gives greater reinforcing effects in relatively smaller tees. As a result the larger

127

tee apparently seems to give higher stress distribution. Moffat et al [43] too, noted that different sized welds at the junction resulted in a considerable difference in stress peaks especially when moment loads were applied.

The weld details used by Moffat et al [43] generally follow a trend with respect to the pipe dimensions. The weld horizontal width increases as D/T and d/D become smaller. The weld height increases as D/T becomes smaller but is not consistent with d/D ratio. It is recommended here that although the BS code guide on weld details is adequate for a range of the branch dimensions, any finite element weld modelling should reflect the variation of d/D and D/T.

Due to M_{xb}, the present model with the smaller weld seam shows a dramatic increase of maximum effective stress by 28% (as in Table 15). Due to in-plane branch moment, the increase is 25%. Other loadings too show substantial but lower increases. With reference to the stresses at the weld, Rodabaugh [81][100] looked at the weld toe as a source of peak stress which reduces the fatigue life of the tee branch.

4.3.3. Hoop and axial stresses

4.3.3.1. Internal pressure

The term 'axial stress' shall be defined as the stress in the axial direction of the pipe it is referring to, and the 'hoop stress' acts in the hoop direction of the pipe. The free pipe ends were capped in the present model, which means that the axial pressure forces were taken into consideration.

The stress field at the intersection of a tee connection is influenced by a combination of the weld around the intersection and three independent geometric parameters, namely, d_m/D_m,

D_m/T (or d_m/t) and t/T. The parameter d_m/D_m describes the weakening of the run pipe by the intersection and t/T indicates the relative stiffness of the run and branch pipes. In a tee branch in which internal pressure is acting, the prevalence of the hoop or axial stresses in the pipes is influenced by these parametric ratios.

Concerning the locations of maximum stress, Taylor and Lind's [107] experiments on tee branches subjected to internal pressure showed two stress peaks along the crotch line; at the crotch corner and at the point where the crotch line intersects the transverse plane. The maximum stress at the crotch corner is the hoop stress and occurs because of the removal of material in the run pipe. The maximum stress in the transverse plane arises because the internal pressure acting normal to the run pipe needs to be balanced by a bending stress at the maximum location, and this bending stress increases with diameter ratio. The maximum stress at the transverse plane is seldom higher than at the crotch corner, hence the hoop stress in the latter case usually governs the design of the pipe.

From the present FEM results, the axial and hoop stress distributions on the inner and outer surfaces of the run and branch pipes are plotted in Figs. 77(a) and (b). The distance S is defined as:-
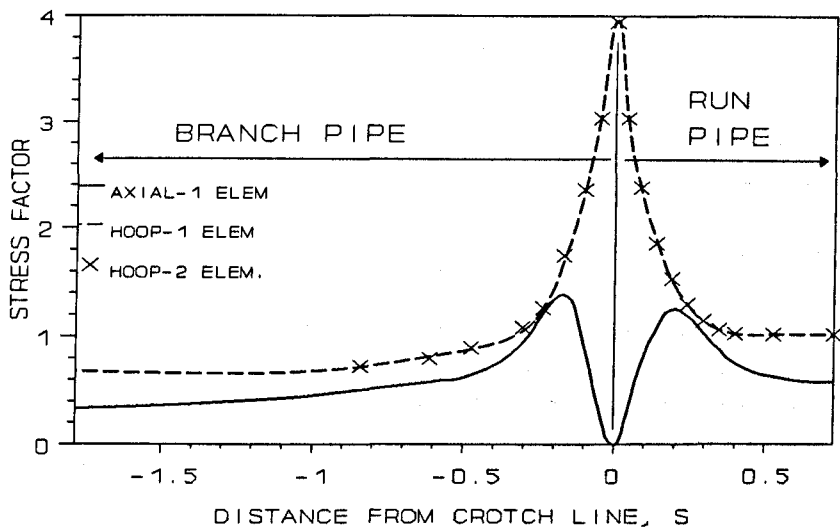
S = distance from the weld centre or crotch line ÷ D_m

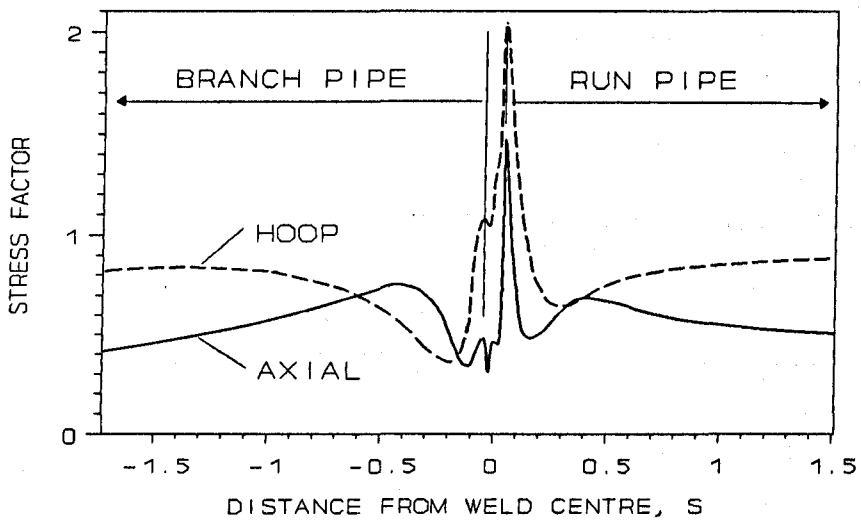and the stress factors are normalised as per Eqn. (44), on Page 60.

In Fig. 77(a) the inner surface hoop stress results are also quoted for the 2-element thick model. The 1-element thick model which was used in the present study shows insignificant difference compared to the 2-element model. The figures show that the maximum hoop stress factor of about 4.0 occurs at the inside corner of the longitudinal plane i.e. the crotch corner. The hoop stresses peak at the intersection and decay rapidly away from the junction, and level

off to a reasonably uniform stress within a distance of $S \approx 0.5$ (i.e. $0.5D_m$) from the crotch line. On the outer surface, the hoop stress peaks at the weld-run pipe junction. A maximum axial stress factor of about 1.5 occurs at the weld-run pipe junction. On the inner surface the axial stresses peak with a stress factor of about 1.2 at $S \approx 0.2$ and, as expected, approach zero at the crotch corner.

The radial stresses are satisfactory considering that only a single layer of elements was modelled. Half way along the length of the pipe limbs, the inner radial stresses were about 10% lower than the magnitude of applied pressure.

FIG. 77. HOOP AND AXIAL STRESS DISTRIBUTIONS (IN LONGITUDINAL PLANE), WHEN SUBJECTED TO INTERNAL PRESSURE.

Note 1. S=distance from weld centre or crotch line /D_m
      2. The stress factors are normalised as per Eqn. (44), Page 60

130

4.3.3.2. Moment loadings

The way various parameters influence the stress factors is complex. Decock [99] subjected tee branches (with d/D = 0.37 to 0.7) to in-plane branch moment loading and noted that when the parameter t/T was reduced from 1 to about 0.5, the maximum hoop or axial stress was decreased by about 10-20%. For out-of-plane branch moment, with a tee branch of d/D = 0.37, the maximum stress increased with decreasing values of t/T. For tee branches of range D/T > 100, Corum et al [36] showed that (for r/R = 1.0 and t = T), the maximum stress was highest for torsional branch moment and lowest for in-plane branch moment.

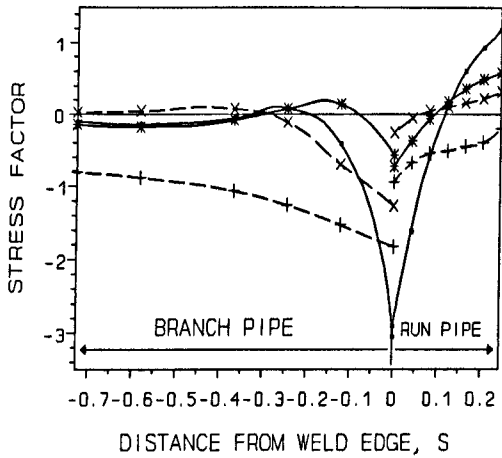### 4.3.4. Bending and membrane stresses

The stress categories of primary, secondary and peak stresses have been quoted in Section 2.4.1. These stress categories are classified according to location in the structure, origin of stress and type of stress. The type of stresses are general membrane and bending stresses. Membrane stresses are relatively uniform across the wall, acting in either compression or tension. Bending stress distributions exhibit a maximum tension on one side and maximum compression on the other side of the wall, with a straight line distribution. In this study, the bending and membrane stresses at a section through the wall thickness are defined as $(\sigma_o - \sigma_i)/2$ and $(\sigma_o + \sigma_i)/2$ respectively.

Mokhtarian and Endicott [53] presented equations for bending and surface stresses in branch junctions subjected to internal pressure. Since the branch pipe behaved differently from the run pipe, they developed separate equations as functions of d/D, D/T and t/T. The equations were found to be fairly accurate within the limitations of D/T < 1000, d/t < 1000 and 0.03 < d/D < 0.5. For internal pressure, Lind [102] pointed out two locations where bending stresses are large; at the pipe junctures in both the transverse and longitudinal planes, shown as points A and B in Fig. 1. At point A, equilibrium in the direction normal to the run pipe

shell is maintained by bending action. The bending stresses at A are localised and are said to be seldom higher than the (run pipe) hoop stresses at B.

The distributions of membrane and bending stresses, for the present model, for in-plane and out-of-plane moments and for internal pressure are shown in Figs. 78(a)-(d). The membrane and bending stresses due to torsional moment loads (not shown) are not as high as in bending moment loads. The term 'longitudinal' refers to the direction in the plane of the section under consideration and parallel to the boundary of the section and 'hoop' refers to the direction normal to the plane of the section.

Moment loads cause higher shell bending than membrane stresses but for internal pressure, the membrane stresses are higher. However, Skopinsky [108] remarked that for pressure loading in thin shells, in the longitudinal direction, bending stress still prevails. For nozzle bending moments, Steele and Steele [51] described the variation of stress factors with T/t for $d/t = 100$. They found that for $T/t \leq 2$ the nozzle was essentially rigid as far as bending stress was concerned but for large T/t the most severe stress was the bending stress in the nozzle. From Figs. 78(a),(b) and (c), due to bending moments, the bending stresses are maximum at the weld edge but the membrane stresses start to dominate over bending stresses at a distance of $S > 0.1 D_m$ (20 mm) from the weld edge. In-plane moment loadings show a change in the direction of longitudinal bending just outside the weld edge. In Fig. 78(d) internal pressure causes the membrane hoop stress to peak at the weld edge. The other hoop and membrane stresses are not much intensified above their nominal stresses.

132

(a) Mxb LOADING.
STRESSES ON TRANSVERSE PLANE.
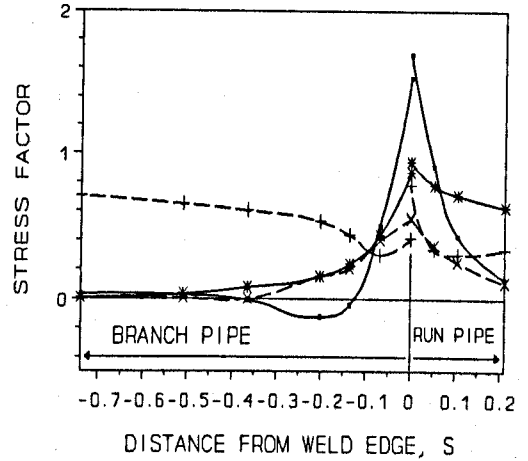
(b) Mzb LOADING.
STRESSES ON LONGITUDINAL PLANE.
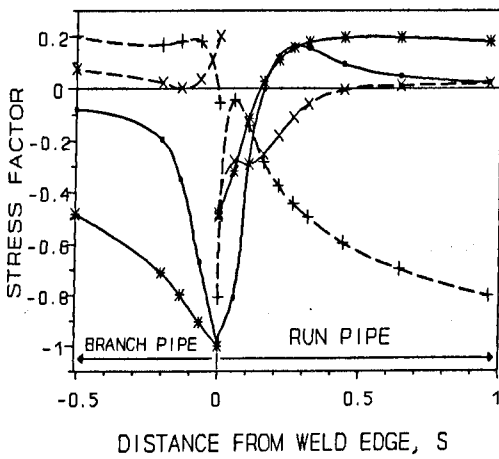
(c) Mzr LOADING.
STRESSES ON LONGITUDINAL PLANE.
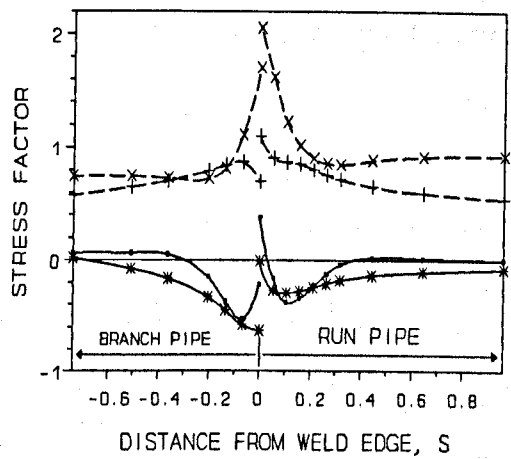
(d) PRESSURE LOADING.
STRESSES ON LONGITUDINAL PLANE.

FIG. 78.   BENDING AND MEMBRANE STRESS (IN HOOP AND AXIAL
DIRECTIONS) DISTRIBUTIONS IN LONGITUDINAL AND
TRANSVERSE PLANES.

Note
1. S = distance from weld edge /D_m
2. Key to markers.
    ■ axial bending stress   + axial membrane stress
    * hoop bending stress   x hoop membrane stress

133

4.3.5. Maximum effective stresses

The von Mises ESF distributions along the weld junctions and the crotch line of the tee branch are shown in Figs. 79(a)-(u). Although general comments about the effects of geometric parameters cannot be made with the present tee branch, Figs. 79(a)-(u) give a graphic comparison between the three critical locations and between individual loadings. Along the crotch line, the loads M_{xr}, M_{zr} and pressure cause high stresses. At both the weld-run pipe and weld-branch pipe junctions, the load M_{xb} is the most critical loading. Similar comparison of locations of maximum stresses can be made from individual loading.

Table 16 shows the absolute maximum von Mises ESFs, and their locations. The maximum ESFs on the transverse or longitudinal plane are also presented. The maximum ESF values occur at locations which are symmetrical about the x-y and y-z planes, hence the results from only one quadrant are shown in Table 16.

Figs. 80(a)-(d) show the distribution of the ESF on the inner and outer surfaces, on the longitudinal and transverse planes. The non-dimensionalised distance S differs from the previous definition, i.e. it is measured from the weld centre. The maximum ESF along these planes are summarized in the second column of Table 16. Due to in-plane and out-of-plane run pipe moments, the absolute maximum von Mises ESFs coincidentally occur on the transverse plane at the crotch line. From Figs. 80(a)-(d), most of the stresses on the run pipe attenuate to reasonably uniform values within $1.5D_m$. The maximum ESFs do not generally occur on the weld itself, but instead at the weld-pipe junctions. In a test on tee branches (d/D=1.0), Moffat [34] observed that in 2 (M_{xr} and M_{yr}) of the 6 moment loads, the maximum stress occurs at different locations for different junctions, implying that these locations are influenced by pipe dimensions. From Moffat et al's [43] fitted curves, for all moment loads, when the D/T and d/D ratios are small the maximum ESFs do not differ much.

134
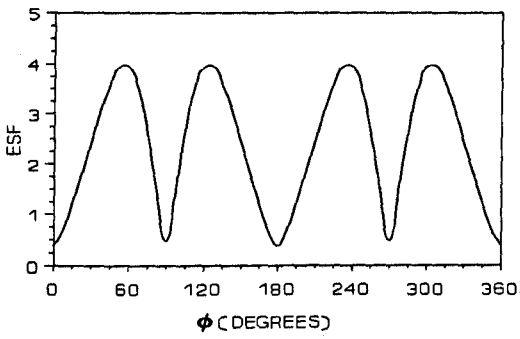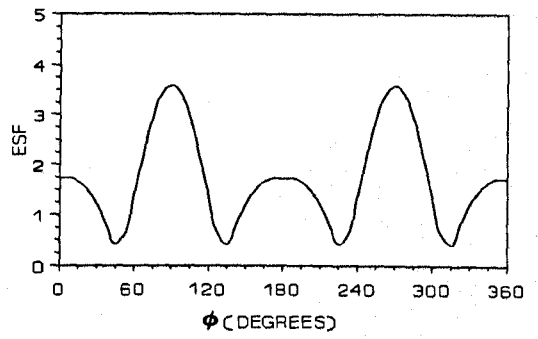
(a) Mxr. CROTCH LINE.

(b) Mzr. CROTCH LINE.
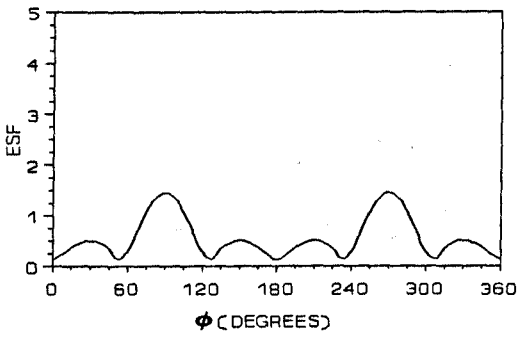
(c) Myr. CROTCH LINE.
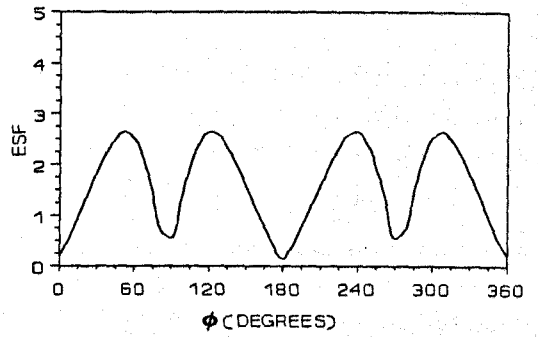
(d) Myb. CROTCH LINE.
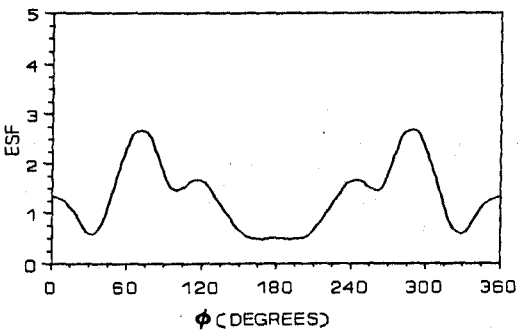
(e) Mzb. CROTCH LINE.
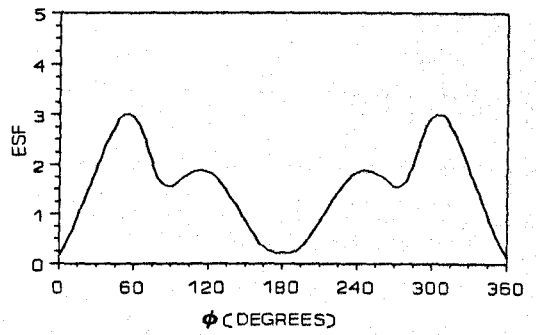
(f) Mxb. CROTCH LINE.
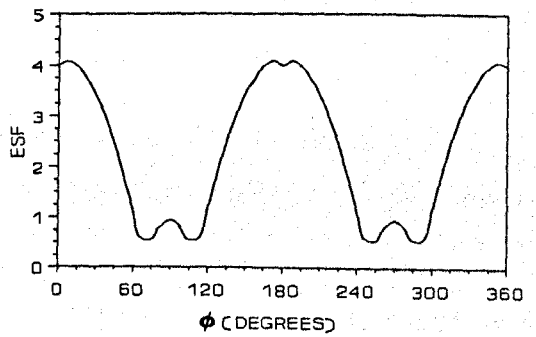
(g) PRESSURE. CROTCH LINE.

FIG. 79.
ESF DISTRIBUTIONS
ALONG CROTCH LINE.

135
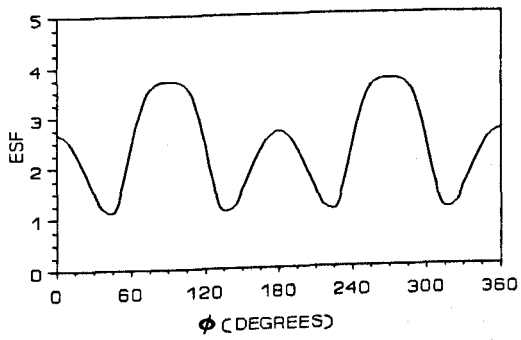
(h) Mxr. WELD-RUN PIPE EDGE.
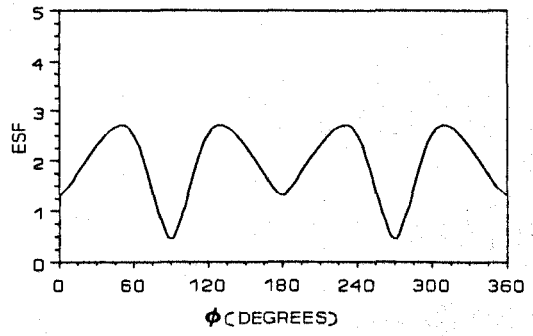
(i) Mzr. WELD-RUN PIPE EDGE.
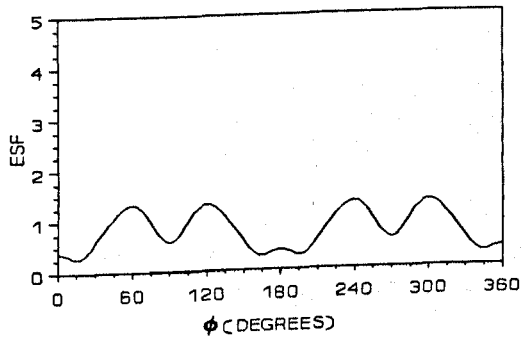
(j) Myr. WELD-RUN PIPE EDGE.
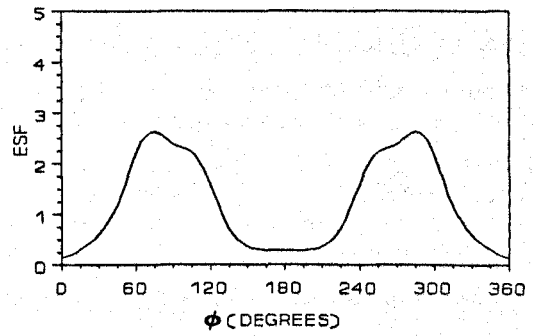
(k) Myb. WELD-RUN PIPE EDGE.
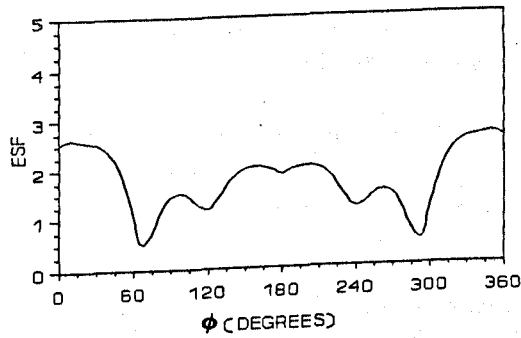
(l) Mzb. WELD-RUN PIPE EDGE.
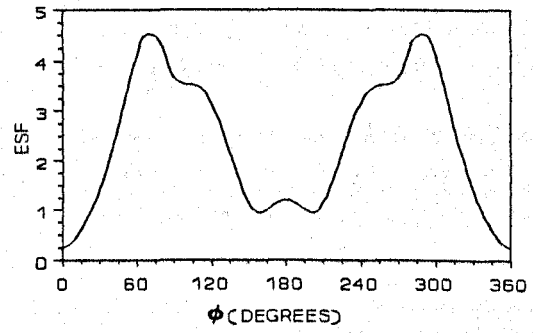
(m) Mxb. WELD-RUN PIPE EDGE.
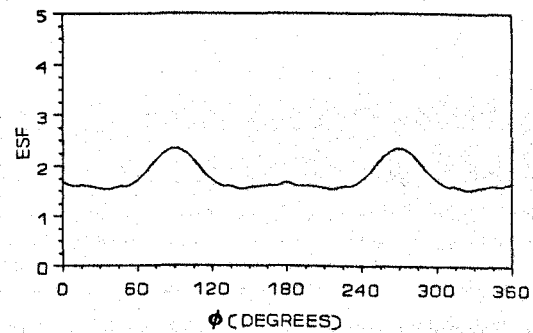
(n) PRESSURE. WELD-RUN PIPE EDGE.

FIG. 79(CONTD.).
ESF DISTRIBUTIONS
ALONG WELD-RUN PIPE JUNCTURE

136
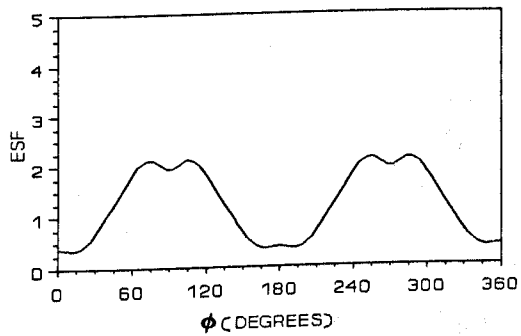
(o) Mxr. WELD-BRANCH PIPE EDGE.
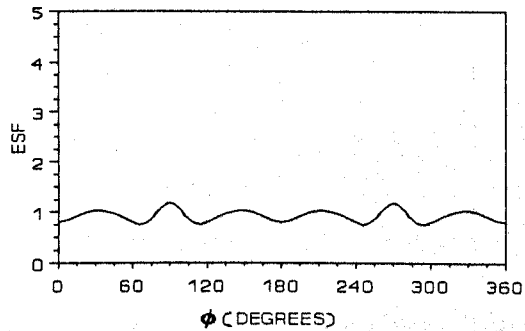
(p) Mzr. WELD-BRANCH PIPE EDGE.
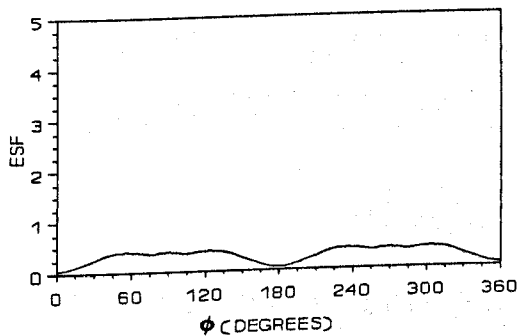
(q) Myr. WELD-BRANCH PIPE EDGE.
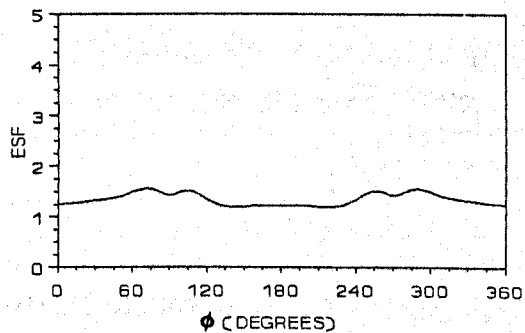
(r) Myb. WELD-BRANCH PIPE EDGE.
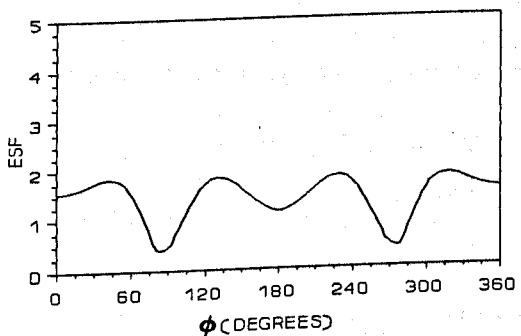
(s) Mzb. WELD-BRANCH PIPE EDGE.
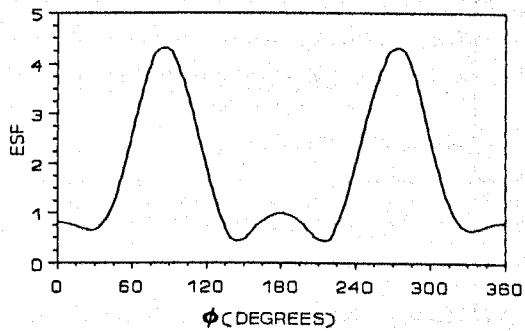
(t) Mxb. WELD-BRANCH PIPE EDGE.
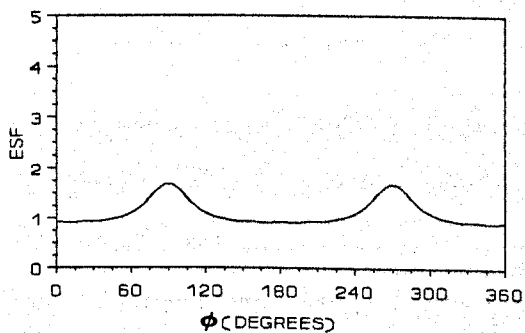
(u) PRESSURE. WELD-BRANCH PIPE EDGE.

FIG. 79(CONTD.).
ESF DISTRIBUTIONS
ALONG WELD-BRANCH
PIPE JUNCTURE

137
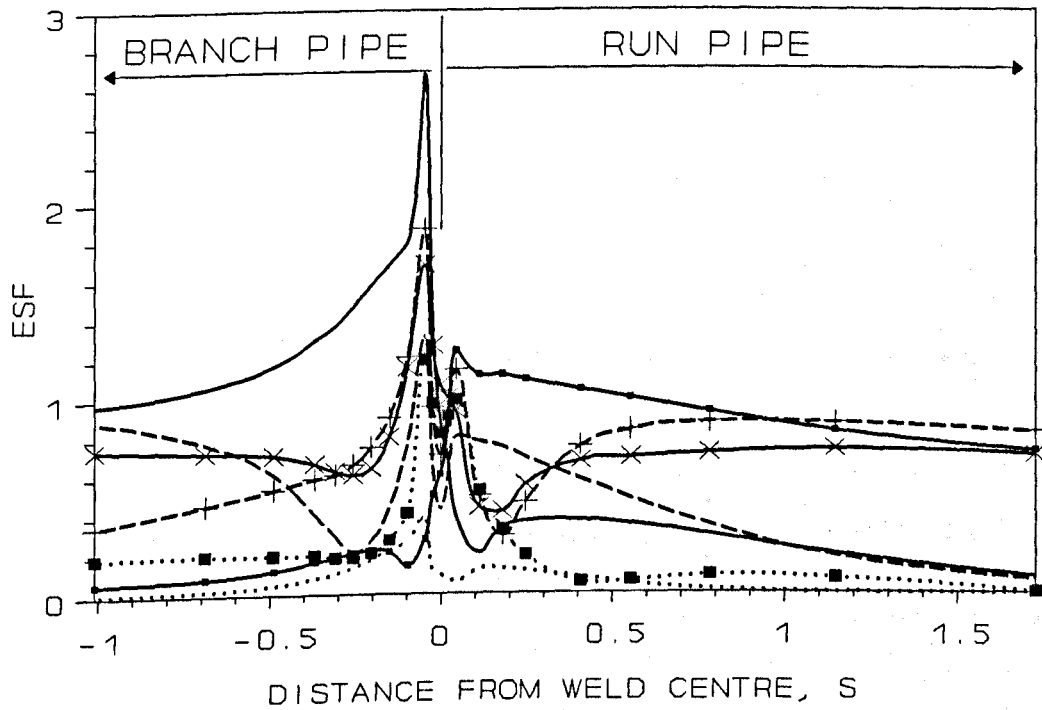
(a) LONGITUDINAL PLANE. OUTER SURFACE.
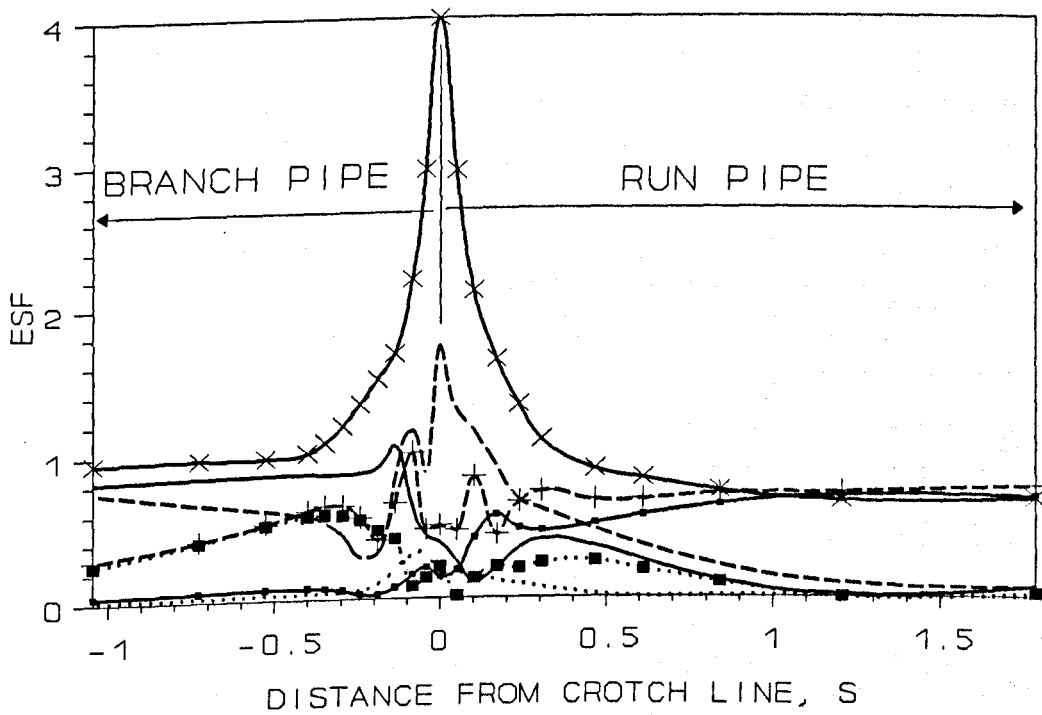
(b) LONGITUDINAL PLANE. INNER SURFACE.

FIG. 80.   ESF DISTRIBUTIONS IN BRANCH AND RUN PIPES. (KEY TO MARKERS AS IN FIG. 80(c))

138
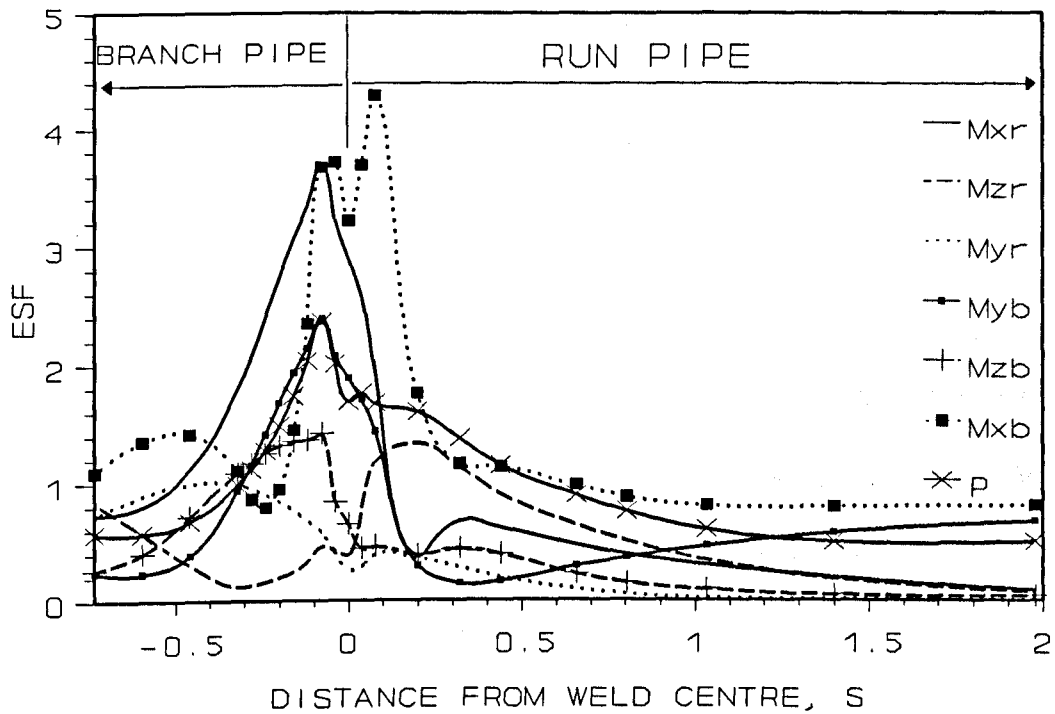
(c) TRANSVERSE PLANE. OUTER SURFACE.
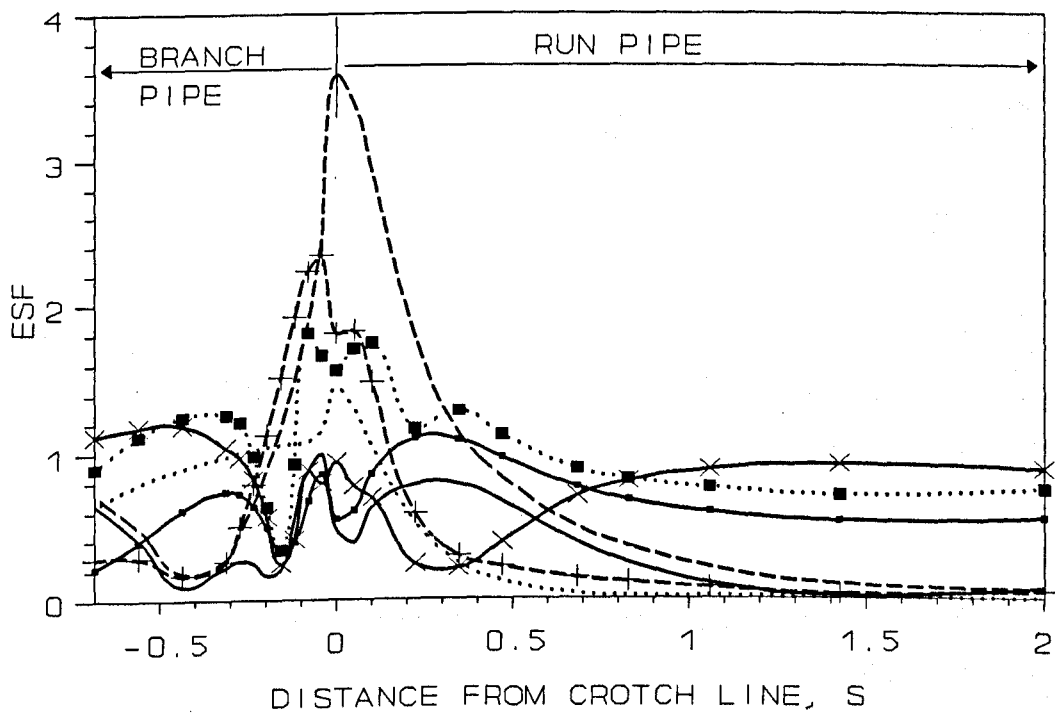
(d) TRANSVERSE PLANE. INNER SURFACE.

FIG. 80(CONTD.).   ESF DISTRIBUTIONS IN BRANCH AND RUN PIPES. (KEY TO MARKERS AS IN FIG. 80(c))

Table 16. <u>Maximum ESFs and locations - absolute values and at transverse or longitudinal plane.</u>

Load	Maximum ESFs at transverse or longitudinal plane[a]	Absolute maximum ESFs
M_{xr}	3.69, weld-run, TP[b]	3.95, 51°, crotch line[c]
M_{zr}	3.58, crotch line, TP	3.58, 90°, crotch line
M_{yr}	1.46, crotch line, TP	1.46, 90°, crotch line
M_{yb}	2.39, weld-run, TP	2.65, 51°, crotch line
M_{zb}	2.34, run pipe, 7.9 mm from crotch line, in, TP	2.66, 73°, crotch line
M_{xb}	4.28, weld-branch, TP	4.51, 67.5°, weld-run
P	4.00, crotch corner, LP	4.08, 0°, crotch corner

[a] TP = transverse plane, LP = longitudinal plane
[b] example: maximum ESF=3.69 on weld-run pipe junction in transverse plane
[c] example: maximum ESF=3.95 at $\phi=51°$ on crotch line

4.3.6. Load interactions

The load interaction diagram is a plot of a combination of two or more loadings that would cause the maximum effective stress in the tee branch to reach the yield stress of the material. For 2-load interactions, from 7 load categories, there are 21 possible pairs of load combination. The interaction diagrams for the tee branch are presented in Figs. 81(a)-(u). The data for these plots are calculated by the computer program FINALT. The load interactions are discussed in the following groups:-

i. dissimilar moment loads on same limb of the branch junction, as in Figs. 81(a)-(f).
ii. similar moment loads on different limbs, as in Figs. 81(g)-(i).
iii. dissimilar moment loads on different limbs, as in Figs. 81(j)-(o).
iv. internal pressure plus moment load, as in Figs. 81(p)-(u).

For the purpose of grouping the loading pairs, $\bar{M}_x:\bar{M}_x$, $\bar{M}_y:\bar{M}_y$ and $\bar{M}_z:\bar{M}_z$ are considered similar moment pairs, while dissimilar moments pairs are $\bar{M}_x:\bar{M}_y$, $\bar{M}_y:\bar{M}_z$ and $\bar{M}_z:\bar{M}_x$. The discussion on load interaction is limited to the results obtained from the tee branch under

140

study. The interaction diagrams can be grouped roughly into two categories; by symmetry and by linearity of the yield loci. Symmetrical yield envelope means that in a combined loading, the sign of one of the loads does not affect the overall first yield.

Out of 21 pairs of interacting loads, 13 pairs exhibit perfect symmetry and the other 8 pairs show tendencies for a reversed load to increase or decrease the maximum effective stress. The pairs which show unsymmetrical behaviour are $\bar{M}_{xb}:\bar{M}_{yb}$, $\bar{M}_{xr}:\bar{M}_{yb}$, $\bar{M}_{yr}:\bar{M}_{xb}$, $\bar{M}_{zb}:\bar{P}$, $\bar{M}_{zr}:\bar{P}$ and all cases of similar moments on the run and branch pipes. The most extreme case of unsymmetry is $\bar{M}_{zr}:\bar{P}$, i.e. when in-plane moment on the run pipe interacts with pressure. In the $\bar{M}_{zr}:\bar{P}$ interaction, a negative in-plane run pipe moment lessens significantly the tendency of the branch pipe to yield. The first yield internal pressure capacity can be increased by as much as 50% and the negative moment can be increased by as much as 30%.

It is difficult to categorize the loading pairs by yield locus symmetry or linearity. There are no definite and simple trends, but simplified and conservative relationships have to be found for further classification. Fig. 82 shows how the various loading pairs can be grouped into 5 simplified diagrams which are made up of circular, linear or square relations in each quadrant. The groups shall be referred to as cases (a)-(e) in Fig. 82.

i. <u>Dissimilar moment loads on same limb</u>

Out of six pairs of moment loads on the same limb, in Fig. 81(a)-(f), only the $\bar{M}_{xb}:\bar{M}_{yb}$ interaction is sign dependent and is best represented by case (e) of Fig. 82. The two $\bar{M}_y:\bar{M}_z$ loadings on the same limb ($\bar{M}_{yb}:\bar{M}_{zb}$ and $\bar{M}_{yr}:\bar{M}_{zr}$) gives a linear relation and the other interactions in this group are close to circular. For simplicity and conservatism, the loading pairs in this group are best represented by a linear relation:-

$$\overline{M}_{1r} + \overline{M}_{2r} \leq 1 \qquad\qquad (84)$$

and $\qquad \overline{M}_{1b} + \overline{M}_{2b} \leq 1 \qquad\qquad (85)$

where $\overline{M}_1$ and $\overline{M}_2$ are any two of the three moments.

ii. Similar moment loads on different limbs

In this group, the $\overline{M}_{xr}{:}\overline{M}_{xb}$ and $\overline{M}_{zb}{:}\overline{M}_{zr}$ interactions are simplified by case (d) of Fig. 82, while the $\overline{M}_{yr}{:}\overline{M}_{yb}$ pair is close to the linear case (b). This loading group can be best represented by a linear relation:-

$$\overline{M}_{1r} + \overline{M}_{1b} \leq 1 \qquad\qquad (86)$$

where $\overline{M}_1$ is any one of the three moments.

iii. Dissimilar moment loads on different limbs

The six pairs of moment combinations are shown in Figs. 81(j)-(o). Two ($\overline{M}_{xr}{:}\overline{M}_{yb}$ and $\overline{M}_{yr}{:}\overline{M}_{xb}$) of the six pairs are sign dependent and four symmetrical pairs show almost linear or circular interaction. For this group, the most conservative relation to describe all the pairs is again a linear interaction:-

$$\overline{M}_{1r} + \overline{M}_{2b} \leq 1 \qquad\qquad (87)$$

iv. Moment + Pressure

For the Moment:Pressure interactions in Figs. 81(p)-(u), the yield loci are not far from circular with the exception of the load pair $\overline{M}_{zr}{:}\overline{P}$. If a linear relation is utilised for the whole group, with the exception of the interaction of positive $\overline{M}_{zr}$ plus pressure loading, the stresses from other load pairs would be much overestimated. A circular relation is thus considered:-

$$\overline{P}^2 + \overline{M}^2 \leq 1 \qquad\qquad (88)$$

In Schroeder et al's [48] study on the limit behaviour of tee branches, the theoretical Moment:Pressure interaction was obtained by superimposing the velocity fields for bending moments onto that for internal limit pressure. Schroeder's limit load interaction for $\bar{M}_{xb}$:P varied from a bilinear to a convex curve (tending to circular), depending on geometric parameters. For the $\bar{M}_{zb}$:P interaction, they obtained a nearly straight line.

To investigate pressure coupling effect, a geometrically nonlinear finite element analysis was carried out using ABAQUS [109] finite element code, with combined loads of M_{xb}= 8.0 kN-m and Pressure= 4 MPa. The present linear finite element analysis gave a maximum Mises stress of 297.0 MPa at the junction between the weld and the run pipe, at $\phi=75°$. At the same location, the nonlinear analysis gave a corresponding effective stress of 290.9 MPa. A check was also made for stresses at a few critical locations on the longitudinal and transverse planes of the branch. The predicted stresses from the nonlinear analysis were lower by not more than 4%, indicating a negligible influence of pressure coupling effect for this model.
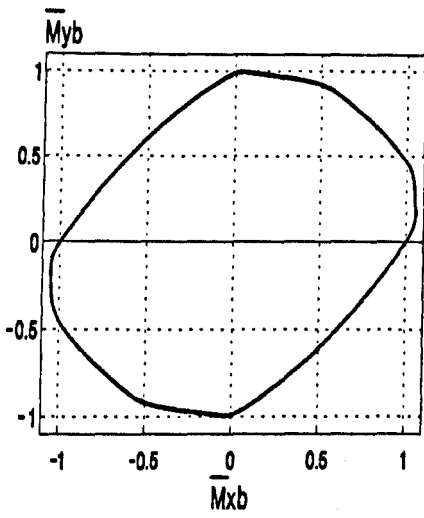
(a)
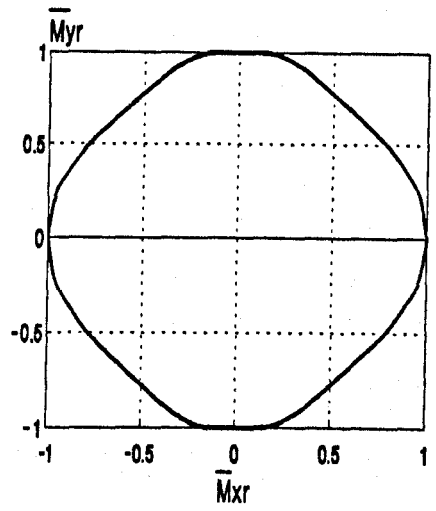
(d)
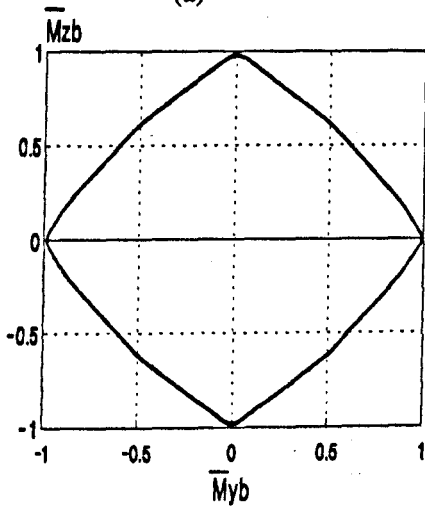
(b)
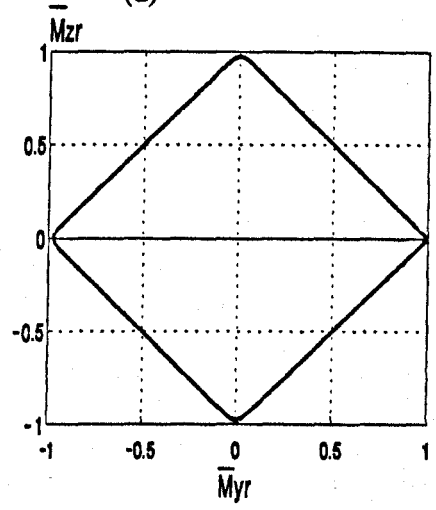
(e)
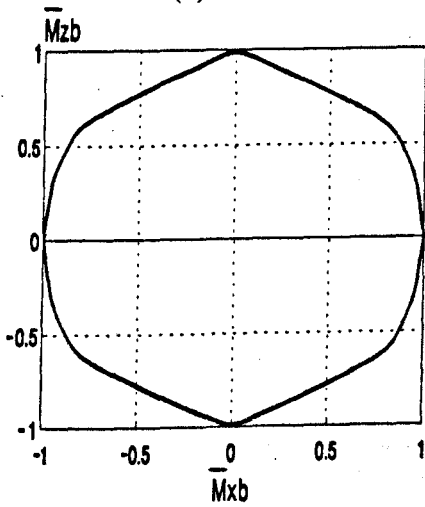
(c)
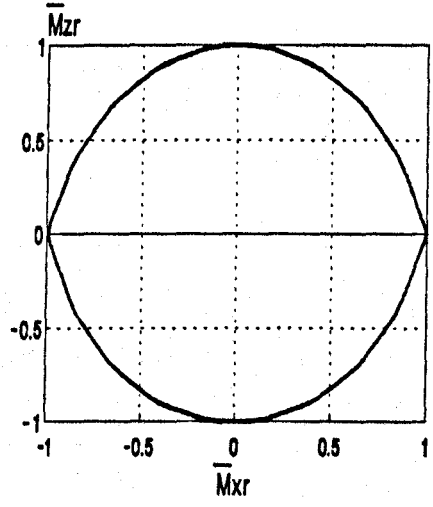
(f)

MOMENTS ON BRANCH PIPE

MOMENTS ON RUN PIPE

FIG. 81. INTERACTION DIAGRAMS - DISSIMILAR MOMENTS ON SAME LIMB.

(g)

(h)

(i)
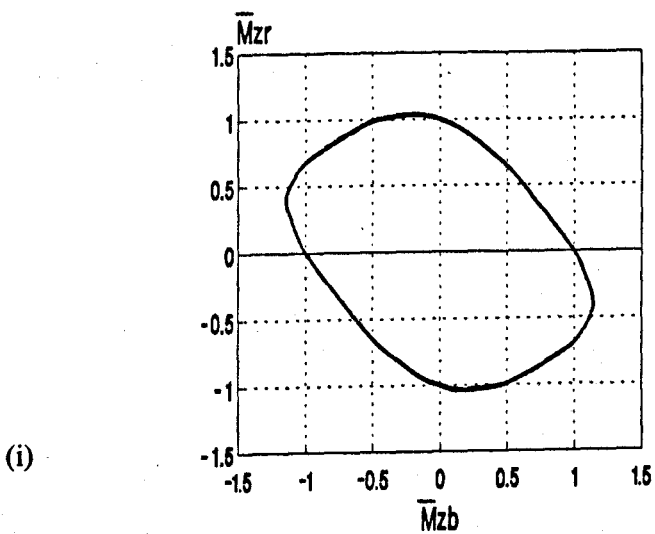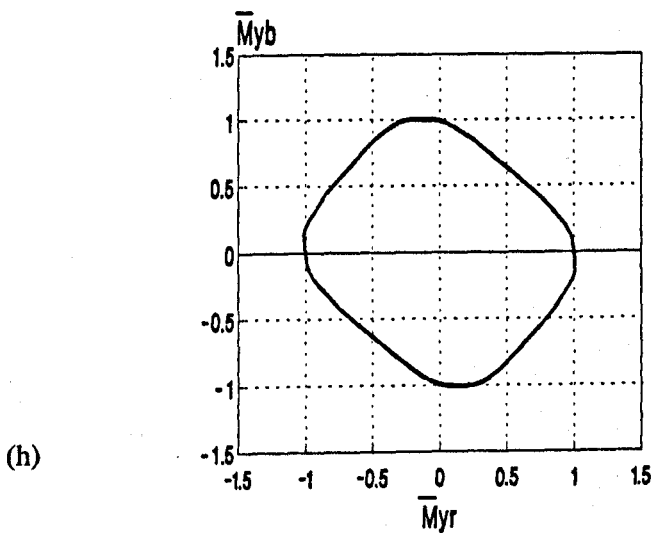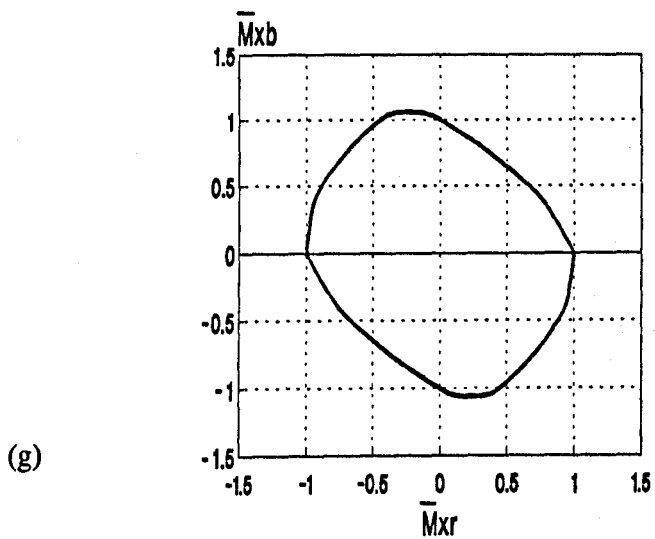
FIG. 81(CONTD.).   INTERACTION DIAGRAMS - SIMILAR MOMENTS ON DIFFERENT LIMBS.
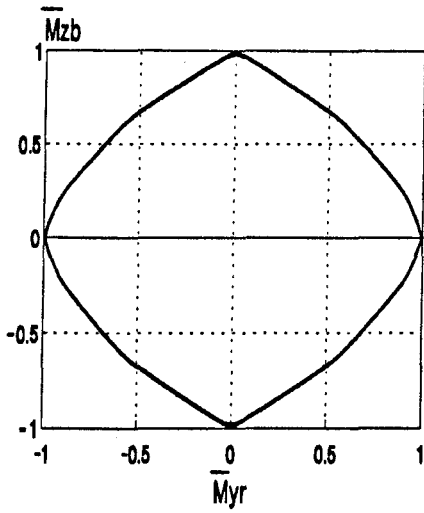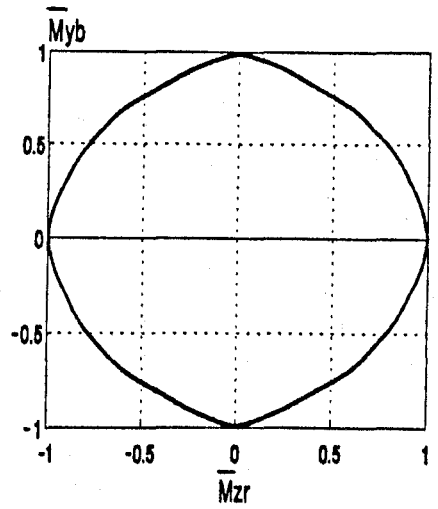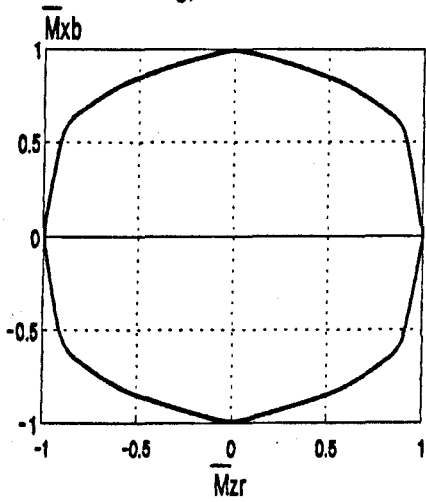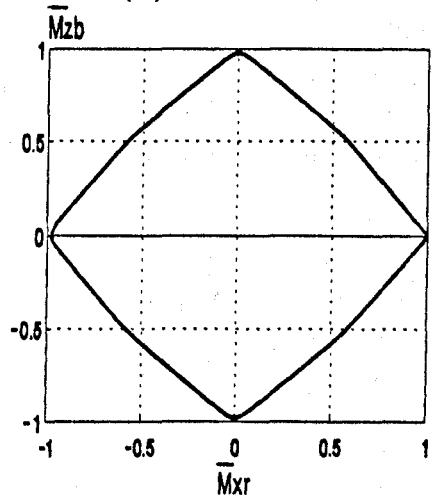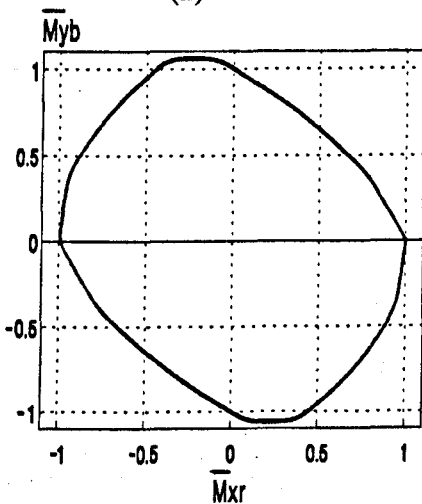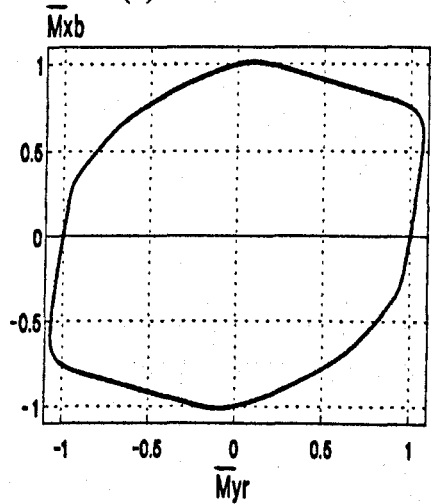
145

FIG. 81(CONTD.).   INTERACTION DIAGRAMS - DISSIMILAR MOMENTS ON
DIFFERENT LIMBS.

146
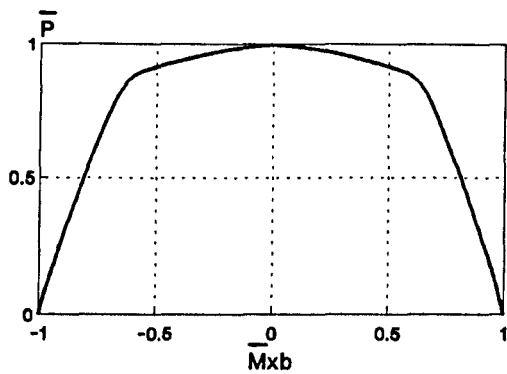
(p)
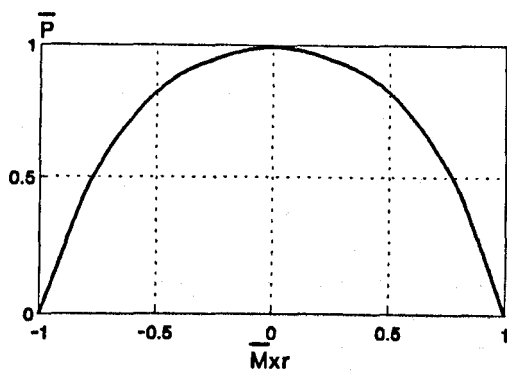
(s)
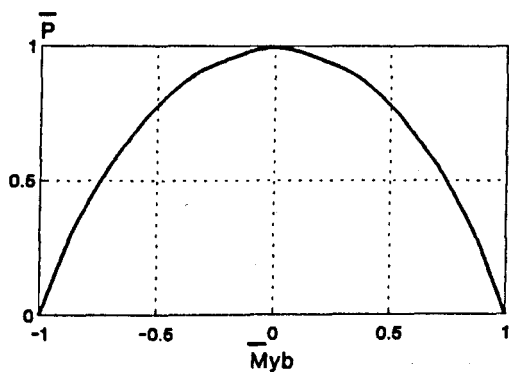
(q)
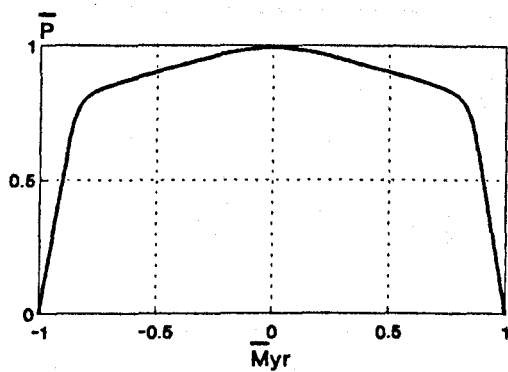
(t)
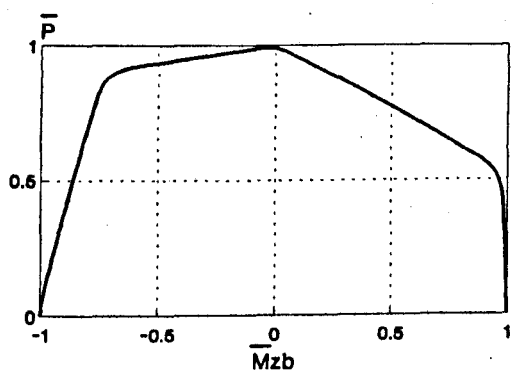
(r)
PRESSURE AND MOMENT
ON BRANCH PIPE
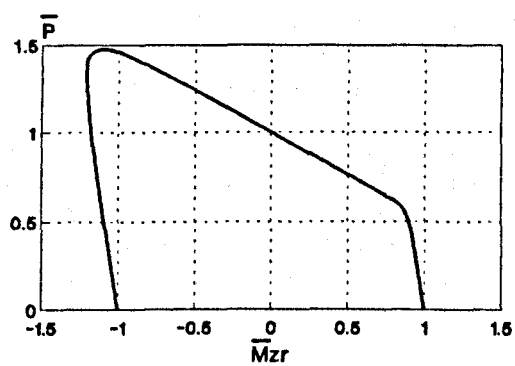
(u)
PRESSURE AND MOMENT
ON RUN PIPE

FIG. 81(CONTD.). INTERACTION DIAGRAMS - PRESSURE AND MOMENTS LOADS.

147
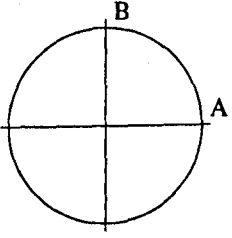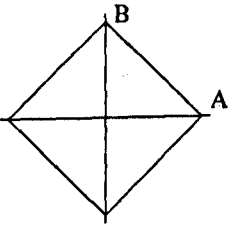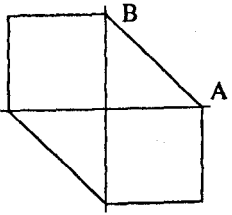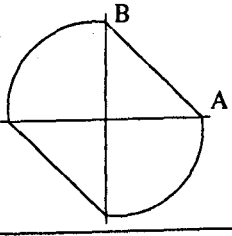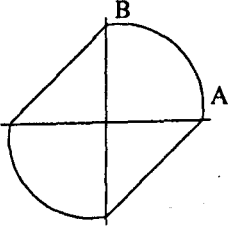
SIMPLIFIED INTERACTION DIAGRAM	PRESENT STUDY d/D=0.8	DIFFERENCE WITH MOFFAT'S [42] ANALYSIS (OTHERWISE SIMILAR)	
		d/D=0.5	d/D=1.0
(a)	Mxr:Mzr	Case (d)	Case (b)
	Mxb:Mzb	Case (e)	Case (b)
	Mzr:Myb		
	Mzr:Mxb		
	All P:M except Mzr:P	Mxr:P Case (e) Mzb:P Case (b)	Mzb:P Case (d)
(b)	Mxr:Myr	Case (a)	
	Myb:Mzb		
	Myr:Mzr		
	Myr:Myb	Case (a)	Case (d)
	Myr:Mzb		
	Mxr:Mzb		
(c)	Mzr:P	Case (d)	
(d)	Mxr:Mxb	Case (e)	
	Mzb:Mzr	Case (a)	Case (c)
	Mxr:Myb		
(e)	Mxb:Myb	Case (a)	Square in 1st and 3rd quadrant
	Myr:Mxb		

FIG. 82. SIMPLIFIED 2-D INTERACTION DIAGRAMS   FOR TEE BRANCH

148

4.3.7. Load interactions from Codes

In branch junctions, the combined effect due to both run and branch moments and internal pressure must be added for stress evaluation. The Codes assume that the locations of the maximum stresses from internal pressure and external moments coincide. From Table 16, the maximum stresses occur at different locations, hence the method of combining stresses in the Codes is conservative. The ASME code allows run moments to be applied at both ends of the run pipes and can be misunderstood. The run moments are moments that exist in the run pipe that are not produced to balance the branch moments. Section NB-3683.1(d) shows how the run moments can be calculated. For the case of the cantilever model, the reaction moments at the fixed end are always equal and opposite to those applied at the run pipe free end. Hence the run moments are simply the moments that are applied at the free end. In ASME Section III NB-3683.1(c), the resultant branch and run pipe moments are determined from a combination of the three moment loadings on the limb,

$$M_b = \sqrt{(M_{xb}{}^2 + M_{yb}{}^2 + M_{zb}{}^2)} \qquad (89)$$
$$\text{and} \qquad M_r = \sqrt{(M_{xr}{}^2 + M_{yr}{}^2 + M_{zr}{}^2)} \qquad (90)$$

The closest resemblance to the study of first yield behaviour is the check on combined primary-plus-secondary stressing. The check ensures that the combined stresses due to nominal stresses and discontinuity effects at the branch junction are within acceptable limits. The combined stress relationship from Eqn. (10) of ASME Section III NB-3653.1(a) is given by:-

$$C_1\frac{PD_o}{2T} + C_{2b}\frac{M_b}{Z_b} + C_{2r}\frac{M_r}{Z_r} \le 3S_m \qquad (91)$$

where the coefficients C are the ASME secondary stress indices.

To see how accurate the ASME code is, Eqns. (89), (90) and (91) are used with the loading groups in the above Section 4.5. When dissimilar moments interact on a pipe limb, Eqn. (89) or (90) combines with Eqn. (91) to give a circular relation:-

149

$$\overline{M}_{1b}^{2} + \overline{M}_{2b}^{2} \leq 1 \tag{92}$$

$$\text{or} \quad \overline{M}_{1r}^{2} + \overline{M}_{2r}^{2} \leq 1 \tag{93}$$

where $\overline{M}_{1}$ and $\overline{M}_{2}$ are any two of the three moments.

Similar calculation applied to the other loading groups by using Eqns. (89), (90) and (91) reveals linear interactions. This means that ASME considers the combined moment load on a limb to be the least critical in the design of tee branches. From the FEM results, ASME seems to have underestimated the maximum stress from the linear $\overline{M}_{yb}{:}\overline{M}_{zb}$ and $\overline{M}_{yr}{:}\overline{M}_{zr}$ interactions. To ensure that a linear interaction is also obtained from dissimilar moment loadings on a limb, it is proposed that the following changes be made:-

replace Eqn. (89) with $M_{b} = (M_{xb} + M_{yb} + M_{zb})$ \hfill (94)

replace Eqn. (90) with $M_{r} = (M_{xr} + M_{yr} + M_{zr})$ \hfill (95)

From the FEM results, the Moment:Moment interactions can simply and conservatively be represented by a linear relation and the Moment:Pressure by a circular relation. From Section 4.5 these representations can lead to slight unconservatism in some loading pairs. Eqn. (10) of ASME is a linear relation between all loading pairs. When pressure is one of the interacting loads, a linear interaction causes the combined stress on the left hand side of the equation to be overestimated. Therefore, based on the FEM results, it is proposed that the ASME equation for combined stresses be modified to a less conservative equation:-

$$\left[C_{1}\frac{PD_{o}}{2T}\right]^{2} + \left[\left[C_{2b}\frac{M_{b}}{Z_{b}}\right] + \left[C_{2r}\frac{M_{r}}{Z_{r}}\right]\right]^{2} \leq (3S_{m})^{2} \tag{96}$$

i.e. a linear relation between interacting moments and a circular relation for Moment:Pressure interactions. The proposed resultant branch and run pipe moments (Eqns. (94) and (95)) will cause slight conservatism for dissimilar moment loads on a limb. The proposed interaction Eqn. (96) will cause slight underestimation of maximum stresses in positive $\overline{M}_{zr}$ plus pressure

150

interaction.

In BS 806, using notations used by BS, the sum of the direct stresses due to pressure, in-plane and out-of-plane moments is given by:-

$$f_B = \frac{p(d_1 + t_a)m}{2t_a} + \frac{r_1}{I}\sqrt{(M_iB_i)^2 + (M_oB_o)^2}$$

(97)

The above Eqn. (97) indicates that the BS code does not consider interaction between moments on different limbs nor torsional moment as one of the interacting loads. The in-plane plus out-of-plane moment loads on the same limb is a circular interaction, compared to the proposed linear relation from FEM results. On the other hand, the Moment:Pressure interactions from BS is linear relation whereas it is proposed here to be a circular one.

Moffat and Mistry [42] suggested combining a circular interaction between pressure and moment loads, with a linear interaction of resultant moment pairs to produce a conservative relation:-

$$\left[C_1\frac{PD_o}{2T}\right]^2 + \left[\left[C_{2b}\frac{M_b}{Z_b}\right] + \left[C_{2r}\frac{M_r}{Z_r}\right]\right]^2 \leq (3S_m)^2$$

(98)

which is similar to the formulation being proposed here. The interaction diagrams of the tee branch under study resembles more of Moffat and Mistry's [42] tee branch with d/D = 1.0. For the tee branch with d/D = 0.5, Moffat and Mistry found the interaction for branch moment plus run moment to be circular. For this range of tee branches, a less conservative circular relation was proposed by Moffat, i.e.:-

$$\left[C_1\frac{PD_o}{2T}\right]^2 + \left[C_{2b}\frac{M_b}{Z_b}\right]^2 + \left[C_{2r}\frac{M_r}{Z_r}\right]^2 \leq (3S_m)^2$$

(99)

However, Moffat and Mistry [42] suggested that the more conservative Eqn. (98) be adopted for all diameter ratios.

151

4.4 TORISPHERICAL HEAD WITH NOZZLE

4.4.1 Elastic stresses

The stress factors used here are stresses which have been normalized according to each loading condition, using the normalizing factors listed below. For pressure loading, the normalizing factor is the membrane stress in the spherical shell; for the nozzle axial force and moments, the membrane stresses in the nozzle were used. The nominal stresses are:-

$$\sigma_n = P2L_m/4T \qquad \text{for internal pressure P}$$
$$\sigma_n = 32Md_o/\pi(d_o^4-d_i^4) \qquad \text{for nozzle bending moment M}$$
$$\sigma_n = 4F/\pi(d_o^2 - d_i^2) \qquad \text{for nozzle compressive force F}$$
$$\sigma_n = 32T_od_o/\pi(d_o^4-d_i^4) \qquad \text{for nozzle torsional moment } T_o$$

Hence, the stress factor, $\bar{\sigma}$, is defined by $\bar{\sigma} = \sigma/\sigma_n$ where σ can be any hoop, meridional, maximum or the von Mises effective stress.

In the elastic analysis, the usual procedure of determining stress is to add the simple membrane action to the effect of edge force and edge moment to ensure compatibility. Studies made by others on the effect on maximum stress of the nozzle-crown parameters found that in all load cases, the maximum stress occurs at the juncture. In the present FEM, the critical stresses for all loads occur in the hoop direction at the root of the outside fillet.

Figs. 83 and 84 show the ESF distribution along the meridional plane due to the four load cases. The non-dimensional meridional distance S is consistent with Drabble's definition. Figs. 83(a) and 83(b) show the von Mises and hoop stress factors when the shell is subjected to internal pressure. Pressure loading gives an overall good correlation with the test except at the weld-crown edge and knuckle-cylinder juncture. The FEM results indicate that when subjected to internal pressure, the inner surface of the knuckle region E is the highest stressed area, but two other regions (the crotch corner and outer surface of the crown located at C)

approach the maximum stress. Internal pressure does not cause high stresses in the nozzle. At the location where the hoop stress changes sign near the sphere-torus juncture, the ESF approaches zero. At the crown, the ESF is greater on the outer surface than on the inside, but in the knuckle region the reverse is true. The critical hoop pressure stress distribution is often the subject of discussion, hence it is also included in Fig. 83(b). The points of interest of Fig. 83(b) is the high hoop stress at the crown-weld edge and the compressive hoop stress at the knuckle outer surface which is likely to cause unsymmetric inward buckling. For high D/T ratios, it is reported that internal pressure can also cause considerable compressive hoop stress on the inner surface of the torus portion and large diameter ratios (d/2L) can cause high meridional stress. A point worth noting is Drabble's pressure stress factor at the crotch corner. His value of 1.73 compares well with the FEM value of 1.82. Leckie and Payne's [110] presented stress concentration factor curves for first yield in spherical pressure vessels with cylindrical nozzles. Using $\rho = (d/2L)\sqrt{(L/T)} = 0.795$ and t=T, the maximum ESF (defined by the maximum shear stress in terms of membrane stress in the sphere) due to pressure, gives about 2.8.

Figs. 84(a)-(c) present the ESF on the inner and outer surfaces of the shell for the remaining load cases. The experimental results for torque are not available for comparison. The agreement with experiments from bending moment and axial force is good at the crown near the intersection but fair in other regions. From axial force and moment loads, the ESFs at the weld-crown junctures are much higher than other areas but due to torque the maximum ESF at the weld-nozzle juncture is not much higher than the stress in the nozzle.

The way in which the model was discretized resulted from the main interest of study. It was decided that the stress peaks should be due to stress concentration from the main vessel geometric discontinuities and not from localized effects; hence the FE method gave lower

153

stresses at the weld toes. Had the stresses at the weld toes been the main concern, these regions would have been finely meshed. From above discussions, the experimental results from axial force and moment loads do not satisfactorily agree with the FEM results. This may be due to the loads not accurately applied. In Drabble's [74] tests, both loads were obtained from transverse forces applied to the ends of an I-beam which was clamped across the top of the nozzle. The most likely source of error in this method of loading is eccentric loading, and thus impure axial force or bending moment.

Table 17. Predicted and experimental absolute maximum Mises effective stress factor.

Load	FEM	BS 5500 [111][1]	Experimental [74]	Location from FEM
Torque, T_o	1.11	-	-	nozzle-weld edge
Moment, M	3.31	7.22	3.21	crown-weld edge, in plane of moment
Pressure, P	1.95	2.2	3.13	inner surface of toroidal knuckle
Force, F	5.27	9.62	5.87	crown-weld edge

[1]   Maximum SCF at sphere-nozzle juncture

Table 17 shows the comparison between predicted and experimental results [74] of maximum Mises ESF. The table indicates that the predicted results correlate fairly with the test. The axial force on the nozzle is the most critical load while torsional moment is the least critical. When subjected to nozzle torsional moment, the nozzle-weld edge is highly stressed while the cylinder and knuckle region are lowly stressed. When bending moment and axial force act on the nozzle of the vessel, the crown-weld edge is subjected to maximum stresses while the cylindrical vessel has low stresses. In Drabble's [74] experiment, the locations of first yield for the three load cases occur at the crown-weld edge. From Table 17, the FEM agrees reasonably with the experimental maximum locations for bending moment and axial force but differs by about 38% for pressure loading.

154
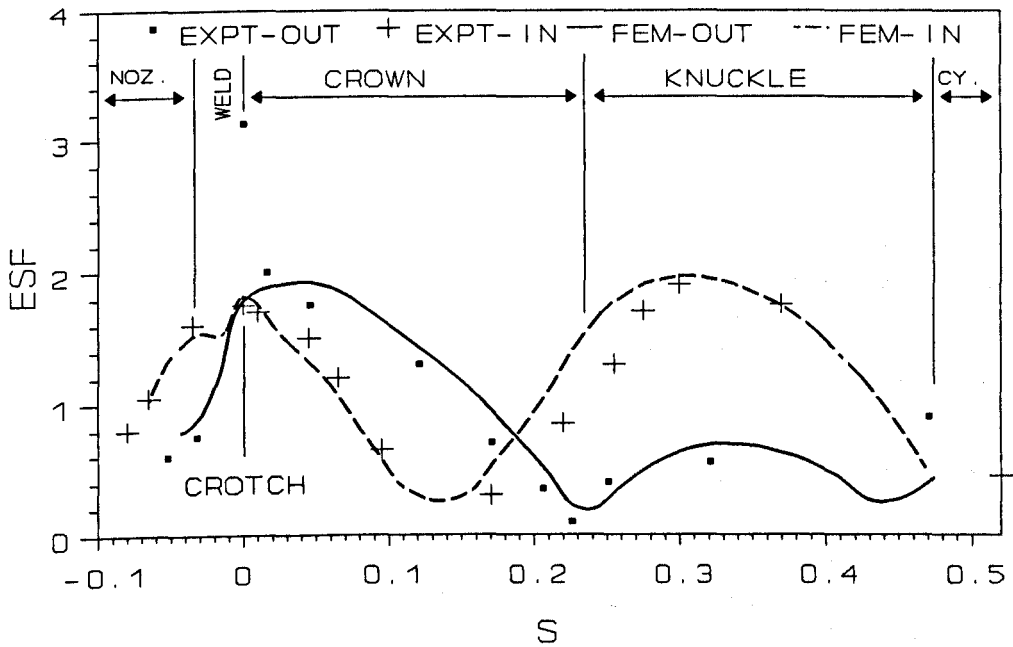
(a) MISES STRESS. INTERNAL PRESSURE.
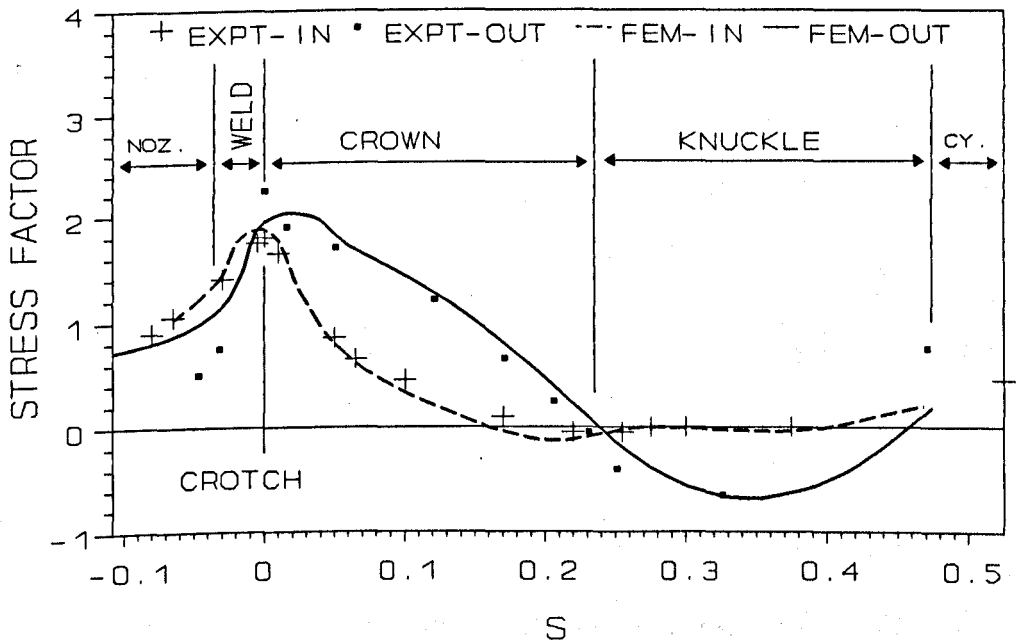
(b) HOOP STRESS. INTERNAL PRESSURE.

FIG. 83.   STRESS DISTRIBUTIONS ON LONGITUDINAL PLANE, DUE TO PRESSURE - A COMPARISON BETWEEN EXPERIMENTAL AND FEM RESULTS. (Note   S=distance from intersection /inner radius of cap).
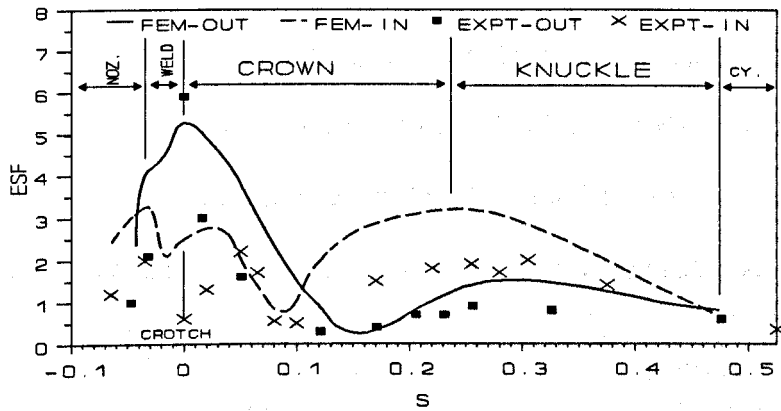
155
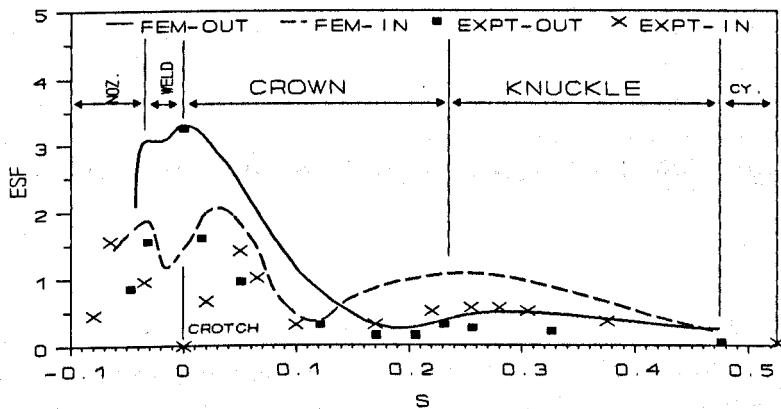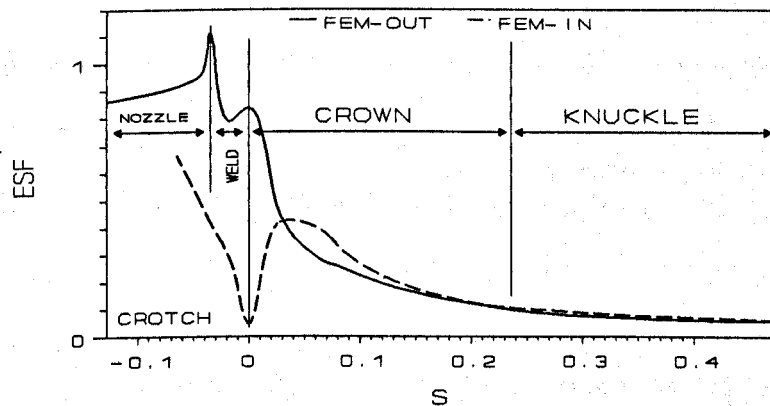
FIG. 84.   STRESS   DISTRIBUTIONS   ON   LONGITUDINAL   PLANE   -   A
COMPARISON BETWEEN EXPERIMENTAL AND FEM RESULTS, FOR
AXIAL FORCE AND BENDING MOMENT. (Note S=distance from
intersection /inner radius of cap).

156

4.4.2 Effects of weld fillet

Experimental studies by other authors, [69][112] and [113], have indicated that the presence of even a nominal fillet at the nozzle-sphere juncture significantly influences stress results on the outer surface. This has been attributed to the added reinforcement at the juncture. The agreement between the thin shell theory and experiment has always been clouded by the large localized effect of the fillet at the juncture between the shell and the nozzle. In elastic thin shell analysis the highest stress at the nozzle base is still overestimated because the presence of the weld fillet in the actual vessel lowers the stress. This is not the case in finite element idealizations where the fillet can be accurately represented by 3-D elements. To model the effects of the weld, the conventional shell theory has been modified by O'Connell and Chubb [114], where the normal forces (to the shell surface) at the juncture were replaced by equivalent bands of pressure.

4.4.3 Effects of geometric parameters

The stress distribution at the local shell-nozzle intersection is characterized by three non-dimensional parameters, i.e. t/T, L/T and $(r/L)\sqrt{(L/T)}$. From parametric studies of other authors, these parameters influence the stress factors and are important in the design process of such pressure vessels. One such variation of stress factor from axial force loading on a nozzle in a torispherical head was described by Chao [115] who, using thin shell theory, varied the stress with t/T while keeping the ratios L/T and $\rho = (r_m/L_m)\sqrt{(L_m/T)}$ constant. Chao found that the maximum ESF first decreases with increasing t/T, but reaches a maximum value prior to increasing with increasing ratio of t/T. This meant that a thicker nozzle does not always lead to a lower stressed structure. Similarly for nozzle bending moment load, there are optimum values of t/T that result in minimum stresses. According to Chao [115], the reason for the optimum t/T is the changeover of stress from hoop to meridional as t/T is increased. From Chao's [115] minimum stress curve of thrust and bending moment loading,

157

the present sphere-cylinder configuration gives minimum stress when t/T is between 0.55 and 0.65. An optimum value of t/T does not apply for the case of internal pressure loading; a higher t/T ratio always results in a stronger structure.

If the stresses in the knuckle were also considered, the magnitude and location of yielding is influenced by additional parameters of the knuckle. Many authors generalize the effects on stress at the intersection of pressure vessels by the sphere and nozzle parameters. According to Mershon [112], there is some evidence that in the reinforced condition, with 2L/T increasing, the hoop stress on the outer surface increases. According to Lind [116], the failure mechanism is restricted to certain ranges of the shape parameters. For a very thin nozzle in a vessel with very thick walls yielding will be entirely in the nozzle. Similarly for low values of the diameter ratio (d/2L less than 0.1) and for thick-walled nozzles, yielding will be in the main vessel. The diameter ratio (d/2L) affects maximum stresses at the nozzle-shell juncture. In general the stresses increase with increasing diameter ratio up to a $d/D \approx 0.8$. after which the stresses either are reduced or level off.

4.4.4 Load interactions

Many stress analyses have been carried out for separate loadings of internal pressure, bending and thrust on the nozzle. In the present analysis torsional moment has been included to study the first yield behaviour at the vessel-nozzle intersection when two loads interact. From the 4 load cases, 6 load interactions could be plotted. Figs. 85(a)-(f) show the first yield load interaction curves at the vessel-nozzle juncture. The applied loading on the nozzle could easily have been wrongly interpreted as a plain pipe problem. In fact, for the same load combination, some of the interaction curves are different from those of the plain pipe, especially if the maximum stress due to the load occurs on the vessel crown.
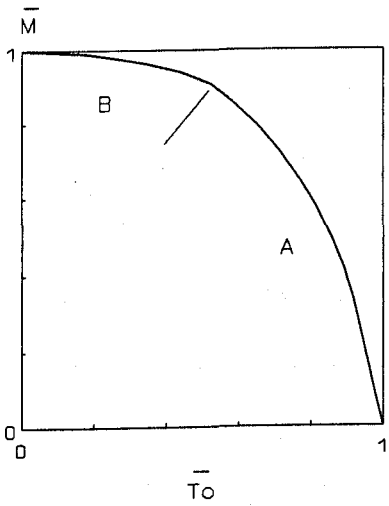
(a) TORQUE:MOMENT
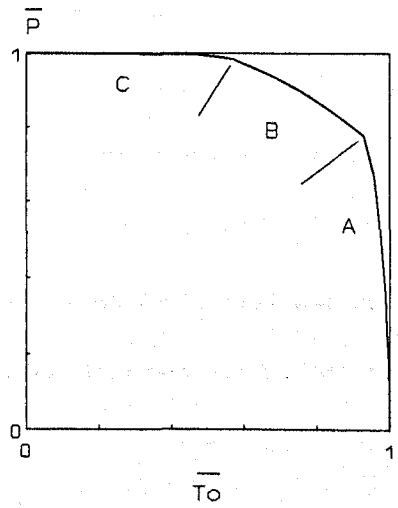
(b) TORQUE:PRESSURE
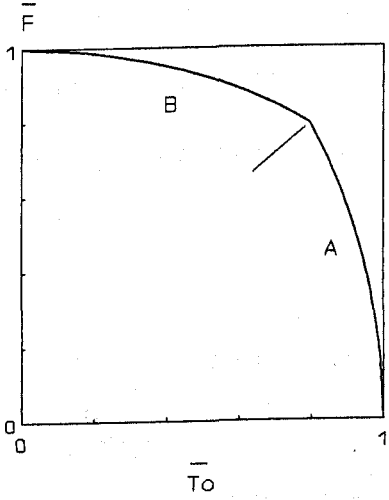
(c) TORQUE:AXIAL FORCE
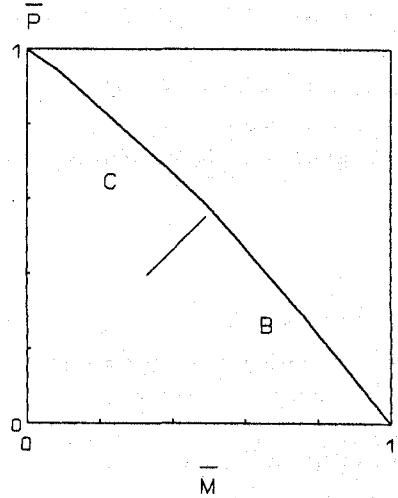
(d) MOMENT:PRESSURE
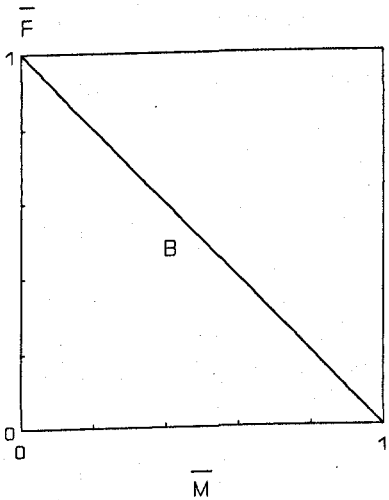
(e) MOMENT:AXIAL FORCE
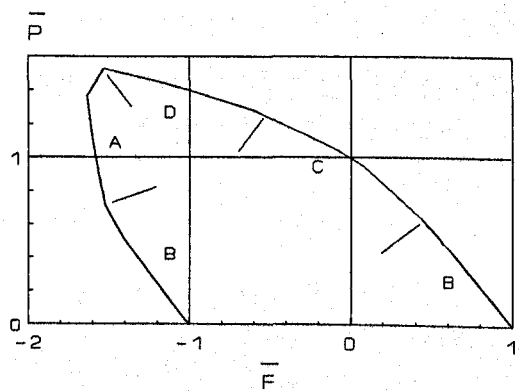
(f) AXIAL FORCE:PRESSURE

FIG. 85.   LOAD INTERACTION DIAGRAMS FOR TORISPHERICAL SHELL WITH NOZZLE. (First yield locations A-E shown in Fig. 14)

159

Two load pairs show the most critical linear interaction, namely, $\overline{M}$:$\overline{P}$ and $\overline{M}$:$\overline{F}$, while three load pairs of $\overline{T}_o$:$\overline{M}$, $\overline{T}_o$:$\overline{P}$ and $\overline{T}_o$:$\overline{F}$ can simply and conservatively be represented by a circular relation. The symmetry of these five pairs, shown only in first quadrant in Figs. 85(a)-(e), means that the yield behaviour is not affected by the sign of both interacting loads. The $\overline{F}$:$\overline{P}$ interaction in Fig. 85(f) can be simply represented by a linear relation for the first and third quadrant and a square relation in the second and fourth quadrant. However if a general and consistent (with geometric parameters) relation is to be assigned to the $\overline{F}$:$\overline{P}$ pair, a linear relation fits well. For the $\overline{F}$:$\overline{P}$ combination, a tensile force on the nozzle plus internal pressure is a critical combination while a nozzle compressive force plus pressure results in low stress field. For this particular vessel configuration, the first yield compressive thrust on the nozzle and pressure can be increased by as much as 60%, provided the interacting loads are of the proper magnitude.

In general, the location of maximum stress from combined loadings can be predicted from the maximum location due to individual loads. From the load interaction curves, sudden changes in slope can be attributed to yielding moving from one location to another. These changes of location are marked on the load interaction diagrams. Point A in Fig. 14 represents a section of the structure which passes through the weld-nozzle edge, and point B is contained in the section through the crown-weld edge. The $\overline{F}$:$\overline{P}$ interaction is a case where the maximum stress can occur at a location which is not critical to either a thrust or pressure loading. From Fig. 85(f), a negative force on the nozzle interacting with internal pressure produces maximum effective stress at locations A or D in Fig. 14..

Drabble [74] constructed a three-load initial yield locus from the available strain gauge readings. From the isometric plot, the general trend of his load interaction agrees well with the present result, but the load magnitude cannot be verified accurately.

As in the stress analysis of elbows, the method of superposition of stress data in some geometries is questionable. In one of the experimental tests, Witt et al [117] conducted a superposed loading on a spherical shell with protruded nozzle. The model which had geometric ratios d/2L=0.078, d/t=9.5 and 2L/T=81.33 was loaded simultaneously with axial force and internal pressure. From inspection of the larger stresses, they remarked that the method of stress superposition was accurate. Apart from the flush nozzle, the present crown geometry which differs slightly (d/2L=0.14, d/t=9.0 and 2L/T=64.0) from Witt's model should exhibit similar valid superposition characteristics.

4.4.5 The BS 5500 code

The high stresses at the intersection are caused by discontinuity shear stresses and moments which exist to maintain compatibility at the juncture. The conventional method of analysis and design of pressure vessels is the use of standard design codes, such as the ASME and BS, which are based on the classical membrane theory and hence involves many inconsistencies and inaccuracies at the geometric junctures. In BS 5500 [111], the design of the opening is carried out by applying a stress concentration factor (SCF) to the nominal stress in the spherical shell rather than in the nozzle. The SCF is based on the maximum principal stress theory and calculated with respect to the sphere membrane stress if the loading is internal pressure. The nominal stresses for other load categories are found in Sect. G.2.5 of BS 5500 [111]. The SCF can be read off from SCF curves once the values of ρ (defined on Page 153) and t/T are known. The SCF does not make any distinction between the inner and outer surface stresses. The SCF values from the Code in Table 17 are therefore meant for the spherical shell, but normalized with the same factors as in the FEM and experimental results. From the comparison in Table 17, with the exception of pressure, the BS code overestimates the FEM values by a large margin. Under the action of combined loading, the BS suggests a conservative estimate of the combined stress by adding the maximum stresses for individual

161

loadings.

CHAPTER 5.   CONCLUSIONS

The study describes the stress analysis of some commonly used piping components. Since only one specific geometry of the tee branch and torispherical shell with nozzle have been investigated, the conclusions apply to the particular vessel. The stress behaviour and load interaction were carried out by the application of the finite element method and for one particular elbow geometry, an experimental test was carried out. The following conclusions are drawn:-

5.1. PLAIN PIPES

1. The finite element model with one layer of 20-node elements through the wall thickness is sufficient to give accurate hoop and axial stresses for both thick and thin pipes.

2. The method of linear superposition of stresses from separate load effects is satisfactory for thick and thin pipes. If buckling does not precede yielding, the set of interaction curves can be used to predict yielding in pipes. With the present set of stress database obtained from four pipes, the computer program allows prediction of first yield interaction for any pipe dimension.

3. For the $\overline{T}_o:\overline{P}$ and $\overline{M}:\overline{P}$ load pairs, as the pipe gets thinner (larger D/T), yielding occurs at lower combined loads. For other load pairs, the interactions are not affected by D/T ratios.

4. Comparison with the BS code shows mixed results because of different yield criteria. The derived BS yield formulations show a large difference for the $\overline{M}:\overline{P}$ pair, slight conservatism for the $\overline{T}_o:\overline{P}$ pair and identical circular relation for the $\overline{T}_o:\overline{M}$ pair.

5. Even when compared with the FEM Tresca criterion, the BS results differ because

of different assumptions.

5.2. PIPE BENDS

1. The FEM results were compared with those from analytical methods and it was shown that the results of thicker elbows ($D/T \leq 20$) agree well.

2. For torque and moment loads, as the elbows get thicker, the maximum ESFs become less affected by b ($= R/r$). For internal pressure, when $D/T > 40$ and $b > 5$, the maximum ESF is not affected by D/T and b.

3. The ASME and Rodabaugh's results for torque loading are suspect. For moment loading, they are more conservative for low values of λ.

4. The $\overline{M}:\overline{T}_0$ and $\overline{T}_0:\overline{P}$ first yield load interactions are not significantly affected by R/r and D/T. The $\overline{M}:\overline{P}$ interaction is not much affected by R/r but significantly affected by D/T.

5. In certain cases, a combined loading of internal pressure and in-plane moment causes a reduction in maximum ESF which can be quite considerable in thin elbows ($D/T > 80$).

6. Compared to the FEM, the BS rules are conservative for $\overline{T}_0:\overline{P}$ interaction. The ASME load interaction agrees with the FEM.

7. From the finite element method, it is proposed that the $\overline{T}_0:\overline{P}$ and $\overline{M}:\overline{P}$ load interactions be taken to be linear and the $\overline{M}:\overline{T}_0$ to be circular. For the $\overline{M}:\overline{P}$ interaction, if the linear relation is assumed, for some elbow geometries, the effective stresses can be significantly conservative.

8. From the limited amount of information available on a thin elbow, the increase in in-plane moment- or torque-carrying capacity is mainly due to the nonlinear load coupling.

9. In both $\bar{M}{:}\bar{P}$ and $\bar{T}_o{:}\bar{P}$ load interactions, the maximum moment- or torque-carrying capacity is not necessarily achieved at high internal pressures. From the thinner elbow model EL01, the maximum von Mises stresses are greatly reduced between $\bar{P}=0.2P_Y$ and $\bar{P}=0.5P_Y$.

10. For the thick elbow, the results from the linear analysis give satisfactory correlation with an analysis which includes geometric nonlinearity and nonlinear coupling effect. Since all the linear load interaction curves are more conservative, the plots which are produced for elbows with about the same geometric parameters as EL07, can be used to predict first yield behaviour with high accuracy.

11. Although slightly less conservative, the BS 806 Code is satisfactory in determining the maximum SCF for moment load.

12. The most appropriate $\bar{P}{:}\bar{M}$ interaction for a thick long radius elbow is linear one.

5.3. TEE BRANCH

1. The good correlation between the present finite element results and Moffat et al's [43] empirical ESFs suggests that finite element method is capable of giving satisfactory results of a complex piping geometry. The resultant first yield load interaction results are also satisfactory provided the principle of superposition holds for the structure.

2. In finite element modelling of the branch junction, the lower order elements are unsuitable even after further mesh refinement. The use of a single layer of higher order 20-node brick elements, with moderate mesh refinement, is suitable.

3. In every loading, except M_{xb}, the maximum ESFs occurred on the inside surface. Apart from pressure loading, the maximum ESF values occurred within $\pm45°$ of the transverse plane. Pressure loading produced a maximum effective stress in the transverse plane.

4. The stresses from the branch pipe loads are more intensified than from run pipe loads. The out-of-plane branch moment loading gives higher maximum stress intensity than by any other loading.

5. For the six moment categories, the effective stress factor can be expressed in the form

$$ESF = Q(R/T)^a(r/R)^b(t/T)^c$$

to reflect its dependence on the various geometric parameters.

6. The effect of increased weld reinforcement is to reduce high stresses at the intersection, especially due to loads on the branch pipe. Due to internal pressure, the weld reinforcement does not play an important role in decreasing the maximum stress at the crotch corner.

7. For all the load cases, the present results agree well with other FEM and experimental results, provided the weld details are nearly identical.

8. The use of the ASME III code beyond the limit of application can result in an overestimation of stresses. The design codes should consider the effects of twisting moments on the branch and run pipes because they are not negligible.

9. For some load combinations, one of the interacting loads has a strengthening effect upon the other. In such cases, the tee branch is capable of sustaining higher loads at specific combinations before yielding sets in. The most prominent case is the negative M_{zr} interacting with internal pressure.

10. For simplification and conservatism, the interaction between moments on the run and branch pipes should be taken to be linear, and the interaction between moment and pressure loads to be circular.

11. The ASME III general equations for checking combined stresses should be modified on two fronts. The proposed resultant moments are:-

$$M_b = (M_{xb} + M_{yb} + M_{zb})$$

166

and $M_r = (M_{xr} + M_{yr} + M_{zr})$

The proposed equation for combined stress is:-

$$\left[c_1 \frac{PD_o}{2T}\right]^2 + \left[\left[c_{2b}\frac{M_b}{Z_b}\right] + \left[c_{2r}\frac{M_r}{Z_r}\right]\right]^2 \leq (3S_m)^2$$

12.   The practical importance of the present load interaction analysis is in the design of similar tee branches. Tee branches of other parameters need further investigation.

5.4. TORISPHERICAL HEAD WITH NOZZLE

1.   The agreement between calculated and experimental results was fair.

2.   For all the load categories, high stresses occurred at the vessel-nozzle juncture because of the geometric discontinuity. For internal pressure, the stress peaks at locations remote from the nozzle juncture were similar to a torispherical vessel without nozzle.

3.   When torque is one of the combined loads, a is circular interaction is proposed. For other load combinations a linear relation is proposed.

CHAPTER 6.   SUGGESTIONS FOR FUTURE WORK

1.   The study assumes the small displacement theory. In reality, when thin-walled structures are subjected to moment loads, large geometric displacements influence the stress history and this has to be taken into account for a more accurate analysis.

2.   A study should be undertaken to develop more advanced design methods and rational design criteria to evaluate elasto-plastic structural behaviour of piping components. Is has been reported by Kirkwood and Moffat [118] that once the first yield limit has been exceeded in branch junctions, the load interactions using other approaches (such as three times elastic slope or five times elastic slope) are significantly different from first yield interactions.

3.   Research work should be carried out to investigate the effect of structural geometric imperfection on load interaction. Due to the nature of manufacturing, the pipe cross-sectional shape may not be perfectly circular and variation of wall thickness is not uncommon. In order to make specific changes to analytical or design procedures more work is needed to provide quantitative data.

4.   For the tee branch, an extension of FEM work on branches with diameter ratios of between 0.8 and 1.0 and $D/T > 100$ should be carried out to confirm the stress behaviour in tee branches in that range. The most likely problem encountered here would be modelling of the weld details at the flanks. Since it has been shown that the weld details highly influence the resulting maximum stresses, the size of the weld should reflect the other pipe dimensions.

REFERENCES

[1] Stokey W.F., Peterson D.B. and Wunder R.A. - *Limit loads for tubes under internal pressure, bending moment, axial force and torsion.* Nuclear Eng. and Design, Vol. 4, 1966, pp. 193-201.

[2] Larson L.D., Stokey W.F. and Panarelli J.E. - *Limit analysis of a thin-walled tube under internal pressure, bending moment, axial force and torsion.* Jour. Appl. Mech., 1974, pp. 831-832.

[3] Franzen W.E. and Stokey W.F. - *The elastic-plastic behavior of stainless steel tubing subjected to bending, pressure and torsion.* Proc. 2nd. Int. Conf. on Pres. Ves. Tech. San Antonio, Texas. 1973, pp. 457-467.

[4] Reilly, P. - *The loading of thin walled pipes with combined torsion and internal pressure to collapse.* Final year project, Liverpool University, 1986.

[5] BS 806: 1986. *Specification for design and construction of ferrous piping installations for and in connection with land boilers.* British Standards Institution.

[6] von Karman T. - *Uber die Formanderung dunnwandiger Rohre, insbesondere federnder Ausgleichsrohre.* Zeit VDI, Vol. 55, 1911.

[7] Vigness I. - *Elastic properties of curved tubes.* Trans. ASME, Vol. 65, 1943, pp. 105-120.

[8] Barthelemy J. - *Bulletin de l'Association Technique Maritime et Aeronautique.* 1946.

[9] Kafka P.G. and Dunn M.B. - *Stiffness of curved circular tubes with internal pressure.* Jour. Appl. Mech., Vol. 23, 1956, pp. 247-254.

[10] Rodabaugh E.C, Iskander S.K. and Moore S.E. - *End effects on elbows subjected to moment loadings.* ORNL/Sub-2913/7, Oak Ridge National Laboratory, TN., 1978.

[11] Natarajan R. and Blomfield J.A. - *Stress analysis of curved pipes with end restraints.* Computers and Structures, Vol. 5, 1975, pp. 187-196.

[12] Thomson G. and Spence J. - *Combined pressure and in-plane bending on pipes with flanges.* 7th Int. Conf. Struct. Mech. in Reactor Tech., Chicago, 1983.

[13] Thomas K. - *Stiffening effects on thin-walled piping elbows of adjacent piping and nozzle constraints.* Jour. Pres. Ves. Tech., Vol. 104, 1982, pp. 180-187.

[14] Ohtsubo H. and Watanabe O. - *Stress analysis of pipe bends by ring elements.* Jour. Pres. Ves. Tech., Vol. 100, 1978, pp. 112-122.

[15] Rodabaugh E.C. and George H.H. - *Effect of internal pressure on flexibility and stress-intensification factors of curved pipe or welding elbows.* Trans. ASME, Vol. 79, 1957, pp. 939-948.

[16]   Findlay G.E. and Spence J. - *Stress analysis of smooth curved tubes with flanged end constraints.* Int. Jour. Pres. Ves. & Piping, Vol. 7, 1979, pp. 83-103.

[17]   Flugge W. - *Stresses in shells.* 4th printing, Springer-Verlag, New York, 1967.

[18]   Ory H. and Wilczek E. - *Stress and stiffness calculation of thin-walled curved pipes with realistic boundary conditions being loaded in the plane of curvature.* Int. Jour. Pres. Ves. & Piping, Vol. 12, 1983, pp. 167-189.

[19]   Lang H.A. - *Toroidal elastic stress fields for pressurized elbows and pipe bends.* Int. Jour. Pres. Ves. & Piping, Vol. 15, 1984, pp. 291-305.

[20]   ASME Boiler and Pressure Vessel Code, Section III, Nuclear Power Plant Components, Division 1, 1992.

[21]   Dhalla A.K. - *Collapse characteristics of a thin-walled elbow: Validation of an analytical procedure.* Trans. of ASME, Vol. 109, 1987.

[22]   Kano T., Iwata K., Asakura J. and Takeda H. - *Stress distribution of an elbow with straight pipes.* 4th Struct. Mech. in Reactor Tech., San Francisco, 1977.

[23]   Spence J. and Thomson G. - *Flanged pipe bends under combined pressure and in-plane bending.* Proc. 5th Int. Conf. on Pres. Ves. Tech., Vol. 1, San Francisco, 1984.

[24]   Hoffmann A. and Roche R. - *Methodes simplifiees d'analyse des tuyauteries-Methode globale-Cas paeticulier des coudes.* Journees de conference du DEMT, 1978.

[25]   Solal P. - *Flexion en ouverture monotone et pincements en fermeture monotone sur un coude en Acier A 106 grade B.* Report CEA/DEMT 77-29, Saclay, 1977.

[26]   Wassermann D.R. - *Experimental investigation of stresses in cold-bent pipes due to internal pressure and in-plane bending.* Int. Jour. Pres. Ves. & Piping, Vol. 14, 1983, pp. 135-151.

[27]   Fujimoto T. and Soh T. - *Flexibility factors and stress indices for piping components with D/T≥100 subjected to in-plane or out-of-plane moment.* Jour. Pres. Ves. Tech., Vol. 110, 1988, pp. 374-386.

[28]   ASME Boiler and Pressure Vessel Code, Section III, Nuclear Power Plant Components, Division 1, 1992.

[29]   Natarajan R. - *Analysis of flexibilities and stress intensification factors in 90 degree bends with end restraints. Design and Analysis of Piping and Components-1990.* Pres. Ves. and Piping, Vol. 188, 1990.

[30]   Thomson G. - *The influence of end constraints on smooth pipe bends.* Ph.D dissertation, University of Strathclyde, 1980.

[31]   Wichman K.R., Hopper A.G. and Mershon J.L. - *Local stresses in spherical and cylindrical shells due to external loading.* Welding Research Council Bulletin 107, 1965.

[32]   Mershon J.L., Mokhtarian K., Ranjan G.V. and Rodabaugh E.C. - *Local stresses in cylindrical shells due to external loads on nozzles - Supplement to Welding Research Council Bulletin 107.* Welding Research Council Bulletin 297, 1984.

[33]   Moore S.E., Greenstreet W.L. and Mershon J.L. - *The design of nozzles and openings in pressure vessels.* Pressure vessels and piping: Design technology - A decade of progress. 1982.

[34]   Moffat D.G. - *Experimental stress analysis of four fabricated equal diameter branch pipe intersections subjected to moment loadings and the implications on branch junction design.* Proc. Instn. Mech. Engrs., Vol. 199, No. A4, 1985, pp. 261-284.

[35]   Gwaltney R.C., Corum J.M., Bolt S.E. and Bryson J.W. - *Experimental stress analysis of cylinder-to-cylinder shell models and comparisons with theoretical predictions.* Jour. Pres. Ves. Tech., Vol. 98, 1976, pp. 283-290.

[36]   Corum J.M., Bolt S.E., Greenstreet W.L. and Gwaltney R.C. - *Theoretical and experimental stress analysis of ORNL thin-shell cylinder-to-cylinder model No. 1/2/3/4.* ORNL-TM-4553/5021/5020/5019, 1972/1975/1975/1975, Oak Ridge National Laboratory.

[37]   Bijlaard P.P. - *Stresses from local loadings in cylindrical pressure vessels.* Trans. ASME, Vol. 77, 1955, pp. 805-816.

[38]   Bijlaard P.P., Dohrmann R.J, and Wang I.C. - *Stresses in junction of nozzle to cylindrical pressure vessel for equal diameter of the vessel and nozzle.* Nuclear Eng. and Design, Vol. 5, 1967, pp. 349-365.

[39]   Eringen A.C., Naghdi A.K., Mahmood S.S, Thiel C.C. and Ariman T. - *Stress concentrations in two normally intersecting cylindrical shells subject to internal pressure.* Welding Research Council Bulletin 139, 1969, pp. 1-34.

[40]   Lekkerkerker J.G. - *The determination of elastic stresses near cylinder-to-cylinder intersections.* Nuclear Eng. and Design, Vol. 20, 1972, pp. 57-84.

[41]   McBride W.L. and Jacobs W.S. - *Design of radial nozzles in cylindrical shells for internal pressure.* Jour. Pres. Ves. Tech., Vol. 102, 1980, pp. 70-78.

[42]   Moffat D.G. and Mistry J. - *Interaction of external moment loads and internal pressure on a variety of branch pipe intersections.* Proc. Int. Conf. Pres. Ves. Tech., Beijing, 1988.

[43]   Moffat D.G., Mwenifumbo J.A.M., Xu S.H. and Mistry J. - *Effective stress factors for piping branch junctions due to internal pressure and external moment loads.* Jour. of Strain Analysis. Vol. 26. No. 2. 1991.

171

[44] Moore S.E. and Rodabaugh E.C. - *Background for changes in the 1981 edition of the ASME nuclear power plant components code for controlling primary loads in piping systems*. Jour. Pres. Ves. Tech., Vol. 104, 1982, pp. 351-361.

[45] Ellyin F. and Turkkan N. - *Lower bound to limit pressure of nozzle to cylindrical shell attachment*. ASME Publication 71-PVP-38, 1971.

[46] Boyle J.T. - *Design and analysis of piping systems*. A short course, University of Strathclyde, 1991.

[47] Rodabaugh E.C. and Moore S.E. - *Stress indices and flexibility factors for nozzles in pressure vessels and piping*. NUREG/CR-0778, 1979.

[48] Schroeder J., Gartenburg J. and Srinivasaiah K.R. - *Part II - Theoretical and experimental results for in-plane and out-of-plane limit couples applied to the branch and their interaction with pressures*. Proc. 2nd. Int. Conf. on Pres. Ves. Tech., San Antonio, Texas, 1973, pp. 305-329.

[49] Leckie F.A. and Penny R.K. - *Solutions for the stresses in nozzles in pressure vessels*. Welding Research Council Bulletin 90, 1963, pp. 8-18.

[50] Donnell L.H. - *Stability of thin-walled tubes under torsion*. NACA Report No. 479, 1933.

[51] Steele C.R. and Steele M.L.- *Stress analysis of nozzles in cylindrical vessels with external loads*. Jour. Pres. Ves. Tech., Vol. 105, 1983, pp. 191-200.

[52] Steele C.R. - *Reinforced openings in large steel pressure vessels: Solution for large openings*. 1978 SHELLTECH Report 84-1, 1984.

[53] Mokhtarian K. and Endicott J.S. - *Stresses in intersecting cylinders subjected to pressure*. Welding Research Council Bulletin 368, 1991.

[54] Prince N. and Rashid Y.R. - *Structural analysis of shell intersections*. Proc. 1st Int. Conf. on Pres. Ves. Tech., Delft, 1969, pp. 245-254.

[55] Bakhrebah S.A. and Schnobrich W.C. - *Finite element analysis of intersecting cylinders*. Civil Engineering Studies, SRS No. 400, University of Illinois at Urbana-Champaign, 1973.

[56] Gantayat A.N. and Powell G.H. - *Finite element analysis of thin and thick-walled tubular joints*. Nuclear Eng. and Design, Vol. 46, No. 2, 1978, pp. 381-394.

[57] Lock J., Carmichael G.D.T. and Moffat D.G. - *Finite element stress analysis on an equal diameter branch pipe intersections subjected to internal pressure and in-plane moment loadings*. Pipework Design and Operation, Instn. Mech. Engrs., 1985, pp. 59-70.

[58] Kirkwood M.G., Carmichael G.D.T. and Moffat D.G. - *Finite element stress analysis of an equal diameter branch pipe intersections subjected to out-of-plane and twisting moments*. Jour. Strain Analysis, Vol. 21, No. 1, 1986, pp. 9-16.

[59] Rodabaugh E.C. and Moore S.E. - *Review of elastic stresses and fatigue-to-failure data for branch connections and tees in relation to ASME design criteria for nuclear power piping systems*. Reported in Welding Research Council Bulletin 368, 1991.

[60] Zhixiang J., Qingjiang Z. and Siding Z. - *Stress and strength analysis of equal-diameter tees*. Jour. Pres. Ves. Tech., Vol. 113, 1991, pp. 55-63.

[61] Batchelor M.J. and Taylor T.E. - *Equivalent torispherical pressure vessel heads*. Jour. Pres. Ves. & Piping, Vol. 7, 1979, pp. 229-243.

[62] Galletly G.D. - *Analysis of discontinuity stresses adjacent to a central circular opening in a hemispherical shell*. David Taylor Model Basin Report No. 870, NS731038, 1954.

[63] Galletly G.D. - *Torispherical shells - A caution to designers*. Jour. Eng. for Industry, 1959, pp. 269-284.

[64] Onat E.T. and Prager W. - *Limit analysis of shells of revolution*. Proc. Royal Nederlands Academy of Science, Vol. 57, 1954, pp. 534-548.

[65] Drucker D.C. and Shield R.T. - *Limit analysis of symmetrically loaded thin shells of revolution*. Jour. Appl. Mech., Vol. 26, 1959, pp. 61-68.

[66] Rose R.T. and Thompson J.M.T. - *Calculated stress concentration factors for nozzles in spherical pressure vessels*. Proc. Symp. Pres. Ves., Research towards better design, 1961.

[67] Lind N.C. - *Plastic analysis of radial outlets from spherical pressure vessels*. Jour. Eng. for Industry, Vol. 86, 1964, pp. 193-198.

[68] Gill S.S. - *The limit pressure for a flush cylindrical nozzle in a spherical pressure vessel*. Int. Jour. Mech. Eng. Sci., Vol. 6, 1964, pp. 105-115.

[69] Rodabaugh E.C. and Cloud R.L. - *Assessment of plastic strength of pressure vessel nozzles*. Jour. Eng. for Industry, 1968, pp. 636-643.

[70] Leckie F.A. - *Shakedown pressures for flush cylinder-sphere shell intersections*. Jour. Mech. Eng. Sci., Vol. 7, No. 4, 1965, pp. 367-371.

[71] Bushnell D. - *Plastic buckling of various shells*. Jour. Pres. Ves. Tech., Vol. 104, 1982, pp. 51-72.

[72] Bushnell D. - *BOSOR 5 (1976) - Program for buckling of elastic-plastic shells of revolution including large deflections and creep*. Comp. and Struct., Vol. 6, 1976, pp. 221-239.

[73] Gross N. - *Experiments on short radius pipe bends*. Proc. Instn. Mech. Engrs., 1952, pp. 465-479.

[74] Drabble F. - *Shakedown of radial nozzle in a pressure vessel end under the action of several loads*. Report No. A/025/76, The University of Liverpool, 1976.

[75]   PATRAN-G Version 2.5 User manuals, PDA Engineering, Santa Ana, California. USA, 1989.

[76]   ASAS-H User manuals, Atkins Research and Development, Surrey, UK, 1989.

[77]   Mwenifumbo J.A.M. - *Stress and flexibility analysis of branch pipe junctions by the finite element method.* MScEng thesis, University of Liverpool, 1988.

[78]   Natarajan R., Widera G.E.O. and Afsari P. - *A finite element model to analyze cylinder-cylinder intersections.* Jour. Pres. Ves. Tech., Vol. 109, 1985, pp. 411-420.

[79]   Bryson J.W., Johnson W.G. and Bass B.R. - *Stresses in reinforced nozzle-cylinder attachments under internal pressure loading analyzed by the finite element method - a parameter study.* ORNL/NUREG-4. Oak Ridge National Laboratory, 1977.

[80]   Chen H.C. and Schnobrich W.C. - *Nonlinear analysis of intersecting cylinders by the finite element method.* Civil Engineering Studies, SRS No. 435, University of Illinois at Urbana-Champaign, 1976.

[81]   Rodabaugh E.C. - *Accuracy of stress intensification factors for branch connections.* Welding Research Council Bulletin 329, 1987.

[82]   Hardenbergh D.E. and Zamrik S.Y. - *Effects of external loadings on large outlets in a cylindrical pressure vessel.* Welding Research Council Bulletin 96, 1964.

[83]   Riley W.F. - *Experimental determination of stress distribution in thin-walled cylindrical and spherical pressure vessel with circular nozzle.* Welding Research Council Bulletin 108, 1965.

[84]   Ellyin F. - *An experimental study of elasto-plastic response of branch-pipe tee connections subjected to internal pressure, external couples and combined loadings.* Welding Research Council Bulletin 230, 1977.

[85]   Decock J.M. - *Experimental and finite element analysis of a thin shell cylinder-to-cylinder model.* ASME Pressure Vessel and Piping Conference, 1971.

[86]   Thomson G. and Spence J. - *Maximum stresses and flexibility factors of smooth pipe bends with tangent pipe terminations under in-plane bending.* Jour. Pres. Ves. Tech., Vol. 105, 1983, pp. 329-336.

[87]   Turner C.E. and Ford H. - *Examinations of the theories for calculating the stresses in pipe bends subjected to in-plane bending.* Proc. Instn. Mech. Engrs., Vol. 171, 1957, pp. 513-515.

[88]   Lang H.A. - *Initial yielding in elbows and curved tubing.* Int. J. Pres. Ves. & Piping, Vol. 21, 1985, pp. 235-241.

[89]   Sobel L.H. and Newman S.Z. - *Comparison of experimental and simplified analytical results for in-plane plastic bending and buckling of an elbow.* Jour. Pres. Ves. Tech., Vol. 102, 1980, pp. 400-409.

[90] Chan K.L.C. and Boyle J.T. - *Creep flexibility and stress factors for pipe bends with ends constraints under in-plane or out-of-plane loading*. Int. Jour. Pres. Ves. & Piping, Vol. 23, 1986, pp. 259-293.

[91] Imamasa J. and Uragami K. - *Experimental study of flexibility factors and stresses of welding elbows with end effects*. Proc. 2nd Int. Conf. on Pres. Ves. Tech., San Antonio, 1973, pp. 417-426.

[92] Boyle J.T. and Spence J. - *The non-linear analysis of pressurised curved tubes*. Proc. 3rd Int. Conf. on Pres. Ves. Tech., Tokyo, 1977.

[93] Smith R.T. - *Theoretical analysis of stresses in pipe bends subjected to out-of-plane bending*. Jour. Mech. Eng. Sci., Vol. 9, No. 2, 1967, pp. 115-123.

[94] Kirkwood M.G. and Moffat D.G. - *Techniques for measuring plastic loads in branch pipe connections loaded by pressure and in-plane moments*. 2nd. Conf. on Pipework Eng. and Operation, Instn. Mech. Engrs., 1989, pp. 197-208.

[95] Greenstreet W.L. - *Experimental study of plastic responses of pipe elbows*. ORNL/NUREG-24, 1978.

[96] Babcock Power Ltd. - Private communication.

[97] Mershon J.L. - *Reinforcement of openings under internal pressure*. Welding Research Council Bulletin 95, 1964.

[98] Decock J. - *Reinforcement method of openings in cylindrical pressure vessels subjected to internal pressure*. Welding Research Abroad, 1975, pp. 9-36.

[99] Decock J. - *External loadings on nozzles in cylindrical shells*. Proc. 4th Int. Conf. on Pres. Ves. Tech., London, Vol. 2, 1980, pp. 127-134.

[100] Rodabaugh E.C. - *A review of area replacement rules for pipe connections in pressure vessels and piping*. Welding Research Council Bulletin 335, 1988.

[101] Money H.A. - *Designing flush cylinder-to-cylinder intersections to withstand pressure*. ASME paper 68-PVP-17, 1968.

[102] Lind N.C. - *Approximate stress concentration analysis for pressurised pipe branch connections*. Pressure vessels and piping: Design and analysis, A decade of progress, 1972, pp. 952-958.

[103] Xie D.S. and Lu Y.G. - *Prediction of stress concentration factors for cylindrical pressure vessels with nozzles*. Int. Jour. Pres. Ves. & Piping., Vol. 21, 1985.

[104] Wordsworth A.C. and Smedley G.P. - *Stress concentrations of unstiffened tubular joints*. European offshore steels research seminar, Cambridge, 1978.

[105] Khan A.S. and Shah S.S. - *A parametric study of two normally intersecting cylindrical shells subjected to out-of-plane moment*. Int. Jour. Pres. Ves. & Piping., Vol. 22, 1986.

[106] Bryson J.W., Johnson W.G. and Bass B.R. - *Stresses in reinforced nozzle-cylinder attachments - A parameter study*. ASME Publication PVP-Vol. 50, 1981.

[107] Taylor C.E. and Lind N.C. - *Photoelastic study of the stresses near openings in pressure vessels*. Welding Research Council Bulletin 113, 1966, pp. 1-24.

[108] Skopinsky V.N. - *Numerical stress analysis of intersecting cylindrical shells*. Jour. of Pres. Ves. Tech., Vol. 115, 1993, pp. 275-282.

[109] ABAQUS General purpose finite element program, User's Manual Version 5.2, Hibbitt, Harlsson and Sorrenson.

[110] Leckie F.A. and Payne D.E. - *Some observations on the design of spherical pressure vessels with flush cylindrical nozzles*. Proc. Instn. Mech. Engrs., Vol. 180, Pt. 1, No. 20, 1965-66, pp. 497-501.

[111] BS 5500: 1988. *Specification for unfired fusion welded pressure vessels*. British Standards Institution.

[112] Mershon J.L. - *Preliminary evaluation of PVRC photoelastic test data for reinforced openings in pressure vessels*. Welding Research Council Bulletin 113, 1966.

[113] Marcal P.V. and Turner C.E. - *Elastic-plastic behaviour of flush nozzles in spherical pressure vessels*. Jour. Mech. Eng. Sci., Vol. 9, No. 3, 1967, pp. 182-189.

[114] O'Connell J.M. and Chubb E.J. - *Improved method of calculating stresses at the intersection of a cylindrical nozzle and a spherical vessel*. Proc. Appl. Mech. Convention, Instn. of Mech. Engrs., Vol. 178, 1964.

[115] Chao Y.J. - *Minimum stress design of nozzles in pressure vessel heads*. Jour. Pres. Ves. Tech., Vol. 110, 1988, pp.460-463.

[116] Lind N.C. - *Plastic analysis of radial outlets from spherical pressure vessels*. Jour. Eng. for Industry, 1964, pp. 193-198.

[117] Witt F.J., Gwaltney R.C., Maxwell R.L. and Holland R.W. - *A comparison of theoretical and experimental results from spherical shells with a single radially attached nozzle*. Jour. of Eng. for Power, 1967, pp. 333-339.

[118] Kirkwood M.G. and Moffat D.G. - *Plastic loads for piping branch junctions subjected to combined pressure and in-plane moment loads*. Procs. Instn. Mech. Engrs., Part E, Jour. of Process Mech. Eng., 1994.

APPENDIX

APPENDIX A. THE ENERGY METHOD [15] COMPUTER PROGRAM

```
c Rodabaugh's elasticity elbow equations for in-plane bending to calculate axial and hoop
stresses.
c Considers stiffening effect of pressure. Modified to include diametral extensibility.
c Uses 10th order approximation. Stresses due to moment only.
c theta=hoop direction, zero at extrados.
c phi=axial direction, zero at mid-section of 90-deg elbow.
c Input units in N-mm, will be converted to lbf-in in program.
      real d(20,21),ro,ri,rm,doo,di,r,m,pr,e,ni,t,s,pi,ii,lam,psi,rr,
     1 theta2,sum,sum1,sum2,sum3,sum4,sum5,sum6,sum7,kp,kf,
     2 sigtheo,sigthei,sigphio,sigphii,p,gam,ksi,sthep,sphip,
     3 stheo,sthei,sphio,sphii
      integer n,np1,i,j,k,theta
      write (6,*)' Outer radius, in mm.='
      read(5,*)ro
      ro=ro/25.4
      doo=ro*2
      write (6,*)' Inner radius, in mm.='
      read(5,*)ri
      ri=ri/25.4
      di=ri*2
      write (6,*)' Bend radius, in mm.='
      read(5,*)r
      r=r/25.4
      write (6,*)' In-plane moment, in N-mm.='
      read(5,*)m
      m=m/(4.448222*25.4)
      write (6,*)' Internal pressure, in N/mm2='
      read(5,*)pr
      pr=pr*1.0e3/6.894757
      write (6,*)' Elastic modulus, in N/mm2='
      read(5,*)e
      e=e*1.0e3/6.894757
      ni=0.275
      n=10
      t=ro-ri
      rm=(ro+ri)/2
      gam=r/rm
      s=pr*rm/t
      pi=4.0*atan(1.0)
      ii=pi*(ro**4-ri**4)/4
      lam=t*r/((rm**2)*sqrt(1.-ni**2))
      psi=s*r**2/(e*rm**2)
c     d's are coeff. of c's
      d(1,1)=5+6*lam**2+24*psi
      d(1,2)=-5.0/2
      d(10,9)=-(2*n-3)*(2*n+1)/2.
      d(10,10)=((4*n**2+1)+(8*n**3-2*n)**2*lam**2/6+
```

177

```
   1 (8*n**2*(4*n**2-1))*psi)
      do 2 i=2,9
      j=i-1
      d(i,j)=-(2*i-3)*(2*i+1)/2.
2     continue
      do 3 i=2,9
      j=i+1
      d(i,j)=-(2*i-1)*(2*i+3)/2.
3     continue
      do 4 i=2,9
      j=i
      d(i,j)=((4*i**2+1)+(8*i**3-2*i)**2*lam**2/6+
   1 (8*i**2*(4*i**2-1))*psi)
4     continue
      d(1,11)=-3.
      do 5 i=2,10
      d(i,11)=0.
5     continue
c     write(6,*)' The dU matrix is'
      do 111 i=1,n
c     write(6,*)(d(i,j),j=1,n)
111   continue
c Gauss-Jordan elimination-to solve simultaneous equations
      np1=n+1
      do 44 k=1,n
      p=d(k,k)
      if (p.ne.0.0) goto 55
      write(6,*)' Zero divide - rearrange equations.'
      goto 1
55    do 77 j=1,np1
77    d(k,j)=d(k,j)/p
      do 88 i=1,n
      if (i.eq.k) goto 88
      rr=d(i,k)
      do 99 j=1,np1
99    d(i,j)=d(i,j)-rr*d(k,j)
88    continue
44    continue
c stress calculation - strain energy method
      write(6,*)'Theta  Hoop stress  Axial stress        VM'
      write(6,*)'      out    in out      in      out in'
c ksi is to change back from psi to N/mm2
      ksi=6.894757/1.e3
      kf=m*ro/ii
      do 100 theta=0,180,15
      theta2=theta+90
      theta2=theta2*pi/180.0
      sum1=0.
      do 21 i=1,n
      sum=0.5*(d(i,11)*(1-2*i)+d(i+1,11)*(2*i+3))*sin((2*i+1)*theta2)
      sum1=sum1+sum
```

```
21    continue
      sum2=0.
      do 23 i=1,n
      sum=0.5*ni*lam*d(i,11)*(2*i-8*i**3)*cos(2*i*theta2)
      sum2=sum2+sum
23    continue
      sum3=0.
      do 24 i=1,n
      sum=0.5*lam*d(i,11)*(2*i-8*i**3)*cos(2*i*theta2)
      sum3=sum3+sum
24    continue
      sum4=0.
      do 25 i=1,n
c --  modification to include hoop extensibility --
      sum=0.5*(1/gam)*(d(i,11)*(1-2*i)+d(i+1,11)*(2*i+3))*
     1 cos((2*i+1)*theta2)*cos(theta2)/(2*i+1)
      sum4=sum4+sum
25    continue
      sum5=0.
      do 26 i=1,n
      sum=0.25*d(i,11)**2*(1-2*i)**2
      sum5=sum5+sum
26    continue
      sum6=0.
      do 27 i=1,n
      sum=(0.0833333*lam**2)*d(i,11)**2*(8*i**3-2*i)**2
      sum6=sum6+sum
27    continue
      sum7=0.
      do 28 i=1,n
      sum=psi*4*i**2*(4*i**2-1)*d(i,11)**2
      sum7=sum7+sum
28    continue
c     kp=1./(1+3*d(1,11)+(9/4)*d(1,11)**2+sum5-2*d(10,11)*d(11,11)*
c    1 (2*10-1)*(2*10+3)+d(11,11)**2*(2*10+3)**2+sum6+sum7)
      kp=1.0/(1+1.5*d(1,11))
      sigthei=(kp*m*rm/(ii*(1-ni**2)))*(-sum3-(1/gam)*(1+1.5*d(1,11))*
     1 (cos(theta2))**2-sum4)
      sigtheo=(kp*m*rm/(ii*(1-ni**2)))*(sum3-(1/gam)*(1+1.5*d(1,11))*
     1 (cos(theta2))**2-sum4)
      sigphio=(kp*m*rm/(ii*(1-ni**2)))*((1+1.5*d(1,11))*sin(theta2)+
     1 sum1+sum2)
      sigphii=(kp*m*rm/(ii*(1-ni**2)))*((1+1.5*d(1,11))*sin(theta2)+
     1 sum1-sum2)
      sthep=0
      sphip=0
c stress factor due to moment only, but with pressure interaction
      write(6,930)theta,sigtheo/kf,sigthei/kf,sigphio/kf,sigphii/kf,
     * (sqrt(sigtheo**2+sigphio**2-sigtheo*sigphio))/kf,
     * (sqrt(sigthei**2+sigphii**2-sigthei*sigphii))/kf
930   format(i4,1x,f7.2,1x,f7.2,1x,f7.2,1x,f7.2,1x,f7.2,1x,f7.2)
```

```
100   continue
  1   continue
      stop
      end




APPENDIX B.        FINALE.FOR - A PROGRAM TO INTERPOLATE STRESSES
                   FOR A GIVEN ELBOW DIMENSION AND EVALUATE LOAD
                   INTERACTIONS
C-----------------------------------------------------------------
C   A PROGRAM TO INTERPOLATE STRESSES AT ALL NODES FOR ANY GIVEN
C   VALUES OF Dm/T AND b OF ELBOWS. DETERMINATION OF STRESSES,
C   FOR ANY GIVEN COMBINATION OF TORQUE, IN-PLANE MOMENT AND
C   INTERNAL PRESSURE.
C-----------------------------------------------------------------
C   STRESS DATA FROM 16 ELBOWS HAVE BEEN PREVIOUSLY GENERATED BY
C   LINEAR FEM. ASSUMES LINEAR SUPERPOSITION OF STRESSES.
C-----------------------------------------------------------------
      COMMON LC,WHE,BBN,DTN,RO,RI,KK2
      DOUBLE PRECISION BBN,DTN,KK2,RO,RI,RR,KKK2,LAM
      INTEGER M
      CHARACTER*10 FILENAME(21)
      DATA FILENAME/'el04.pop','el03.pop','el02.pop','el01.pop',
     *         'el08.pop','el07.pop','el06.pop','el05.pop',
     *         'el12.pop','el11.pop','el10.pop','el09.pop',
     *         'el16.pop','el15.pop','el14.pop','el13.pop',
     *      'intpe1.pop','intpe2.pop','intpe3.pop','intpe4.pop',
     *      'intpe5.pop'/
1507  WRITE(6,*)'VALID  FOR  Dm/T=10    TO  150'
      WRITE(6,*)'     AND     b=2    TO  7'
      WRITE(6,*)'OR       LAMBDA = 0.0267 TO   1.4'
      WRITE(6,*)'---------------------------------------'
      WRITE(6,*)'OUTER RADIUS, IN mm?'
      READ(5,*)RO
      WRITE(6,*)'INNER RADIUS, IN mm?'
      READ(5,*)RI
      WRITE(6,*)'BEND RADIUS, IN mm?'
      READ(5,*)RR
      DTN=(RO+RI)/(RO-RI)
      BBN=2.*RR/(RO+RI)
      LAM=2.0*BBN/DTN
      WRITE(6,*)
      WRITE(6,*)' NEW Dm/T      NEW b RATIO     NEW LAMBDA'
      WRITE(6,1161)DTN,BBN,LAM
1161  FORMAT(F9.4,10X,F7.4,10X,F7.4)
      IF (DTN.LT.10.0.OR.DTN.GT.150.0.OR.BBN.LT.2.0.OR.BBN.GT.7.0) THEN
      WRITE(6,*)' ELBOW DIMENSIONS OUT OF RANGE!! - PLEASE TRY AGAIN'
      GOTO 1507
      ENDIF
C   STRESSES IN DATA FILES ARE STRESS FACTORS
```

```fortran
C     CREATING FILE intpe1.pop

OPEN(UNIT=10,FILE='intpe1.pop',STATUS='UNKNOWN',FORM='FORMATTED')
      WRITE(10,301)DTN
301   FORMAT(' PIPE WITH NEW Dm/T ',F7.3)
      M=4
      DO 1 I=1,M
      FILENAME(I)=FILENAME(I)
1     CONTINUE
      CALL GENFILE(DTN,BBN,M,KK2,FILENAME)
      CLOSE(10)
C     CREATING FILE intpe2.pop
      OPEN(10,FILE='intpe2.pop',STATUS='UNKNOWN',FORM='FORMATTED')
      WRITE(10,301)DTN
      M=4
      DO 2 I=1,M
      FILENAME(I)=FILENAME(I+4)
2     CONTINUE
      CALL GENFILE(DTN,BBN,M,KK2,FILENAME)
      CLOSE(10)
C     CREATING FILE intpe3.pop
      OPEN(10,FILE='intpe3.pop',STATUS='UNKNOWN',FORM='FORMATTED')
      WRITE(10,301)DTN
      M=4
      DO 3 I=1,M
      FILENAME(I)=FILENAME(I+8)
3     CONTINUE
      CALL GENFILE(DTN,BBN,M,KK2,FILENAME)
      CLOSE(10)
C     CREATING FILE intpe4.pop
      OPEN(10,FILE='intpe4.pop',STATUS='UNKNOWN',FORM='FORMATTED')
      WRITE(10,301)DTN
      M=4
      DO 4 I=1,M
      FILENAME(I)=FILENAME(I+12)
4     CONTINUE
      CALL GENFILE(DTN,BBN,M,KK2,FILENAME)
      CLOSE(10)
C     CREATING FINAL FILE intpe5.pop
      OPEN(10,FILE='intpe5.pop',STATUS='UNKNOWN',FORM='FORMATTED')
      WRITE(10,302)DTN,BBN
302   FORMAT('PIPE WITH NEW Dm/T=',F7.3,'  AND B=',F7.3)
      M=4
      DO 5 I=1,M
      FILENAME(I)=FILENAME(I+16)
5     CONTINUE
      CALL GENFILE(BBN,BBN,M,KKK2,FILENAME)
      CLOSE(10)
      CALL STRESS
      STOP
      END
```

```
      SUBROUTINE GENFILE(DTN,BBN,M,KK2,FILENAME)
C     READING DATA FROM 4 DATA FILES AND GENERATE INTERPOLATED FILE
      COMMON/BLOCK1/STRES(9,858,3),ALOAD(3),SIGMA(6),STR(9),
     * PI,XVAL(361),YVAL(361),ZVAL(361),XVALT(361),YVALT(361),
     * ALOADT(3)
      CHARACTER*10 TITLE,FILENAME(21)
      DOUBLE PRECISION BBB(4),X(4),F(4),YY,DT(4),STRE(9,858,3,4),
     * ANS(9,858,3),DTN,BBN,KK2
      INTEGER M,MAXLOC,LOCASE
      DO 101 LL=1,4
      OPEN(UNIT=20,FILE=FILENAME(LL),STATUS='OLD')
      REWIND 20
      READ(20,333)TITLE
333   FORMAT(A72)
      READ(20,200)MAXLOC
      READ(20,200)LOCASE
      READ(20,*) BBB(LL)
      READ(20,*) DT(LL)
      DO 13 KK=1,LOCASE
      DO 14 JJ=1,MAXLOC
      READ(20,* )(STRE(II,JJ,KK,LL),II=1,9)
14    CONTINUE
13    CONTINUE
      CLOSE(20)
101   CONTINUE
      WRITE(10,200)MAXLOC
      WRITE(10,200)LOCASE
200   FORMAT(I6)
      WRITE (10,445) DTN
      WRITE (10,445) BBB(1)
445   FORMAT (F7.3)
      DO 506 KK=1,LOCASE
      DO 505 JJ=1,MAXLOC
      DO 504 II=1,9
      DO 503 LL=1,M
      X(LL)=DT(LL)
      F(LL)=STRE(II,JJ,KK,LL)
503   CONTINUE
      CALL SPLIN(X,F,DTN,YY)
C     INTERPOLATING SEPERATELY FOR EVERY 4 SETS OF DATA
      ANS(II,JJ,KK)=YY
504   CONTINUE
      DO I=3,8
      STR(I)=ANS(I,JJ,KK)
      END DO
      CALL SIGCAL
11    FORMAT(3(1PE11.4,1X))
C     MISES STRESS IN intpe 1-5.pop CALCULATED IF SIGMA(6) USED
      WRITE(10,601) STRE(1,JJ,KK,1),STRE(2,JJ,KK,1),
     * (ANS(II,JJ,KK),II=3,8),SIGMA(6)
C     ABS(ANS(9,JJ,KK)) THIS VALUE GIVES INTERPOLATED MISES STRESS
```

```
505   CONTINUE
506   CONTINUE
601   FORMAT(F8.1,1X,8(F7.3,1X))
      RETURN
      END
      SUBROUTINE SPLIN(X,Y,DTN,ANS)
C     CUBIC SPLINE FIT TO N DATA POINTS. ENDCON=1 SELECTED BUT
C     USER MAY SPECIFY ANY ONE OF 4 DIFFERENT END CONDITIONS.
C     DTN=NEW X VALUE FOR WHICH Y IS TO BE DETERMINED
C     ENDCON = 1 FOR A NATURAL SPLINE FIT
C     ENDCON = 2 FOR Y1" = Y2" AND YN" = YN+1"
C     ENDCON = 3 FOR EXTRAPOLATED Y"-S AT ENDS
C     ENDCON=4 FOR CASES 1 & 3 AVERAGED
      IMPLICIT REAL*8(A-H,O-Z)
      INTEGER ENDCON
      DIMENSION A(48),B(48),C(48),S(48),Z(48),X(50),Y(50),H(49),YPP(50)
      N=4
      ENDCON=1
      DO 26 I = 1,N-1
      H(I) = X(I+1) - X(I)
26    CONTINUE
      DO 27 I = 1,N-2
      S(I) = 6.*(Y(I+2) - Y(I+1))/H(I+1) - 6.*(Y(I+1) - Y(I))/H(I)
27    CONTINUE
      DO 28 I = 1,N-3
      C(I) = H(I+1)
      A(I+1) = C(I)
28    CONTINUE
      DO 29 I = 1,N-2
      B(I) = 2.*(H(I) + H(I+1))
29    CONTINUE
      GO TO(33,30,31,32)ENDCON
C     CASE 2 (Y1" = Y2" AND YN" = YN-1")
30    B(1) = B(1) + H(1)
      B(N-2) = B(N-2) + H(N-1)
      GO TO 33
C     CASE 3 (EXTRAPOLATED Y"-S AT ENDS)
31    B(1) = (H(1) + H(2))*(H(1) + 2.*H(2))/H(2)
      A(N-2) = (H(N-2)*H(N-2) - H(N-1)*H(N-1))/H(N-2)
      B(N-2) = (H(N-2) + H(N-1))*(2.*H(N-2) + H(N-1))/H(N-2)
      GO TO 33
C     CASES 1 AND 3 AVERAGED
32    B(1) = (H(1) + H(2))*(H(1) + 4.*H(2))/(2.*H(2))
      C(1) = (2.*H(2)*H(2)-H(1)*H(1))/(2.*H(2))
      A(N-2) = (2.*H(N-2)*H(N-2) - H(N-1)*H(N-1))/(2.*H(N-2))
      B(N-2) = (H(N-2) + H(N-1))*(4.*H(N-2) + H(N-1))/(2.*H(N-2))
33    CALL TRIDI(N-2,A,B,C,S,Z)
      GO TO(34,35,36,37)ENDCON
C     CASE 1
34    YPP(1) = 0.
      YPP(N) = 0.
```

```
      GO TO 38
C     CASE 2
35    YPP(1) = Z(1)
      YPP(N) = Z(N-2)
      GO TO 38
C     CASE 3
36    YPP(1) = (Z(1)*(H(1) + H(2)) - Z(2)*H(1))/H(2)
      YPP(N) = (Z(N-2)*(H(N-2) + H(N-1)) - Z(N-3)*H(N-1))/H(N-2)
      GO TO 38
C     CASES 1 AND 3 AVERAGED
37    YPP(1) = (Z(1)*(H(1) + H(2)) - Z(2)*H(1))/(2.*H(2))
      YPP(N) = (Z(N-2)*(H(N-2) + H(N-1)) - Z(N-3)*H(N-1))/(2.*H(N-2))
C     ASSIGN VALUES OF Z(1) THROUGH Z(N-2) TO YPP(2) THROUGH YPP(N-1).
38    DO 39 I = 2,N-1
      YPP(I) = Z(I-1)
39    CONTINUE
C     WRITE OUT Y VALUES FOR X VALUES AS SPECIFIED
      XX = DTN
      XMAX=X(4)
43    DO 44 I = 1,N-1
      IF(XX .GE. X(I) .AND. XX .LE. X(I+1))GO TO 45
44    CONTINUE
45    ANS = YPP(I)/6.*((X(I+1)-XX)**3/H(I)-H(I)*(X(I+1)-XX))
     *  +YPP(I+1)/6.*((XX-X(I))**3/H(I)-H(I)*(XX-X(I)))
     *  +Y(I)*(X(I+1)-XX)/H(I)+Y(I+1)*(XX-X(I))/H(I)
47    RETURN
      END
      SUBROUTINE TRIDI(N,A,B,C,S,X)
C     SUBROUTINE TO SOLVE A TRIDIAGONAL SYSTEM OF N EQUATIONS USING
C     GAUSSIAN ELIMINATION.
      IMPLICIT REAL*8(A-H,O-Z)
      DIMENSION A(1),B(1),C(1),S(1),X(1)
      NM1 = N-1
      DO 1 I = 1,NM1
      B(I+1) = B(I+1) - A(I+1)*C(I)/B(I)
      S(I+1) = S(I+1) - A(I+1)*S(I)/B(I)
1     CONTINUE
      X(N) = S(N)/B(N)
      DO 2 L = 1,NM1
      I = N-L
      X(I) = (S(I)-C(I)*X(I+1))/B(I)
2     CONTINUE
      RETURN
      END
      SUBROUTINE RETR
C     SUBROUTINE TO RETRIEVE STRESSES AT THE PARTICULAR NODES.
C     858 LOCATIONS, 3 LOADCASES, 25 POINTS OF INTEREST
C     ISURF=INNER SURFACE, OSURF=OUTER SURFACE
      COMMON LC,WHE,BBN,DTN,RO,RI,KK2
      DIMENSION STR(9,858,3),IM(858),OM(858),ISURF(25),OSURF(25)
      INTEGER K,L,P,N,I,LC,MAXLOC,LOCASE,WHE
```

```fortran
      REAL ANG,FAC
      DOUBLE PRECISION RO,RI,BBN,DTN,PI
      DATA ISURF/2805,2800,2790,2780,2770,2760,2750,2740,2730,
     * 2720,2710,2700,2692,2694,2705,2715,2725,2735,2745,2755,
     * 2765,2775,2785,2795,2805/
      DATA OSURF/2804,2799,2789,2779,2769,2759,2749,2739,2729,
     * 2719,2709,2699,2691,2693,2704,2714,2724,2734,2744,2754,
     * 2764,2774,2784,2794,2804/
      OPEN(20,FILE='intpe5.pop',STATUS='OLD')
      REWIND 20
      READ(20,333) TITLE
333   FORMAT(A72)
      READ(20,*) MAXLOC
      READ(20,*) LOCASE
      READ(20,*) BBN
      READ(20,*) DTN
      READ(20,*) (((STR(L,P,N ),L=1,9),P=1,MAXLOC),N=1,LOCASE)
      CLOSE(20)
      PI=4.0*ATAN(1.0)
      WRITE (6,*) 'WHICH LOADCASE?'
      WRITE(6,*) '1=TORQUE  2=IN-PLANE MOMENT  3=PRESSURE'
      READ (5,*) LC
      IF (LC.EQ.1) THEN
      LOCASE=LOCASE-2
      FAC=1.0*4*RO/(PI*(RO**4-RI**4))
      ENDIF
      IF (LC.EQ.2) THEN
      LOCASE=LOCASE-1
      FAC=1.0*4*RO/(PI*(RO**4-RI**4))
      ENDIF
      IF (LC.EQ.3) THEN
      LOCASE=LOCASE
      FAC=1.0*(RO+RI)/(2*(RO-RI))
      ENDIF
      ANG=0.
      OPEN (10,FILE='elbvm.pop',STATUS='UNKNOWN',FORM='FORMATTED')
      DO 200 K=1,25
      I=1
      J=1
2001  CONTINUE
      IM(I)=ISURF(K)-STR(1,I,LOCASE)
      IF(ABS(IM(I)).GT.(0.5)) THEN
      I=I+1
      GOTO 2001
      ENDIF
3001  CONTINUE
      OM(J)=OSURF(K)-STR(1,J,LOCASE)
      IF(ABS(OM(J)).GT.(0.5)) THEN
      J=J+1
      GOTO 3001
      ENDIF
```

```
      ANG=15.0*(K-1)
C     MISES STRESSES IN elbvm.pop ARE CALCULATED
      WRITE (10,222) ANG,STR(9,I,LOCASE),STR(9,J,LOCASE)
222   FORMAT(F6.1,4X,F7.3,4X,F7.3)
200   CONTINUE
      CLOSE(10)
      OPEN(20,FILE='elbvm.pop',STATUS='OLD')
      CALL UNI1(LC)
      CLOSE(20)
      RETURN
      END
      SUBROUTINE UNI1(LC)
      RETURN
      END
      SUBROUTINE STRESS
C     PROGRAM TO CALCULATE AND GENERATE LOAD INTERACTION.
C     INPUT DATA FILE IS READ FROM INTERPOLATED OUTPUT
C     (2+7) STRESSES, 858 LOCATIONS AND 3 LOADCASES
      COMMON/BLOCK1/STRES(9,858,3),ALOAD(3),SIGMA(6),STR(9),
     * PI,XVAL(361),YVAL(361),ZVAL(361),XVALT(361),YVALT(361),
     * ALOADT(3)
      COMMON/BLOCK2/LOC(858),MAXLOC,LOCASE,ILOC,IX,IY,IZ,NDEV
      COMMON/BLOCK3/TITLE
      COMMON LC,WHE,BBN,DTN,RO,RI,KK2
      DOUBLE PRECISION RO,RI,BBN,DTN
      CHARACTER*80 TITLE
      NDEV=20
      OPEN(UNIT=NDEV,FILE='intpe5.pop',STATUS='OLD')
      READ(NDEV,333)TITLE
333   FORMAT(A72)
      WRITE(6,333)TITLE
C     STRESSES IN DATA FILES ALREADY NORMALISED, HENCE
      ALOAD(1)=1.0
      ALOAD(2)=1.0
      ALOAD(3)=1.0
      DO I=1,3
      ALOADT(I)=ALOAD(I)
      END DO
      CALL DATA
1011  CONTINUE
1111  WRITE(6,101)
101   FORMAT(' SELECT OPTION FOR ANALYSIS:',/,
     *       ' 1 = MAX. MISES STRESS AND PLOT, AROUND ELBOW',/,
     *       '     MID-SECTION, FROM COMBINED LOADS',/,
     *       ' 2 = 2-LOADCASE INTERACTION DIAGRAM.',/,
     *       '     DATA IN FILE elb2id.pop',/,
     *       ' 3 = 3-LOADCASE INTERACTION DIAGRAM.',/,
     *       '     DATA IN FILE elb3id.pop',/,
     *       ' 4 = MISES ESF PLOT, AROUND ELBOW',/,
     *       '     MID SECTION, FROM SEPARATE LOADS',/,
     *       ' 5 = QUIT',//)
```

```fortran
      READ(5,*)NOPT
      GOTO (1,2,3,4,5),NOPT
      GOTO 1111
5     GOTO 200
1     CALL STRES1
      GOTO 1011
2     CALL INTER2(0)
      GOTO 1011
3     CALL INTER3
      GOTO 1011
4     CALL RETR
      GOTO 1011
200   CONTINUE
300   RETURN
      END
      SUBROUTINE DATA
C     READ IN FROM DATA FILE
      COMMON/BLOCK1/STRES(9,858,3),ALOAD(3),SIGMA(6),STR(9),
     * PI,XVAL(361),YVAL(361),ZVAL(361),XVALT(361),YVALT(361),
     * ALOADT(3)
      COMMON/BLOCK2/LOC(858),MAXLOC,LOCASE,ILOC,IX,IY,IZ,NDEV
      COMMON LC,WHE,BBN,DTN,RO,RI,KK2
      DOUBLE PRECISION BBN,DTN,RO,RI,INA
      READ(NDEV,*)MAXLOC
      READ(NDEV,*)LOCASE
      READ(NDEV,*)BBB
      READ(NDEV,*)DT
      READ(NDEV,*)(((STRES(I,J,K),I=1,9),J=1,MAXLOC),K=1,LOCASE)
      PI=4.0*ATAN(1.0)
      INA=(PI/4.0)*(RO**4-RI**4)
C     STRESSES CHANGED TO ABSOLUTE STRESSES PER UNIT LOAD,
C     FOR NEW ELBOW
      DO 612 J=1,MAXLOC
      DO 613 I=3,9
      STRES(I,J,1)=STRES(I,J,1)*RO/INA
      STRES(I,J,2)=STRES(I,J,2)*RO/INA
      STRES(I,J,3)=STRES(I,J,3)*(RO+RI)/(2.0*(RO-RI))
613   CONTINUE
612   CONTINUE
      DO 10 I=1,LOCASE
      DO 5 J=1,MAXLOC
      LOC(J)=STRES(1,J,1)
      DO 4 K=3,9
      STRES(K,J,I)=STRES(K,J,I)/ALOAD(I)
4     CONTINUE
5     CONTINUE
10    CONTINUE
      DO I=1,9
      END DO
      CLOSE (20)
      RETURN
```

```fortran
      END
      SUBROUTINE RETR1
C     SUBROUTINE TO RETRIEVE STRESSES AT THE PARTICULAR NODES AND
C     PLOT THE GRAPH FOR COMBINED LOADINGS - ABSOLUTE STRESSES GIVEN
C     858 LOCATIONS, 3 LOADCASES, 25 POINTS OF INTEREST
C     ISURF=INNER SURFACE, OSURF=OUTER SURFACE
      COMMON LC,WHE,BBN,DTN,RO,RI,KK2
      DIMENSION STR(9,858,3),IM(858),OM(858),ISURF(25),OSURF(25)
      INTEGER K,L,P,I,LC,MAXLOC,LOCASE,WHE,N
      REAL ANG
      DOUBLE PRECISION RO,RI,BBN,DTN
      DATA ISURF/    2805,2800,2790,2780,2770,2760,2750,2740,2730,
     * 2720,2710,2700,2692,2694,2705,2715,2725,2735,2745,2755,
     * 2765,2775,2785,2795,2805/
      DATA OSURF/   2804,2799,2789,2779,2769,2759,2749,2739,2729,
     * 2719,2709,2699,2691,2693,2704,2714,2724,2734,2744,2754,
     * 2764,2774,2784,2794,2804/
      OPEN(20,FILE='comelb.pop',STATUS='OLD')
      REWIND 20
      READ(20,333) TITLE
333   FORMAT(A72)
      READ(20,*) MAXLOC
      READ(20,*) LOCASE
      READ(20,*) BBN
      READ(20,*) DTN
      READ(20,*) (((STR(L,P,N),L=1,9),P=1,MAXLOC),N=1,1)
      CLOSE(20)
      OPEN (10,FILE='elbvm.pop',STATUS='UNKNOWN',FORM='FORMATTED')
      ANG=0.
      WRITE(6,*)'COMBINED VON MISES STRESSES AT ELBOW MID-SECTION'
      WRITE(6,*)'THETA      INNER SURFACE  OUTER SURFACE'
      DO 200 K=1,25
      I=1
      J=1
2002  CONTINUE
      IM(I)=ISURF(K)-STR(1,I,1)
      IF(ABS(IM(I)).GT.(0.5)) THEN
      I=I+1
      GOTO 2002
      ENDIF
3002  CONTINUE
      OM(J)=OSURF(K)-STR(1,J,1)
      IF(ABS(OM(J)).GT.(0.5)) THEN
      J=J+1
      GOTO 3002
      ENDIF
      ANG=15.0*(K-1)
      WRITE (10,222) ANG,STR(9,I,1),STR(9,J,1)
      WRITE (6,222) ANG,STR(9,I,1),STR(9,J,1)
222   FORMAT(F6.1,4X,1PE11.4,4X,1PE11.4)
200   CONTINUE
```

```fortran
      REWIND 10
      CALL UNI1C
      RETURN
      END
      SUBROUTINE UNI1C
      RETURN
      END
      SUBROUTINE STRESST
C     CALCULATE SIGMA-1, SIGMA-2 AND TR EFF.STRESSES AT ONE LOCATION
      COMMON/BLOCK1/STRES(9,858,3),ALOAD(3),SIGMA(6),STR(9),
     * PI,XVAL(361),YVAL(361),ZVAL(361),XVALT(361),YVALT(361),
     * ALOADT(3)
      COMMON/BLOCK2/LOC(858),MAXLOC,LOCASE,ILOC,IX,IY,IZ,NDEV
      DO I=3,9
      STR(I)=0.
      END DO
      DO 10 I=1,LOCASE
      DO 5 J=3,9
      STRS=STRES(J,ILOC,I)
      STR(J)=STR(J)+STRS*ALOADT(I)
5     CONTINUE
10    CONTINUE
      CALL SIGCAL
      RETURN
      END
      FUNCTION FIND(IMAX)
C     FINDING VON MISES' MAX.EFF.STRESS AND LOC.
      COMMON/BLOCK1/STRES(9,858,3),ALOAD(3),SIGMA(6),STR(9),
     * PI,XVAL(361),YVAL(361),ZVAL(361),XVALT(361),YVALT(361),
     * ALOADT(3)
      COMMON/BLOCK2/LOC(858),MAXLOC,LOCASE,ILOC,IX,IY,IZ,NDEV
      SMAX=0.
      DO 100 ILOC=1,MAXLOC
      CALL STRESSV
      IF(SMAX.GT.SIGMA(6))GOTO 100
      IMAX=ILOC
      SMAX=SIGMA(6)
100   CONTINUE
      FIND=SMAX
      RETURN
      END
      FUNCTION FINDT(IMAXT)
C     FINDING TRESCA'S EFF.STRESSES AND LOC.
      COMMON/BLOCK1/STRES(9,858,3),ALOAD(3),SIGMA(6),STR(9),
     * PI,XVAL(361),YVAL(361),ZVAL(361),XVALT(361),YVALT(361),
     * ALOADT(3)
      COMMON/BLOCK2/LOC(858),MAXLOC,LOCASE,ILOC,IX,IY,IZ,NDEV
      SMAXT=0.
      DO 100 ILOC =1,MAXLOC
      CALL STRESST
      IF (SMAXT.GT.SIGMA(5))GOTO 100
```

```fortran
      IMAXT=ILOC
      SMAXT=SIGMA(5)
100   CONTINUE
      FINDT=SMAXT
      RETURN
      END
      SUBROUTINE STRES1
C     SUBROUTINE FOR STRESS CALCULATION
      COMMON/BLOCK1/STRES(9,858,3),ALOAD(3),SIGMA(6),STR(9),
     * PI,XVAL(361),YVAL(361),ZVAL(361),XVALT(361),YVALT(361),
     * ALOADT(3)
      COMMON/BLOCK2/LOC(858),MAXLOC,LOCASE,ILOC,IX,IY,IZ,NDEV
      COMMON LC,WHE,BBN,DTN,RO,RI,KK2
      DOUBLE PRECISION BBN,DTN,RO,RI
      character*20 fdat
      WRITE(6,5999)
5999     FORMAT(' TOTAL MISES EFFECTIVE STRESS FOR COMBINED
     LOADINGS.',/)
      WRITE(6,6030)
6030  FORMAT(' ENTER INTERACTING APPLIED LOADS.',//)
      WRITE(6,6031)
6031  FORMAT(' TORQUE, IN N-mm=' /)
      READ(5,*)ALOAD(1)
      WRITE(6,6032)
6032  FORMAT(' IN-PLANE MOMENT, IN N-mm=' /)
      READ(5,*)ALOAD(2)
      WRITE(6,6033)
6033  FORMAT(' INTERNAL PRESSURE, IN N/mm2=' /)
      READ(5,*)ALOAD(3)
      WRITE(6,604)ALOAD
604   FORMAT(//,' APPLIED LOADS, IN N-mm UNITS, ARE : ',/,
     * ' TORQUE          =',1PE10.3,/,
     * ' IN-PLANE MOMENT  =',1PE10.3,/,
     * ' INTERNAL PRESSURE =',1PE10.3)
602   FORMAT(/,1X,'NODE NO. SIG-X  SIG-Y  SIG-Z  (SIG-TR-CAL)',
     * '  SIG-VM-CAL ',/)
      SMAX=0.
      DO 100 ILOC=1,MAXLOC
      CALL STRESSV
C     DO NOT USE STR HERE - INDIVIDUAL STRESSES PROPORTIONED AND
      SUMMED
      IF(SMAX.GT.SIGMA(6))GOTO 99
      SMAX=SIGMA(6)
      IMAX=ILOC
99    CONTINUE
100   CONTINUE
601   FORMAT(I5,1X,6(F9.2,2X))
      WRITE(6,605)
605   FORMAT(//,'  MAXIMUM VM EQUIVALENT STRESS FOUND AT ',/)
      ILOC=IMAX
      CALL STRESSV
```

```fortran
      WRITE(6,602)
      WRITE(6,601)LOC(ILOC),STR(3),STR(4),STR(5),
     * SIGMA(5),SIGMA(6)
C    * SIGMA(5),SIGMA(6),STR(9)--STR(9) IS INTERPOLATED MISES STRESS
C     MISES STRESSES IN comelb.pop ARE CALCULATED
C     IF RUNNING MANY LOAD COMBINATIONS FOR AN ELBOW AND SEPARATE
C     DATAFILES ARE NEEDED FOR SPECIAL PURPOSES, THEN
C     WRITE(6,*)' DATAFILE TO BE OPENED?'
C     READ(5,*)FDAT
C     OPEN(15,FILE=FDAT,STATUS='UNKNOWN',FORM='FORMATTED')
      OPEN(10,FILE='comelb.pop',STATUS='UNKNOWN',FORM='FORMATTED')
      WRITE(10,*)'ABSOLUTE STRESSES FROM COMBINED LOADINGS'
      WRITE(10,*)MAXLOC
      WRITE(10,*)LOCASE
      WRITE(10,*)BBN
      WRITE(10,*)DTN
      WRITE(15,*)'ABSOLUTE STRESSES FROM COMBINED LOADINGS'
      WRITE(15,*)MAXLOC
      WRITE(15,*)LOCASE
      WRITE(15,*)BBN
      WRITE(15,*)DTN
      DO 1101 ILOC=1,MAXLOC
      DO I=3,9
      STR(I)=0.
      END DO
      DO 10 I=1,LOCASE
      DO 5 J=3,9
      STRS=STRES(J,ILOC,I)
      STR(J)=STR(J)+STRS*ALOAD(I)
5     CONTINUE
10    CONTINUE
      CALL SIGCAL
C     VON MISES STRESS CALCULATED FROM SIGCAL
      WRITE(10,56)STRES(1,ILOC,1),STRES(2,1,1),STR(3),STR(4),STR(5),
     * STR(6),STR(7),STR(8),SIGMA(6)
      WRITE(15,56)STRES(1,ILOC,1),STRES(2,1,1),STR(3),STR(4),STR(5),
     * STR(6),STR(7),STR(8),SIGMA(6)
56    FORMAT(F8.1,1X,F5.1,1X,7(1PE11.4,1X))
1101  CONTINUE
      CLOSE(10)
      CALL RETR1
      RETURN
      END
      SUBROUTINE STRESSV
C     CALCULATE SIGMA-1, SIGMA-2 AND VM EFF.STRESSES AT ONE LOCATION
      COMMON/BLOCK1/STRES(9,858,3),ALOAD(3),SIGMA(6),STR(9),
     * PI,XVAL(361),YVAL(361),ZVAL(361),XVALT(361),YVALT(361),
     * ALOADT(3)
      COMMON/BLOCK2/LOC(858),MAXLOC,LOCASE,ILOC,IX,IY,IZ,NDEV
      DO I=3,9
      STR(I)=0.
```

```fortran
      END DO
      DO 10 I=1,LOCASE
      DO 5 J=3,9
      STRS=STRES(J,ILOC,I)
      STR(J)=STR(J)+STRS*ALOAD(I)
5     CONTINUE
10    CONTINUE
      CALL SIGCAL
      RETURN
      END
      SUBROUTINE INTER2(NALL)
C     INTERACTION FOR SELECTIVE AND ALL LOADCASES.
      COMMON/BLOCK1/STRES(9,858,3),ALOAD(3),SIGMA(6),STR(9),
     * PI,XVAL(361),YVAL(361),ZVAL(361),XVALT(361),YVALT(361),
     * ALOADT(3)
      COMMON/BLOCK2/LOC(858 ),MAXLOC,LOCASE,ILOC,IX,IY,IZ,NDEV
      COMMON/BLOCK3/TITLE
      CHARACTER*80 TITLE,FFNN
      OPEN(10,FILE='elb2id.pop',STATUS='UNKNOWN',FORM='FORMATTED')
C     IF WRITING DATA TO SEPARATE FILE FOR SOME PURPOSES,
C     WRITE(6,*) 'FILENAME TO WRITE STRESS INTERACTION DATA?'
C     WRITE(6,*) 'TAKE CARE NOT TO OVERWRITE EXISTING FILE!!'
C     READ(5,*)FFNN
C     OPEN(22,FILE=FFNN,STATUS='UNKNOWN',FORM='FORMATTED')
      WRITE(6,601)
601   FORMAT(' FOR INTERACTION DIAGRAM.',/,
     *       ' LOADCASE  1 = TORQUE ',/,
     *       '          2 = IN-PLANE MOMENT ',/,
     *       '          3 = INTERNAL PRESSURE ',//,
     * ' ENTER 2 INTERACTING LOADCASES, SEPARATED BY A SPACE.'/,
     * ' THE FIRST ENTRY WILL BE ON THE X-AXIS.')
      READ(5,*)IX,IY
      CALL INTACT(2)
      OPEN(20,FILE='elb2id.pop',STATUS='OLD')
      REWIND 20
      CALL UNI2(IX,IY)
      RETURN
      END
      SUBROUTINE INTER3
C     INTERACTION FOR THREE LOADS
      COMMON/BLOCK1/STRES(9,858,3),ALOAD(3),SIGMA(6),STR(9),
     * PI,XVAL(361),YVAL(361),ZVAL(361),XVALT(361),YVALT(361),
     * ALOADT(3)
      COMMON/BLOCK2/LOC(858 ),MAXLOC,LOCASE,ILOC,IX,IY,IZ,NDEV
      COMMON/BLOCK3/TITLE
      CHARACTER*80 TITLE
      OPEN(10,FILE='elb3id.pop',STATUS='UNKNOWN',FORM='FORMATTED')
      WRITE(6,601)
601   FORMAT(' LOADCASES  1 = TORQUE      ',/,
     *       '          2 = IN-PLANE MOMENT ',/,
     *       '          3 = INTERNAL PRESSURE ',//,
```

```
      * ' ENTER 3 INTERACTING LOADCASES, SEPARATED BY A SPACE.',/,
      * ' THEY WILL CORRESPOND TO THE X-,Y- AND Z-AXES LOADS.',/,
      * ' THE THIRD LOADCASE HAS NO NEGATIVE VALUES.')
        READ(5,*)IX,IY,IZ
        CALL INTACT(3)
        OPEN(20,FILE='elb3id.pop',STATUS='OLD')
        REWIND 20
        CALL UNI3(IX,IY,IZ)
        RETURN
        END
        SUBROUTINE UNI3(IX,IY,IZ)
        RETURN
        END
        SUBROUTINE INTACT(NDIM)
C     INTERACTION DATA SUBROUTINE
        COMMON/BLOCK1/STRES(9,858,3),ALOAD(3),SIGMA(6),STR(9),
      * PI,XVAL(361),YVAL(361),ZVAL(361),XVALT(361),YVALT(361),
      * ALOADT(3)
        COMMON/BLOCK2/LOC(858),MAXLOC,LOCASE,ILOC,IX,IY,IZ,NDEV
        REAL MVM(361),MTR(361),BLOAD(3),BLOADT(3),SMAXT,SXT,SYT
        PI=4.0*ATAN(1.0)
        DO 1 I=1,3
        BLOAD(I)=ALOAD(I)
        BLOADT(I)=ALOADT(I)
        ALOAD(I)=0.
        ALOADT(I)=0.
1       CONTINUE
        ALOAD(IX)=1.
        ALOADT(IX)=1.
        SMAX=FIND(IMAX)
        SMAXT=FINDT(IMAXT)
        SX=1./SMAX
        SXT=1./SMAXT
        WRITE(6,605)IX,SMAX,LOC(IMAX)
605     FORMAT(' LOAD NO.',I2,'. MAX VM EFF.STR. PER UNIT LOAD IS',
      * 1PE10.3,' AT NODE ',I5)
        ALOAD(IX)=0.
        ALOADT(IX)=0.
        ALOAD(IY)=1.
        ALOADT(IY)=1.
        SMAX=FIND(IMAX)
        SMAXT=FINDT(IMAXT)
        SY=1./SMAX
        SYT=1./SMAXT
        WRITE(6,605)IY,SMAX,LOC(IMAX)
        IF(NDIM.EQ.3)GOTO 606
        WRITE(6,603)
603     FORMAT(//,' 2-D INTERACTION DIAGRAM STRESS DATA',/,
      * ' IN FILE elb2id.pop, IN THE FORM OF:-',/,
      * ' X-LOAD      Y-LOAD',//)
        DO 10 I=1,361
```

```
         ANGLE=REAL(I-1)*1.0*(PI/180.)
         X=COS(ANGLE)
         Y=SIN(ANGLE)
         ALOAD(IX)=X*SX
         ALOAD(IY)=Y*SY
         ALOADT(IX)=X*SXT
         ALOADT(IY)=Y*SYT
         SMAX=FIND(IMAX)
         SMAXT=FINDT(IMAXT)
         XVALT(I)= X/SMAXT
         YVALT(I)= Y/SMAXT
         MTR(I)=SQRT(XVALT(I)**2+YVALT(I)**2)
         XVAL(I)=X/SMAX
         YVAL(I)=Y/SMAX
         MVM(I)=SQRT(XVAL(I)**2+YVAL(I)**2)
         ANGLE=ANGLE*180./PI
C    IF TRESCA STRESSES AND LOCATIONS OF MAX. STRESSES ARE NEEDED
C    WRITE(6,602)XVALT(I),YVALT(I),LOC(IMAXT),XVAL(I),YVAL(I),
C    * LOC(IMAX)
         WRITE(10,666)XVAL(I),YVAL(I)
         WRITE(22,666)XVAL(I),YVAL(I)
666   FORMAT(1X,F8.4,3X,F8.4)
10      CONTINUE
602   FORMAT(F7.4,3X,F7.4,3X,I5,3X,F7.4,3X,F7.4,3X,I5)
         GOTO 19
606   CONTINUE
         S3=FLOAT(IZ)
         S3=S3/ABS(S3)
         IZ=IABS(IZ)
         ALOAD(IY)=0.
         ALOAD(IZ)=1.
         SMAX=FIND(IMAX)
         SZ=1./SMAX
         WRITE(6,605)IZ,SMAX,LOC(IMAX)
         WRITE(6,604)
604   FORMAT(/,'3-D INTERACTION DIAGRAM STRESS DATA, IN FILE',/,
      * ' elb3id.pop, IN THE FORM OF:-',/,
      * ' LOAD-X          LOAD-Y          LOAD-Z',//)
         NCASES=1
         FI=0.
         DFI=.48*PI/20
         DO 500 K=1,21
         Z=SIN(FI)/COS(FI)
         ALOAD(IZ)=Z*SZ*S3
         DO 400 I=1,33
         ANGLE=FLOAT(I-1)*PI/16.
         X=COS(ANGLE)
         Y=SIN(ANGLE)
         ALOAD(IX)=X*SX
         ALOAD(IY)=Y*SY
         SMAX=FIND(IMAX)
```

```fortran
      XVAL(I)=X/SMAX
      YVAL(I)=Y/SMAX
      ZVAL(I)=Z*S3/SMAX
      ANGLE=ANGLE*180./PI
C     IF LOCATIONS NEEDED
C     WRITE(6,607)XVAL(I),YVAL(I),ZVAL(I),LOC(IMAX)
      WRITE(10,608)XVAL(I),YVAL(I),ZVAL(I)
608   FORMAT(1X,3(1PE12.3,1X))
400   CONTINUE
      FI=FI+DFI
500   CONTINUE
607   FORMAT(1X,3(1PE12.3,3X),I10)
      X=0.
      Y=0.
      Z=S3
19    CONTINUE
      DO 20 I=1,3
      ALOAD(I)=BLOAD(I)
20    CONTINUE
      CLOSE(10)
      RETURN
      END
      SUBROUTINE SIGCAL
C     STRESSES CALCULATIONS
      COMMON/BLOCK1/STRES(9,858,3),ALOAD(3),SIGMA(6),STR(9),
     * PI,XVAL(361),YVAL(361),ZVAL(361),XVALT(361),YVALT(361),
     * ALOADT(3)
      COMMON/BLOCK2/LOC(858),MAXLOC,LOCASE,ILOC,IX,IY,IZ,NDEV
      DOUBLE PRECISION J1,J2,J3,B1,B0,B11,PHI,B111,
     * BB,Y1,Y2,Y3,S11,S22,S33,PHI1
      PI=4.0*ATAN(1.0)
      J1=STR(3)+STR(4)+STR(5)
      J2=STR(3)*STR(4)+STR(4)*STR(5)+STR(5)*STR(3)
     * -STR(6)**2-STR(7)**2-STR(8)**2
      J3=STR(3)*STR(4)*STR(5)+2*STR(6)*STR(7)*STR(8)-STR(3)*STR(7)**2
     * -STR(4)*STR(8)**2-STR(5)*STR(6)**2
      B1=(3*J2-J1**2)/3
      B0=(-2*J1**3+9*J1*J2-27*J3)/27
      B11=-3/B1
      PHI1=(-B0/2)*B11**1.5
      IF (PHI1.GE.1.0) THEN
      PHI1=0.999999999
      END IF
      IF (PHI1.LE.-1.0) THEN
      PHI1=-0.999999999
      END IF
      PHI=ACOS(PHI1)
      B111=-B1/3
      BB=2*B111**0.5
      Y1=BB*COS(PHI/3)
      Y2=BB*COS(PHI/3+2*PI/3)
```

195

```
      Y3=BB*COS(PHI/3+4*PI/3)
      S11=Y1+J1/3.
      S22=Y2+J1/3.
      S33=Y3+J1/3.
      SIGMA(1)=STR(3)
      SIGMA(2)=STR(4)
      SIGMA(3)=MAX(S11,S22,S33)
      SIGMA(4)=MIN(S11,S22,S33)
      SIGMA(5)=SIGMA(3)-SIGMA(4)
      SIGMA(6)=S11**2+S22**2+S33**2-S11*S22-S22*S33-S33*S11
      SIGMA(6)=SQRT(SIGMA(6))
  11  FORMAT(6(1PE11.4,1X))
      RETURN
      END
      SUBROUTINE UNI2(IX,IY)
      RETURN
      END
```

Note:
1. Graph plotting subroutines not included.

APPENDIX C.   LOCATION OF IMPORTANT NODES IN ELBOW MODELS.

Node locations

Node number	θ (in degrees)	ϕ (in degrees)	Location
2692	180	0	outer surface of intrados
2719	135	0	outer surface
2739	105	0	outer surface
2744	90	0	outer surface of crown
2745	90	0	inner surface of crown
2754	285	0	outer surface
2759	75	0	outer surface
3060	240	-15	outer surface
3218	225	22.5	outer surface
3233	120	-22.5	outer surface

196